THE ORIGIN AND FATE OF METALS DURING DIESEL ENGINE COMBUSTION

A THESIS

SUBMITTED TO THE FACULTY OF THE GRADUATE SCHOOL

OF THE UNIVERSITY OF MINNESOTA

BY

Arthur L. Miller

IN PARTIAL FULFILLMENT OF THE REQUIREMENTS

FOR THE DEGREE OF

DOCTOR OF PHILOSOPHY

Dr. David B. Kittelson, Adviser

Dr. Michael R. Zachariah, Adviser

August, 2005

UNIVERSITY OF MINNESOTA

This is to certify that I have examined this copy of a doctoral thesis by

Arthur L. Miller

And have found that it is complete and satisfactory in all respects,

and that any and all revisions required by the final

examining committee have been made.

Dr. David B. Kittelson Dr. Michael R. Zachariah

Name of Faculty Advisers

David Kittelson

Signature of Faculty Advisers

Aug 20, 2005

Date

GRADUATE SCHOOL

Acknowledgements

I am forever thankful to the many people who helped me during the long process of studying and writing this dissertation. There are too many to name, but I'd especially like to thank:

- My wife and two daughters who put up with me for the entire time.
- My parents and 21 siblings who were cheering from the sidelines.
- Two very talented advisors for their guidance.
- The many generous and helpful grad school classmates and fellow diesel geeks who often carried me when things got tough.
- The folks at NIOSH-LTT who believed in me enough to fund this adventure.
- My colleagues at NIOSH for their support and encouragement.
- Finally, my colleague and friend Dr. Dong Geun Lee, who is now teaching and researching at the Pusan National University in South Korea. Dr. Lee contributed greatly to the success of the single particle mass spectrometry experiments, cheerfully working long hours when necessary to help acquire dependable data.

Executive Summary

The numerous by-products of combustion (literally thousands of compounds) are continually reacting, evolving, and forming particles as they leave the combustion zone and eventually join the atmosphere where we breathe them directly into our lungs. One of the primary contributors to such ambient pollution is the diesel particulate matter (DPM) generated by engines. In order to shed light on the correlation between DPM and health effects, it is important to understand how the various gaseous species and small soot particles are formed and how they behave after leaving the combustion zone.

Recent epidemiological studies have demonstrated a correlation between adverse health effects and exposure to airborne particulate matter, especially DPM. Subsequent studies have been conducted in attempts to identify the source and/or causal mechanisms for the observed health effects. This dissertation reviews highlights of previous work and investigates a hypothesis that considers metal-bearing DPM as a possible contributor. Literature is cited which supports a hypothesis that by-product metals are produced during diesel combustion and reside on small particles that can easily be deposited in the lungs by inhalation. To investigate that hypothesis, research experiments were designed and conducted utilizing a diesel engine to generate particles and subsequent analysis of the particles using techniques including electron microscopy, x-ray diffraction, and single particle mass spectrometry.

Chapter 1 provides background information and justification for this research and entails a summary of research regarding the toxicology and the potential adverse health effects associated with particulate matter (PM) and diesel particulate matter (DPM). Chapter 2 is a short overview of particle mechanics with a focus on particle formation

pathways. Chapter 3 expands on the issue of particle formation and provides more detail concerning DPM formation. It covers the roles of soot and organic carbon as well as non-carbon species and also touches on the issue of technologies aimed at DPM reduction. Chapter 4 is a short statement of the dissertation hypothesis.

Chapters 5-8 summarize the bulk of my dissertation research which was aimed at providing a better understanding of the role of metals during diesel combustion. Each chapter represents a set of experiments designed to quantify the fate of various metals during the combustion process. The chapters appear in the order in which the research was conducted and represent an evolution of refinement in terms of the quantification of the metals in DPM. Chapter 5 represents the most easily quantifiable case, that in which the fuel was doped with relatively large amounts of iron (20-60ppm), while the last of those chapters (Chapter 8), describes the least quantifiable case i.e. where there was no doping at all. The latter case addresses real world conditions and in that sense is the most critical. However, the previous experiments provided valuable insight into the dynamics of the particle formation processes and in that regard stand on their own in terms of advancing the body of knowledge in this field.

Research results are presented and illustrate that for both doped and undoped conditions, trace metals are associated with particles in the size range of about 20-300 nm mobility diameter. For some cases the metal to carbon ratios for these particles are inversely proportional to particle diameter, suggesting condensation of metal vapors onto carbon particles. Results also show that for the doped cases, the slightly higher metal content in the system leads to formation of metal-rich nanoparticles.

Table of Contents

List of Figures

Page

List of Tables

Page

Chapter 1 - Background and Motivation for Current Research

This research was supported by the National Institute for Occupational Safety and Health (NIOSH), and as such was motivated by the issue of worker exposure to diesel particulate matter (DPM). Worker exposure to DPM is currently a pressing health concern and new air quality regulations have been put in place to protect workers (Federal Register, 30 CFR). Adverse health effects stemming from DPM exposure, including cancer, have been demonstrated (Bhatia, et al, 1998; Lipsett, et al, 1998), but no causal mechanisms have been clearly identified. This first chapter entails a review of key portions of the extensive body of literature on the toxicology and health effects associated with exposure to fine and ultrafine particulate matter (PM) and more specifically to DPM.

1.1 Health Effects of PM and DPM

Drastic negative health effects originating from air pollution such as the famous London Fog of 1952 that resulted in over 4,000 deaths, have been recorded in several instances in the past. Tragedies in the U.S. as recent as 1950 (Davis, 2002) have brought the issue to the forefront of the health research field. Although such events are rare, the effects of chronic exposures to air pollution are a topic of great concern and much research. Although the composition of atmospheric aerosols can vary widely, the term PM is often used generically to describe the particulate matter in the air we breath. The term DPM (diesel particulate matter) is used more specifically to describe the aerosol

emitted from a diesel engine. In the following sections are discussions of some of the adverse health effects associated with both PM and DPM.

When a person is exposed to PM, their body's response will depend on what portion of the PM is retained by the body. This material, called the "burden," can be thought as the difference between the amount of exposed material deposited in the body and the "clearance" or removal of material by the body. These processes, in addition to being complex in their own right, are both time dependent. To model such events, epidemiologists must therefore integrate the exposure, deposition, and clearance mechanisms in time to get accurate estimates of burden. For the purpose of the following discussion, the role of particle deposition is highlighted.

The deposition of particles in the respiratory tract is greatly affected by their material properties. Because the particles have great variation in size, shape, and density, rather than making time consuming physical measurements for each aerosol, in many cases it suffices to use an "equivalent diameter" to describe the particles. For particles larger then around 100nm, it is possible to use the metric of "aerodynamic equivalent diameter" (AED). This metric is based on mass and aerodynamic drag and compares particles in terms of aerodynamic behavior (i.e., terminal settling velocity), thus incorporating the properties of size, shape, and density. The baseline for comparison is the settling velocity of rigid spheres of unit density (1 gm/cc). Many of the common aerosol size measurement instruments in use today incorporate this metric and so give results of particle size distribution in terms of aerodynamic diameter. For smaller particles i.e. those less than about 100nm, particle mobility is less dependent on mass, while the effects of diffusion and elemental charge more strongly affect particle

dynamics. For these smaller particles the size metric of choice is thus mobility diameter, which is determined by giving the particles a unit charge and measuring their velocity in an electric field of known strength.

Size distributions of most aerosols of practical importance are "polydisperse" and in fact due to a unique natural phenomenon, many have size distributions which are roughly lognormal. This is a very powerful result, and has allowed the development of many sophisticated modeling techniques which would have been otherwise cumbersome or impossible. The evolution and stability of the lognormal size distribution has been verified theoretically and experimentally (Hinds, 1999). It has been shown that in a very short time, an aerosol of random size distribution (most notably a monodisperse system) will evolve into an aerosol with "self-preserving" (approximately lognormal) size distribution.

For such lognormal size distributions, the logarithmic mean is the median of the distribution, and the measure of variability around that median is the geometric standard deviation (σg). Sometimes called "sigma-g," this metric is simply the ratio of the 84^{th} (or 16^{th}) percentile particle size to the 50^{th} percentile size. Thus, knowing the median value and the σg, the (lognormal) distribution is known.

In measuring aerosol size distributions, the results are typically expressed in terms of number count per size class, or alternately in terms of surface area or volume (or mass, assuming spheres of unit density). Using these three approaches may give differing results in terms of the shape of the size distribution, and so it is important to use the method which best represents the particle properties under question, i.e., when investigating particle surface chemistry, the distribution of particle surface area for

various sized particles would likely be of most interest. In any case, since the size distribution functions are often fairly lognormal, it is customary to refer to the mean or median diameter when describing particle size distributions.

The nature of the aerosol size distribution plays an important role in particle deposition in the human respiratory system since particle size is key to the deposition behavior of particles (EPA, March 2001, pp. 7-14). As the body inhales particulate aerosols, many of the particles are deposited within the respiratory system, while the remainder escape with the exhaled air. The respiratory tract can be described in terms of three main sections as noted in Figure 1.1. The airways act somewhat like a three stage filtering mechanism in removing particles from the inhaled aerosol. The ET and TB sections have high fluid velocities and complex geometries. This results in larger particles not being able to follow the flow streamlines, resulting in significant particle impaction. Large particles i.e. those greater than about 1 um in diameter, are thus removed in the upper airways by impaction or by gravitational settling. The very fine particles make their way easily into the alveolar region. The slower velocities and longer residence times there allow them to deposit by diffusion. Much like a filter, the "mid-sized" particles i.e. those in the 100-300 nm range, are only partially removed by settling and impaction, and since they are too large for efficient diffusion, they are the most likely to escape during exhalation.

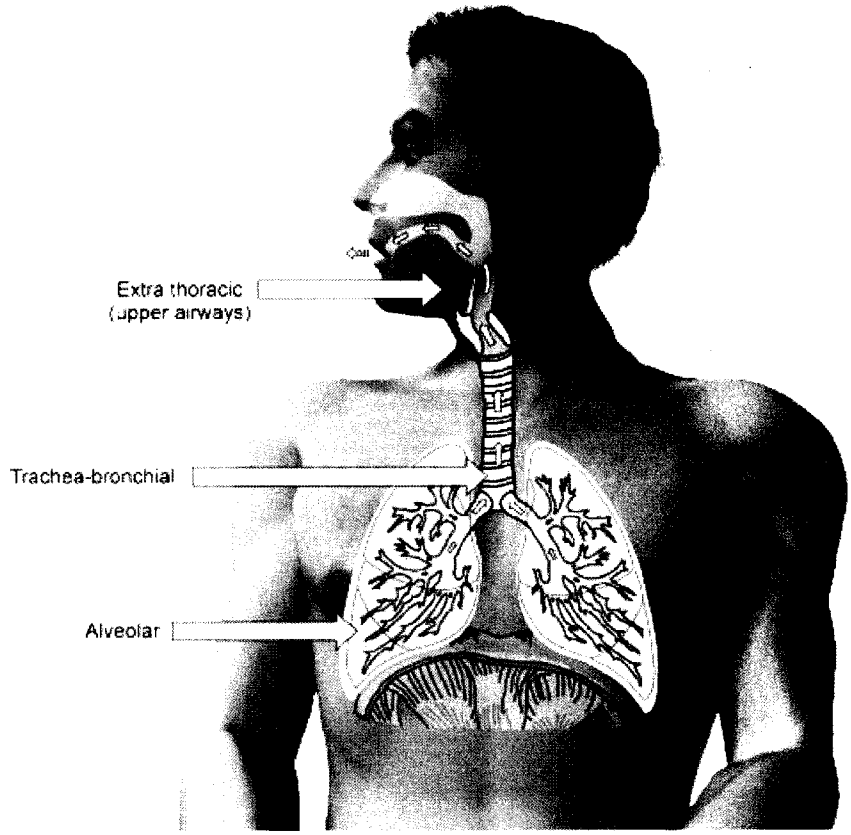

Figure 1.1 - Sketch showing the three main regions of the respiratory system, i.e., the extra thoracic, trachiobronchial, and alveolar regions.

1.1.1 PM10 and PM2.5

The EPA has collected a large amount of air pollution data over the last several decades, including the time weighted average (TWA) concentrations of airborne particulates. Originally they designed collectors which captured all particle less than 10 micrometers in size (aerodynamic diameter), and this data is generally called the "PM 10" data. Subsequently they gathered similar data for particles less than 2.5 micrometers in diameter and this data is referred to as PM 2.5 data. Due to recent concern about the potential hazards of ultrafine particulate matter, current data collection efforts also include information on "ultrafines" i.e. particles smaller than 100nm in diameter.

Over 300 recent articles are cited in a recent EPA report (EPA, 2001), all of which are related to the potential health effects associated with PM exposure. In general, it is difficult to compare the results of multiple studies because of the considerable variation in some of the key variables as well as potential confounders. Factors such as the level and duration of exposure may vary significantly. Exposure to multiple contributors also brings into question the validity of correlations between exposure (of a particular substance) and observed health effects. In spite of drawbacks to inter-study comparisons, there is surprising similarity in many of the published results.

The epidemiological studies thought to yield the best overall estimate of the relation between particle size and health effects are the multi-city studies. With the exception of some anomalies caused by local influences such as steel mills, dust storms, and mold growth, the results are very consistent. Comparison of four multi-city studies (EPA, 2001, pp. 6-267) showed the percent excess deaths per 50 $\mu g/m^3$ increase in 24-hour PM levels to be in the range 2.0% to 4.5%. (Note- excess deaths are determined by the increase in annual death rates over and above a baseline death rate measured in the relative absence of air pollution).

This data is reproduced in Figure 1.2 and shows not only a significant correlation between mortality and PM levels, but a striking similarity in results for the different multi-city studies, suggesting that the trend is not a unique phenomenon. Some regional effects have been demonstrated using this approach (for example higher levels of windblown dust in the southwestern US can effect the comparison with other cities), but in general for many cities the trend is surprisingly similar.

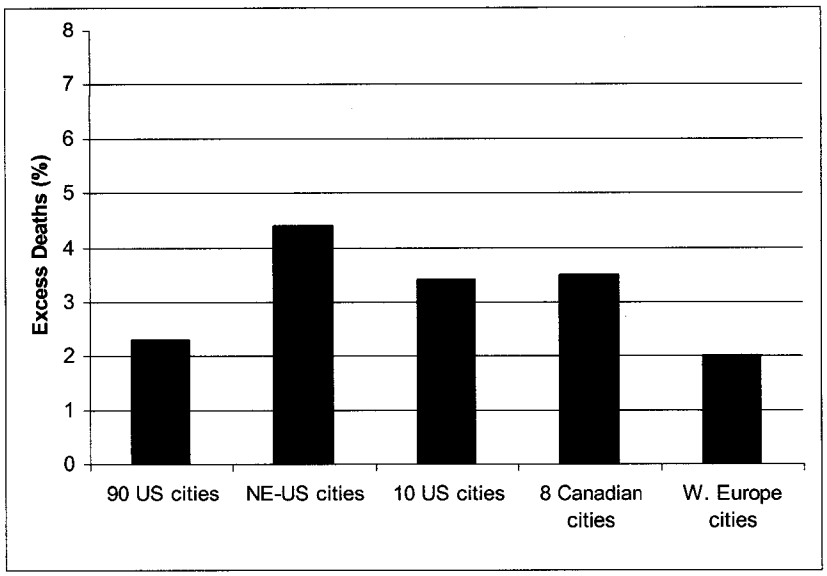

Figure 1.2 - Excess deaths per 50 ug/m3 increase in 24-hour PM10 levels, after (EPA, 2001).

Epidemiological studies of PM exposure are often broken down into categories by exposure duration (long versus short) and by airborne concentrations of a particular size range of particles (PM10, PM2.5, PM10-2.5, and ultrafines). The observed effects are also broken down into serious health effects such as death, cardio-vascular diseases, respiratory diseases, and fetal growth effects, and more acute effects such as bronchitis or asthma exacerbations. The more serious effects are generally indexed by mortality or hospital admissions and are associated with long-term exposure to PM over and above the accumulation of the more acute effects of short-term exposures. Simply put, short-term exposures (on the order of days) are associated with acute effects like bronchitis, while long-term exposures are linked to serious chronic health effects.

New work in the area of health effects includes an association between particle exposure (PM10-2.5) and asthma exacerbation. Another emerging issue stems from data

that shows association between PM exposure during pregnancy/early post-natal and slowed fetal growth or infant mortality (EPA, 2001, pp. 6-267).

Demonstrated adverse health effects are of great concern and have driven the creation of new air quality regulations and procedures. The EPA has developed the National Ambient Air Quality Standards (NAAQS). In order to protect exposed populations from the chronic effect associated with relatively low levels of exposure. Chronic effects may include such things as respiratory and cardiovascular disease, neurotoxic effects and cancer.

Ideally it would be possible to gather exact scientific data to demonstrate a cause and effect relationship between exposure and health effects, in order to set exposure limits including a margin of safety. Unfortunately in regards to PM exposure, there are usually too many variables involved to establish such a precise correlation. These might include multiple/variable constituents as well as other compounding outside stressors. Because of this, correlations between exposure and health effects of PM are generally estimated using a combination of epidemiological and toxicological studies along with studies focused on smaller groups (cohorts) who are occupationally exposed (Godish 2003, pp. 138). Thus the data of Figure 1.2, which is derived from large-scale epidemiological studies, were used along with other data in developing the NAAQS. Some of this data included toxicological studies of various constituents of PM. One key component of PM which has been shown to contain toxic substances is Diesel Particulate Matter (DPM). The bulk of this dissertation work will focus on that unique subcategory of PM.

1.1.2 DPM

Although PM is typically referred to in terms of PM10 and PM2.5, there is great interest in a size class of particles called ultrafines, generally meaning those particles with diameter less than 100 nm. Since these particles are much too small to have been mechanically generated, i.e., via physical communution, they typically do not include mineral dusts. Such ultrafine particles may be formed in the atmosphere by photochemical processes involving both natural and anthropomorphic emissions, and may also be generated anthropomorphically by processes such as high temperature combustion. The aerosols currently in our atmosphere contain a great number of such particles, many of which originate from internal combustion engines. Since many of these are from diesel engines, detailed characterization of DPM is called for and this dissertation research will therefore focus mainly on DPM.

The DPM particles are typically made up of many tiny "spherules" of elemental carbon that coagulate to form chain-like agglomerate particles as depicted in Figure 1.3. These agglomerate particles form inside the engine at high temperature and as they subsequently cool, take on other species (mainly organic carbon compounds) by surface interactions. This will be described in more detail in subsequent chapters.

It is known that diesel engines produce a tri-modal (and fairly lognormal) size distribution of DPM (Kittelson, 1998). The three modes or size ranges of particles are generally called the nucleation mode (diameters approximately 3-30nm), the accumulation mode (diameters approximately 30-500 nm) and the coarse mode (diameters larger than about 1000 nm). The number of nano-size particles, i.e., those in

the "nucleation" mode, is quite variable and can be attributed in many cases to the self-nucleation of volatile species during the dilution and simultaneous cooling of the exhaust.

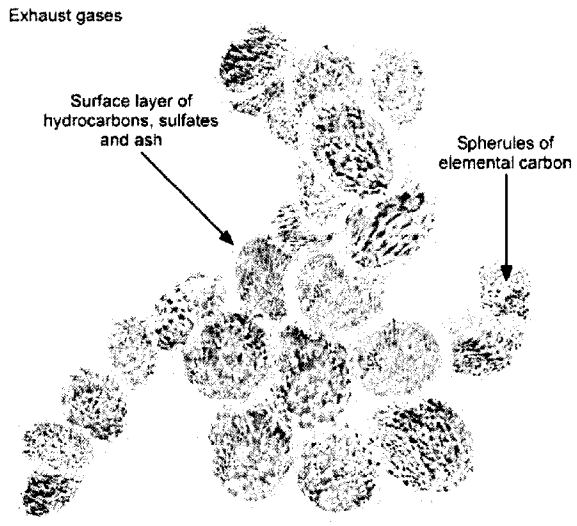

Figure 1.3 - Artist's sketch of a "typical" particle of DPM

In some cases nanoparticles may also form prior to dilution (Du, et al., 1998; Skillas, et al., 2000). The accumulation mode typically makes up the bulk of the particle mass and consists mainly of chain agglomerates as mentioned in the preceding paragraph. The coarse mode is generally believed to consists of clumps of chain agglomerates, and is most probably due to build up and shedding of material from the inside surfaces of the exhaust system.

Several recent studies have demonstrated a correlation between DPM exposures and both acute and chronic health effects, including cancer (Mauderly, et al., 1987). Figure 1.4 is recreated from data that show a significant increase in cancer risk for railroad workers exposed to DPM on the job (Garshick, et al., 1988).

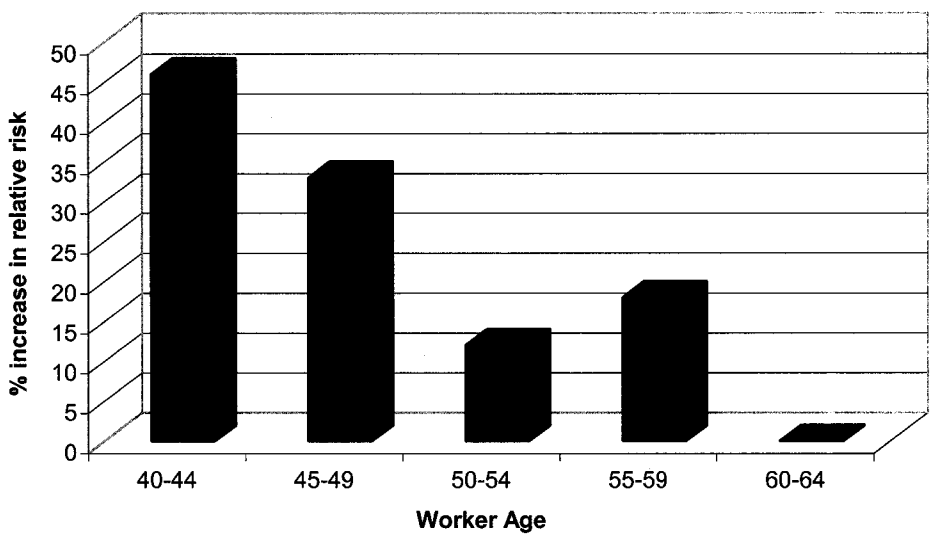

Figure 1.4 - Increased levels of cancer risk for railroad workers exposed to DPM.

Other studies have confirmed this correlation (Bhatia, et al., 1998; Lipsett, et al., 1998) as well as correlations to various respiratory dysfunctions including asthma. In response to such health effects data, some countries have created new regulations to control the allowable emission levels and/or worker exposure to DPM. One unique example of this is the new air quality regulations for underground mines recently implemented in the U.S. by the Mine Safety and Health Administration (MSHA). Both the allowable exposure levels and the measurement metric for DPM were litigated extensively during the formation of that regulation. This was due in part to the shortage

of data for dose/response relationships as well as a cause/effect relationship for the health effects in question. For situations such as this, it is common to use a combination of epidemiology, toxicology, and cohort studies along with considerations for implementation feasibility, to derive a regulation which uses a variety of existing data to reasonably protect workers.

1.2 Theories for DPM Toxicity

Many early health studies simply addressed the combined effects of DPM exposure, with little or no idea as to the sources of the deleterious effects. More recent studies (including this dissertation work) have been undertaken to investigate potential sources and causal mechanisms of the observed negative health effects.

Assigning the toxicity of DPM to a particular element or compound is difficult, since there are many possibilities. Early studies focused on the presence of polynuclear aromatic hydrocarbons (PAH's), which are a whole family of long chain hydrocarbon compounds, many of which have been shown to be toxic. Other theories include the "particle effect" based on the body's response to small particulates, and the toxic metal theory, which addresses the issue of the body's response to metals entering the body in conjunction with small particles. These three theories are described in more detail in the following paragraphs.

1.2.1 PAH's

During the post-WWII expansion of industrial technologies in the U.S., scientists began looking closely at the health effects of industrial processes, and in particular at the

issue of combustion by-products. Early studies identified the mutagenicity of several of the many polynuclear-aromatic-hydrocarbons (PAH's) which are prevalent in combustion emissions (Heinrich, et al, 1986) and researchers initially began studying combustion emissions with an eye toward learning more about PAH's. It was initially shown that PAH's are generally associated with the surfaces of solid particles. Electron micrographs were used at MIT to study particle morphology (Howard and Longwell, 1983), in combination with a "molecular beam flame probe" to gather samples from flames. Work at MIT during the 1980's also involved the use of laser scattering to detect in-situ changes in particle concentration in flames.

Based on the work of that early era, the process of combustion-generated PM formation was postulated to be an evolution from heavy hydrocarbon gases created in the combustion process, to small "spherules" of mainly carbon and finally to agglomerate soot particles containing PAH's (as well as other components) on their surfaces. Since many of the PAH species identified were known to be toxic, it was theorized that they might be responsible for the observed negative health effects, but causal mechanisms are still under investigation.

1.2.2 Particle Effects

A 1990 article (Oberdoerster and Yu, 1990) pointed out that comparing results of exposure studies conducted using both particles of inert black carbon and DPM (Heinrich, 1990; Mauderly et al, 1987), yielded no correlation between lung tumor potency for rats and particle mass or number, but that the surface area of particles did show a correlation. This suggested that the particle specific surface area might be

critical. However, attempts to extrapolate this to DPM exposure data for humans indicated there are likely other forces at work. Other studies (Costa and Dreher, 1997; Lison, et al, 1997) have demonstrated the importance of particle size, mainly in association with bioavailability. From these studies it appears that particle size is important and that it enhances the body's response (to toxins associated with particles) rather than creating a response that is attributable only to the particles themselves.

The importance of particle size and composition was amplified in a study that showed no pulmonary inflammatory response for rats dosed heavily with magnesium particles, in contrast to significant response from rats dosed similarly with zinc oxide particles (Kuschner, et al, 1997). This inter-relation of size and chemistry-dependence was investigated and it was shown that the biological response from nanoparticle exposures varies significantly between nickel oxide (NiO) and nickel sulfide (NiSO4) particles, for the same size particles and exposure dose (Miller, et al, 2001).

A recent study by two medical specialists (Utell and Frampton, 2000), postulated a biological mechanism in response to ultra-fine particles. Their theory is that the high number of these particles that are potentially deposited in the airways and lungs are alone enough to aggravate the tissue and produce vascular inflammation, which leads to coronary events. Work is ongoing to substantiate this hypothesis.

1.2.3 Metals

Environmental studies have shown significant amounts of metals in urban air (Fortoul, et al, 1996; Cass, et al, 2002), from sources such as industrial incinerators (Biswas, et al, 1992), power plants (Costa and Dreher, 1997), and automobiles (Silva and

Prather, 1997). Clinical studies using mice have demonstrated the potential for small metallic particles to induce cell damage (Lison, et al, 1997) and it has also been documented that adverse biological effects in rats can be correlated with exposure to the levels of metallic species found in combustion aerosols (Costa and Dreher, 1997). The data of Figure 1.5 are derived from the latter reference and show such a correlation. The acronyms in the figure are denoted as follows: LDH - lactate-dihydrogenase, a protein used as a marker for cell damage; BAL - bronchio-alveolar lavage, a technique for collecting tissue samples from the respiratory tract; SAL - saline; DOFA - domestic furnace fly ash; ROFA - residential furnace fly ash; and CFA - coal fly ash.

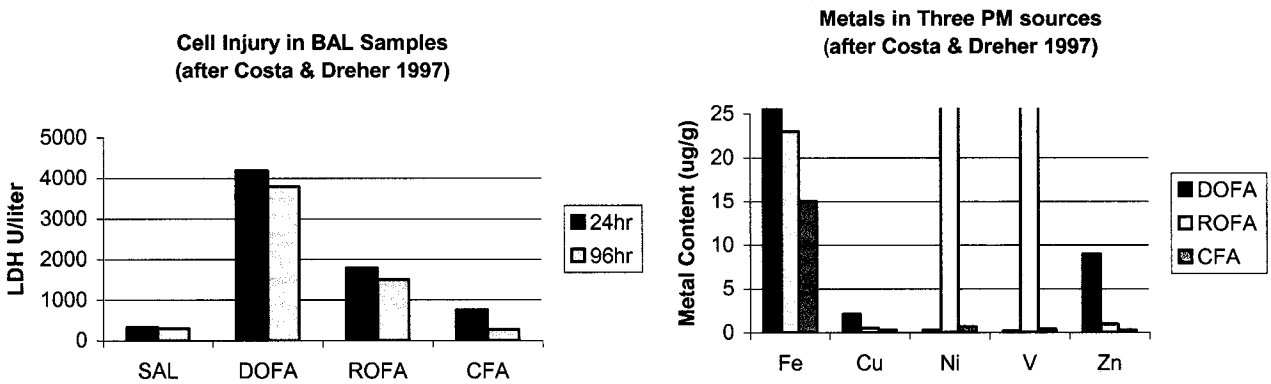

Figure 1.5 - Correlation between cell damage in rats and metal content of fly ash.

This combined information points to a hypothesis of metal-toxicity as a possible causal mechanism for the observed health effects of PM and/or DPM exposure. This hypothesis has stimulated many recent investigations and various researchers are currently trying to quantify sources and fates of metals in the atmosphere as well as their potential health effects.

It has also been shown that metals can form nanoparticles during combustion cooling and that this would greatly enhance the biological effects. The drastic increase in bioavailability for such nano-size metallic particles (due to their high surface area) and the subsequent impact on health effects is demonstrated in Figure 1.6.

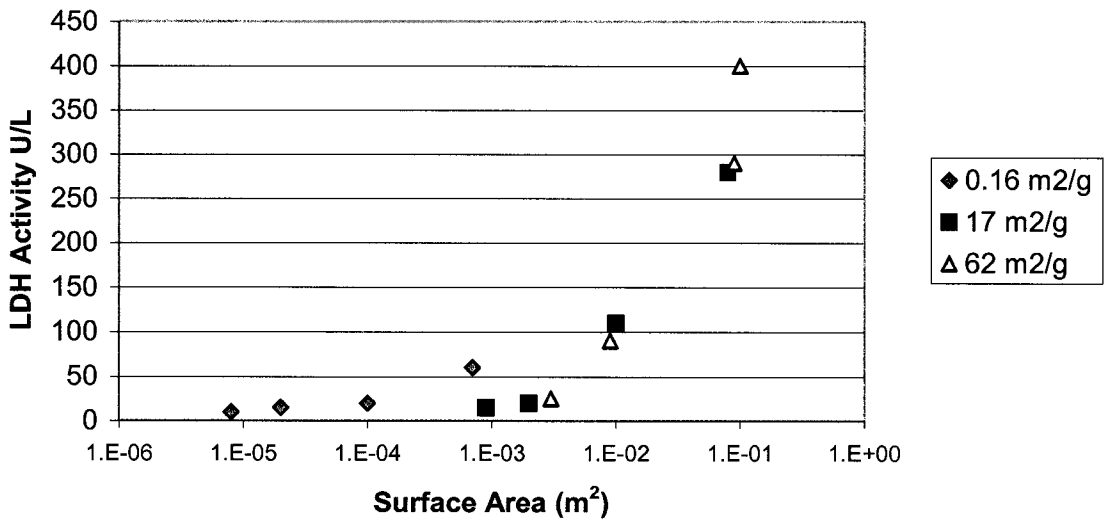

Figure 1.6 - Cell damage (LDH activity) as a function of particle surface area for mice exposed to four different dose levels of three different sized MnO_2 particles. Data recreated from (Lison, et al, 1997).

At a lecture sponsored by the University of Minnesota, Mechanical Engineering Department, it was suggested by Dr. Pratim Biswas that our bodies effectively "concentrate" the sub-micron portion of an inhaled aerosols by selectively removing the larger particles. This affect is due to the noticeable dip in the lung deposition curve (ICRP, 1990) in the size range of 100-300nm. This assessment may help explain discrepancies in historical data, i.e., if the sub-micron portion of test aerosols was not well characterized, and it was preferentially depositing in the lungs, it could dominate in

terms of its effect on biological responses, giving a response that has nothing to do with the chemical composition of the main constituency (super-micron portion) of the aerosol.

1.3 Summary

Adverse health effects from exposure to PM and DPM have been demonstrated in studies conducted in the last few decades. Because PM and DPM represent complex and variable aerosols, finding strong correlations for dose/response and cause/effect relationships have proven elusive and are still under investigation. One possible cause/effect relationship for adverse health effects of DPM may stem from metallic nanoparticles and/or trace metals in the carbonaceous particles found in DPM. Another possibility is that the small size of certain particles and their associated greater surface area per unit mass, may produce deleterious effects. It was the combination of these two possibilities that motivated this dissertation research and delineated the two main goals, which are to investigate the role of metals in DPM formation and more specifically investigate the possibility for formation of metallic nanoparticles.

1.4 References

Air Quality Criteria for Particulate Matter. Vol. II, EPA Draft Report, March 2001.

Bhatia, Rajiv, P. Lopipero, and A. H. Smith. Diesel Exhaust Exposure and Lung Cancer. *Journal of Epidemiology,* Vol. 9, January, pp. 84-91, 1998.

Biswas, P., W. Y. Lin, et al. Formation and Emission of Metalic Aerosols from Incinerators. J Aerosol Sci, Vol. 23, pp. 273-276, 1992.

Cass, G., A. Dilner, and K. Prather. Ultrafine Particles: Characterization, Health Effects and Pathological Mechanisms. University of Rochester - EPA, PM Center, Progress Report, June 2002.

Costa, D. L., and K. L. Dreher. Bioavailable Transition Metals in Particulate Matter Mediate Cardiopulmonary Injury in Healthy and Compromised Animal Models. Env. Health Perspectives, Vol. 105, Suppl. 5, pp. 1053-1060, 1997.

Davis, D. When Smoke Ran Like Water- Tales of Environmental Deception and the Battle Against Pollution. ISBN 0-465-01521-1, 2002.

Du, C. J., J. Kracklauer, and D. Kittelson. Influence of an Iron Fuel Additive on Diesel Combustion. SAE Tech Paper 980536, pp. 1-13, 1998.

Federal Register, October 29, 1998. 30 CFR, Part 57, vol. 63, No. 209, pp. 58104-58222. Diesel Particulate Exposure of Underground Metal and Nonmetal Miners (Proposed Rule).

Fortoul, T. I., L. S. Osorio, A. T. Tovcar, D. Salazar, M. E. Castilla, and G. Oliaz-Fernandez. Metals in Lung Tissue from Autopsy Cases in Mexico City Residents: Comparison of Cases from the 1950's and the 1980's. Env. Health Persp., Vol. 104, No. 6, pp. 630-632, 1996.

Garshick, E., M. B. Schenker, A. Munoz, M. S. Segal, T. J. Smith, S. R. Woskie, K. S. Hammond, and F. E. Speizer. A Retrospective Cohort Study of Lung Cancer and Diesel Exhaust Exposure in Railroad Workers. Am. Rev. Resp. Dis. 137, pp. 820-825, 1988.

Godish, Thaddeus. Air Quality. 4th ed. Boca Raton, FL: CRC Press, July 2003.

Heinrich, U., F. Pott, U. Mohr, R. Fuhst, and J. Doing. Lung Tumors in Rats and Mice after Inhalation of PAH-rich Emissions. Exp. Path., 29, pp. 29-34, 1986.

Hinds, W. C. Aerosol Technology: Properties, Behavior and Measurement of Airborne Particles. 2nd edition. John Wiley and Sons Inc, 1999.

Howard, J. B., and J. P. Longwell. Formation Mechanisms of PAH and Soot in Flames. Polynuc. Aero. Hydrocarbons: Formation, Metabolism and Measurement: 7th Int. Symp., Battelle: Columbus, pp. 27-62, 1983.

ICRP (International Commission on Radiological Protection), Publication 60: 1990 Recommendations of the International Commission on Radiological Protection - Annals of the ICRP Volume 21/1-3, ISBN:0080411444.

Kittelson, D. Engines and Nanoparticles: A Review. J. Aerosol Sci., vol. 29, No. 5/6, pp. 575-588, 1998.

Kuschner, W.G., H. Wong, and P. D. Blanc, et al. Human Pulmonary Responses to Experimental Inhalation of High Concentration Fine and Ultrafine Magnesium Oxide Particles. Environ Health Perspect., Vol. 105, pp. 1234-1237, 1997.

Lipsett, M., and G. Alexeeff. Appendix C: Quantitative Meta-Analysis on the Relationship of Occupational Exposure to Diesel Exhaust and Lung Cancer. In Health Risk Assessment for Diesel Exhaust, Draft. California Environmental Protection Agency, Office of Environmental Health Assessment, February 1998.

Lison, D., C. Lardot, F. Huaux, G. Zanetti, and B. Fubini. Influence of Particle Surface Area on the Toxicity of Insoluble Manganese Dioxide Dusts, Arch Toxicol (1997), vol. 71: pp. 725-729.

Mauderly, J. L., R. K. Jones, W. C. Griffith, R. F. Henderson, and R. O. McClellan. Diesel Exhaust is a Pulmonary Carcinogen in Rats Exposed Chronically by Inhalation. Fund. and Appl. Tox., vol. 9, pp. 208-221, 1987.

Miller, C. R., P. Biswas, and G. D. Leikauf. Combustion-Generated Nickel Species Aerosols: Role of Chemical and Physical Properties on Lung Injury. Aerosol Sci and Tech., vol. 35, pp. 829-839, 2001.

Oberdoerster, G., and C. P. Yu. The Carcinogenic Potential of Inhaled Diesel Exhaust: A Particle Effect? J. Aerosol Sci., Vol. 21, Suppl 1, pp. S397-S401, 1990.

Silva, P., and K. A. Prather. On-line Characterization of Individual Particles from Automobile Emissions. Enviro. Sci. Tech, Vol. 31, No. 11, pp. 3074-3080, 1997.

Utell, M. J., and M. W. Frampton. Acute Health Effects of Ambient Air Pollution: The Ultra-fine Particle Hypothesis. Journal of Aerosol Medicine, 13, pp. 355-359, 2000.

Chapter 2 - Overview of Particle Formation and Behavior

There are many mechanisms that contribute to the formation and interaction of particles. If you limit yourself to the case of DPM, this simplifies the issue somewhat, but the thought of predicting the formation and ultimate fate of DPM particles is still daunting. As a prelude to more detailed discussions in subsequent chapters involving the formation and behavior of DPM particles, in this chapter I describe the three main processes which control the formation of DPM during and after the diesel combustion event. I also review some of the physical forces which act on particles, namely those forces which determine when and how the particles might precipitate out of the aerosol. Those forces are what control the deposition of particles as they are inhaled into the body and as such are key to predicting the potential for particles to induce adverse health effects.

2.1 Particle Formation Mechanisms

Because I am mainly interested in diesel exhaust particles I will focus my discussion here to the origin of particles that form during cooling of superheated vapors. For this case, which reflects conditions that occur during the diesel combustion process, there are three main processes that are generally considered. These are homogeneous nucleation, heterogeneous nucleation or "particle growth" and coagulation. Each of these three processes can be treated individually and this has been done in many different ways historically.

In the field of aerosol science and engineering, the problem of modeling the formation and interaction of various aerosol constituents is elusive. One obvious hurdle is that many aerosols are composed of numerous constituents that have the potential to interact in a variety of ways. This problem is greatly simplified when you limit yourself to individual constituents, but even in this case scientists and engineers have struggled for years to develop a model that is simple and effective under a variety of conditions.

The cornerstone of most numerical models is a population balance equation for individual particles of all sizes. Historically the population balance equation for aerosols has been dubbed the "general dynamic equation" or simply "GDE". The GDE is based on the concept that the number of particles of all sizes will change in time based on a variety of different influences. Following is a brief overview of the roles played by each process in the overall population balance of an aerosol.

2.1.1 Nucleation Theory

The process of nucleation is the formation of stable particles from individual molecules and clusters of molecules. As these very small entities collide and form larger groups, there is an associated bulk energy change arising from changes in chemical potential i.e. due to phase changes during cluster evolution or change in surface energy (a product of the surface tension and the increasing surface area). These coupled together result in a change in free energy associated with the formation of such particles. (Zachariah et al, 1996; Holland and Castleman, 1982) Using classical nucleation theory this change in free energy can be expressed as:

$$\Delta G_g = \sigma \, s_g + \Delta\mu \, g \qquad (2\text{-}1)$$

Where σ is surface tension, s_g is particle surface area, g is number of monomers in the resultant cluster/particle and $\Delta\mu$ is the change in chemical potential due to phase changes i.e. $\Delta\mu = kT \ \ell n\, S$ (here k is Boltzman's constant, T is temperature in Kelvin and S is saturation ratio. This expression (equation 2-1) is parabolic and its maximum represents a "free energy barrier" to the formation of particles. Because this expression is key to the development of nucleation models, many scientists have sought methods of simplifying it. The most popular is the "capillarity approximation". In that approximation, the surface tension appearing in equation 2-1 is assumed to be a constant, independent of particle size. Since the free energy expression is a function of particle diameter (via the s_g term), setting the derivative of equation 2-1 to zero (for the case of maximum ΔG_g by using the capillarity approximation) and rewriting in terms of particle diameter yields a critical diameter often called d* (equation 2-2). Particles smaller than d* are unstable and will tend to evaporate, while those larger than d* are more likely to remain intact and undergo subsequent coagulation and surface growth.

$$d^* = \frac{4\sigma v_1}{kT \ \ell n\, S} \quad (v_1 \text{ indicates the monomer volume}) \qquad (2\text{-}2)$$

In terms of population balance, homogeneous nucleation "contributes" new particles of size d* to the population at a rate generally denoted by "I" or "J" (equation 2-3). In this equation, I is the nucleation rate, n_1 is the monomer concentration, g is the number of monomers in a "g-mer" (between one and some larger number "m"), k_g is the forward rate constant of reaction between a monomer and a "g-mer", p1 and p0 are the monomer and total partial pressures, k is Boltzman's constant, T is the temperature in

Kelvin and ΔG_g the change in free energy associated with the formation of a "g-mer" from "g" monomers (see equation 2-1)

$$I = n_1^2 \{\sum_{g=1}^{m} [k_g (p_1/p_\circ)^{g-1} \exp\left(\frac{-\Delta G_g}{kT}\right)^{-1}\}^{-1} \quad (2\text{-}3)$$

This rate is considered to be the net number of clusters per unit time that grow past the critical size d*. In a nucleation and growth model such as the sectional model derived here, the particles of size larger than d* are assumed to grow via their interactions with monomers as per a "growth rate" governed by heterogeneous condensation theory, while nucleation is only considered to add particles of size d* to the system.

In an attempt to use this expression (equation 2-3) for modeling actual nucleation rates, approximations were introduced as follows, resulting in what is called the "Classical Nucleation Theory". First, a non-dimensional surface tension was introduced:

$$\theta = \frac{s_1 \sigma}{kT} \quad (2\text{-}4)$$

where s_1 is the monomer surface area. Using this expression, equation 2-1 can be written as: $\Delta G_g = kT\,\theta\, g^{2/3} - g\,kT\,\ln S$ (2-5)

Substituting this into equation 2-3 and adding the impingement rate from kinetic theory β_{g^*} (for collisions between a monomer and the critical cluster size, g*) in place of the forward reaction rate term (k_g), one can rewrite equation 2-3 as:

$$I_{cl} = \frac{\beta_g n_1}{3S} \sqrt{\frac{\theta}{\pi}}\, g^{*\,-2/3} \exp\left(\frac{-4}{27}\frac{\theta^3}{(\ell n\, S)^2}\right) \quad (2\text{-}6)$$

Where: $\beta_{g^*} = \frac{p_1}{(2\pi m kT)^{1/2}}\left(1+\frac{1}{g^*}\right)^{1/2}\left(1+g^{*1/3}\right)^2 s_1$ (2-7)

and s_1 is monomer surface, m_1 the molecular weight of the monomer. This "Classical Nucleation Theory" approximation was later refined by adding a self-correcting term (Girschick and Chiu 1990) yielding:

$$I_k = n_s^2 \, Sv_1 \left(\frac{2\sigma}{\pi m_1}\right)^{1/2} \qquad \exp\left(\theta - \frac{4\theta^3}{27(\ln S)^2}\right) \tag{2-8}$$

where n_s is the monomer concentration at saturation.

Although these models have been difficult to verify experimentally, they are still quite useful for estimating nucleation, especially in specific applications where homogeneous nucleation (without chemical reactions) is the primary process of particle formation. An example of this is the particle formation that ensues when running saturated vapors through a diverging nozzle (Hoare, 1980). Nucleation rate often plays a secondary role in population balances of general engineering interest because the time scale on which it occurs is much smaller than that of other processes/interactions between particles. The most important role it plays in an overall model is to provide a source of stable particles that can then grow by heterogeneous nucleation and coagulation. Since it is dependent on the saturation ratio, it will also be dependent on the dynamics of an aerosol system, since when the saturation ratio approaches unity, nucleation approaches zero.

2.1.2 Condensation-Growth Theory

The growth of stable particles by condensation of monomers to their surfaces (sometimes called heterogeneous nucleation) is generally defined as the rate of change in particle volume due to the addition of monomers onto the particle surface. In typical

aerosol systems, since the super saturation level is not too high and numerous "large" particles already exist, available monomers are much more likely to interact with the larger particles than with each other. Thus, "heterogeneous nucleation" is more likely than the creation of new particles by homogeneous nucleation and clustering as described above.

For particles larger than the mean free path of the carrier gas, volume growth rate can be modeled using diffusion theory, yielding

$$\frac{dv}{dt} = \frac{2\pi D v_1 d_p}{k T} (p_1 - p_s) \qquad (2\text{-}9)$$

Where D is the diffusion coefficient, v_1 the monomer volume, d_p the original particle diameter and (p_1-p_s) the difference between monomer concentration and saturation concentration, i.e., the "partial pressure driving force". For particles smaller than the mean free path, growth is expressed as the rate of impingement of monomers onto the surface. Using kinetic theory this results in:

$$\frac{dv}{dt} = \frac{\pi d_p^{\,2} v_1 (p_1 - p_s)}{(2\pi m_1 kT)^{1/2}} \qquad (2\text{-}10)$$

Where the additional variable, m_1, is the molecular weight of a monomer. Growth laws have also been developed to predict the particle growth due to both surface reactions and droplet phase reactions. Additionally, an interpolation formula has been developed for growth of particles in the transition regime (Friedlander, 2000, pp. 284).

2.1.3 Coagulation Theory

Unlike particle growth, for which the modeling depends on the saturation level of monomers in the system, the driving force for coagulation is simply the probability of collision between two particles. Key to this approach is the concept that particle interactions are similar to molecular interactions in that the rate at which they interact is a function of the concentration of the two interacting species and is controlled by a rate constant, or collision frequency function of some sort. In its basic form, the expression that describes coagulation can be written in terms of a collision frequency N_{ij} as follows:

$$N_{ij} = B_{i,j}\, n_i n_j \qquad (2\text{-}11)$$

Note that the collision frequency depends on the concentration of the two colliding species (n_i and n_j), and some rate function B (generally called the collision frequency function). This term is strongly dependent on the relative size of the colliding particles, and also depends on gas temperature, particle charge and other gas and aerosol properties.

This concept is the basis for development of the "kinetic equation". For a polydisperse system of particles it can be written by applying equation 2-11 and assuming that the rate of change in concentration with time of a class of particles of size "k", (i.e. $\frac{dn_k}{dt}$), is the sum of all particles "i" and "j" which collide and form a particle of size k = i+j. This gives:

$$\frac{dn_k}{dt} = \frac{1}{2}\sum_{i+j=k}^{\infty} B_{ij} N_i N_j - \sum_{i=1}^{\infty} B_{ik}\, N_i\, N_k \qquad (2\text{-}12)$$

Where the first term on the right indicates the rate of gain of k-sized particles or "k-mers" and the second term indicates the loss of k-mers (due to collisions with other-sized particles).

The difficulty of applying this expression to real systems is that the probability of collision can be influenced by many such factors, which may each vary considerably over the range of interest. Also, physical properties of particles will generally be distributed continuously across the entire particle population and may range over several orders of magnitude (such as is the case with particle size). Keeping track of all the possible collisions that could ensue is an insurmountable task and therefore most people attempting to develop predictive models will use some simplifying assumptions.

A landmark breakthrough in that regard was the work of Smoluchowski around 1917. He showed that by making the assumptions of a monodisperse system of particles in the continuum regime, with constant collision frequency function or "coagulation coefficient", and Brownian coagulation, equation 2-12 can be rewritten in much simpler form (Friedlander, 2000, pp. 193). After simplification, integrating once in time results in the following expression:

$$N_{\infty} = \frac{N_{\infty}}{1+(BN_{\infty}(0)t/2)} \qquad (2\text{-}13)$$

Using this expression along with the kinetic equation gives the result:

$$n_k = \frac{N\infty(0)\,(t/\tau)^{k-1}}{(1+t/\tau)^{k+1}} \qquad (2\text{-}14)$$

Where: $$\tau = \frac{2}{BN_{\infty}(0)} = \frac{3\mu}{4kTN_{\infty}(0)} \qquad (2\text{-}15)$$

And: $$B = \frac{8kT}{3\mu} \qquad (2\text{-}16)$$

Equations 2-14 to 2-16 represent a very simple expression for coagulation of monodisperse aerosols. This approach is surprisingly useful and accurate if applied to situations where the aerosol size distribution is close to monodisperse and the time frame is short enough that the size distribution does not change significantly. However, when the size distribution changes, the assumptions that govern Smoluchowski's method i.e. interactions of equal sized particles and constant coagulation coefficient, are no longer valid.

In the 1960's Smoluchowski's method was verified experimentally, and it is often used in predicting the transient behavior of aerosols that are approximately monodispersed. Later models for Brownian coagulation also included adjustments for particle force fields, (Van der Waals and Coulomb forces) as well as flow field effects, but experimental verification of these has proven to be a bit elusive. The predictions of several such approaches are presented in the literature (Friedlander, 2000).

The main drawback of Smoluchowski's method is that it is based on the assumption of monodisperse particles and not very many typical aerosols are even close to monodisperse. Also, if you have a coagulating monodisperse aerosol of size "k", in order to keep track of all particles you need to calculate the changes in all multiples of k (usually called "k-mers). Monomeric particle sizes of interest are often very small, and coagulation usually results in particles several orders of magnitude larger than the monomers. Therefore, even for this very simple model you would need to calculate the rate of change of many different particle sizes, and this is cumbersome.

Because of these limitations to Smoluchowski's method, and because coagulation is such an important part of many aerosol problems of practical interest, various attempts have been made to develop analytical and numerical solutions which will predict the coagulation of polydisperse aerosols. The basis for such modeling methods is the "kinetic equation" (equation 2-12). In general the solution to this equation depends greatly on the collision frequency function "B". An expression for this function has been derived for particles larger than the mean free path of the carrier gas i.e. particles in the continuum regime, using a diffusion theory approach, and also for the free-molecular regime, using kinetic theory. Additionally, for the transition regime, an interpolation formula has been developed (Fuchs, 1964) which bridges the gap between the other two regimes.

One of the most important features of coagulation is that in nature, aerosol systems will (fairly quickly) adjust to a self-preserving size distribution. The time required for this has been well documented (Friedlander, 2000, pp. 213) and a good test of any model is whether it mimics that behavior. The characteristic time scale on which this happens is also important and this has been calculated for systems that start out as monodisperse (Friedlander, 2000, pp. 217).

In recent years some scientists have also attempted to solve the kinetic equation in its integral form i.e., using a continuous distribution of particle sizes (and thus collision frequency function). Although a direct solution for this case was not in general possible, the use of similarity transforms has been shown to give closed form solutions for some limited cases (Friedlander, 2000, pp. 202).

2.1.4 Methods for Solving the GDE

Trying to solve the general dynamic equation for all possible cases is not a good engineering approach, but if proper assumptions are made, simplified versions of the GDE may yield very useful results. The most logical approach is to solve the equation simultaneously for the three main physical processes, i.e., nucleation, growth and coagulation, using as few simplifying assumptions as necessary to get a meaningful solution. That is the approach which I took for my work, and other models have been developed to do this as well. The most widely used models are the moment and sectional models, and those are described below. The method which I used for this work is a modified version of a sectional model conceived by Dr. Zachariah at the UMN (Prakash, et al, 2003) and is also described below.

2.1.4.1 Moment Model

One well-known and successful approach for simultaneous solution of nucleation growth and coagulation is the method of moments (Pratsinis, 1988). Although the method is somewhat complicated and requires extensive derivation of moment equations, it yields results that are physically representative and is considered to be a good predictive method. The basis of the method entails writing the kinetic equation in integral form for volume space. It can be shown that by making the assumption of lognormal size distribution (reasonable for many aerosols) and using the definition for "moments" of the volume distribution function, equations for time rate of change in moments may be derived. Subsequently, once the moment equations are solved, the

volume and number distribution are also known. Since many common aerosols have fairly lognormal size distributions, this method works well and produces good results.

2.1.4.2 Sectional Model

Another tack that has been somewhat successful is the sectional approach. In sectional models, the size distribution is divided into ranges or sections and the particle interactions are monitored for each section. Some tricks have been developed to assure mass conservation between sections and in general this approach has been considered more versatile than other methods. (Gelbard, 1980). A modified sectional method was developed at the University of Helsinki in Finland that is simpler and lends itself well to numerical solution. The method used in this report is a modified version of the Finnish sectional model, and it is described in the following section.

2.1.4.3 Modified Sectional Model

A sectional model was developed by Dr. Michael Zachariah at the UMN that is a modified version of the model presented by Dr. Kari Lehtinen from the University of Helsinki. The method is designed to be robust yet simple enough to run in a reasonable time on current vintage personal computers. The key to the simplicity of the model is that it is based on a small number of "volume nodes" spaced at predetermined intervals across the volume space of interest (logarithmic spacing was used in my model but any spacing would work). The key to the accuracy of the method is a size-splitting scheme which insures mass conservation.

The model treats all nucleation, growth and coagulation events as particle collisions in volume space. When a collision occurs between two particles i and j, it will result in a particle of volume "Vnew", which will lie somewhere in volume space between two nodes of known volume. The splitting scheme then allows the resultant volume to be "divvied up" between two nodes, based on its location in volume space relative to the two known nodes, thus insuring mass conservation. The beauty of this approach is that the number of nodes can be relatively small and the model will still yield meaningful results as will be shown in the next section of this chapter. To illuminate this point, the number of size classes for the modified sectional model presented here is 41, whereas if I had used a discrete approach where each particle was a multiple of a 1.0 nm "k-mer", the number of size classes would have been 1,000,000,000,000! In spite of this, the model gives reasonable results (greatly due to the use of the size-splitting scheme) and is computationally very inexpensive.

2.1.5 Predicting Particle Formation using the Modified Sectional Model

With an eye toward understanding the effect of time scales and temperature gradients during particle formation inside an engine, I developed an algorithm for the modified sectional model and wrote a FORTRAN program to predict particle formation from superheated vapors. The program was designed specifically to solve the modified sectional form of the GDE for transient conditions typical in condensers, where heated vapors enter the inlet and cooled aerosols exit at the outlet. The following discussion describes the application of the program to the self nucleation and subsequent coagulation of aluminum particles from superheated vapor.

The initial parameters included a high temperature source of saturated Al vapor and an adiabatic cooling rate of 1000 K/sec. As can be seen in Figure 2.1, at first no new particles appeared. After some cooling had taken place and the saturation ratio reached a threshold value, nucleation started adding particles (stable clusters of size d* as defined in equation 2-2) to the system and as their numbers increased they began coagulating. Particle numbers were initially high as nucleation began (Figure 2.1) but quickly coagulation effects reduced this number. The average particle diameter began to grow (Figure 2.2) and coagulation resulted in a lognormal self-preserving size distribution (Figure 2.3).

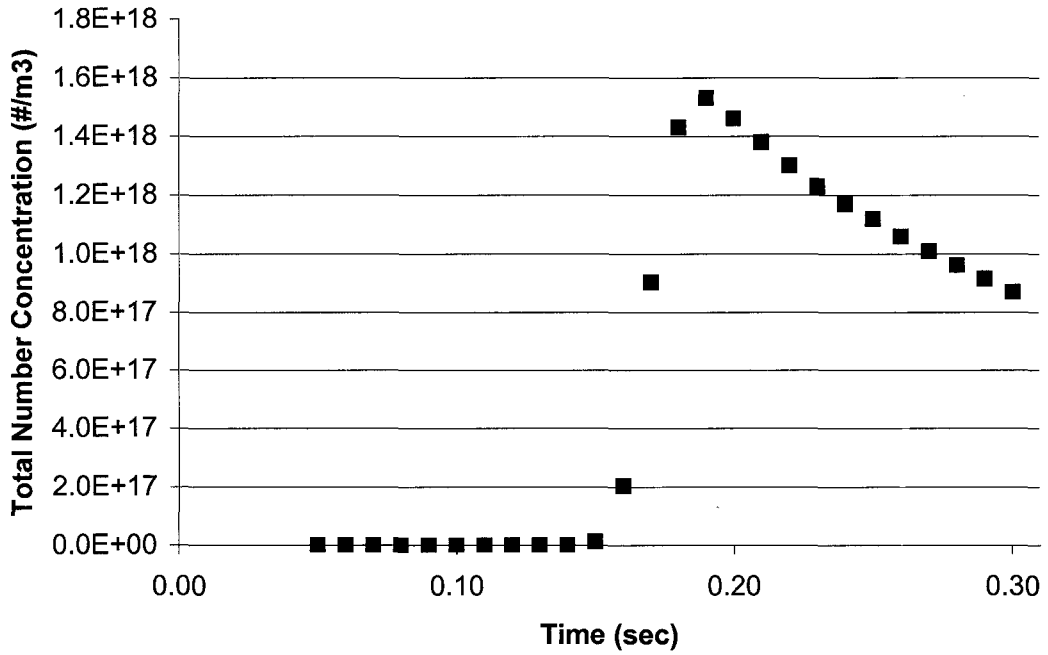

Figure 2.1 - Calculations predicting initial rise and subsequent reduction in particle number concentration for simultaneous nucleation and coagulation of Al particles from supersaturated vapor cooling at 1000 K/s.

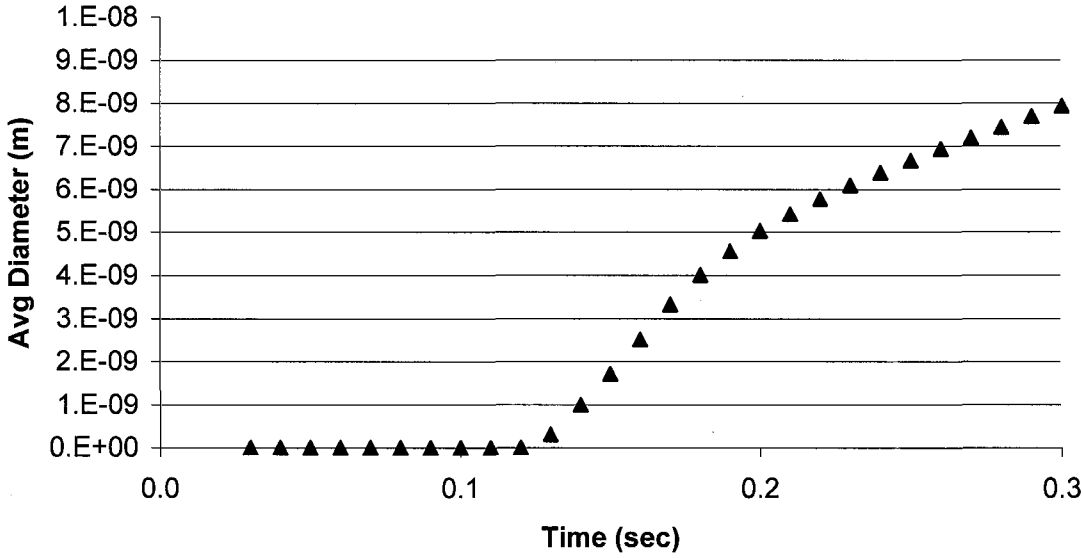

Figure 2.2 - Predicted particle growth during nucleation and coagulation of Al particles.

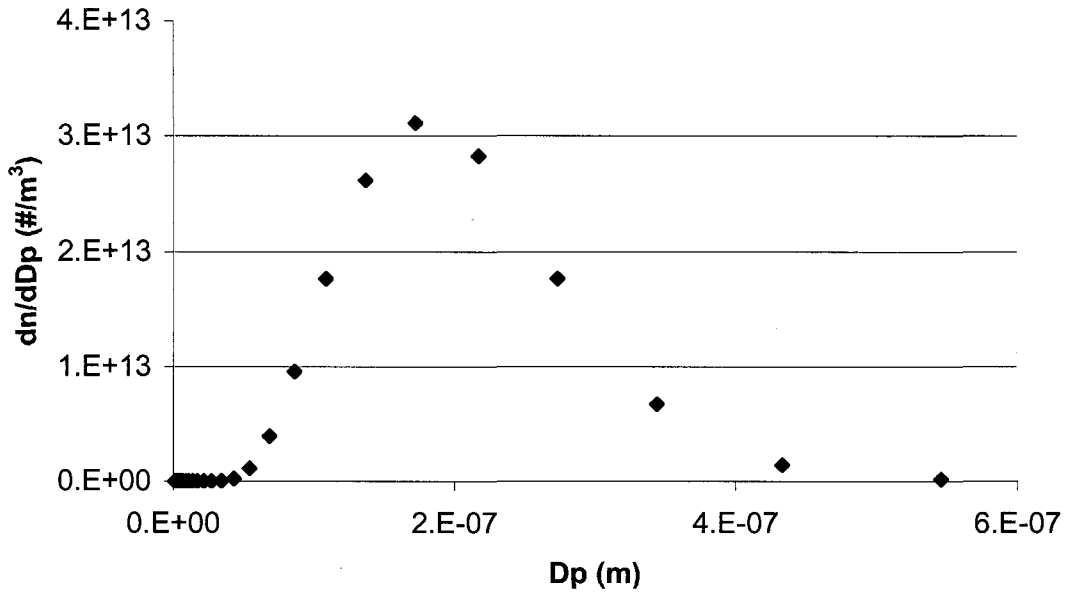

Figure 2.3 - Self preserving size distribution for nucleating and coagulating Al particles, after 0.3 seconds, using 1000 K/s cooling rate.

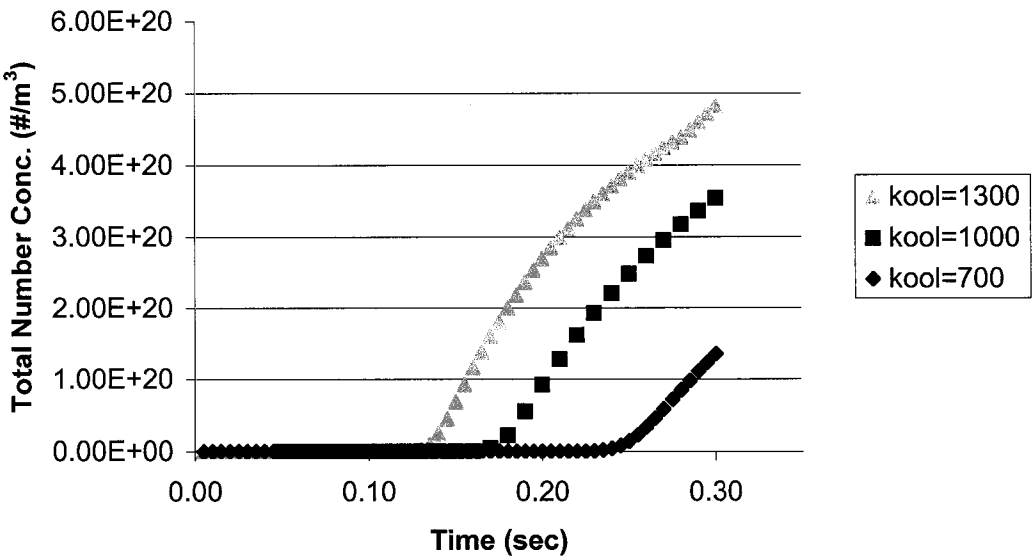

Figure 2.4 - Predicted effect of cooling rate on dynamics of particle formation: Total number concentration of (self nucleated) particles versus time. Note kool=cooling rate in K/sec.

The program was next used to study the effects of cooling on system dynamics. In Figure 2.4, data are plotted which demonstrate the effect of cooling. In general, the higher cooling rates result in quicker dynamics of the system, as expected. This modeling study provided insight into the dynamics of particle formation in an engine, namely that the interaction of supersaturation ratio and temperature gradient drive the self nucleation of particles.

The essence of this model is captured in Figure 2.5, which is an artist's sketch of how such a particle formation process proceeds (from left to right) during cooling of a superheated vapor. Note that this simple model treats only one species. When many species are present, this process still takes place, but is complicated by physical and chemical interactions between the constituents. The results may be similar in terms of

particle sizes and number concentrations, but particle composition may vary drastically depending on the time/temperature history of the system, which influences the multi-specie interactions.

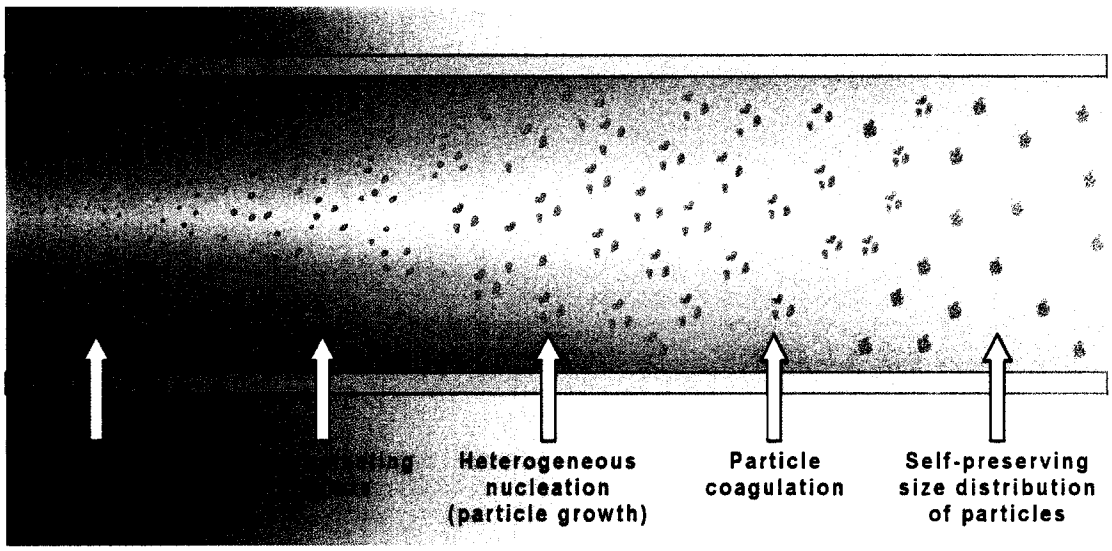

Figure 2.5 - Artist's sketch of the idealized (single species) particle formation process.

Inside the cylinder of a diesel engine, when the ignition event occurs, the system is at high pressure (~150 atm) and temperatures inside the resulting diffusion flame (where soot precursors are forming) are on the order of ~1500K. At the periphery of the diffusion flame localized flame front temperatures are on the order of 2500K, resulting in burnout of most of the soot. As the diffusion flame recedes and the piston retracts, both pressure and temperature drop suddenly and the hot exhaust is pushed out the tailpipe where it encounters cool ambient air. During this sequence, there are three events that produce the conditions necessary for self nucleation, i.e., rapid cooling which raises the supersaturation ratio very quickly. The first is at the flame front where combustion

products may transition from 2500+K to 1500+K in a fraction of a millisecond (that is described in more detail in section 3.1 of this dissertation). The second is during piston retraction where the combustion byproducts cool from 1500^{+}K to ~1000K over about 10 milliseconds. The third event is when the exhaust aerosol leaves the tailpipe and temperature drops from ~600K to ~300K very quickly.

Each of these events has the potential for driving self nucleation, but the volatility of the subject vapors also plays an important role. Therefore the first event will affect only species of very low volatility while the second event affects species of moderate volatility and the final event affects the highly volatile species. This gives some insight into the formation pathways of particles in an engine. In subsequent chapters I will show data which verify that the timing of these events and the corresponding local temperatures correlate well with occurrence of certain types of particles, most notably self nucleated metallic particles.

2.2 Particle Mechanics

During and after formation, particles are subject to many forces which control their behavior and interactions with their surroundings and with each other. Since "particles" come in many different sizes and shapes, it is sometimes difficult to globally prescribe their properties and behavior using simple approaches. However, making some basic simplifying assumptions (as was done in Section 2.1 regarding coagulation theory), can sometimes yield meaningful results. This section is intended to provide an overview of some of the key forces that control behavior of particles. I will focus my discussion on

the forces that are dominant in determining particle deposition since those forces play a key role in the eventual fate of particles.

2.2.1 Gravitational Settling of Particles

Gravity acts on particles at all times and for larger particles it is often the dominant force, causing them to settle downward and deposit onto whatever surface is available. The gravitational settling of particles can be calculated quite accurately for well characterized particles and in its simplest form is a balance between gravity acting on the particle mass and the aerodynamic drag on the particle. If one assumes the particle is spherical and the surrounding air has no movement, Stokes drag law can be used to determine the settling velocity.

Stokes showed that if you solved the Navier-Stokes equation for flow around a sphere using the assumption that inertial forces were negligible and viscous forces dominated, you get a simple solution for drag force which is expressed in terms of fluid viscosity "μ" , particle diameter "Dp" and relative velocity of particle "V":

$$Fd = 3\pi\mu D_p V \qquad (2\text{-}17)$$

Assumptions he made included:

- Continuum flow
- inertial forces negligible compared to viscous forces
- incompressible fluid flow
- zero velocity at particle surface, i.e., "no slip" condition
- isolated, rigid sphere in steady flow.

These assumptions and thereby his law have been shown to be very accurate at Reynolds numbers less than about 1.0. The error in drag force calculation using Stokes Law is about 12% at Re = 1.0 and 5% at Re = 0.3. Since many aerosol applications involve low Reynolds numbers, Stokes Law is used often in aerosol calculations.

Stokes Law can be applied in calculating the speed at which a particle settles in still air i.e. gravitational settling. Equating the gravitational force on a particle (mg) with the Stokes force resisting it, and neglecting buoyancy effect on the mass term gives:

$$3\pi\mu VDp = \left(\frac{\ell p \pi Dp^3 \, g}{6} \right) \tag{2-18}$$

which can be rewritten in terms of settling velocity as:

$$V_s = \frac{\ell p Dp^2 g}{18\mu} \tag{2-19}$$

where ℓp is the particle density.

If particles are significantly smaller than the mean free path of the gas molecules around them, Stokes Law does not work very well, because it is the molecular bombardment of the "still" air that ultimately translates into drag force. This will happen as particles get smaller i.e., for air at STP, particles less than the mean free path of air (λ=65 nm) will certainly experience some slip i.e. reduction in drag force and in fact it is found that slip is quite significant for particles less than about 1.0 μm in air at STP. Slip is a result of a change in particle/gas interactions. When Knudson number (λ/Dp) is large, like it is for submicron particles, the gas molecules are spaced much farther apart relative to particle size, so the particle experiences less molecular bombardment. The

limiting case for this is a particle in vacuum ($\lambda = \infty$) where a particle experiences no stokes drag at all, and "slips" freely downward. This effect was first documented by Millikan in one of his most famous experiments. More recently (Allen and Raabe, 1985) experimental measurements have yielded the following relation for slip in terms of mean free path of aerosol gas "λ" and particle diameter Dp.

$$Cc = 1 + \lambda / Dp \, [2.34 + 1.05 \exp (-0.39 \, Dp/\lambda)] \qquad (2\text{-}20)$$

The settling velocity expression of equation 2-19 is valid for particles between 1.5-75 μm, but if used with the Cunningham slip correction factor (equation 2-20) as in equation 2-21 below, it is valid for particles as small as 0.001 μm (or 1.0 nm).

$$Vs = \frac{\ell P Dp^2 g Cc}{18\mu} \qquad (2\text{-}21)$$

Other terms sometimes used in calculating gravitational settling include Stokes Number, mechanical mobility, relaxation time and stopping time. Those are summarized in the following paragraphs.

Stokes number is the ratio of stopping distance to some other length scale characterization of a particular problem. Physically speaking, it is a measure of the ability for particles to follow the flow streamlines as opposed to continuing their own straight-line trajectory. This is especially pertinent to the design of impactors. The ratio of stopping distance to jet radius is used as the Stokes number for jet orifice impactors. Impactor performance (collection efficiency) is then measured, and plotted against the square root of Stokes number (which is proportional to particle size). This calibration can then be used for any geometrically similar impactor.

Mechanical mobility "B" of a particle is simply defined as the terminal velocity divided by the force producing that velocity. Using Stokes drag, this is written as:

$$B = \frac{V}{F} \tag{2-22}$$

For originally stationary particles accelerating in a (steady) flow, the terminal velocity would be the flow velocity and the force producing it would be Stokes drag force. For a given flow speed and high drag force (as in slow moving liquid stream), the particle quickly reaches the flow velocity. In this case where the particle is more easily accelerated by the flow, the value of mechanical mobility is smaller. This term is often applied to the case of particles falling through still gas, and the above equation can be written as:

$$Vs = FgB \tag{2-23}$$

Relaxation time is a measure of how long it takes a particle to respond to changes in the velocity of the surrounding fluid. It can be determined by looking at the acceleration (or deceleration) of a particle in a fluid, writing the basic F = ma equation, and using the definition of mechanical mobility (F = V/B), which yields mB dv/dt = -v. The product "mB" is defined as relaxation time i.e., τ = mB. Integrating the above expression gives $v = v_o e^{-t/\tau}$, so time t = τ is the relaxation time, which is the time it takes for a moving particle to slow to 1/e = 38% of its original velocity (assuming no other forces than drag). Using the above equations allows rewriting this as:

$$\tau = \frac{Dp^2 \ell pC}{18\mu} \tag{2-24}$$

Another associated term is stopping distance, and this is defined as the distance a particle travels (given an initial velocity), before it comes to rest. Using the above approach where final velocity is assumed zero, and integrating over time gives $S = v_o \tau$ i.e. S is defined as stopping distance and is simply the product of initial velocity and relaxation time.

2.2.2 Impaction Deposition of Particles

The radial velocity of a particle experiencing a 90° trajectory, i.e., trying to follow the streamlines of the impactor jet as it deflected by the flat plate can be calculated by using the centrifugal acceleration and the particle relaxation time. This is analogous to the equation for settling velocity using gravitational acceleration i.e. $V_s = g\tau$

For the impactor case this simplified approach is often used and the radial velocity estimated by the equation: $Vr = \alpha\tau = \frac{u^2}{R}\tau$ (2-25)

Using this expression you can calculate the time for a particle to precipitate a distance "h" i.e. the jet half-width:

$$t_1 = \frac{h}{Vr} = \frac{hR}{\tau u^2} \quad (2\text{-}26)$$

You can then calculate the time it takes a particle to traverse the 90° trajectory of the impactor streamlines: $t_2 = \frac{\pi R}{4u}$ (2-27)

and note that if $t_1 = t_2$ the particle will impact the plate. This inequality can be expressed as:

$$\frac{\tau u}{h} \geq \frac{2}{\pi} \tag{2-28}$$

Since τu is the stopping distance, the left term is the Stokes Number for this system and $2/\pi$ is termed the critical Stokes Number:

$$Stk_{crit} = \frac{\tau u}{h} = \frac{2a^2 \rho C u}{9\mu h} \tag{2-29}$$

In impactor design, it is common to use $\sqrt{Stk} = \left(\frac{2\rho C u}{9\mu h}\right)^{1/2} a$ (2-30)

as a dimensionless particle size and often the impaction efficiency measurements will be graphed with $\sqrt{Stk}$ on the x axis. A basic recipe for cascade impactor design is to design, build, and test one impactor then calculate the values of u, h, and a that would give the same Stokes Number for the desired particle size a, then simply build a geometrically similar impactor and it will perform just as the original one did. For multi-orifice impactors, it is a good idea to first determine the allowable pressure drop across the orifice, then use that to set the target velocity. This velocity can then be used with relaxation time and Stokes Number to get characteristic jet dimension:

$$R = \frac{\tau u}{Stk} \tag{2-31}$$

This is typically used to calculate the flow through a single orifice of an impactor, and the number of orifices required simply depends on desired total flow through system.

2.2.3 Diffusion of Particles

A system of aerosol particles will typically be subject to two types of diffusion processes. The first is called convective or Eddy diffusion and is the process by which a system of suspended particles diffuses on a macro scale due to fluctuations in the flow of the carrier gas. This generally takes place when the physical scale is large and the diffusion process might be thought of as the transport and rearrangement of "packets" or "parcels" of flow, each containing numerous particles. In such large-scale conditions, this process tends to be the dominant diffusion force in an aerosol system.

The second process is often called thermal diffusion and is a process which drives particle diffusion even in the absence of a flow field. In thermal diffusion the particles are driven by Brownian motion. In 1827, Robert Brown first observed a mysterious random motion of pollen grains, and in the late 1880's it was shown that the motion was similar to that of gas molecules as predicted by the kinetic theory of gasses. In short, Brownian motion of particles is caused by random fluctuations in the net forces on the particle due to that many collisions with molecules of the carrier gas.

This Brownian motion drives the diffusion of particles, i.e., the net transport of particles from a region of high concentration to that of a lower concentration. The rate at which this happens is characterized by the "diffusion coefficient" D and the process obeys Fick's Law of Diffusion :

$$J = -D \frac{dn}{dx} \qquad (2\text{-}32)$$

where J is the flux of particles and $\frac{dn}{dx}$ is the concentration gradient.

The diffusion coefficient for a particle can be shown to be a function of the properties of both the carrier gas and a typical particle derivation, using the Stokes-

Einstein Derivation. In this approach the force driving the particles to the region of lower concentration (called the net osmotic force, shown by Einstein) is equated with the viscous drag force for rigid spheres derived earlier by Stokes, using the Navier-Stokes equations.

Equating these gives: $\frac{-kT}{n}\frac{dn}{dx} = \frac{3\pi\eta VDp}{Cc}$ (2-33)

which can be written as: $nV = \frac{-RT\,Cc}{3\pi\eta\,Dp}\frac{dn}{dx}$ (2-34)

Noting that this expression is in the exact same form as equation 2-32 above, yields the relation: $D = \frac{\kappa TCc}{3\pi\eta\,Dp}$ (2-35)

Equation 2-35 is called the Stokes-Einstein equation and defines the diffusion coefficient of a particle. This coefficient along with the gradient in particle concentration drives the thermal diffusion of particles.

The most important thing about thermal diffusion is that it drives particle movement in the absence of fluid flow. Since diffusing particles stick to the walls of flow conduits due to van der Waals force, resulting in a concentration of zero at the wall, diffusion drives particles toward the walls. This means that it can and does drive particles through the boundary layer at the surfaces of flow conduits where they stick to the conduit surfaces resulting in particle deposition and in some cases significant losses in particle concentrations, especially for particles smaller than about 100 mm.

When an aerosol is being transported through flow conduits, particle deposition to the walls, sometimes called "diffusion losses," will take place. This is of great practical importance especially in a laboratory setting where the properties of the aerosol are under

investigation and deposition losses may affect the results. Deposition by diffusion has been well characterized for the limiting case of stagnant, infinite aerosol volumes adjacent to a flat wall (Hinds, 1999, pp. 160). Mathematical solutions have also been obtained for fully developed laminar flow in a tubular conduit. A simplified version of this (Hinds, 1999, pp. 163) is expressed in equation 2-36 in terms of penetration P which is the ratio of particle concentration entering to that leaving and the term

$\mu = \frac{DL}{Q}$ which is a dimensionless deposition parameter.

$$P = \frac{Nout}{Nin} = 1 - 5.5\,\mu^{\frac{2}{3}} + 3.77\,\mu \quad \{\text{for } \mu < .009\} \qquad (2\text{-}36)$$

or

$$P = 0.819 \exp(-11.5\,\mu) + 0.0975 \exp(-70.1\,\mu) \quad \{\text{for } \mu \geq 0.009\} \qquad (2\text{-}37)$$

The (perhaps surprising) result of this solution is that the penetration is independent of tube diameter for equal volume tubes. The longer radial distances that the particles must diffuse to get to the wall is just offset by the shorter length of conduit (this assumes a constant volumetric flow rate). In short, the most critical issue is residence time in the tube. This expression has been shown to be accurate to 1% for all $\mu's$.

2.3 Summary

It is difficult to define a "particle," since there are so many different sources of fine and ultrafine particulate mater. If we consider only those particles emitted by diesel engines, we can more easily discuss the origins of particles. DPM originates directly from the combustion process inside the engine cylinder and particles are formed through

an intricate process of self nucleation, coagulation and surface growth, the latter being dependent on processes such as adsorption and condensation. When DPM becomes part of the ambient aerosol that we breath, the particles are acted upon by forces such as gravitational settling, diffusion and impaction. It is these forces that determine the fate of particles as they are inhaled into the body.

The following chapter will describe in more detail how DPM forms inside the engine and how the formation history may determine particle morphology and chemistry. That chapter also includes a short section describing methods of reducing the DPM emitted by diesel engines.

2.4 References

Allen, M. D., and O. G. Raabe. Slip Correction Measurements of Spherical Solid Aerosol Particles in an Improved Millikan Apparatus. Aerosol Sci. and Tech., Vol. 4, pp. 269-286, 1985.

Friedlander, S. K. Smoke Dust and Haze: Fundamentals of Aerosol Dynamics, 2nd Edition, Oxford Univ. Press, 2000.

Fuchs, N. A. Mechanics of Aerosols, Pergamon, New York, 1964.

Girschick, S. L., and C. Chiu. Kinetic Nucleation Theory. J. Chem. Phys., Vol. 93, No.2, July 1990.

Gelbard, F., Y. Tambour, and John Seinfeld. Sectional Representations for Simulating Aerosol Dynamics. J. Colloid and Interface Sci., Vol. 76, No.2, August 1980.

Hinds, W. C. Aerosol Technology: Properties, Behavior and Measurement of Airborne Particles. 2nd edition. John Wiley and Sons Inc, 1999.

Hoare, M. R., P. Pal, and P. Wegener. Argon Clusters and Homogeneous Nucleation: Comparisons of Experiment and Theory. J. Colloid Interface Sci., Vol. 75, No.1, May 1980.

Holland, P.M., Castleman, A.W., Journal of Physical Chemistry Vol. 86, No. 4181, 1982.

Prakash, A., A. P. Bapat, and M.R. Zachariah. A Simple Numerical Algorithm and Software for Solution of Nucleation, Surface Growth and Coagulation Problems. Aerosol Sci. and Tech- In press 2003.

Pratsinis, J. Colloid Interface Sci 124, 416, 1988.

Zachariah M.R. et al, Journal of Physical Chemistry, Vol. 100, No.36, 1996.

Chapter 3 - The Formation and Mitigation of DPM Emitted by Modern Engines

Since Rudolph Diesel invented his famous engine back in the 1890's, diesel engines have been a cornerstone in the world's dependence on mobile power. Diesel's engine design capitalized on the unique properties of the relatively low-volatile diesel fuel blends. Such fuels allow the fuel/air mixture to be compressed until it self ignites and provides a relatively long, even burn in the engine. For this reason diesel engines are sometimes called "compression ignition" engines. Since the volatility of the fuel is so low, it is possible to use very high compression ratios in compressing the fuel/air mixture, which contributes to the relatively high thermal efficiency and fuel economy of Diesel engines. Many modern diesel engines also employ turbocharging to increase both specific power output and efficiency.

Compression ignition engines have historically been used mainly for heavy-duty applications. Their popularity for use in personal automobiles was hindered by their reputation for being excessively noisy as well as "dirty", since they generate more soot than some other engines. This is changing rapidly however. In the last few decades, advances in engine technologies, most notably the advent of sophisticated electronic fuel injection systems, have resulted in cleaner, quieter diesel engines.

Most recently, further improvements in fuel efficiency have resulted from use of "direct injection" of fuel into the cylinders. Previous designs used "indirect injection" whereby fuel was injected into a prechamber. That design resulted in a quieter engine but sacrificed some fuel economy. The new direct injection engines were made possible by

new advances in engine design that reduced the noise generation usually associated with direct injection.

The diesel engine's reputation for being "dirty" is also slowly waning. The principal emissions from diesel engines are particulate matter (DPM) and oxides of nitrogen, both but especially DPM have been sharply reduced in recent years by the introduction of advance air and fuel management systems and electronic control. However as air quality regulations become increasingly stringent, continued use of diesel engines for on-road applications will likely require use of exhaust treatment systems as described in Section 3.4 of this chapter.

The solid particles that are emitted by diesel engines are the focus of this dissertation work. Such particles have been called diesel smoke, soot, and diesel exhaust particulate, but I will use the term diesel particulate matter (DPM) in most of my discussions.

In the first three sections of this chapter I review the three main components of DPM namely elemental carbon (EC), organic carbon (OC) and the inorganic material or what is sometimes called "non-carbon ash."

3.1 The Role of Elemental Carbon in DPM Formation

DPM contains a host of elements and compounds in varying amounts, but elemental carbon typically comprises the majority of the volume and mass of the DPM. As shown in Figure 1.3, this EC is in the form of small "primary particles" composed of layers of carbon atoms. These primary "spherules" of EC coagulate into the chain-like agglomerate particles as seen in Figure 1.3. To present insight into the chronology of the

particle formation process and to present the current theories pertaining to the role of EC in that process, in this first section I present a review of the diesel combustion process with an eye toward understanding the role of EC in the formation of DPM. The roles of OC and non-carbon ash during this particle formation process will be discussed in the subsequent sections of this chapter.

3.1.1 Summary of the Diesel Combustion Process

Prior to the 1990s there was little hard data on the structure of the diesel flame. Early computational models developed in the 1970s often assumed a dense fuel-rich core for the fuel spray jet, surrounded by "layers" of progressively leaner mixtures. For steady state conditions these layers were "fed" a steady stream of entrained air near the base of the jet (Espey and Dec, 1993). By the late 90s this approach evolved into a steady state diffusion flame model (Naber and Siebers, 1996), in which the jet core disintegrated into droplets which quickly vaporized yielding a tear-drop shaped cloud of droplets and vapor at the boundaries of which a diffusion flame was maintained. The pyrolysis of fuel into soot was thought to occur in a thin layer on the fuel rich side of this diffusion flame.

In the early 1990s researchers at Sandia Labs designed a test set up that revolutionized our understanding of diesel combustion (Dec, 1997). They built a production based single cylinder research engine with optical access to the combustion chamber for using two dimensional laser diagnostics. In just a few years they generated valuable optical data which shed much light on the structure of the steady state diesel flame, including the following:

1. Liquid-phase fuel distributions using Mie scattering.
2. Fuel-air mixture images and temperature fields by Rayleigh scattering.
3. Soot concentration by LII (Laser-Induced Incandescence.)
4. Soot size distributions by combining LII and Raleigh scattering.
5. LIF (Laser-Induced Fluorescence) for PAH, OH distributions.
6. LIF of NO radical to show onset of NOx.
7. Natural Chemi-luminescence to identify auto-ignition and soot development.

Combining these results (Flynn, et al, 1999) led to new conceptual models for both transient and quasi steady state combustion. Figure 1 is a schematic of the current conceptual model for steady state combustion. The important new insights of this model include rapid vaporization of fuel as the jet entrains and accelerates hot air at the shear interface near the nozzle. The resulting stream of heated vapors and air thus begins oxidizing as it enters the main body of the ensuing jet plume, while final oxidation takes place at the plume periphery. The model shows liquid disappearance and delineates the reaction zones. It also shows regions of high OH concentration, which coincide with vigorous diffusion burning as predicted in previous work (Chiu, et al., 1976).

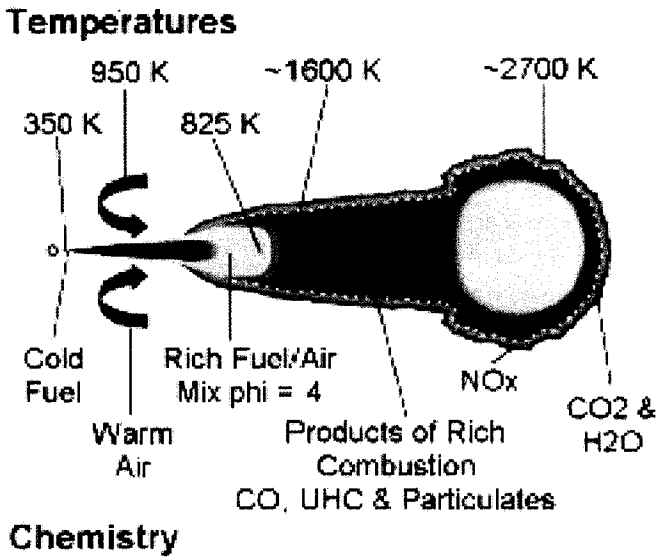

Figure 3.1 - Schematic of current diesel combustion model (from Flynn, et al., 1999).

By linking the results of chemical kinetics analyses with the spatial and temporal data from laser diagnostics, a team of researchers (Flynn, et al., 1999) were able to present a unified picture of our current understanding of the diesel combustion process. They were also able to postulate a new "refined" view of the combustion process and confirm their hypothesis experimentally.

Many kinetic models of hydrocarbon fuel combustion have been developed over the last 30 years, and have become more and more complex in that time. Computational times are highly sensitive to the number of intermediate species as well as the number of carbon atoms in the fuel molecule. Current models can account for numerous intermediate species as well as combustion of complex molecules like normal heptane. Recent computational successes include demonstrating that unburned hydrocarbons are in fact not caused by wall quenching as was previously thought, and that early injection stratified charged combustion can increase unburned hydrocarbon significantly.

One of the problems with modeling diesel combustion is that diesel fuel is an ill-defined mix of hundreds of hydrocarbon species, many of which have more than 10-15 carbon atoms. In addition this illusive mix is variable day-to-day even from the same vendor. To side step this issue, most models are based on a surrogate fuel such as Iso-Octane or normal heptane.

A group of researchers recently used the HCT code to model a constant pressure reaction of normal heptane and air for the conditions typically found in a diesel engine (Flynn, et al., 1999). They were able to quantify the rapid evolution of many species including soot precursors such as C2H2, C2H4, and C3H3. Most notably they evaluated the times scales for 50% reaction completion and showed that temperatures above about 900K are required for reactions to advance as quickly as necessary in an engine (i.e., at time scales on the order of tenths of milliseconds). They also plotted a relation between cylinder temperature and reaction rates.

The disintegration and vaporization of the liquid jet was studied (Naber and Siebers, 1996), which resulted in a correlation between jet length and cylinder temperatures. Using this along with the above correlation between temperature and reaction rate, it was possible to describe the spatial and temporal evolutions of the diesel flame in terms of fuel vaporization, reaction onset, subsequent re-entrainment of reaction products, temperature rise of the jet, and finally the establishment of a steady state diffusion flame.

Using this information a two-stage combustion model was developed (Flynn, et al., 1999), in which the first stage is a low temperature reaction of the fuel-rich jet using the limited oxygen available in the fuel and entrained gases. This reaction produces

H_2O, CO, CO_2 and many partially burned fuel fragments, and peaks at temperatures of about 1600K. When these products reach the jet periphery, they encounter oxygen diffusing through the flame and rapidly oxidize in a second stage reaction reaching temperatures of around 2500K.

Combustion Initiation

As injection begins, relatively cool fuel is atomized into a plume and warmed by the air in the cylinder. Evaporation of the plume yields vapors which begin reacting to form hydrocarbon compounds at a critical temperature of about 850K (Figure 3.1). Such reactions continue until available oxygen is depleted yielding a larger plume of a reaction by products (soot precursors) at around 1600K (Figure 3.1). At the periphery of this plume, a diffusion flame forms across which oxygen travels from the surrounding air to react with this hydrocarbon-rich inner plume (Figure 3.1). The bulk of the heat release occurs at this flame boundary and temperatures rise to approximately 2700K. Although there is still speculation, it is hypothesized that soot is formed from precursors in this very thin highly-reactive zone, and is completely oxidized by combustion reactions with the exception of a very small portion (0.1%) that survives due to quenching, and it is this small portion that represents the soot we observe in the system after combustion is complete. This two stage initiation results in a steady state flame as shown in Figure 3.1.

Heat Release

In this work, injection of diesel fuel starts at about 10 or 11° before top dead center. About 6 or 7° after injection, the beginning of the ignition event triggers an initial

heat release which is very short i.e. about 3-5 crank angle degrees (CAD). This marks the transition of the forming diffusion flame to a quasi steady state. This quasi-steady state diffusion flame (Figure 3.1) is established very near top dead center of the piston travel. Once established, the bulk of the fuel is combusted in the diffusion flame. This represents about 85-90% of the fuel combustion, all happening over a period of about 15 CAD, right after the piston passes top dead center.

In spite of considerable work in this area, there is still much speculation about the details of the origin of exhaust particulates. Many believe that the fuel fragments resulting from the first stage reaction event will grow into particles inside the jet plume, and laser diagnostics support this. However, other tests (Lee, et al., 1990) show that all such particles are consumed across the diffusion plane i.e., during the second stage reaction. Flynn, et al., state that DPM emissions may be simply a result of some limited/undetectable quenching in this second oxidation reaction. Other work which supports this includes work by Miyamoto et al. in which the use of 25% oxygenated fuel led to near-zero Bosch smoke output. Those authors investigated this by modeling N-Heptane combustion with addition of di-methyl ether (DME) to increase oxygen content of the fuel (using the HCT code). They noted that this resulted in a significant drop in precursor production, which suggests that the availability of precursors is directly responsible for particulate formation.

Based on the above observations is it is evident that the spherules of EC form early in the combustion process. Since temperature is very high in the flame, most other species are volatilized and either do not participate in the early formation of the spherules, or are restructured across the flame, freeing other species. The result is a high

number of "pure" spherules of EC which coagulate quickly after passing through the flame due to their high number concentration. Once formed, these agglomerate particles then take on other species by adsorption, by condensation, or via self nucleation of nanoparticles followed by additional coagulation.

3.2 The Role of Organic Carbon Compounds in DPM Formation

The numerous by-products of combustion (literally thousands of compounds) are continually reacting and evolving as they leave the combustion zone and eventually join the atmosphere where we breathe them directly into our lungs. Many of these products are organic carbon compounds, some of which have been shown to be carcinogenic. During the combustion process, these compounds usually deposit onto particle surfaces where they may be held indefinitely. Because of this obvious health issue, it is important to understand how the various gaseous species and small soot particles are formed and how they behave after leaving the combustion zone.

The role of organic carbon compounds during particle formation has been studied from a variety of angles. During the post-WWII expansion of industrial technologies in the US, scientists began looking more closely at the health effects of industrial processes, and in particular at the issue of combustion by-products. Early studies identified the mutagenicity of several of the many polynuclear-aromatic-hydrocarbons (PAH's) which are prevalent in combustion emissions and researchers initially began studying combustion emissions with an eye toward learning more about PAH's. By 1983 it had been shown that PAH's are generally associated with the surfaces of solid particles. Detailed studies at MIT used electron micrographs to investigate particle morphology, as

well as a "molecular beam flame probe" to gather samples from flames (Howard and Longwell, 1983) . Work at MIT during the 1980's also involved the use of laser scattering to detect in-situ changes in particle concentration in flames. Based on theirs and other work of that era, the process of post-combustion PM formation was postulated to be an evolution from heavy hydrocarbon gases created in the combustion process, to small "spherules" of mainly carbon and finally to agglomerate soot particles containing PAH's (as well as other components) on their surfaces. Subsequent works focused on the finer points of particle formation, i.e., how the spherules agglomerate and how the hydrocarbon gases condense and/or adsorb onto the particle surfaces.

The following review highlights some of the approaches that have been taken in the investigation of the deposition of volatile organic carbon species onto soot particles. Since PAH's have been the focus of much of the recent research in this area, I will focus to some degree on PAH's.

3.2.1 Review of Publications Concerning the Role of Organic Carbon

In the early 1980's, work was done which led to our current understanding of the basic structure of combustion PM, i.e., agglomerate particles composed of small (10-30 nm) "spherules" of carbon, clinging together not unlike bunches of grapes (Howard and Longwell, 1983). The role of PAH's in particle formation was also studied, by mass spectrometry of gases withdrawn from pre-mixed flames at various heights. It was shown that at low positions (1-4 cm above the burner) the volume concentration of heavy hydrocarbons was significant, but that higher up, the concentration was attributable mainly to soot. This transition from heavy hydrocarbon gases to soot particles was

postulated to be a rapid evolution beginning with spherules of mainly carbon and ending with agglomerate particles containing PAH's and other volatiles on their surfaces.

Subsequent work (Prado and Lahaye, 1983) focused on the formation/destruction of PAH's in two classes:

1) PAH's containing only carbon and hydrogen

2) PAH's containing heteroatoms of sulfur, nitrogen and oxygen

The latter are not found in laboratory flames but abound in practical systems. They also have mutagenic activity in the absence of an enzyme activation unlike the PAH's containing only C and H.

Prado and Lahaye showed that when using gas chromatography mass spectrometry (GC/MS) to analyze the volatile fraction extracted from flames, the chromatographs were strikingly similar for a variety of fuels both aromatic and aliphatic and for various flame types i.e. pre-mixed and diffusion flames (both laminar and turbulent). PAH formation was studied using a molecular beam mass spectrometry system to measure both stable and radical species in the flame. This species information was used to deduce possible pathways for PAH formation. They concluded that PAH build up is likely due to aliphatic fragments attaching to aromatic rings. They also conducted tests with a residential oil burner which demonstrated that leaner fuel to air ratios (F/A) produce less soot, but because of the chemistry of PAH formation, actually produce more PAH's by an order of magnitude. Since PAH's were known to be carcinogenic, this was a significant result in terms of its potential impact on legislating exposure to combustion PM.

In the late 1980's a Swiss team (Burtscher and Schmidt-Ott, 1986) introduced the use of the aerosol photoemission (APE) technique to study adsorption and condensation coating of ultra fine particles. They produced carbon particles using the spark or "sputter" method and passed them through a perylene condensation chamber. (Perylene is a fairly non-toxic planar 5-ring PAH). They measured the particles' photoelectric activity in response to a pulsed Xe arc lamp as a function of condenser temperature. Using a screen type diffusion battery, they also measured the size change (i.e., coating thickness) evident from the change in penetration rate through the battery. In this way, they generated data which quantified the relation between PAH (perylene) coating thickness and photoemission rates.

The APE technique was subsequently used to study the adsorption/desorption of perylene from combustion aerosols (Steiner et al., 1990). A sample was drawn from the tailpipe of a spark ignition engine and run through a differential mobility analyzer (DMA) to obtain a monodisperse aerosol. This aerosol was reheated and passed through a carbon denuder to remove any volatile compounds. Next perylene was added in a well-controlled furnace (+/- 2 deg C) and the mixture cooled to trigger condensation onto the mono-disperse particles. The APE analyzer was used to measure photoemissions as a function of surface coating. A second heater and denuder downstream of the coating furnace also allowed determination of the desorption temperature.

Their results showed a surprising correlation between particle shrinkage due to desorption of the condensed PAH layer and the photo yield of the APE sensor, which proved their hypothesis that the APE technique might be useful for measuring the content of PAH's on combustion particles.

In the early 1990's another Swiss team investigated the adsorption of volatile compounds onto particle surfaces by in essence reversing the growth process (Steiner and Burtscher, 1993). Their primary experiments entailed using a furnace to reheat diluted exhaust effluent and demonstrating the change in particle properties as the furnace temperature was increased from 20 to 330 deg C. For generating test aerosols, they used three different types of combustion sources i.e. an oil burner, a diesel engine and a spark ignition (SI) engine. Changes in particle characteristics during the experiments were recorded by several methods. Total particle mass was measured with a Beta meter, mass of black carbon (BC) with an aethalometer, and particle mobility diameters were ascertained using a differential mobility analyzer (DMA). Very small changes in furnace temperature were shown to correlate with small changes in particle diameter (Dp) and in most cases also a pronounced change in photoemissions as measured with an aerosol photoemission (APE) analyzer. The changes in APE were used to determine the amount of polynuclear aromatic hydrocarbons (PAH's) on the particle surfaces as described in a related work (Niessner et al., 1986). The small changes in diameter resulting from particle shrinkage due to desorption as the temperature was raised, were measured using a screen type diffusion battery. To accomplish this, two aerosol electrometers (AEM) were used, one on the inlet and one on the outlet of the diffusion battery, and the difference in their readings used to determine the fraction of particles passing through the battery. Based on diffusion theory, this difference was translated into particle diameter-changes of a few angstroms.

The work of Steiner and Burtscher was in effect an experimental "proof" of the contribution of adsorbed species to particle make-up. It also demonstrated the "layering"

of species by showing the shrinkage of particles as a function of temperature, and a diagram of a proposed layering model was presented. The temperature versus shrinkage data were used to derive desorption energies, and this result compared to the work of other researchers. It was noted that some of the PAH's stayed on the particles until much higher temperatures were reached, which supports a realistic adsorption model where species of various volatilities are adsorbed based on the temperature during different stages of particle formation.

The Swiss team also conducted a test that illuminated the relation between metals and organic carbon. Using leaded fuel in a spark ignition engine, they demonstrated that inorganic species can significantly effect particle formation. They noted that the fraction of organic carbon associated with emitted particles decreased for the leaded fuel case. They did not determine, however, whether this was due to soot suppression or to metal enhanced oxidation, and this question is still the topic of some controversy. It is possible that the lead on particle surfaces leads to oxidation of carbonaceous species as the particle transits the exhaust system. It is also possible that the lead acts as a scavenger of free radicals during the combustion process and thus affects the equilibrium chemistry of combustion. Further investigation concerning the reaction mechanisms involved might clarify the correlation between free radical scavenging (especially of H atoms) and the net production of volatile hydrocarbons.

Steiner and Burtscher's work represented a good example of how carefully executed experiments can provide insight for the support of a theoretical or hypothetical model. The results not only supported the layering model for combustion particle morphology, but also illuminated the similarities and differences in combustion particles

from three common sources. The results also provided insight into a potential new research tangent. In this case the results pointed the way to potential studies of the effects of inorganic material on particle morphology, which is the subject of the next section of this chapter.

In the mid 1990's another team studied the emissions of PAH's from a diesel engine as a function of the PAH content of the fuel and lube oil (Schramm, et al., 1994). They used pyrene as a representative PAH and insured that pyrene was the sole PAH contained in the fuel and oil used for experiments. The amount of pyrene added to the oil (400 ppm) was based on typical PAH levels in used engine oil, so their data for pyrene emissions were comparable to total PAH emissions for a typical engine.

They found that significant amounts of PAH are transported from the lubricant to the exhaust gases and that the emissions contained much more PAH than that derived from oil consumption alone. They concluded that PAH's first dissolve in the oil and then are released during combustion. They also showed that the survivability of PAH's is 40-100 times greater for oil than for fuel. This was postulated to be due to the release of PAH's from oil much later in the expansion stroke (when temperatures are lower and cylinder surface area exposed to exhaust gases is higher). They also completed parametric tests of the effect of engine speed and load on the PAH emissions but the results were inconclusive.

In an effort to better quantify the carbon collected on filter samples, NIOSH researchers published a standard thermal-optical method that allows speciation of organic, carbonate and elemental carbon in a two stage process via temperature and atmosphere control (Birch and Cary, 1996). The method entails placing a sample (a

small punch from a quartz filter) into an oven and controlling the temperature and gas environment. In stage one the atmosphere is Helium and the temperature stepped to about 820 deg C. In this stage, evolved carbon from organics and carbonates ("OC") is reduced to CH4 and quantified by a flame ionization detector (FID). The transmittance of He-Ne laser light through the sample filter is also monitored and it decreases in stage one due to pyrolytically generated char building up on the sample filter. In stage two, oxygen (10%) is added to the atmosphere. This first causes oxidation of the EC that was left as char on the filter. Correction for the char contribution to the total EC is accomplished by measuring the amount of char oxidation required to return the filter to its original transmittance value. The temperature is then raised to about 860 deg C and the remaining EC oxidized and quantified by the FID. The mass of carbon is deduced directly from the FID signal, and the "split" between OC and EC is set at the point at which the filter transmittance indicates that all the pyrolytically generated char has been oxidized. This method has been well accepted and is used for determining OC/EC content of particles for regulatory purposes.

Thermo gravimetric analysis (TGA) has been used extensively to quantify evaporation rates of volatile organic compounds (Pichon, et al., 1997). Experimental results have been shown to be consistent with a 1-D theoretical mass transfer evaporation model and demonstrate the influence of heating rate and ambient pressure on evaporation rates.

In the late 1990's, the adsorption of volatile organic hydrocarbons (VOC's) onto soot particles was investigated using combustion residue from an oil furnace which burned #2 fuel oil (Goss and Eisenreich, 1997). Cleaned particles were placed in a

stainless steel column and put into the gas chromatograph (GC) oven. One of six different VOC's was introduced isothermally at various temperatures. The velocity of the carrier gas was slow enough to insure adsorption equilibrium. In this arrangement, the retention time is a direct measure of adsorption intensity and allows direct calculation of sorption coefficients. Their method also entailed saturation of the carrier gas (purified air) at some temperature below the experimental temperature which allowed precise control over the relative humidity (RH), a problem often associated with this type of experiments. These results demonstrated the kinetics of adsorption and served as a baseline for estimating adsorption under less controlled conditions.

Much of the work done regarding adsorption was done using approaches that relied on "thermal desorption" i.e. the volatilization of species from a surface due to energy provided by the heat of the substrate itself (Hueglein, et al., 1997). They generated particles using a spark discharge generator with nitrogen as a carrier gas. The particles had mobility diameters of about 25 nm with spherule size around 2 nm as determined by a scanning electron microscope (SEM). They coated the particles with perylene as in the work of the Swiss team (Steiner and Burtscher, 1993). Immediately after dilution with pure air, the particles entered a photoemission tube and desorption began due to the low vapor pressure of perylene in the diluted mixture. At various times thereafter, the aerosol was irradiated for 20 ns with an excimer laser (wavelength = 193 nm) and subsequently all electrons and negatively charged ions were precipitated out by an electric field. The remaining positively charged particles create a signal via a current amplifier as they exit the phototube. For thinly coated particles this current is proportional to the amount of adsorbed perylene. By varying the time, i.e. position in

tube, of the irradiation, the subsequent signals can be used to determine a desorption rate. This result was significant in that it represented a new technique for learning more about the rate at which PAH's desorb.

In the last decade, considerable research has focused on diesel particles. A novel method for determining the volatile fraction of DPM in-situ using a combination of laser induced desorption and light scattering was demonstrated (Witze, 2002). The method involves using two laser pulses spaced closely in time so as to "freeze" the flow of exhaust aerosol. The first pulse delivers enough energy to desorb the volatile component of each particle, and simultaneously produces "elastic light scattering" which is proportional to the total volume of DPM in the aerosol. The second pulse is used to get another scattering signature and gives the resulting volume change caused by the laser desorption.

Another method for characterizing DPM employed a tandem DMA (TDMA) system to measure the size distributions of total PM and the solid fraction of PM for particles emitted from a diesel engine (Franz, et al., 2002). The experimental setup included extracting a sample from the tailpipe, cooling and diluting it, and passing it through the first DMA. The size distribution was measured by varying the voltage to the DMA stepwise and measuring particle number with a condensation nuclei counter (CNC) at each voltage (corresponding to a particle mobility diameter). The sample was then run through a heater and denuder to remove the volatile fraction and then through the second DMA to re-measure the size distribution. In this way they directly measured particle shrinkage due to desorption over the entire particle size range. This (TDMA) approach was also used by UMN researchers (Sakurai, et al., 2003). Combining that technique

with the use of a thermal desorption mass spectrometer, they showed that certain organic compounds are associated with the smaller sized DPM, and the identified compounds in fact correlate closely with the organic compounds found in engine lube oil. That work confirmed earlier evidence which suggested that much of the organic carbon associated with DPM originated from the lube oil consumed during normal engine operation.

3.2.2 Contribution of Organic Carbon to DPM

In summary, an evolution of experimental methods has led to a better understanding of the relation between the volatile and non-volatile fractions of DPM. The non-volatile fraction constitutes the cores of particles and is made up of agglomerated primary particles of elemental carbon, while the volatile fraction is made up of any of a great number of organic carbon compounds. Much of the organic fraction originates from lube oil. PAH's have been shown to build up in lube oil and so will take a similar pathway onto particles as do the lube oil compounds. The lube oil that is deposited onto the cylinder walls by the piston action is subsequently volatilized inside the cylinder and the resulting vapors then adsorb or condense onto particles as the system cools. The details of this process depend on many variables including engine temperature, oil consumption, and volatility of subject species and cooling rate of the system. The exact chemistry of post-combustion particle formation has only been touched on and this is an area requiring more research. Because of the complex chemistry involved, studies should best be undertaken using single species of interest, modeling their chemical pathways and then verifying the models experimentally.

3.3 The Role of Non-Carbonaceous Species in DPM formation

Environmental studies have shown significant amounts of metals in urban air from sources such as industrial incinerators (Biswas, et al., 1992), power plants (Costa and Dreher, 1997), and automobiles (Silva and Prather, 1997). Clinical studies using mice and rats have demonstrated the potential for small metallic particles to induce cell damage (Lison, et al., 1997). This combined information points to a hypothesis of metal-toxicity as a possible causal mechanism for the observed health effects of PM exposure. This hypothesis has stimulated many recent investigations and various researchers are currently trying to quantify sources and fates of metals in the atmosphere as well as their potential health effects. The work described in section 3 of this report is an example of such ongoing research.

3.3.1 Metals in Combustion-Related PM

It has been documented that many combustion processes produce metal by-products in particulate form. Examples of such by-product metals are lead, nickel, chromium, cadmium, arsenic, zinc, mercury and their many associated compounds. It has also been documented that negative biological effects can be correlated with exposure to the levels of metallic species found in combustion aerosols (Costa and Dreher, 1997). The diesel engine is one unique (and frequently used) combustion source which is capable of producing metallic particles.

3.3.2 Metals in DPM

The formation of DPM stems primarily from carbon particles, but during combustion there are many other species present in smaller amounts and these will all play a role in the make up of the exhaust emissions. As mentioned in the previous chapter, the processes of adsorbtion, condensation, self nucleation and coagulation are all taking place, as well as a multitude of chemical reactions. It is postulated that these processes act to convert gases to particles along a timeline that reflects the local temperature and cooling rate, and that the conversions will take place more or less in the order of the volatility of the gaseous species. Because I have chosen to address the fate of metals in this dissertation work, I will limit the following discussion to metallic species. These may originate from sources such as trace metals in the fuel or from the use of metallic fuel additives for enhancing regeneration of diesel particulate filters, but under normal operating conditions most are believed to originate from lube oil additives that enter the combustion chamber via blow-by of the piston rings. This is evidenced by the existence of a significant amount of unburned oil in the diesel exhaust (Sakurai, et al., 2003).

Table 3.1 lists the constituents of a fairly typical lube oil used in a diesel engine (Kittelson and Watts 2002). As seen in the table, many trace elements are either available from the original crude, added to enhance lubricity, viscosity, and other fluid properties, or accumulate due to engine wear. Many of these elements do not combust well and are not very volatile, so rapid cooling during the expansion stroke may result in condensation of their vapors onto existing carbon particles and/or self-nucleation of the

Table 3.1 - Examples of trace metals in engine lube oil (Kittelson and Watts, 2002)

Additive Metals	Low Sulfur Lube Oil Concentration, ppm*	E-43 Lab Lube Oil Concentration, ppm
Ca	3323	2881
Ba	4	7
Mg	7	98
Zn	14	1090
P	16	998
B	356	12
Mo	<1	<1
Wear Metals		
Fe	2	2
Sn	< 1	< 1
In	< 1	< 1
Cu	< 1	< 1
Cr	< 1	< 1
Al	0	< 1
Contaminant Metals		
Si	2	4
Na	1	2
Viscosities		
40C cST	90.48	106.9
100C cST	13.22	14.33
Index	146	137
Soot by IR wt %	0.44	0.58
Total base KOH equiv mg/g	11.6	9.7
IR oxidation	0.06	0.06
IR nitration	0.03	0.03
Total Sulfur ppm	385	4000

*Tested after use

vapors into nanoparticles. Thus, they will usually exit the tailpipe as part of the DPM. Preliminary data on DPM samples taken from an engine exhaust stream (Zielinski, et al., 2002) show measurable amounts of these lube-oil additives.

Sulfur is prevalent in both fuels and oils and its role in DPM formation has been studied extensively. Because of its high volatility it tends to exit the engine mainly in gaseous form and has been shown to add greatly to the production of nano-aerosols during post-tailpipe dilution and subsequent cooling. It may, however, contribute significantly to the ash content of DPM due to its prevalence in the fuels and oils. Since its behavior is well documented and it can be minimized by the use of ever more popular low sulfur fuels, and because its role in particle formation occurs mainly beyond the engine exit, I will not address sulfur to any great degree in my comments concerning non-carbon ash emissions.

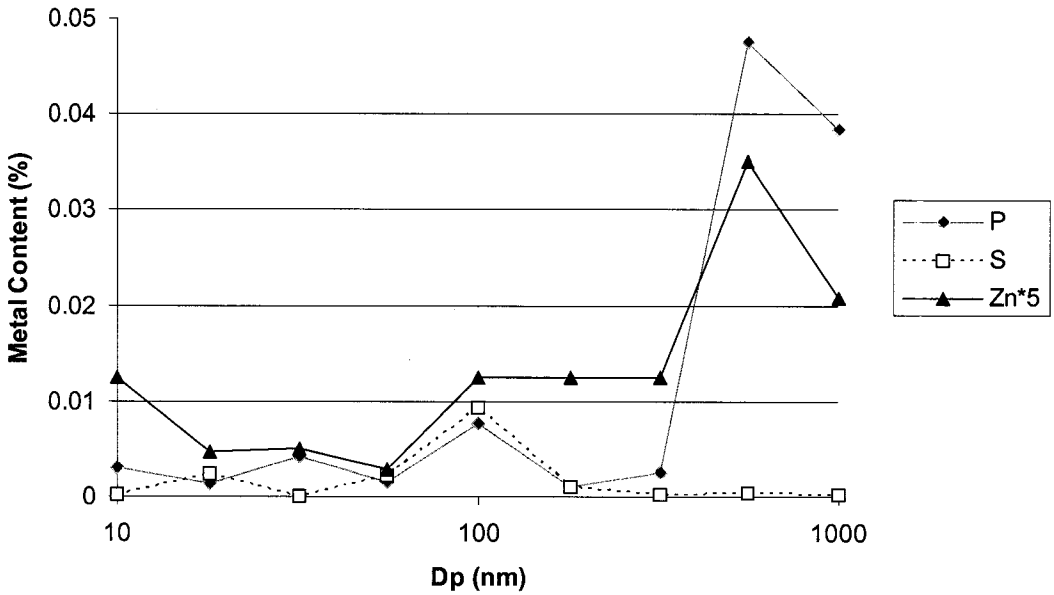

Figure 3.2 - Trace metals measured in DPM samples, after Zielinski.

3.3.3 Current Research on Metals in DPM

The use of diesel fuel is prevalent in our society and the emissions from diesel combustion have a significant impact on air pollution levels including metallic species

(Silva and Prather, 1997). Epidemiological studies have demonstrated a correlation between DPM exposure and cancer risk (Mauderly, et al., 1987; Garschick, et al., 1988), but no definitive causal mechanism has been established. Based on the above-cited references, we know that both acute and chronic health effects have been associated with DPM. We also know that the potentially large number of ultrafine particles and their characteristic high lung-penetration efficiency may play a role in this correlation, and that the presence of metals may be a contributor. To address these issues, I conducted a joint investigation with my colleagues to quantify the trace metals in DPM and show where they reside, i.e., how they are apportioned across the particle size distribution. The following sections of this report summarize preliminary findings. The research aims at providing insight into how diesel combustion leads to the formation of metal-rich nanoparticles via self-nucleation as well as the overall distribution of metals across a wider range of particle sizes due to condensation and coagulation.

From the perspective of diesel engine designers, the concern about metals emissions comes in part from advancements in "clean engine technology." Simply put, if the newer engines drastically reduce soot emissions, the particles they emit will have a higher proportion of non-carbon species such as metals and could potentially be even more toxic than the previously-generated higher-carbon particles.

One could argue that the advent of diesel particulate filter systems as described in the next section, may negate such concerns about particle toxicity. There are two counter-arguments to that. First, it is certain that such exhaust filtration systems will not be utilized on all engines and in fact the "cleaner" engines will be less likely to have filters installed and it is exactly those engines that may generate the more toxic particles.

Second, the issue of particle formation pathways during combustion and how they affect particle toxicity is an important area of research and has implications far beyond diesel engine technology.

3.4 Summary of DPM Reduction Technologies

Since health studies conducted in the last two decades have indicated a correlation between DPM exposure and cancer, new regulations are being adopted worldwide to reduce DPM exposures. Several countries have adopted regulations specific to tailpipe emissions and air quality in mines (McKinnon, 1999). In 1999, the U.S. Environmental Protection Agency set new emissions guidelines (Federal Register, 40 CFR) that include limits on DPM generation by non-mining off-highway vehicles. The Mine Safety and Health Administration (MSHA) has followed suit by promulgating DPM regulations for underground mines (Federal Register, 30 CFR). There are many ways to reduce DPM exposure. In fact, MSHA has developed a whole Atoolbox@ full of DPM reduction techniques for the mining industry (see www.msha.gov). Perhaps the most effective method is to reduce DPM at the source, i.e., to reduce an engine=s output of DPM. Methods for DPM reduction at the engine fall into four categories: engine design, maintenance, fuels, and exhaust treatments. A number of techniques for reducing DPM are available in each category. It is expected that in the future, equipment operators will use a combination of techniques to design a DPM-reduction strategy. The following is a brief overview of some of the more promising technologies for reducing DPM output. New technologies for DPM reduction are continually emerging and many are reviewed in the literature (McKinnon, 1999; McGinn, 2000).

3.4.1 Engine Design

Engine manufacturers are continually investigating ways to increase combustion efficiency in an attempt to design cleaner-burning diesel engines. Each manufacturer has its own bag of tricks, which may include such things as special cylinder head designs, turbochargers, precise combinations of valve and fuel injection timing, and so on. Considerable improvements have been made just in the last 5 years or so, and many of today's engines emit just a fraction of the DPM that their recent predecessors did.

The advent of emission control modules (or ECMs) has had a huge impact on engine emissions. An ECM is a microprocessor-based control unit that analyses feedback from sensors monitoring engine parameters, such as rpm, fuel flow, and crankshaft speed. It utilizes this information to optimize fuel flow to the engine under transient conditions. Since overfueling probably contributes more to increased DPM than any other factor, this technique alone has led to dramatically cleaner engines. Many of the newer engines also employ exhaust gas recirculation (EGR) to help reduce emissions and some even incorporate real time variable-EGR, where the central ECM controls EGR in order to optimize combustion. Application of ceramic cylinder coatings and superoxygenation of inlet air supply have both been shown to enhance combustion, thereby significantly reducing DPM output. However, neither of these technologies have been commercialized to date.

Combinations of these and other combustion-enhancing technologies, along with modern diesel fuel blends, are resulting in a new generation of clean-burning diesel engines. Some manufacturers are even confident that they can meet upcoming DPM standards without the use of any exhaust treatment.

3.4.2 Engine Maintenance

Although good maintenance is generally considered a given when discussing emission standards, it is worth noting here with regard to DPM generation. Two extensive studies (Spears, 1997; McGinn, 2000) have been done recently on the role of maintenance in reducing DPM. Both document the tradeoffs that occur during tuning of diesel engines. Notable is the tradeoff between DPM and oxides of nitrogen: when you reduce one, the other generally increases.

These studies also document the effect of engine tuning on overall emissions, including DPM. In addition, they show that regular monitoring of emissions using a dependable gas analyzer can be a powerful maintenance tool and can detect problems such as faulty injectors or inlet leakage. This issue is of particular interest to miners and other off-road equipment operators, since inlet leaks are often hard to detect, yet can have devastating effects on engine life when operating in dusty environments. A detailed method of assessing such inlet leakage is available in the literature (McGinn, 2000).

3.4.3 Fuels

Fuels play a key role in the generation of DPM by an engine. There are many different blends of what would be considered Astandard@ diesel fuel available on the market. Although some may be slightly better than others in terms of their contribution to the DPM output of an engine, none of them will effect a drastic reduction in DPM (Clark, et al, 1999). There are however some alternative fuel options that may have a greater impact on DPM production.

The use of synthetic fuels derived from natural gas and/or plastic wastes,Abiodiesel@ blends, and emulsions of diesel fuel and water using proprietary stabilizers have all been shown to significantly reduce DPM. A variety of data is available (Watts, et al., 1998; McDonald and Spears, 1995; Schnakenberg, et al., 2003) that show DPM reductions ranging from 20% to 65%. Biodiesel fuel blends have the advantage of significantly reducing the elemental carbon (pure soot) portion of the emissions, but the cost is still slightly high compared to normal diesel fuel (DOE, 2004). Synfuels and emulsions are currently more cost effective at approximately 5 to 15 cents per gallon more than regular diesel and are also commercially available. Emulsion fuels have the added advantage of reducing oxides of nitrogen, although there is a penalty in power output. These alternative diesel fuels have been shown to be very effective at reducing DPM as well as other harmful emissions, but it is unlikely that the use of an alternate fuel alone will be sufficient to reduce DPM enough to meet the standards that will be set in the future.

3.4.4 Exhaust Treatment

Although DPM is a very complex mixture, it consists of two main components: elemental carbon and organic carbon (sometimes referred to as EC and OC). Elemental carbon (the pure carbon that makes up about half of total DPM), is very difficult to oxidize, which means it must be physically removed. This fact gave rise to the many Atrapping@ technologies for filtering it out of exhaust. Soot filters, particle traps, and diesel particulate filter systems (DPFS's) are all names given to devices that physically remove DPM from an uncooled exhaust stream. Organic carbon, which refers to any of

numerous carbon compounds, is more easily destroyed (via oxidation) by catalytic-convertor-type technologies. The many different options for exhaust treatment, therefore, tend to fall into two categories: physical removal of DPM and conversion or oxidation of DPM. Below are summaries of technologies that trap or filter out DPM, followed by those that oxidize the organic fraction of DPM.

There are two common types of particle traps: the monolith-style filters, which are typically made from ceramics or silicarbon, and the fiber-based filters, which are made from a fibrous glass or ceramic material. The monolith filters are actually a honeycomb-type structure of long, narrow passages in which the ends of adjacent passages are plugged off. Half the passages are connected directly to the exhaust manifold and the other half to the downstream side, i.e., the tailpipe exit. The exhaust gases from the engine pass through the thin honeycomb structure, leaving the soot trapped on the walls of the upstream passages. The fiber-based filters may be wound, woven, or knitted and are typically akin to an oil filter in that the gas enters the inner part of a cylinder, which is tightly wrapped with many layers of fiber. The gas passes outward through the fibers and in doing so gives up soot onto the fibers.

Soot eventually builds up in both types of filters, and they must be regenerated by heating to a temperature hot enough to burn off the soot. Although this is sometimes done by removing the filter and baking it, many new auto-regenerating filters incorporate catalysts (either in the fuel and/or embedded on the filter medium), which allows the soot to be burned off at peak operating temperatures during normal engine operation. Since sulfur tends to poison surface catalytic coatings, such catalyst-based traps generally require matching the catalyst loading with the sulfur content of the fuel. Many of these

new systems have been tested in Europe and have been shown to perform well even after thousands of hours of operation. The advantage of soot filters is that they are extremely efficient and have been demonstrated to remove as much as 90% of total carbon (which includes both elemental and organic carbon) from the exhaust stream.

As a precursor to selecting particle traps to install on engines, dataloggers are often employed to measure temperature profiles during normal duty cycles. State-of-the-art particle traps are designed to be maintenance free and therefore must incorporate a method of periodically burning off the soot that accumulates on the filters. Although most particle traps use some type of a catalyst to enhance this process, it is still critical for the engine to maintain adequate exhaust temperatures for a certain portion of its duty cycle, i.e., long enough for the regeneration of the trap to take place. For this reason, the first step in matching an on-board regenerating trap to a particular engine is to measure an engine=s exhaust temperature profile during its normal duty cycle using a datalogger and use this profile to select a trap.

As a way to get around the need for adequate regeneration temperatures during operation, a Aswap-out@ trap has been designed for smaller rigs (less than 100 hp) that do not reach exhaust temperatures high enough for on-board regeneration. The swap-out trap to be tested comes complete with a wall-mounted, 220-V regenerating station. The trap is designed with over-center locking clamps for quick exchange. It is insulated and has lifting handles so the operator can grab the trap as it is released. The filters are sized to be effective for one full shift. Regenerating time is approximately 30 to 60 min, depending on how dirty the filter is.

Paper filters have also been shown to remove DPM from the exhaust efficiently, as long as exhaust temperatures are low enough to prevent burning the filters. There are two types of systems available based on different methods of exhaust cooling. The scrubber systems, which are used to cool the exhaust stream on the permissible engines used in coal mines, have been shown to reduce DPM by the scrubbing action alone. In addition, exhaust thus cooled can be routed through a submicrometer paper filter system to remove still more DPM. Such postscrubber filter systems have been shown to be extremely effective, and some have already been deployed in coal mines. Maintenance on such systems includes cleaning or replacing the scrubber liquid and changing the paper filters.

A second paper-filter-type system is the dry gas system. This is a relatively new technology designed to compete with both scrubbers and particle traps. Exhaust gases are cooled by a radiator-type heat exchanger and then passed through a paper filter to remove DPM. Scrubber maintenance is eliminated, but the filters must still be checked and/or changed regularly.

In addition to the various particle filtration systems, there are many catalytic convertors on the market designed for diesel engines. These convertors remove organic compounds using a process of chemical oxidation. Depending on exhaust temperature and formulation, they may reduce CO and volatile hydrocarbons (which give diesel its peculiar odor), by over 90% and 80%, respectively. Since around half the total DPM typically consists of organic carbon compounds, these convertors are often capable of reducing DPM considerably, although the particles of soot (EC) remain intact. The fact that the soot is much more stable and not as readily subject to catalytic oxidation is a limitation of this technology in that the soot is generally considered the more prominent

marker of DPM. In some countries, it is measured as an indicator of DPM levels. Another issue is that, depending on the fuel used, the oxidation process can produce particles of sulfate or increased levels of other potentially harmful constituents, such as NO_2. These constituents should always be monitored in the field. A big advantage of this approach is that the cost of the convertors is typically quite low.

3.5 Summary

Typical DPM particles are agglomerates of elemental carbon. The formation and agglomeration of these particles happens inside the engine cylinder early in the combustion process, at or near the flame front and just after ignition. Other gaseous combustion by-products (notably hundreds of different organic carbon compounds), interact with the surfaces of the carbon agglomerates. As the piston retracts and the system cools, the organic carbon compounds and other species such as metals, will adsorb and/or condense onto surfaces and may also self nucleate if conditions warrant. The resulting aerosol exits the tailpipe and is what we call DPM.

Due to health considerations, new DPM regulations have been put in place to reduce emissions and in the case of the mining industry, to control worker exposures. A variety of new methods and products for reducing DPM are becoming available and mining companies as well as on-road truck manufacturers are developing strategies for DPM reduction. The current technology most likely to achieve the reductions stipulated by the new regulations is the particle trap (soot filter). This technology has been demonstrated on heavy duty engines in mining applications and upcoming regulations for on-road heavy duty vehicles may also necessitate the use of soot traps for those vehicles.

Although such traps are the most effective technology available for reducing DPM, it is expected that equipment operators will rely on a variety of control measures in the future to suit their individual requirements.

3.6 References

Birch, M. E., and R. A. Cary. Elemental Carbon-Based Method for Monitoring Occupational Exposure to Particulate Diesel Exhaust. Aerosol Sci and Tech., 25:3, pp. 221-241, 1996.

Biswas, P., and W. Y. Lin, et al. Formation and Emission of Metalic Aerosols from Incinerators. J Aerosol Sci, Vol. 23, pp. 273-276, 1992.

Chiu, W. S., S. M. Shahed, and W. T. Lyn. A Transient Spray Mixing Model For Diesel Combustion. SAE Transactions, Vol. 85, pp. 502-512, SAE 760128, 1976.

Clark, N. N., C.M. Atkinson, G. J. Thompson, and R. D. Nine. Transient Emissions Comparison of Alternative Compression Ignition Fuels. SAE Technical Paper Series 1999-01-117. SAE International, Warrendale, PA. Reprinted from Alternative Fuels for CI Engines (SP-1412), 1999.

Costa, D. L., and K. L. Dreher. Bioavailable Transition Metals in Particulate Matter Mediate Cardiopulmonary Injury in Healthy and Compromised Animal Models. Env. Health Perspectives, Vol. 105, Suppl. 5, pp.1053-1060, 1997.

Dec, J. E. A Conceptual Model of DI Diesel Combustion On Laser-Sheet Imaging. SAE 970873, 1997.

DOE (US Dept of Energy). Biodiesel handling and use guidelines. DOE/GO-102004-1999, Sept 2004.

Espey, C., and J. E. Dec. Diesel Engine Combustion Studies In a Newly Designed Optical-Access Engine Using High-Speed Visualization and 2-D Laser Imaging. SAE Transactions, Vol. 102, Sec. 4, pp. 703-723, SAE 930971, 1993.

Federal Register. Oct. 29, 1998. 30 CFR, Part 57. Vol. 63, No. 209, pp. 58104-58222. Diesel Particulate Exposure of Underground Metal and Nonmetal Miners (Proposed Rule).

Federal Register. October 23, 1998. 40 CFR, Parts 9, 86, and 89. Control of Emissions of Air Pollution from Nonroad Diesel Engines. Rules and Regulations, Environmental Protection Agency [AMS-FRL-6155-3], RIN 2060-AF76. Vol. 63, No. 205.

Flynn, P., R. Durrett, G. Hunter, A. Loye, O. C. Akinyemi, J. Dec, and C. Westbrook. Diesel Combustion: An Integral View Combining Laser Diagnostics, Chemical Kinetics, and Empirical Validation. SAE Technical Paper 1999-01-0509, 14 pp., 1999.

Franz, B., T. Eckhardt, T. Kauffeldt, and P. Roth. H2O2 Addition to Diesel Engine Exhaust Gas and its Effect on Particles. J. Aerosol Sci. 31:415-426, 2000.

Goss, K. U., and S. J. Eisenreich. Sorption of Volatile Organic Compounds to Particles from a Combustion Source at Different Temperatures and Relative Humidities. Atmos. Enviro., Vol 31, No. 17, pp. 2827-2834, 1997.

Howard, J. B., and J. P. Longwell. Formation Mechanisms of PAH and Soot in Flames. Polynuc. Aero. Hydrocarbons: Formation, Metabolism and Measurement: 7th Int. Symp., Battelle: Columbus, pp. 27-62, 1983.

Kittelson, D. B., and Winthrop Watts (principle investigators). Diesel Aerosol Sampling Methodology- CRC-43, Cummins Final Report. Available from the authors at the University of Minnesota, Minneapolis, MN, USA, 2002, 71 pp.

Hueglein, Ch., Paul, J. Scherrer, and K. Siegmann. Direct Observation of Desorption Kinetics with Perylene at Ultrafine Aerosol Particle Surfaces. J. Phys. Chem. B, Vol.101, No. 45, pp. 9335-9341, 1997.

Lee, W., C. E. Solbrig, T. A. Litzinger, R. J. Santoro, and D. A. Santavicca. Planar Laser Light Scattering for the In-Cylinder Study of Soot In a Diesel Engine. SAE Transactions, Vol. 99, Sec. 3, pp. 2222-2235, SAE 902125, 1990.

Lison, D., C. Lardot, F. Huaux, G. Zanetti, and B. Fubini. Influence of Particle Surface Area on the Toxicity of Insoluble Manganese Dioxide Dusts. Arch Toxicol (1997), Vol. 71: pp. 725-729.

Mauderly, J. L., R. K. Jones, W. C. Griffith, R. F. Henderson, and R. O. McClellan. Diesel Exhaust is a Pulmonary Carcinogen in Rats Exposed Chronically by Inhalation. Fund. and Appl. Tox., Vol. 9, pp. 208-221, 1987.

McDonald, J. F., D. L. Purcell, and B. T. McClure. Methyl Ester Oxygenated Fuels for Diesel Mining Applications. Presentation at 7th U.S. Mine Ventilation Symposium, June 5-7, 1995.

McDonald, J. F., and M. W. Spears. Field Trials of Soy Methyl Esters as a Fuel for Diesel-Powered Equipment in Underground Mines. U.S. Bureau of Mines CRADA 6200-0063, 1995.

McGinn, Sean. The Relationship Between Diesel Engine Maintenance and Exhaust Emissions. Final Report www.deep.org (November 20, 2000).

McKinnon, Dale. Diesel Emission Control Strategies Available to the Underground Mining Industry. www.meca.org, 1999.

Miyamoto, N., H. Ogawa, N. M. Nurun, K. Obata, and T. Arima. Smokeless, Low NOx High Thermal Efficiency, and Low Noise Diesel Combustion With Oxygenated Agents as Main Fuel. SAE 980506, 1998.

Naber, J. D., and D. L. Siebers. Effects of Gas Density And Vaporization on Penetration and Dispersion of Diesel Sprays. SAE 960034, 1996.

Naber, J. D., and D. L. Siebers. Effects of Gas Density and Vaporization on Penetration and Dispersion of Diesel Sprays. SAE 960034, 1996.

Niessner, R. The Chemical Response of the Photoelectric Aerosol Sensor (PAS) to Different Aerosol Systems. J. Aerosol Sci. 17, pp. 705-714, 1986.

Pichon, C., V. Risoul, G. Trouve, W. A. Peters, P. Gilot, and G. Prado. Study of Evaporation of Organic Pollutants by Thermogravimetric Analysis: Experiments and Modelling. Thermochimica Acta, Vol. 306, pp. 143-151, 1997.

Prado, G., and J. Lahaye. Mechanisms of PAH Formation and Destruction in Flames Relation to Organic Particulate Emissions. NATO SI Ser., Ser. C., 112 (Mobile Source Emiss. Incl. Polycyclic Species), pp. 259-275, 1983.

Sakurai, Hiromu. Tobias, Herbert J. Park, Kihong. Zarling, Darrick, Docherty, Kenneth S. Kittelson, David B. McMurry, Peter H. Ziemann, Paul J. On-Line Measurements of Diesel Nanoparticle Composition and Volatility. Atmospheric Environment, Vol. 37, No. 9-10, pp. 1199-1210, March 2003.

Schnakenberg, G., and A. Bugarski. Phase-I report for M/NM Diesel Partnership, 2003.

Silva, P., and K. A. Prather. On-Line Characterization of Individual Particles from Automobile Emissions. Enviro. Sci. Tech, Vol. 31, No. 11, pp. 3074-3080, 1997.

Spears, Mathew W. An Emission-Assisted Maintenance Procedure (EAMP) for Diesel-Powered Equipment. Evaluation of Technology to Reduce Diesel Particulates, Revised Task One Report (Contract USDI/1432 C)369004). University of Minnesota, Center for Diesel Research, Minneapolis, MN, 84 pp., 1997.

Steiner, D., S. Diserens, H. Burtscher, and H. C. Siegman. Adsorption and Desorption of PAH's on Combustion Aerosols. J. Aerosol Sci., Vol. 21, Suppl. 1, pp. S27-S30, 1990.

Watts, W., Jr., M. Spears, and J. Johnson. 1998. Evaluation of Biodiesel Fuel and Oxidation Catalyst in an Underground Metal Mine. Revised final report submitted to DEEP Technical Committee September 24, 1998. www.deep.org. Nov. 20, 2000.

Witze, P. O. Real-Time Measurement of the Volatile Fraction of Diesel Particulate Matter Using Laser-Induced Desorption with Elastic Light Scattering (LIDELS). SAE paper 2002-01-1685, 2002.

Zielinski, B., W. Goliff, and M. McDaniel, et al. Chemical Analysis of Collected Diesel Particulate Matter Samples in the CRC E-43 Project. Draft Report for CRC E-43 project headed by D. Lawson at the Nat Renewable Energy Lab in Golden, CO, 48 pp, 2002.

Chapter 4 - Hypothesis/Thesis Statement

DPM has been linked to various adverse health affects including cancer, but the causal mechanisms remain undetermined. Ultrafine particles and their unique surface area properties may play a key role and it is suspected that metals could also be a factor. The presence of metals in very small particles has been linked to oxidative stress on epithelial cells and associated with increased lung tumors in rats. For these reasons, this research project was designed to better quantify the origin and fate of metals in DPM.

As an introduction to the possible pathways for particle formation I used a modified sectional model to predict particle formation dynamics. I used this together with my knowledge of the diesel combustion process to form my hypothesis concerning the origin and fate of metals in DPM. I predicted that in the diesel combustion chamber the carbon would first form soot particles and soon thereafter, low volatile vapors derived from trace metals in the lube oil would condense onto the particles, and more volatile species would in turn do the same. I also predicted that if the metal to carbon ratio gets high enough, the metals would self-nucleate into nanoparticles. My hypothesis is stated below.

4.1 Dissertation Hypothesis

It is hypothesized that as a part of the diesel combustion process, trace metals from the fuel, lube oil and/or engine wear will vaporize and subsequently adsorb or condense onto the surfaces of carbon (soot) particles. If the metal to carbon ratio during combustion reaches a critical level, they may also form self-nucleated nanoparticles, which may exist independently and/or coagulate with other particles.

Chapter 5 - Characterizing Iron-Bearing Particles Using the Single Particle Mass Spectrometer (SPMS)

As a first step in addressing my research hypothesis, I designed an experiment to investigate the fate of a known metal during diesel combustion. This chapter describes the results of that experiment. For this study, DPM was generated by a 1.5 liter engine and ferrocene was added to the fuel to raise the level of metal (Fe) in the system. The exhaust particles were analyzed in real time using a recently developed single particle mass spectrometer (SPMS) that has the capability of ablating each particle down to its elemental constituents, thereby yielding the relative mass of elements in each particle. Particle-size calibration of the instrument was achieved by correlating the SPMS signal intensity with measured DPM size. Using this approach, I was able to measure size and composition resolved elemental species distributions for both the nuclei mode and ultrafine portion of the accumulation mode of DPM. Results show that when the fuel is doped with ferrocene, iron-rich nanoparticles are formed and their number and size increase with level of doping. Larger iron-bearing particles are also formed, but it is observed that the metal to carbon ratios increase for smaller particle sizes. Hydrogen to carbon ratios were measured as a function of particle size, which allowed determination of the relative amounts of organic carbon and elemental carbon in the particles and showed that the hydrogen to carbon ratios increase for smaller sized particles. The combined results are used to discuss the effects of metal doping level and engine load on particle nucleation and mechanisms of DPM formation.

5.1 Introduction

It is known that diesel engines produce a tri-modal size distribution of diesel particulate matter (DPM) (Kittelson, 1998). The newer "cleaner" engines, although they produce less mass of particles, can sometimes produce a greater number of nano-size particles (Bagley, et al, 1996; Kittelson, et al, 2000, 2002), although many new engines reduce number and mass simultaneously. This "nuclei mode" of particles is quite variable and can be attributed in many cases to the self-nucleation of volatile species during the dilution and simultaneous cooling of the exhaust aerosol as it exits the tailpipe. It has also been shown that some nanoparticles may form prior to dilution and that this phenomenon can be enhanced by introducing trace amounts of metals into the fuel (Du, et al, 1998; Higgins, et al, 2002). The increase in nuclei mode particles is thought not to be a direct function of how "clean" the engine is, but rather to depend on the ratio between carbon (soot) and the nucleating species. One of the main goals of the experiment described in this chapter was to study the onset of self nucleation and to gather information about the make up of the resulting nanoparticles.

5.1.1 DPM Formation

The dynamics of particle formation during and after combustion is a topic of much interest and investigation. A recent summary of the diesel combustion process (Flynn, et al, 1999) describes how the fuel jet quickly disintegrates as it exits the nozzle and vaporizes as it entrains hot air, subsequently forming a plume of fuel-vapor and air mixture with a diffusion flame at its periphery. It has been shown that soot precursors originate from partial oxidation of fuel in the fuel-rich region of this plume. It is

postulated that within the plume, the precursors form soot primary particles that are spherical. Such particles begin to agglomerate and subsequently encounter the diffusion flame and are mostly oxidized at temperatures around 2500K, but it is thought that some survive due to localized quenching and remain in the combustion chamber. As the piston moves downward, the system cools rapidly. At this stage, if there are other non-volatile gaseous species (such as metals) with very high concentrations, they will deposit on the carbon particles or may alternatively self-nucleate if the rapid cooling drives their saturation ratios high enough. As the resulting aerosol travels through the exhaust system, further cooling causes semi-volatile species such as polycyclic aromatic hydrocarbons (PAH's) to condense onto the particles. When the aerosol exits the tailpipe it again cools rapidly and other more volatile species condense suddenly and/or self-nucleate into nanoparticles. The resulting complex mixture of particles is what we call DPM.

5.1.2 DPM Chemistry

Both chronic and acute health effects have been shown to be associated with DPM and one theory suggests that the ultrafine and nano-sized particles, i.e., particles less than about 100 nm in diameter, may play a key role in this (Utell and Frampton, 2000; Donaldson and Stone, 2003). Although techniques have been developed to characterize the size of such small particles (Kittelson, 1998; Abdul-Khalek, et al, 1998, 1999), more important factors resulting in adverse health effects may be related to their chemical composition (Costa and Dreher, 1997). Traditionally, the chemical analysis of aerosols requires sample collection followed by off-line analysis. Such analysis can suffer

from artifacts arising from reactions within the collected sample itself or between the sample and the substrate (Appel and Tokiwa, 1981) and can often only give results corresponding to bulk properties. Several newer methods utilizing mass spectrometry for chemical analysis of single particles provide simultaneous size information (Suess and Prather, 1999), but most such mass spectrometers employ light scattering for sizing the DPM. Since the intensity of scattered light reduces sharply for particles below 200 nm, the lower limit of measurable particle size is typically around 200 nm. Tobias et al. (2000) reported that a thermal desorption mass spectrometer could simultaneous measure the size and chemical composition of ultrafine particles, but their evaporation method (electrical heater in quadrupole cell) allows only the measurement of the volatile species coating the DPM, or the self nucleated particles of sulfate or organic carbon. The issue of chemical composition and its links to particle formation scenarios is, therefore, complex and remains elusive. When I designed the experiment described in this chapter, I predicted that the recently developed SPMS, employing a much strong laser, might overcome the above current limitations.

The work described here specifically addresses the issue of metals in DPM. Metals in diesel exhaust may originate from sources such as trace metals in the fuel, the use of metallic fuel additives for enhancing regeneration of diesel particulate filters (Stratakis and Stamatelos, 2003), or from lube oil additives that enter the combustion chamber via reverse blow-by of the piston rings. The role of such metals in the chemistry of DPM formation remains a challenging topic of investigation. The research described here aims at providing insight into the formation of metal-rich nanoparticles via self-nucleation as

well as the overall distribution of metals across a wider range of particle sizes due to adsorption, condensation and coagulation.

5.1.3 Research Approach

The main goals of this work are to quantify the amount of metal in various sizes of DPM and to investigate how metal levels during combustion may affect the chemistry of particle formation. The research approach taken was to use a diesel engine to generate exhaust particles and to dope the fuel supply with ferrocene to introduce metal (iron) into the combustion process. The resulting iron-bearing diesel exhaust particles were analyzed using a recently developed single-particle mass spectrometer (SPMS) that is capable of determining the elemental composition of both fine and ultrafine particles (Mahadevan, et al, 2002), and as outlined in the following sections, the particle size may also be derived from the same measurement.

Lab testing entailed running the diesel engine and routing a sample of the diluted exhaust aerosol to a scanning mobility particle sizer (SMPS) and to the SPMS for analysis. (Note the similarity in acronyms.) The latter generated mass spectra for large numbers of individual particles. Subsequent analysis of the spectral data provided insight into not only the elemental composition of particles that make up the DPM aerosol but also the size-preference of the elements. Additional offline particle analysis was conducted using transmission electron microscopy (TEM) and energy dispersive spectroscopy (EDS). The offline results are covered only briefly, as the bulk of that work will be described in chapter 6.

The following section describes the experimental setup including details about the SMPS, SPMS and its aerodynamic lens inlet, the data processing software and the engine and sampling arrangement. The subsequent section includes various presentations of the SPMS data that show elemental composition of particles, as well as discussion of those results. In that section, three distinct classes of particles are identified and data presented which support that observation. The final section summarizes the highlights of the data analysis.

5.2 Experimental Setup and Procedures

The source of diesel particulate for this work was an Onan-Cummins "QuietDiesel" genset powered by a three cylinder, 1.5 liter Isuzu engine. This unit is capable of providing 10 kW of continuous AC power at a fuel flow rate of about 4 kg/hr. In order to maintain a steady 60 Hz of AC current from the generator, the fuel flow to the engine is controlled by an electronic governor actuator that maintains a constant engine speed of 1800 rpm. The load on the engine is provided by loading the generator outlet with a resistive load bank made by the Simplex Company. For most of our experiments, the engine was run at two conditions, i.e., no-load and 6 kW load. The corresponding fuel flow rates were 1.0 kg/hr and 2.25 kg/hr. It should be noted that the size distribution of particles generated by this relatively small engine varies somewhat from that of typical heavy duty engines. Under normal operating conditions it produces no discernable nuclei mode and the accumulation mode decreases with engine load rather than increases as it does for most larger engines.

The fuel used for all tests was #2 diesel fuel with nominal sulfur level of 350 ppm. To dope the fuel with iron, small amounts of ferrocene powder/crystals, i.e., $(C_5H_5)_2Fe$, were measured using a milligram scale and mixed with about 200ml of fuel in a beaker. This was heated on a hot plate to 60 deg C and stirred with a magnetic stirrer for 30 minutes until all the ferrocene was dissolved. The solution was then blended with the appropriate amount of diesel fuel to achieve the desired doping level. For example mixing 4 gm ferrocene (0.301 mass fraction Fe), with 20 kg fuel yielded about 60 ppm of Fe in the fuel.

5.2.1 Particle Sampling

The particulate matter for SPMS analysis is drawn from the tailpipe as shown in Figure 5.1. The 3.8 cm diameter exhaust line is connected to a fume hood system via a 10-cm-diameter pipe, and a 20-cm-long, 3 mm-ID stainless steel probe draws a sample about 15 cm from the muffler exit at a flow rate of about 5 lpm. The probe is inserted through the tailpipe wall and directed into the exhaust stream. The opposite end of the probe is attached to the inlet of an AirVac-TD260H vacuum pump that acts as an ejector dilutor as described in previous work (Abdul-Khalek, et al, 1999). The dilutor is fed a supply of 30 psi (200 kPa) dry air at room temperature. Cold-flow calibration using a bubble flow meter at the dilutor inlet and a rotameter at the outlet, yielded a dilution ratio of approximately 10:1 for this setup. For measurements of particle size distribution with the SMPS, the flow was further diluted as shown in Figure 5.1 using a second ejector dilutor. Note that all SMPS data in this report have been dilution-corrected to represent tailpipe conditions.

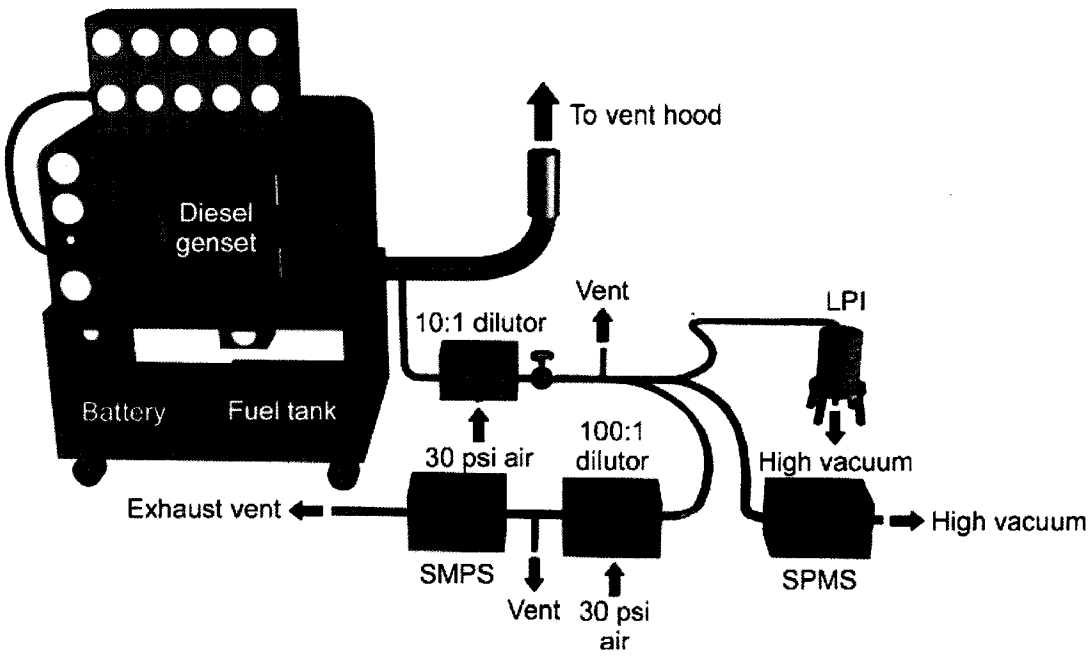

Figure 5.1 - Sampling and dilution of DPM using exhaust probe and ejector dilutor.

5.2.2 Particle Size Measurement Using the Scanning Mobility Particle Sizer

Particle size distributions were measured using an SMPS (Wang and Flagan, 1989). The SMPS system used in this experiment was built in-house at the UMN and is a modified version of a TSI instrument, consisting mainly of a particle neutralizer (Po210), a "long-column" differential mobility analyzer (DMA), a TSI model 3010 condensation particle counter (CNC), and data acquisition PC. The incoming aerosol enters the system through a critical orifice at a flow rate of 1.0 lpm and filtered sheath air is recirculated in the system at 10 lpm by an adjustable blower. The PC computer interfaces with the DMA voltage supply and scans the voltage from zero to ten kilovolts and back, over a four-minute period. The data acquisition stores voltage and particle number counts which are then used to determine size distribution after correction for charge distribution, aerosol residence time and voltage ramping effects.

5.2.3 Single Particle Mass Spectrometry

A schematic diagram of the SPMS used in this study is shown in Figure 5.2, and is slightly modified from that described in a recent publication (Mahadevan, et al, 2002). The components of the system consist of an aerodynamic lens inlet, three-stage differential pumping system, free-firing dissociation/ionization laser and optics system, linear time-of-flight mass spectrometer, and data acquisition system composed of a high-speed digital storage oscilloscope and a PC. Details of the components and their working principles are described elsewhere (Mahadevan, et al, 2002).

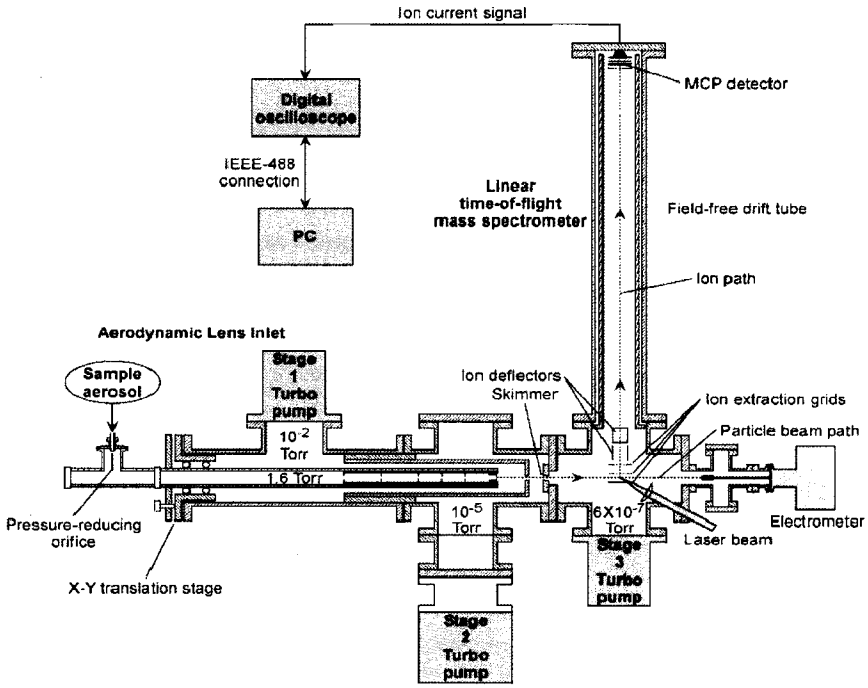

Figure 5.2 - Schematic of the time-of-flight single particle mass spectrometer (SPMS).

The pressure in the inlet tube downstream of the pressure-reducing orifice is 1.6 Torr when the pressure upstream of the inlet is maintained at 1 atm, while the pressure in the first stage vacuum chamber, which is pumped by a 250 L/sec turbo molecular pump, is $2x10^{-2}$ Torr. The second and third stages are pumped with a 1000 L/sec turbo pump and a 210 L/sec turbo pump, which maintain pressures of $1x10^{-5}$ and $6x10^{-7}$ Torr, respectively when the system is sampling. At a distance of 30 mm downstream of the aerodynamic lens inlet, the narrowly focused aerosol beam intersects a laser beam at the center of the extraction plate (see Figure 5.2). The laser used in the system is a frequency-doubled Nd:YAG laser operated at 10 Hz in the internal Q-switch mode. The laser energy measured before the laser entrance window of the mass spectrometer is about 100 mJ/pulse. The power density of a 5 ns laser pulse focused at the center of the extraction region (see Figure 5.2) is estimated to be approximately 2.8×10^{10} W/cm^2 assuming the beam diameter at the focal point is 0.3 mm. Each laser shot is detected with a photodiode sensor to initiate time-of-flight measurement in the data acquisition system.

When the laser hits and disintegrates a particle, atomic ions comprising the particle are generated in the extraction field of the mass spectrometer. The positive ions with one or more elemental charges are accelerated along the one meter long, linear-time-of-flight tube and detected by microchannel plates. The temporal ion signals are captured by a 500-MHz digital storage oscilloscope and stored on PC via GPIB connection.

Examples of typical particle mass spectra are shown in Figures 5.3a-c. Note that although there are some molecular fragments (C_x, N_2, O_2/S), the particles were generally ablated to their elemental constituents. The peaks at m/z = 32 are likely a combination of O2 derived from dilution air and sulfur derived from the fuel or oil. Though much of the

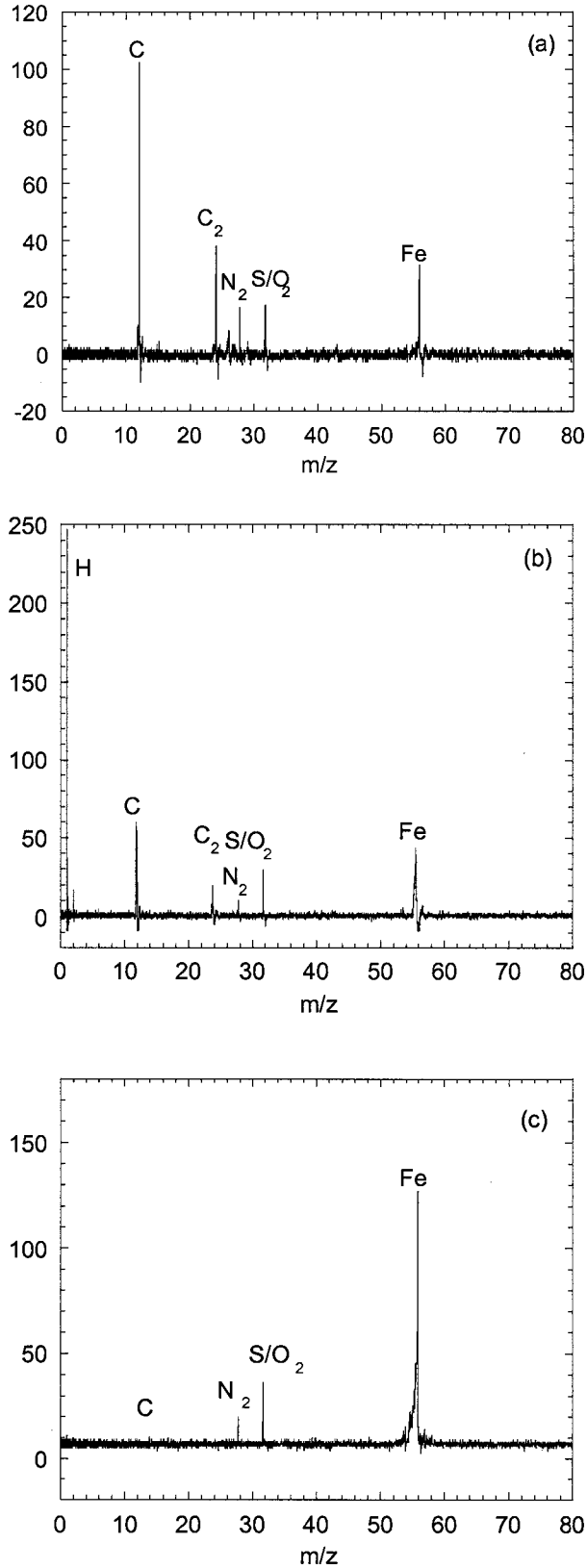

Figure 5.3 - Classified examples of diesel SPMS (a) elemental carbon, (b) organic carbon, and (c) pure iron with possible small carbon content.

sulfur leaves the tailpipe as SO_2, a few percent of sulfur is known to convert to particulate sulfate and could thus contribute to that peak. We also considered the effect of background (BG) ions or molecules such as N_2 and O_2, which may give or take electrons via collision with primary ions or neutrals generated from the particle. This so-called "matrix effect" or "charge transfer effect" is likely not significant here, for the following reasons. First, there are relatively few collisions due to the very low pressure surrounding the laser focal volume. Second, the mean absolute BG signal intensity in the presence of particles is quite similar to that with no particles introduced to the SPMS, i.e., the BG signal originates from direct ionization of BG due to the high intensity of the laser used.

Thousands of such spectra were collected during the course of this work. Each spectrum is unique, as is each particle. Key to our analysis of the particles is the application of customized software developed for quickly sorting data files, and providing statistical analysis of the relative size of all spectral peaks for multiple elements. The software also allows for rejection of "bad hits", which are spectra containing only BG signals, or dominated by BG noise. For our purposes, all O_2 and N_2 signals were considered to be noise, induced by the presence of air in the aerosol stream.

5.2.4 Correlating Particle Size with SPMS Signal Intensity

In principle if all atoms in the particle were converted to ions and the flight tube transported all ions to the microchannel plate, the integrated ion spectra would yield a direct mass measurement for the particle. However, we know that the above constraints

are never met in our system. We have however developed a way of determining particle size from the SPMS signal intensity.

This was done using the following procedure. The transmission efficiency of nanoparticles through the lens and skimmers was first measured as a function of size by measuring the electrical current generated by size-selected charged particles of NaCl before and after the inlet assembly. Next, PSL spheres of known size were sampled and the SPMS signal intensity was correlated with their volume, yielding a correction factor. Finally, the size distribution of the diesel aerosol was measured using an SMPS, while numerous single particle mass spectra were collected using the SPMS. The signal intensities of the spectra were used along with the correlation factor to estimate the original particle volume. It is notable that the correlation is not linear but rather is best fitted by a power function. This is ascribed to the size-dependent ion losses during their transport from the laser focus to the detector, due to the size dependence of energetic ion formation. Details on this topic will be described in subsequent publications (Lee, et al, 2004).

It is notable that the above procedure is based on data generated using relatively compact particles of NaCl and PSL. The more complex shape factor of diesel particles and thus variability in aerodynamic diameter will influence how well they are focused by the aerodynamic lens. In spite of this limitation, the estimated size distribution of SPMS-sampled particles correlates reasonably well with SMPS data from the diesel particles (Figure 5.4).

From the measured size correlation factors, we found that $D_v=29.135\ PA^{0.71}$ where PA is the total peak area of the SPMS signal. Using this nonlinear size correlation

function, volume-equivalent sizes of original particles were obtained straightforwardly from a large set of mass spectra. The resulting size distribution is then correlated with the original size distribution of particles by dividing the SPMS-measured distribution by the transmission efficiency. Since the mass of diesel exhaust PM has been shown to be well correlated with mobility size (volume = 5.1523 $D_m^{2.31}$) (Park, et al, 2003), the volume data (SPMS) was converted to D_m to allow direct comparison between results from the SPMS and the SMPS. The mobility size distribution for the volume data from the SPMS (dN/dD_m) is then obtained by counting the number of mass spectra of particles whose size lies in each constant bin and then dividing the number by the bin_size. As for the SMPS data, it is usually presented as $dN/d\log D_m$ rather than dN/dD_m due to its intrinsic size-dependent mobility bandwidth (dZ_p). Since the size/bin allocation of particles passing through the DMA slit is proportional to their size, converting from dN/dlogDm (SMPS) to dN/dD_m requires multiplying by a constant $\Delta\log D_m$ (0.06235) and then dividing by the appropriate size D_m, i.e. the relation dN/dDm=dN/dlogDm(SMPS)/(Dm*ln(10)) is used in converting from dN/dlogDm (SMPS) to dN/dDm for direct comparison of the two data sets as shown in Figure 5.4. Note that since the y-axis units of the two distribution curves were not the same, we normalized them by multiplying each data point by the ratio of peak values for the two curves.

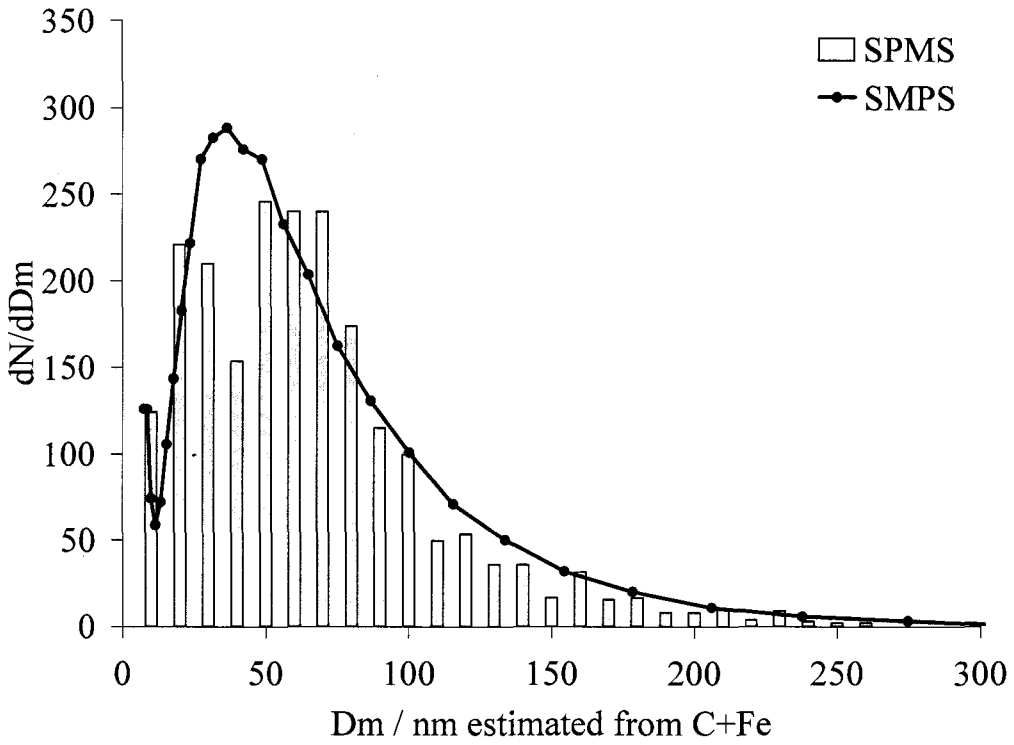

Figure 5.4 - Comparing SMPS size distribution and SPMS-derived mobility diameters for Fe-doped diesel exhaust at 0 kW engine load.

The match of the two size distributions indicates reasonable correlation of signal intensity to particle size and the agreement is especially good for the larger particles. The smaller particles, due to their high diffusivity, have poor collimation in the aerodynamic lens, and therefore poor transmission efficiencies to the ablation laser. This is evident in that the mobility sizing (SMPS) measurements under both engine load conditions (especially for the higher doping case) show high concentrations of particles less than 30 nm for which our mass-spectrometer only occasionally registered hits. It should be noted that the electrical current measurements, used for the estimation of transmission efficiency, were lower for smaller particle sizes and were eventually comparable to noise for particles less than 30 nm, partly due to low concentration of

nanoparticles in the calibration aerosol. The transmission efficiency was thus assumed to be constant in the range 10-30 nm.

5.3 Results and Discussion

In this section we discuss the determination of particle composition from the SPMS data, with an eye toward quantifying the distribution of iron on particles of various sizes. For these experimental conditions, the vast majority of the particulate matter consists of H, C, and Fe, so we will focus on those three elements. The relative proportions of these elements were derived from the ratios between peak areas in the particle mass spectra, the validity of this assumption has been reported in our prior work (Mahadevan, et al, 2002). We thus determined both the size and elemental composition for each of many particles and used this to investigate the distribution of a particular element (say Fe) across the measured particle size range.

(a)

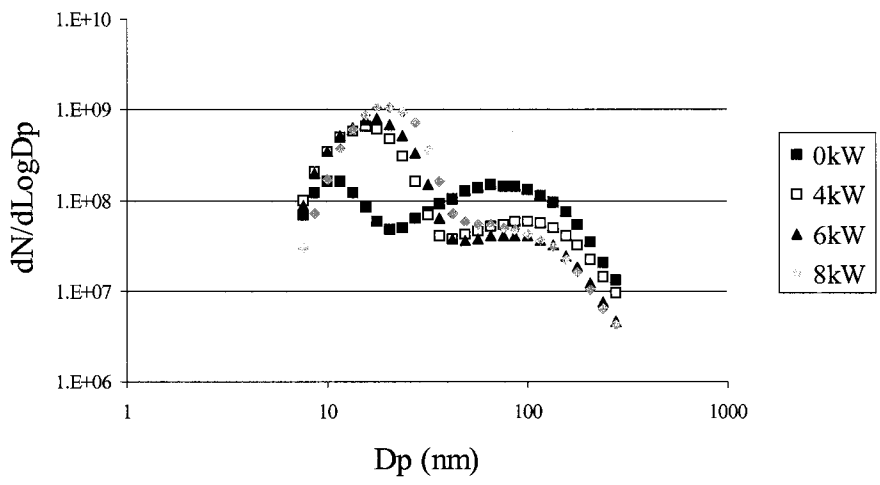

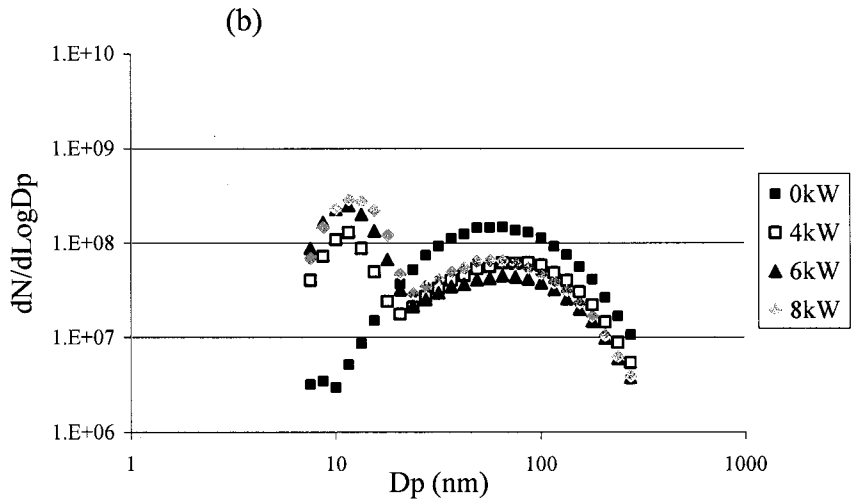

Figure 5.5 - Number-weighted size distribution of diesel particles at different engine loads (a) with 60 ppm iron added to the fuel and (b) with 20 ppm iron added to the fuel.

5.3.1 Particle Size Distribution

Figure 5.5a shows that when the fuel is doped with 60 ppm iron, the size distribution of particles contains a distinct nuclei mode that increases with engine load. This increase in self nucleated metal particles reflects higher Fe concentration in the system. The higher concentration results from the simultaneous increase in load and thus fuel flow rate. Since the rpm is constant, metal throughput increases. As the doping rate is reduced to 20 ppm (Figure 5.5b), the iron content is lowered and the nuclei mode eventually disappears at 0 kW engine load as illustrated in the figure. Note the difference of the vertical axis in Figure 5.5 ($dN/dlogD_m$) compared to dN/dD_m in Fig. 5.4. For both doping levels (Figures 5.5a and 5.5b), the size distribution is strongly bimodal in the range measured by the SMPS and the dilution-corrected total number concentrations vary from about $5x10^7$ #/cc to about $5x10^8$ #/cc (higher numbers being reflective of the increasing number of nuclei mode particles at high engine load). The accumulation mode

particles are shown to decrease as load (and thus both engine temperature and metal content) goes up, especially during the initial increase from 0 kW to 4 kW load. That is not surprising since this engine produces less soot at higher loads, but it is also possible that the metal-enhanced oxidation of carbon may play a role as observed in an earlier work (Jung, et al, 2004).

We surmised that if the appearance of the nuclei mode is directly attributable to self-nucleation of iron then there should be a direct correlation between the Fe concentration in the system and the volume of nuclei mode particles (~ less than 20 nm) for each condition. Figure 5.6 shows the relationship between Fe concentration and total volume of particles less than 20 nm measured by the SMPS, i.e., as in Figure 5.5, for several different engine conditions. The Fe concentration was obtained for each operating condition as the product of doping level and fuel flow rate, divided by the volumetric flow rate through the engine. It is evident from the first two data points on the left that there is a "baseline" volume of small particles for this engine that is independent of the presence of metal. This baseline we attribute to the "tail" of the non-iron containing accumulation mode. Note that if the assumption of unit density were made, the Y axis units could be converted to ug/m3, and one could use the slope of the data curve to speculate on the recovery rate of iron. If the specific gravity were assumed to be around 5 or 6 (a reasonable assumption for iron oxide particles), the data would suggest a recovery rate higher than 100%. This of course is not feasible and may be clouded by the contribution of non-iron species to the nuclei mode volume, however it suggests that the nuclei mode may contain a significant amount of the iron in the system.

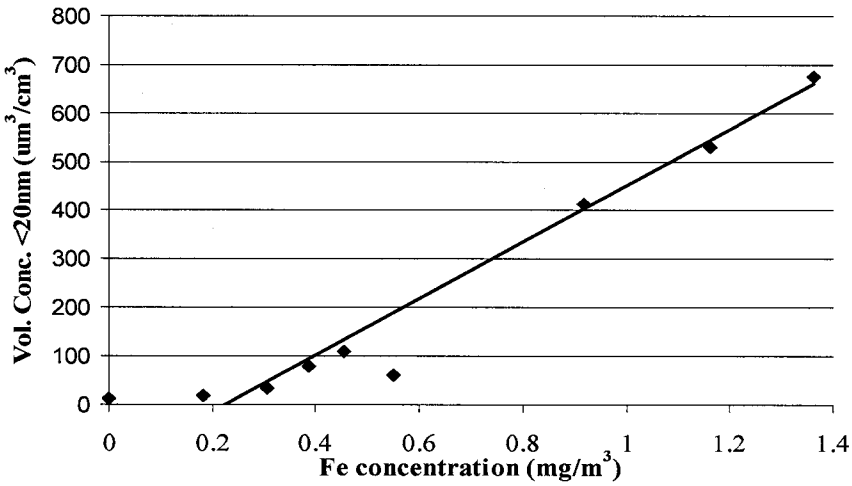

Figure 5.6 - Total volume of nuclei mode particles (<20 nm) as a function of Fe concentration in the exhaust.

The data show that starting at a "threshold" value of about 0.2-0.25 mg/m^3 of Fe in the system, the volume (and thus mass) of self-nucleated particles increases linearly with increase in the Fe concentration. This threshold value corresponds to a critical Fe/C ratio at which self-nucleation of metallic particles first begins. Further increase in Fe input simply adds to the number and size of such nucleated particles. This is an important result in view of new engine technology designed to meet future emission standards, which employs precise control of high-pressure fuel injection to reduce NO_x and particulate (carbon) emissions. These "cleaner" engines, which have a reduced carbon particulate matter emission, will presumably have increases in the metal to carbon ratio and enhance the likelihood for formation of metal nanoparticles.

5.3.2 Particle Mass Spectra Sorted by Class

Due to the wide distribution of aerosol composition as observed in the mass-spectra, we found it useful to sort the spectra by general class. To do this we counted on previous knowledge of particle morphology in the nuclei and accumulation modes of typical diesel exhaust. The nuclei mode of DPM is generally considered to consist of two particle types; nonvolatile inorganic ash that nucleates at high temperatures in the engine (Abdul-Khalek, et al, 1998; Kittelson, et al, 2002), and condensed volatile materials such as sulfates and unburned fuel or oil which self nucleate later during the dilution/cooling of the exhaust aerosol (Sakurai, et al, 2003). The accumulation mode on the other hand, which would be the third type of particle, is said to consist mainly of "spherules," i.e., primary particles of elemental carbon, coagulated into agglomerates, with other materials adsorbed onto the surface. To verify this for our case we took DPM samples for TEM/EDS analysis using a low-pressure cascade impactor (LPI) (Hering, et al, 1979). Figure 5.7 shows a TEM image which contains all three of the above mentioned particle types. This sample was taken from the final impactor plate of the LPI and represents particles with aerodynamic diameter around 50 nm. EDS analysis of the two small, dense particles in Figure 5.7 indicate they are composed mainly of iron.

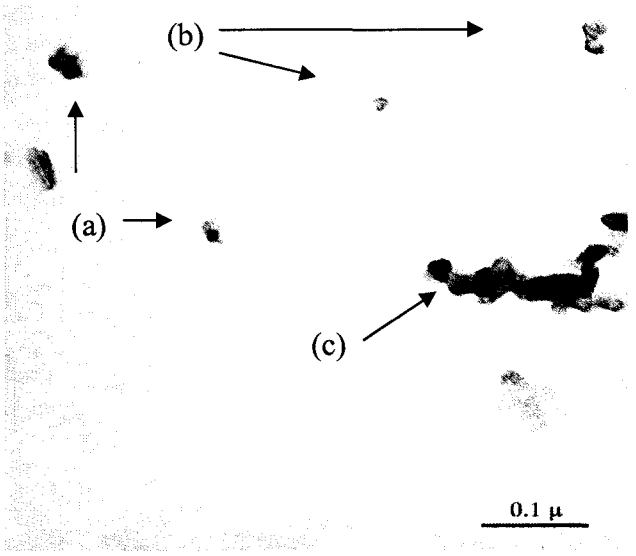

Figure 5.7 - TEM micrograph of size-selected DPM, showing: a) nucleated iron particles, b) hydrocarbon particles, and c) chain agglomerate particle (6 kW load, 60 ppm doping rate).

For the purposes of the following discussion, the particle mass-spectra were sorted into three basic particle types as follows. Note that the values of C, H, and Fe, are molar ratios and are obtained from the areas under the elemental peaks of the individual mass spectra.

1) "Elemental Carbon (EC)" particles, are defined as those where H/C < 1. These are particles containing greater relative amounts of elemental carbon (typically agglomerates of primary carbon spherules).
2) "Organic Carbon (OC)" particles are defined as those where H/C >1. They are typically nanoparticles containing fuel or oil residues rich in organic carbon i.e. rich in hydrogen.
3) "Pure iron" particles, are those where Fe/C > 10. These are the nanoparticles of iron (presumably self nucleated in the engine).

Before looking at detailed particle stoichiometry, we present the SPMS results for these three particle types, in terms of the frequency distribution of each type as a function of particle size. Figures 5.8 and 5.9 show the number-weighted mobility size distributions, for each of the three particle types at two different engine conditions and two different doping rates of iron. Note that particle sizes presented in all figures for the SPMS are mobility sizes transformed from Dv. Although these particle types are by no means definitive, some significant trends are noticeable.

Figure 5.8a shows that at low engine load and high ferrocene doping rate, the "elemental carbon" particles are widely distributed, with a peak at around 70nm, and constitute the bulk of the particulate material, which coincides with the distribution of agglomerate particles i.e. the accumulation mode particles shown in Figure 5.5. Figure 5.8a also shows that the "organic carbon" particles are distributed in the lower size range (< 50 nm), i.e., the lower-side tail of the accumulation mode. Under the conditions for Figure 5.8a we see virtually no "pure iron" particles. This is probably due to higher carbon generation at low load, preferentially facilitating Fe adsorption onto carbon particles rather than nucleation of Fe. The result is that at the lower load, the nuclei-mode iron particles as measured by mobility diameter (Figure 5.5a), are fewer in number and almost all less than 30 nm in diameter, and in that range the mass-spectrometer has poor particle transmission efficiency.

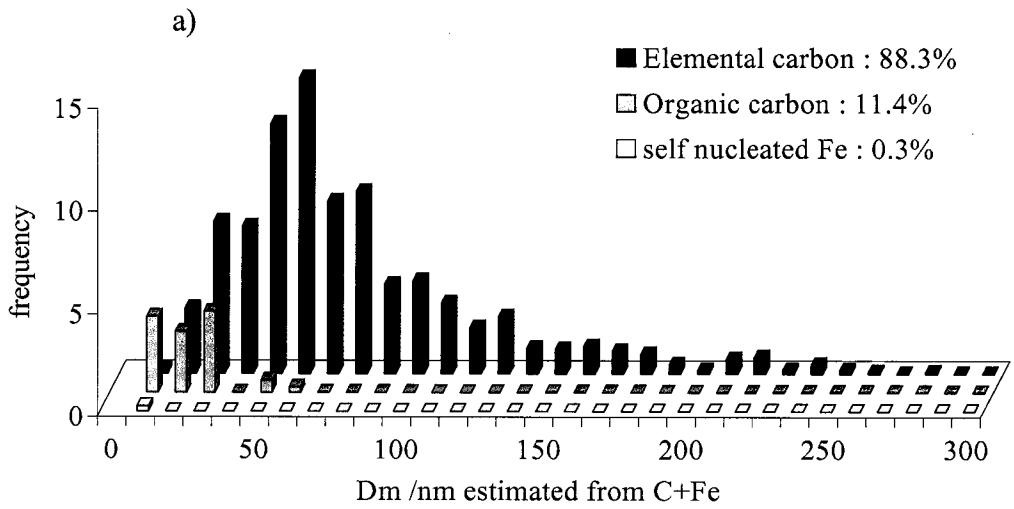

Figure 5.8a - Size distributions for three classes of diesel exhaust particles generated at engine load of 0 kW, using 60ppm Fe doping of the fuel. Note: Percent distributions refer to frequency of occurrence.

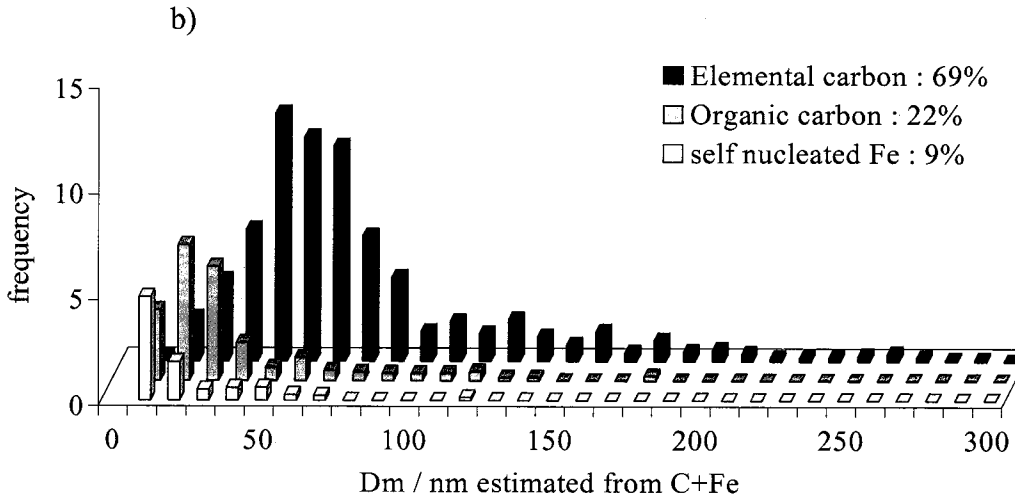

Figure 5.8b - Size distributions for three classes of diesel exhaust particles generated at engine load of 6 kW, using 60ppm Fe doping of the fuel. Note: Percent distributions refer to frequency of occurrence.

At higher engine load, the increase in Fe concentration combined with inherent soot reduction yields a higher Fe/C ratio, so the pure iron particles have increased in number and grown in size to a point where the aerodynamic lens is able to transmit them more efficiently to the ionization laser. This improved transmission of iron nano particles is enhanced by their greater density and thus increased aerodynamic diameter. For this reason it is probable that they are over-represented as compared to say organic carbon nanoparticles. Figure 5.8b shows that at 6kW engine load, about 9% of the detected particles (by number) are pure iron nanoparticles. Note that in this figure the size distribution of the elemental carbon particles has not changed significantly, which is consistent with the SMPS measurement in Figure 5.5a.

For the lower iron doping case (Figure 5.9ab), size distributions are similar to those for the higher doping case (Figure 5.8ab). Again at the low load, we see an absence in the mass-spectra of pure iron particles and as discussed previously we attribute this to a transmission efficiency effect. The lower load gives a wider size distribution of the elemental carbon particles (Figure 5.9a) and one might be tempted to see in the data a bimodal distribution. It should be kept in mind that the definition we employed to distinguish organic and elemental carbon is arbitrary and the bimodal-looking distribution may be associated with particles that are of an organic carbon type but did not fulfill our definition of H/C of > 1. A further discussion of that point is presented in the next section.

(a)

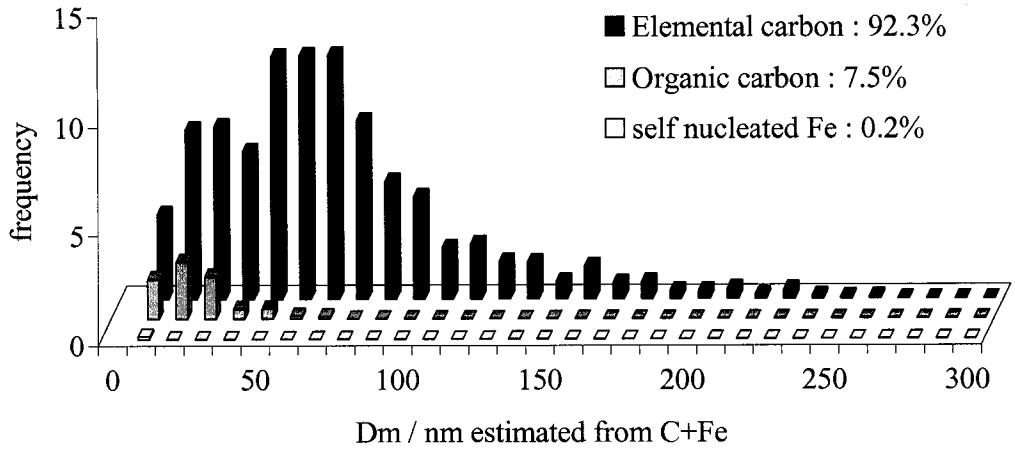

Figure 5.9a - Size distributions for three classes of diesel exhaust particles generated at engine load of 0 kW, using 20ppm Fe doping of the fuel. Note: Percent distributions refer to frequency of occurrence.

(b)

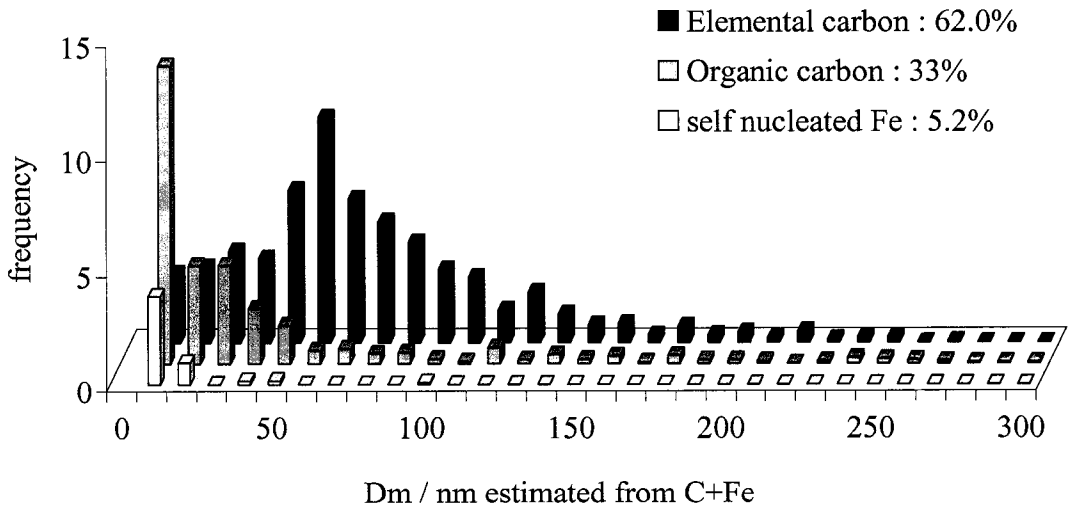

Figure 5.9b - Size distributions for three classes of diesel exhaust particles generated at engine load of 6 kW, using 20ppm Fe doping of the fuel. Note: Percent distributions refer to frequency of occurrence.

In general we see that the appearance of self-nucleated particles is promoted at high engine load because of the higher fuel flow rate and therefore higher iron injection rate, combined with lower carbon (soot) content. The effect of increasing the iron doping rate is to directly increase the iron content in the nuclei mode, while the effect of engine load is coupled with doping rate via the rate of fuel flow. The combined effect of both these influences is perhaps best reflected in Figure 5.6. The relative number of "organic carbon" particles was shown to be greater for the higher engine load cases which can be attributed in part to reduced emissions of elemental carbon as engine load goes up (somewhat unique to this engine), which results in apparent increase in organic carbon relative to elemental carbon. Further discussion of the latter point will be included in the following section. The relative frequency of elemental and organic carbon particles varied somewhat, possibly due to the fact that our distinction between these two classes based on a fixed ratio of H/C is somewhat arbitrary and the fact that on a shot-to-shot basis, hydrogen content of particles varied greatly.

5.3.3 Detailed Elemental Composition

In the following discussion we look more closely at the composition of the diesel exhaust particles. We present results (Figures 5.8-5.14) that illustrate the analysis of numerous mass spectra to observe trends in particle properties, namely the amount of various elements in each particle.

Elemental Carbon Particles

The data in Figures 5.8 and 5.9 show that the distribution of EC particles measured by the mass-spectrometer is similar to the accumulation mode of the particle size

distribution as measured by the SMPS, and is relatively independent of iron addition. It is also notable that as load and thus Fe concentration increases, the absolute number of these accumulation mode particles decreases (note the difference between the no-load and 4kW cases in Figure 5.5). Such reduction is somewhat expected since this engine produces less soot at higher loads, but it is also possible that metal-enhanced oxidation of carbon is taking place. This is suggested by earlier studies (Gratz, et al, 1992; Bonczyk, 1991: Otto, et al, 1980; Miyamoto, et al, 1987), which describe how the presence of metal deposited onto carbon particles leads to oxidation of carbon late in the combustion process. It may also be related to soot suppression in the early combustion stages as suggested by one study (Miyamoto, et al, 1987).

The latter issue is a matter of considerable discussion in the literature. It has been shown that for premixed flames (Ritrievi, et al, 1987), addition of metal triggers the self nucleation of metal oxide nanoparticles, which form prior to the soot, and in fact enhance soot production by supplying sites for subsequent condensation of carbon, thus encouraging soot formation. However, it is not clear at this moment whether such metallic-core particles would have any different surface reactivity than pure carbon particles. On the other hand, laminar diffusion flames, which in theory are more akin to diesel combustion flames, have been shown to display the same behavior i.e. early generation of metal-oxide nanoparticles (Bonczyk, 1991), but (perhaps due to reduced oxygen availability) this process appears to be limited, leaving sufficient metal vapor in the system to form metal oxide partial coatings on the soot particles, evidenced by their high rate of oxidation later in the flame. Neither of these studies indicated that metal played a role in suppression of soot during the combustion process. However, an earlier

study involving diesel engines (Miyamoto, et al, 1987), in which soot concentration was measured in the cylinder as a function of crank angle, suggested that during diesel combustion of metal-doped fuel, soot is not only oxidized due to its metallic coating, but that its formation is also suppressed. In that work, however, the soot measurements were not necessarily taken near the main diffusion flame, so it is still unclear whether the data is applicable here.

Our definition of elemental carbon particles is primarily used to distinguish them from the organic type carbon particles, however it should not be used to imply that these particles do not contain iron. In fact many accumulation-mode particles, which are mainly elemental carbon, also contain some iron. Such particles will be discussed further in the latter part of this section.

Organic Carbon Particles

"Organic Carbon " particles, based on our definition, are more prevalent in the smaller size ranges, which is consistent with a previous observation (Sakurai, et al, 2003) that documented the increase in volatile hydrocarbon species on particles of smaller sizes. The existence of these more volatile hydrocarbon species is reflected in the data of Figure 5.10a-b, which show the relative amounts of hydrogen and carbon for all hydrogen-containing particles at the higher Fe doping rate. The "Organic Carbon (OC)" particles, as defined by H/C>1, are those data points lying above the carbon curve.

Note that for this and subsequent figures, each point on a graph represents the area under one elemental peak from one unique mass spectrum (i.e., one particle). The x-axis reflects the size of the particle analyzed i.e. the mobility diameter calculated using

the correlation described in the previous section. The values on the y-axis reflect the relative amount of each element determined by calculating the area under that elemental peak. For carbon, due to molecular fragments, we sometimes had more than one peak and in that case the area under all carbon-containing peaks would be summed to give the amount of carbon for that particle. These area summations represent the relative contribution of each element in the particle, and therefore give mole fraction or particle elemental stoichiometry. The validity of this has been discussed in our previous work (Mahadevan, et al, 2002).

We observe in Figure 5.10 that the H/C ratios are clearly greater for smaller particles, but the scatter in the data demonstrates how elusive it would be to define a "typical" H/C ratio for diesel particles. The variation in H/C may reflect the locally varied temperature history that the particles underwent, which results in local variation in the (partial) burning of fuel and lube oil, as well as variation in the vapor deposition history.

Note that for particle size estimation we use two different schemes. Since the mean diameter of primary carbon particles is around 25~30 nm, if the measured D_v is larger than 30 nm, the D_v is converted to D_m as described above, while if $D_v < 30$ nm, we set $D_m = D_v$, i.e., we assume the particles are spherical. For this reason in Figure 5.10 and subsequent figures, there is a slight inflection in the carbon curve at 30 nm.

The solid line in Figure 5.10 was drawn to indicate that the amount of hydrocarbon deposited to the preexisting iron-bearing carbon particles scales as D_m^2, i.e., approximately to the surface area of the accumulation mode PM. This might imply that a significant portion of the volatile hydrocarbon condenses near the tail pipe, before and

during dilution cooling. Under those conditions the very small sized PM would undergo free-molecular condensation, i.e., where condensation rate is proportional to the surface area of particle cores. At the lower doping level, this same dependence on size (D_m) was found at both engine loads (not shown here). Note that the horizontal axis in the figures corresponds to mobility size of composite particles estimated from the sum of carbon and iron peak areas.

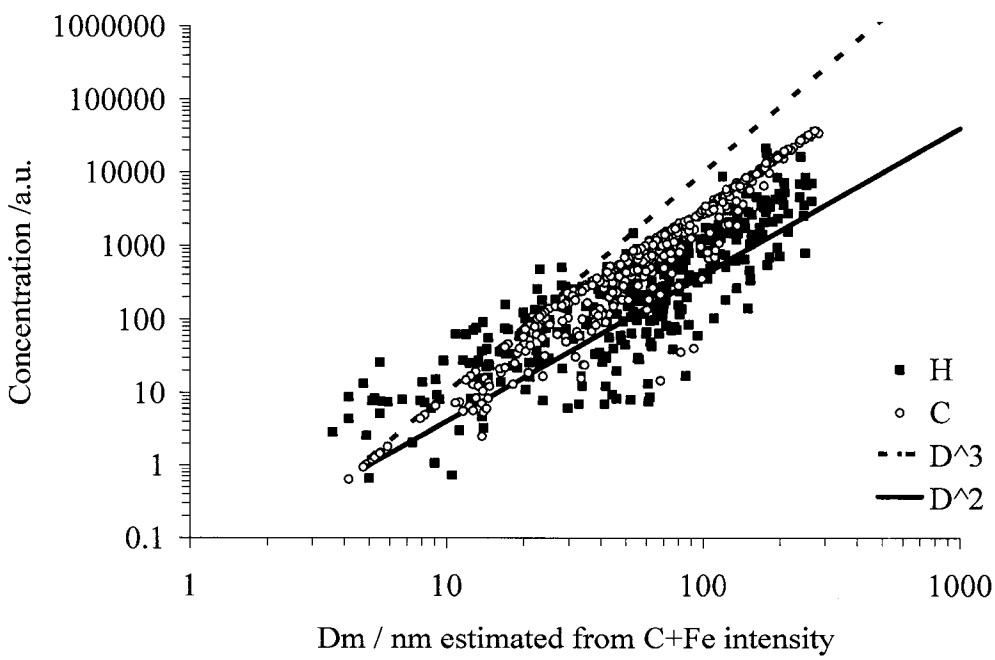

Figure 5.10 - Size dependence of carbon and hydrogen in diesel exhaust particles generated at 6kW engine load using 60ppm Fe doping of the fuel. (Note: Solid line through data shows $D_{m,c}^2$ dependence of elemental concentration).

Pure Iron Particles

We noted earlier that the "pure iron" particles are detected by the SPMS only at high engine loads. At this condition, the concentration of Fe more than doubles due to increased fuel flow rate, while the soot concentration decreases. The combined effect heightens the Fe/C ratio, effectively increasing the super-saturation ratio of iron vapor in the combustion chamber, in turn causing the nuclei mode particles to grow larger and more numerous. At the size of around 25-30 nm they are large enough to penetrate the aerodynamic lens and therefore are detectable. This is best seen in Figures 5.11a-b, which show, for the higher doping rate, higher iron levels for the especially small particles. At the lower engine load (Figure 5.11a) the data shows a tightly banded distribution of iron and a relatively low iron fraction over much of the particle size range i.e. lower engine loads produce less iron relative to carbon because the engine produces more carbon and less fuel is consumed to provide iron. In comparison, Figure 5.11b shows that at higher engine load, many of the smaller particles lie above the carbon curve, suggesting they are "pure iron" particles, while many of the larger particles have iron content similar to the low load case. Overall, the relative amount of Fe is also higher and more variable over the entire size range for the high load case. The latter can be explained by the dominance of mutual coagulation i.e., over nucleation and condensation, between the three types of particles.

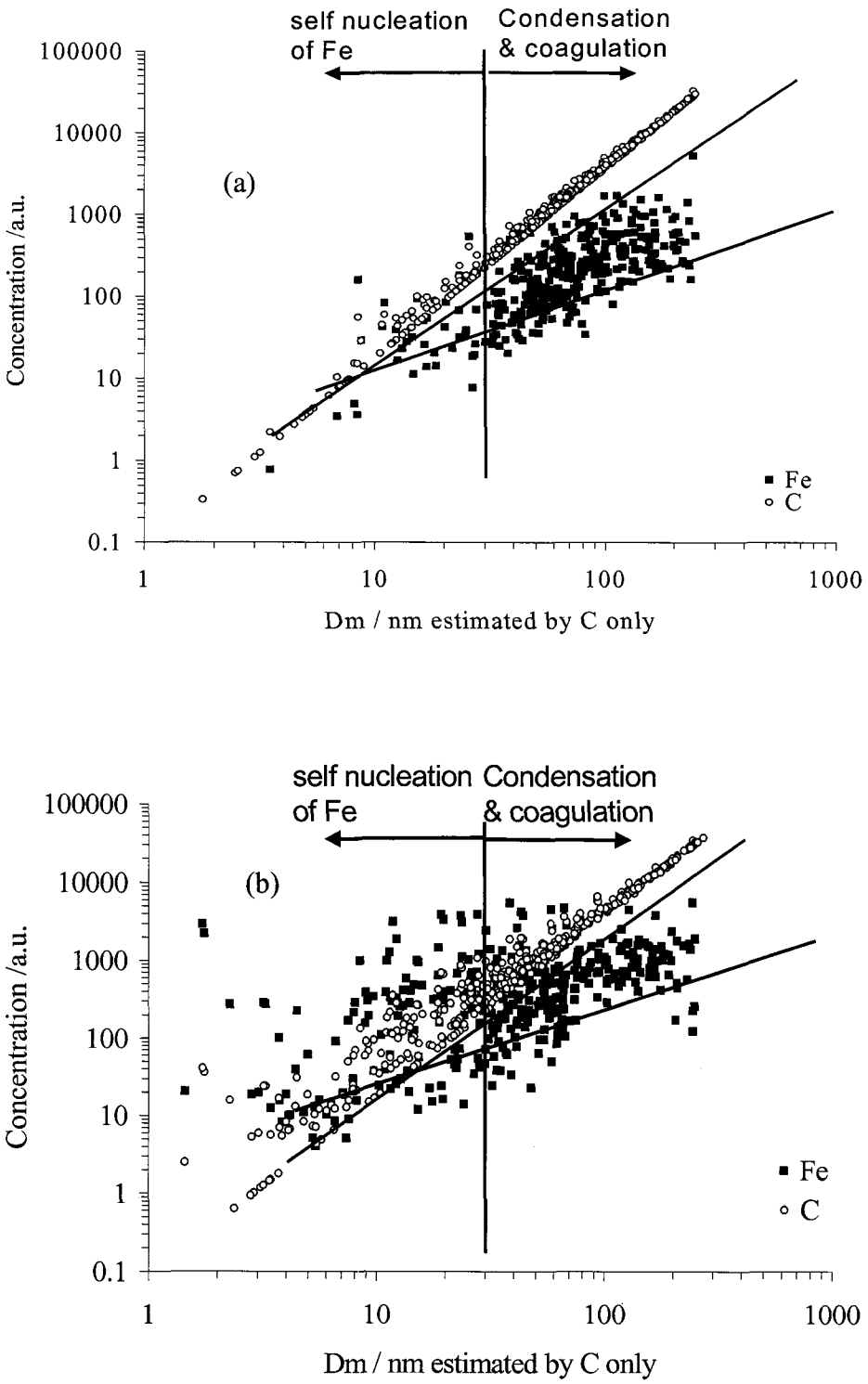

Figure 5.11 - Size dependence of iron and carbon fractions in diesel exhaust particles for the case of 60ppm Fe doping: (a) 0 W load, and (b) 6 kW load. (Note that upper line shows $D_{m,c}^{2}$ while lower line shows $D_{m,c}^{1}$).

Note that in Figure 5.11 the mobility size corresponds to carbon core mobility diameter that was estimated from the carbon peak area only. This was done because we wanted to investigate whether or not the Fe vapor condenses onto preexisting carbon, not the whole PM size (though they are in fact very similar). We postulated that the iron is condensed to the preexisting carbon core or self-nucleated inside the engine cylinder due to its very low vapor pressure. If this is the case, the behavior of particles may lie in the continuum regime, for which the deposition rate of Fe is proportional to diameter (Friedlander, 1977). The slope of the plotted data Fe vs $D_{m,c}$ lies indeed between $D_{m,c}^{1}$ and $D_{m,c}^{2}$, (indicated by lower and upper solid lines, respectively), which is obviously smaller than the slope of H vs D_m in the previous figure. This is not surprising because inside the engine the pressure is very high, moving the particle behavior toward continuum conditions, where the deposition rate of Fe is proportional to $D_{m,c}^{1}$. The results might reflect that the present condition for incorporating Fe is fairly close to the continuum regime. This supports the previous conclusion that the iron deposition is dominated by coagulation of iron primary particles, with each other and/or with larger agglomerates. This is especially true for the higher doping case (Figure 5.11b), which is expected since the population of self nucleated iron particles is much higher for that case.

For lower doping and at low load (Figure 5.12a), the lowest Fe/C ratios are seen, as is the tightest grouping of data. This tight grouping suggests less coagulation effect, and the data points are closer to the lower solid line ($D_{m,c}^{1}$) representing pure condensation in the continuum regime as explained above. For the higher load case (Figure 5.12b), small particles of pure iron are evident (those above the carbon curve), and the effect of their coagulation with larger carbon particles makes the data grouping less tight.

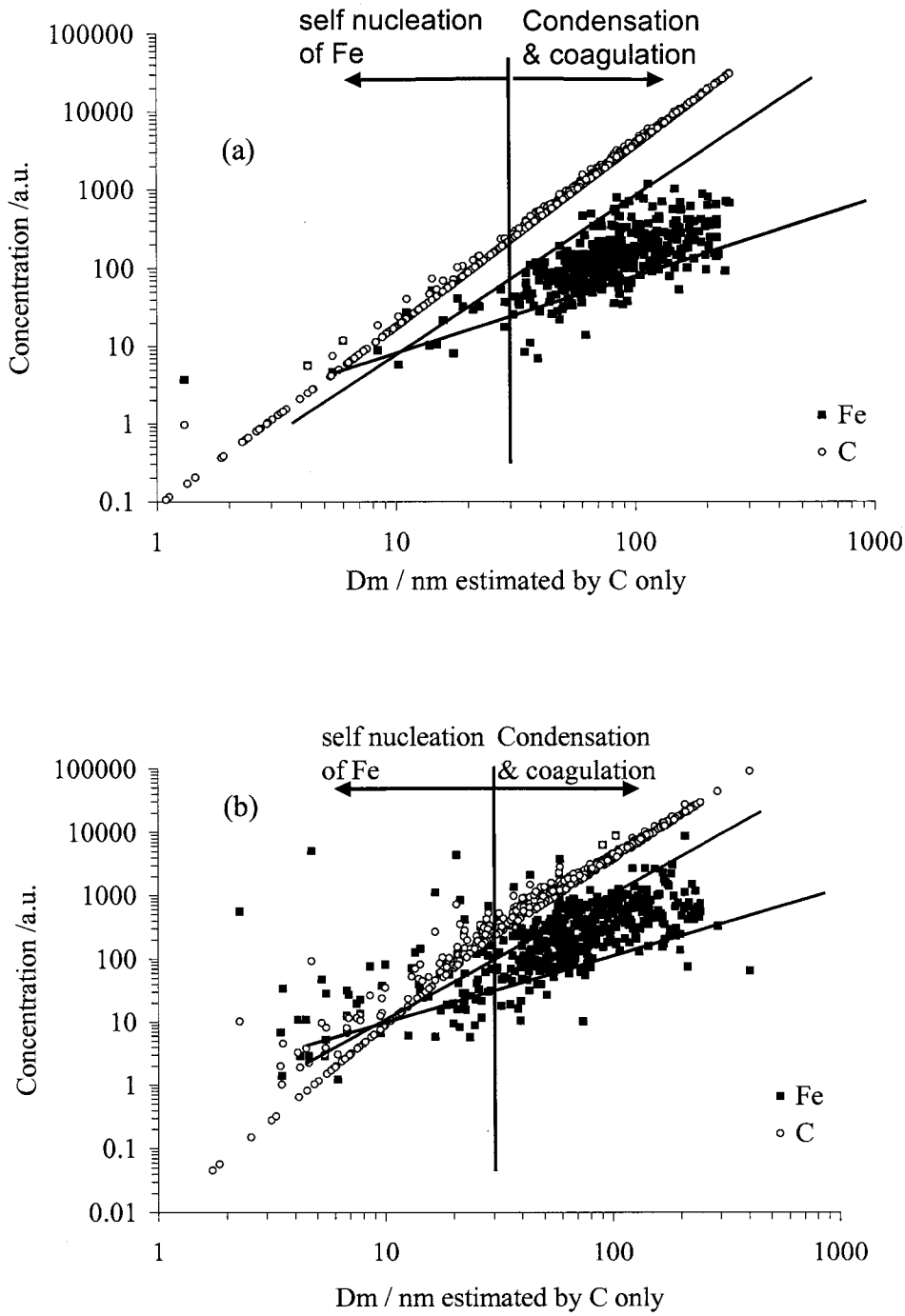

Figure 5.12 - Size dependence of iron and carbon fractions in diesel exhaust particles for the case of 20ppm Fe doping of the fuel: (a) 0 W load, and (b) 6 kW load. (Note that the upper line shows $D_{m,c}^{2}$ while the lower line shows $D_{m,c}^{1}$).

Plotting the Fe fraction of the DPM against $D_{m,c}$ clearly shows the relationship between iron content and particle size. Figure 5.13a shows that at low load and high Fe doping, the iron content increases sharply for smaller particles. At high load (Figure 5.13b) the trend is similar but significantly more particles are high in iron while very few (those on the x-axis) have no iron. In contrast to Figure 5.13a, the data of Figure 5.13b show a similar behavior of iron content, but with increased data scatter. The scatter is believed to be a result of a trend toward coagulation dominance in the aerosol system, which would tend to scramble the distribution. This coagulation is driven by the increase in size and number of self-nucleated iron particles observed at the higher load, i.e. when there is more iron available.

The evidence of condensation is seen most clearly at low Fe doping (Figures 5.14a-b). Similar to the high doping case, the Fe content increases sharply for smaller particles as seen in Figure 5.14b. The data for the low load (Figure 5.14a) represent the lowest Fe/C conditions of all the cases we investigated and for this reason we graphed them in log scale to better show the diameter dependence of iron content under those low-Fe conditions, where little if any self nucleation is taking place. Note that the trend line reflects $D_{m,c}^{1.31}$, suggesting condensation in the continuum regime. This supports the argument that prior to self nucleation, iron is depositing onto the active surface of particles via condensation. In general we see that higher iron concentration, either through higher doping or the indirect effect of higher engine loads (increased fuel flow rate) tends to produce more scatter in the iron size distribution. At low iron doping the results are consistent with a heterogeneous condensation of iron onto carbon. At the higher iron concentrations we observe a much larger nucleation mode consistent with a

higher super-saturation of iron vapor which favors homo vs. heterogeneous nucleation. The self nucleated particles would subsequently coagulate with the accumulation mode particles and thus scramble the tight iron distribution that is depicted in Figure 5.11.

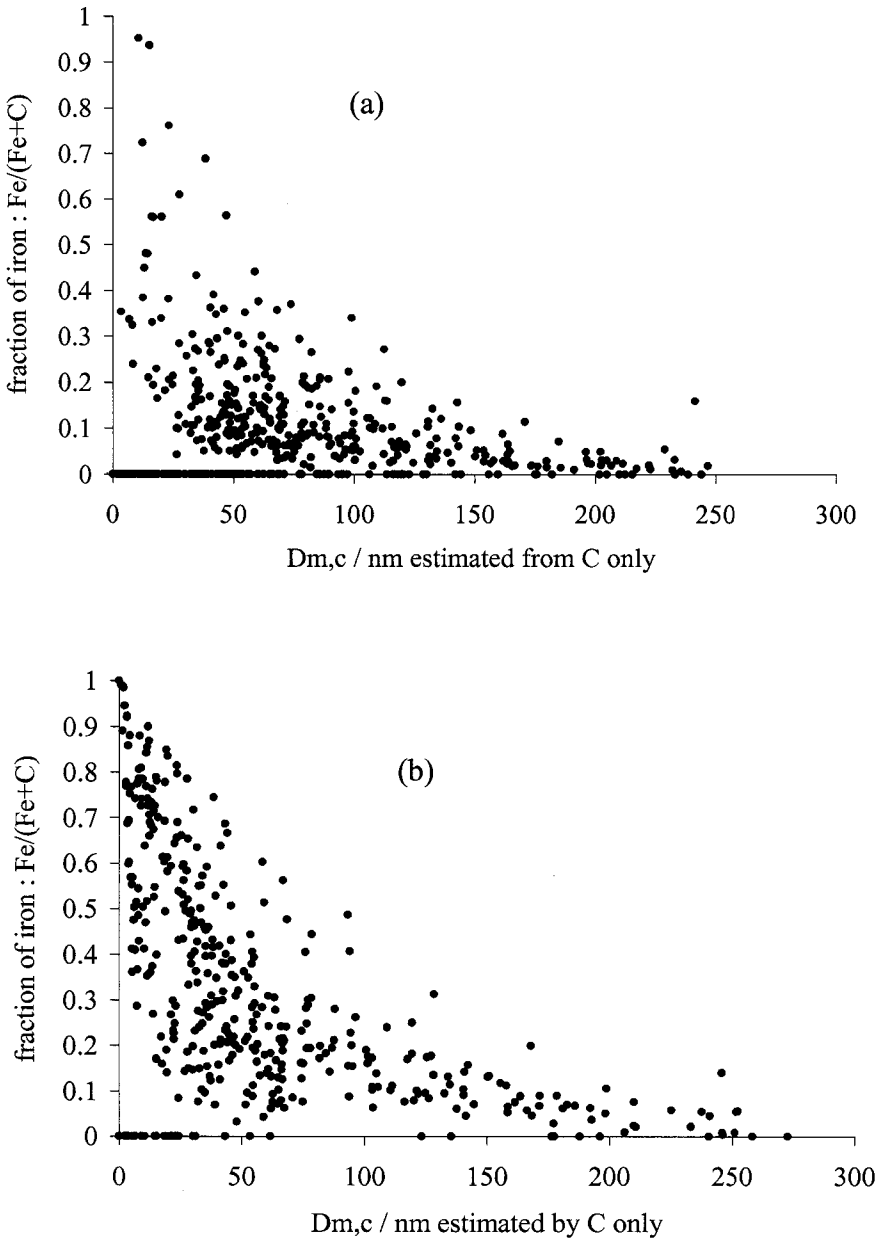

Figure 5.13 - Size dependence of iron fraction in diesel exhaust particles for the case of high (60ppm) Fe doping: (a) 0 W load, and (b) 6 kW load.

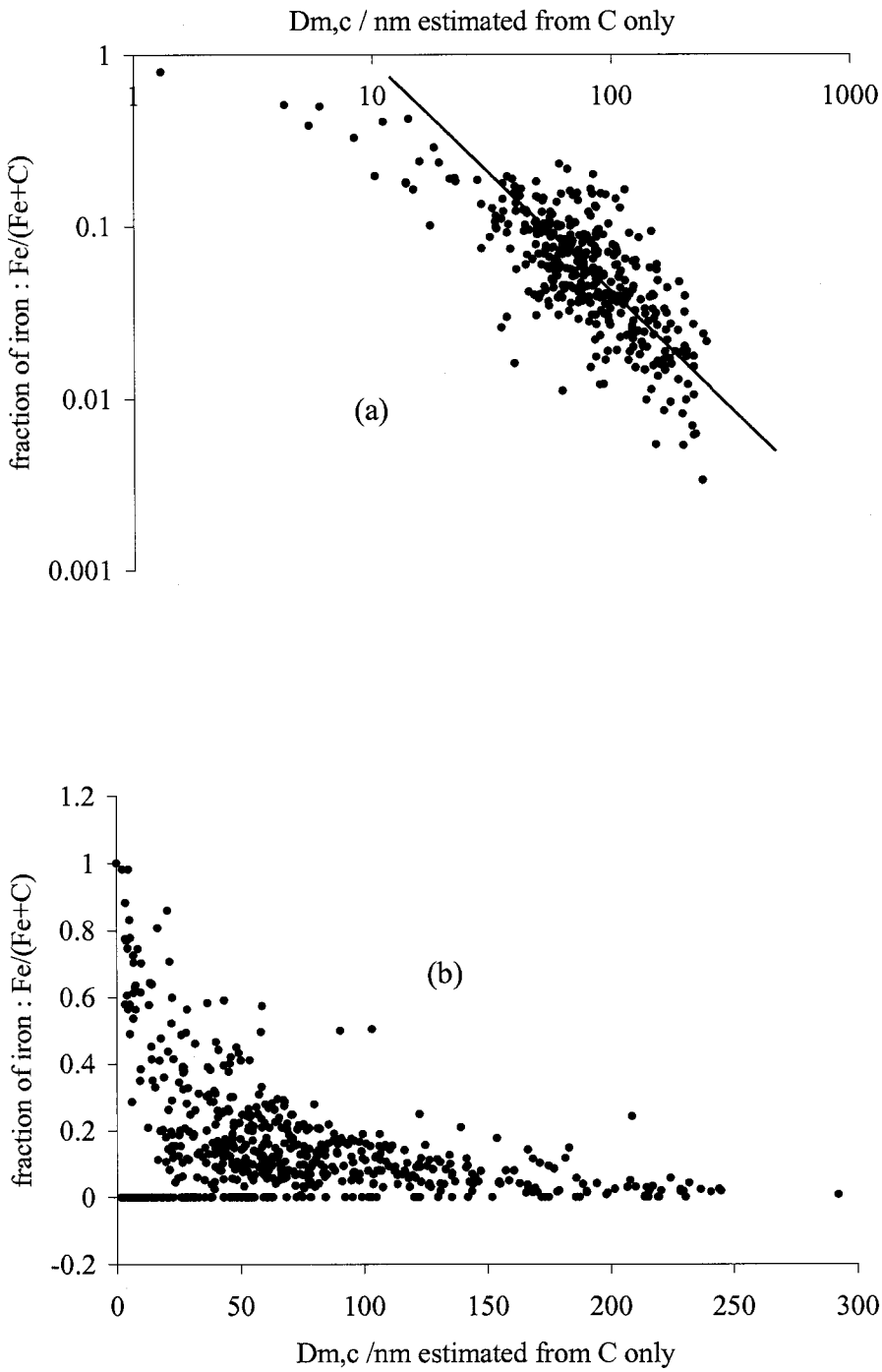

Figure 5.14 - Size dependence of iron fraction in diesel exhaust particles for the case of low (20ppm) Fe doping: (a) 0 W load, and (b) 6 kW load. (Note: solid line through data shows $D_{m,c}^{1.31}$ dependence).

5.4 Conclusions

In this chapter I described the application of single particle mass spectrometry to obtain the size and composition resolved statistics needed to gain insight into the formation mechanisms of metal-bearing diesel particles, for the full size range of DPM, including nanoparticles. For this assessment the DPM was divided into three main particle types: self-nucleated metal-rich nanoparticles, ultrafine particles rich in organic carbon, and larger elemental carbon agglomerates containing small amounts of metal (each type containing a certain amount of adsorbed hydrocarbons).

At the lowest metal doping level, below the onset of apparent self nucleation, metal to carbon ratio as a function of size is well fitted with a $1/D_p$ curve, implying that for this case, metal condensation onto preexisting carbon is a dominant mechanism for DPM to contain metal. In contrast, at higher doping level and higher engine load (higher flow rates of metal-doped fuel), the metal to carbon ratio is greatly scattered over the entire size range, suggesting that coagulation with metal-rich nanoparticles dominates the distribution of metals. Somewhere between these two extremes lies a set of conditions which triggers the onset of metal self-nucleation. This threshold condition will be dependent on the quantity of metal vapors in the combustion chamber, the cylinder temperature, the adiabatic cooling rate and the particle surface area available for vapor deposition. Changes in these parameters will directly affect the way in which metals are distributed in the DPM. For my test conditions, increase of engine load can be interpreted in terms of an increase in the Fe concentration, along with a decrease in soot formation, consequently increasing the probability for self-nucleation and subsequent coagulation.

5.5 References

Abdul-Khalek, I. S., D. B. Kittelson, B. R. Graskow, Q. Wei, and F. Brear. Diesel Exhaust Particle Size: Measurement Issues and Trends. *SAE Tech. Paper* 980525:1-14, 1998.

Abdul-Khalek, I. S., D. B. Kittelson, and F. Brear. The Influence of Dilution Conditions on Diesel Exhaust Particle Size Distribution Measurements. SAE Paper No. 1999-01-1142: 1-9, 1999.

Appel, B. R., and Y. Tokiwa. Atmospheric Particulate Nitrate Sampling Errors Due to Reactions with Particulate and Gaseous Strong Acids. *Atmos. Environ.* 15:1087-1089, 1981.

Bagley, S. T., K. J. Baumgard, L. D. Gratz, J. H. Johnson, and D. G. Leddy. Aftertreatment Device Effects on Diesel Emissions. Health Effects Institute. Cambridge, MA, Research Report No. 76, 1996.

Bonczyk, P. A. Effect of Ferrocene on Soot in a Prevaporized Iso-Octane/Air Diffusion Flame. *Combust. Flame* 87:233-244, 1991.

Costa, D. L., and K. L. Dreher. Bioavailable Transition Metals in Particulate Matter Mediate Cardiopulmonary Injury in Healthy and Compromised Animal Models. *Env. Health Perspectives* 105(5):1053-1060, 1997.

Donaldson, K. and V. Stone. Current Hypotheses on the Mechanisms of Toxicity of Ultrafine Particles. *Ann Ist Super Sanita* 39(3):405-410, 2003.

Du, C. J., J. Kracklauer, and D. Kittelson. Influence of an Iron Fuel Additive on Diesel Combustion. *SAE Tech. Paper* 980536:1-13, 1998.

Flynn, P., R. Durrett, G. Hunter, A. Loye, O. C. Akinyemi, J. Dec, and C. Westbrook. Diesel Combustion: An Integral View Combining Laser Diagnostics, Chemical Kinetics, and Empirical Validation. *SAE Tech. paper* 1999-01-0509:1-14, 1999.

Friedlander, S. K. Smoke Dust and Haze. John Wiley & Sons, New York, p. 251, 1977.

Hering, S., S. Friedlander, J. Collins, and W. Richards. Design and Evaluation of a New Low-Pressure Impactor (Part 2). *Environ. Sci. Tech.* 13(2):184-188, 1979.

Higgins, K., H. Jung, D. B. Kittelson, J. T. Roberts, and M. R. Zachariah. Size-Selected Nanoparticle Chemistry: Kinetics of Soot Oxidation. *J. P-Chem.* 106(1):96-103, 2002.

Jung, H., D. B. Kittelson, and M. R. Zachariah. The Influence of Cerium Additive on Kinetics of Diesel Nanoparticle Oxidation. In preparation, 2004.

Kittelson, D., D. Johnson, and W. Watts. Diesel Aerosol Sampling Methodology, CRC E-43 Final Report available at http://www.crcao.com, 2002.

Kittelson, D.B., J. Johnson, W. Watts, Q. Wei, M. Drayton, D. Paulsen, and N. Bukowieki. Diesel Aerosol Sampling in the Atmosphere. *SAE Tech. paper* 2000-01-2212:1-8, 2000.

Kittelson, D. Engines and Nanoparticles: A Review. *J. Aerosol Sci.* 29(5/6):575-588, 1998.

Knutson, E. O., and K. T. Whitby. Aerosol Classification by Electric Mobility: Apparatus, Theory, and Application. *Journal of Aerosol Science* 6:443-451, 1975.

Lee, D., K. Park, and M. R. Zachariah, M.R. Determination of Size Distribution of Polydisperse Nanoparticles Using Single Particle Mass Spectrometry. In preparation, 2004.

Park, K.H., F. Cao, D. B. Kittelson, and P. H. McMurry. Relationship Between Particle Mass and Mobility for Diesel Exhaust Particles. *Env Sci & Technology* 37 (3): 577 – 583, 2003.

Mahadevan, R., D. Lee, H. Sakurai, and M. R. Zachariah. Measurement of Condensed-Phase Reaction Kinetics in the Aerosol Phase Using Single Particle Mass Spectrometry, *J. Phys. Chem. A* 106:11083-11092, 2002.

Miyamoto, N., H. Zhixin, A. Harada, H. Ogawa, and T. Murayama, T. *SAE Tech. Paper* 871612:1-7, 1987.

Otto, K, M. H. Sieg, M. Zinbo, and L. Bartosiewicz. The Oxidation of Soot Deposits from Diesel Engines. *SAE Tech. Paper* No. 800336:277-289, 1980.

Ritrievi, K. E., J. P.Longwell, and A. F. Sarofim. The Effects of Ferrocene Addition on Soot Particle Inception and Growth in Premixed Ethylene Flames, *Combust. Flame* 70:17-31, 1987.

Sakurai, H., H. J. Tobias, K. Park, D. Zarling, K. S. Docherty, D. B. Kittelson, P. H. McMurry, and P. J. Ziemann. On-Line Measurements of Diesel Nanoparticle Composition and Volatility. *Atmos. Environ.* 37:1199-1210, 2003.

Stratakis, G.A., and A. M. Stamatelos. Thermogravimetric Analysis of Soot Emitted by a Modern Diesel Engine Run on Catalyst-doped Fuel, Combust. Flame 132:157-169, 2003.

Suess, D. T., and K. A. Prather. Mass Spectrometry of Aerosols. *Chem. Rev.* 99:3007-3035, 1999.

Tobias, H. J., P. M. Kooiman, K. S. Docherty, and P. J. Ziemann. Real-Time Chemical Analysis of Organic Aerosols Using a Thermal Desorption Particle Beam Mass Spectrometer. *Aerosol Sci. Tech.* 33:170-190, 2000.

Utell, M. J., and M. W. Frampton. Acute Health Effects of Ambient Air Pollution: The Ultra-fine Particle Hypothesis. *J. Aerosol Med.* 13:355-359, 2000.

Wang, S.C. and R.C. Flagan [1989]. "Scanning Electrical Mobility Spectrometer". Division of Engineering and Applied Science, CA Institute of Technology, Pasadena, CA 91125, pp138-178.

Chapter 6 - Characterizing Iron-Bearing Diesel Particles Using TEM/EDS

The work described in this chapter is an extension of the work described in Chapter 5 and was intended to compliment it. The same experimental setup was used to combust iron-doped diesel fuel to generate metal-bearing diesel particles, but for this work the subsequent analysis of the particles was done using transmission electron microscopy and energy dispersive spectroscopy (TEM/EDS). For this study, as for the work in Chapter 5, DPM was generated by a 1.5-liter diesel engine and the fuel was doped with ferrocene to enhance the level of iron in the system. The exhaust particles were collected on TEM grids and analyzed using the Philips CM12 TEM/EDS instrument. Results show that when the iron to carbon ratio (Fe/C) in the engine is low, the exhaust particles have morphologies similar to the undoped case, but at a threshold Fe/C value of 0.013 (for this engine), self-nucleated metallic nanoparticles are formed. The number and size of these nanoparticles increase with level of doping. Metal-bearing particles that span a larger size range are also formed. Agglomeration of metallic and carbon particles is observed in two distinct modes i.e., attachment of iron primary particles (5-10nm in diameter) to carbon agglomerates, and coagulation of iron agglomerates (20-200nm in diameter) with carbon agglomerates. Results of this work imply that as new engine technologies reduce carbon levels in the engine, this could foster the generation of metallic nanoparticles, potentially creating an additional health concern associated with DPM exposure.

6.1 Introduction

Both chronic and acute health effects have been shown to be associated with DPM and one theory suggests that the ultrafine and nano-sized particles, i.e., particles less than about 100 nm in diameter, may play a key role in this association (Utell and Frampton, 2002; Pope, et al, 1995). Although new techniques have been developed to characterize size and morphology of such small particles, the issue of chemical composition and its links to particle formation scenarios is complex and remains elusive. The role of trace metals is of particular interest due to their possible toxicity (Ghio, et al, 2000; Aust, et al, 2002) as well as their potential roles in atmospheric chemistry and the current work therefore focuses on the fate of metals in DPM, and their effects on particle morphology.

Metals in diesel exhaust may originate from sources such as trace metals in the fuel (Wang, et al, 2003) or from the use of metallic fuel additives for enhancing regeneration of diesel particulate filters, but under normal operating conditions most are believed to originate from lube oil additives and by-products of engine wear, that enter the combustion chamber via reverse blow-by of the piston rings (De Petris, et al, 1996). The research reported in this chapter aims at providing insight into this issue by investigating the morphology and chemistry of particles resulting from the diesel combustion process and more specifically the formation of metal-rich nanoparticles via self-nucleation as well as the overall distribution of metals across a wider range of particle sizes due to vapor deposition and coagulation.

6.2 Research Approach

The main goals of this work are to quantify the fate of fuel-borne metals during diesel combustion and to investigate how metal levels during combustion may affect the particle formation process. The research approach taken was to use a diesel engine to generate exhaust particles and to dope the fuel supply with ferrocene to introduce additional metal (Fe) into the combustion process, in amounts above the normal trace levels. Lab testing entailed running the diesel engine and routing a sample of the diluted exhaust aerosol to a low-pressure impactor (LPI) or electrostatic precipitator (ESP). The size distribution of the diesel aerosol was also measured using a scanning mobility particle sizer (SMPS). The resulting metal-bearing diesel exhaust particles were analyzed using transmission electron microscopy (TEM) and energy dispersive spectroscopy (EDS).

Results include TEM images that show the morphology of various sizes and types of metal-bearing diesel exhaust particles, and demonstrate the influence of metals on the morphology of the particles. Using a combination of TEM/EDS on selected particle samples demonstrates the wide variation in morphology and elemental composition and thus sheds further light on the particle formation process.

The following section describes the setup and procedures, while the third section presents a discussion of the results. The discussion of results focuses on the five main types of particle morphologies observed. In the final section, some explanations are offered for plausible particle formation pathways that describe the fate of metals during combustion.

6.3 Experimental Setup and Procedures

The engine and particle sampling setup used for this experiment were the same as those described in Chapter 5 (Figure 5.1). The engine is a 1.5 liter Isuzu engine controlled by an electronic governor actuator that maintains a constant engine speed of 1800 rpm. The load on the engine was provided by loading the generator outlet with a resistive load bank made by the Simplex Company. For the purposes of our experiments, the engine was run at four conditions, i.e., 0kW, 2kW, 4kW, and 6kW load. The corresponding fuel flow rates were 1.1, 1.4, 1.8, and 2.2 kg/hr. The fuel used for all tests was #2 diesel fuel with nominal sulfur level of 350 ppm, doped with 1% lube oil, yielding a fuel mixture containing ppm levels of several metals as outlined in Table 7.1.

The particulate matter for sampling/analysis was drawn from the tailpipe as described in Chapter 5. For measurements of particle size distribution with the SMPS, the flow was diluted as in previous experiments and all SMPS data in this report have been dilution-corrected to represent actual tailpipe conditions. It should also be noted that the size distribution of particles generated by this engine varies somewhat from that of typical heavy-duty engines. Under normal operating conditions it produces no discernable nuclei mode and the accumulation mode does not increase significantly with engine load as it does for larger engines.

6.3.1 Particle Sampling

Two methods were used to collect particles on TEM grids. The first method employed a low-pressure cascade impactor (LPI) to collect size-selected samples of particles larger than 50nm (aerodynamic diameter). The second collection method

employed an electrostatic precipitator (ESP), which does not yield a representative sample of particles due to charge-biasing, but has the advantage of collecting a wide variety of particle sizes on one grid, including particles less than 50nm (aerodynamic diameter). The samples were collected on 200 mesh copper TEM grids coated with either carbon (carbon coated "formvar") or SiO films. The carbon films are more robust (therefore less damaged by the impactor jets) and since they are thinner, yield better TEM images. The SiO films, since they contain no carbon, allow better EDS analysis of the carbonaceous particles.

The LPI is a simple method for classification of particles by size (Hering, et al, 1979). It consists of several sizing stages, which are stacked on top of each other. The aerosol is drawn through the stack by using a relatively low-pressure vacuum pump, which is where the LPI gets its name. Each stage has a nozzle at the center that focuses the particle-laden aerosol and accelerates it to a pre-determined velocity based on local pressure and nozzle size, which causes particles to impact onto a plate. The cascading stages are designed so that the first stage collects the largest cut size and each sequential stage collects smaller and smaller particles. In this way, the aerosol sample can be divided into predetermined size classes for analyses that entail size-dependent aerosol characteristics. The LPI used in this work was designed to operate at approximately 10 kPa (abs) outlet pressure and 1.0 lpm flow rate. For sample collection, cellophane tape was used to attach the TEM grids onto the impactor plates of the final three stages i.e. stages 6, 7 and 8, which have design cut points of 120nm, 75nm, 50nm (aerodynamic dia) respectively.

The ESP used for these experiments was built in house and is a simplified version of the Rochester design (Cheng, et al, 1981). It consists of a brass tee plumbed so that the aerosol flows through the straight section. A small probe with a molybdenum platform is inserted into the tee connection with a TEM grid attached to the platform. The base end of the probe consists of a high voltage coaxial fitting, wired such that the probe is at high voltage while the tee fitting is grounded. This design, unlike the point-to-plane (Rochester) design, does not generate a corona discharge and so depends on the intrinsic charge of particles to attract them onto the grid. For this reason its collection efficiency is much less, and the particles are collected with a charge-bias (likely enhanced by the influence of metals on particle charging) . Despite these limitations, it provided a simple and effective way to collect a variety of particles from the aerosols sampled.

6.3.2 Particle Imaging and Analysis

Particles were imaged and photographed using a Philips CM12 TEM (FEI Company, Hillsboro, OR, USA) operating at 60kV accelerating voltage and using TEM spot size settings of 2-5. Images were recorded on Kodak Electron Microscopy Film 4489 and developed in Kodak developer D-19 at full strength for 3.0 minutes at 22°C. Particles and nearby support substrate backgrounds (C and SiO films) were analyzed for elemental composition using a Power MX EDS system (EDAX, Inc., Mahwah, NJ. USA) fitted with Super Ultra Thin Window x-ray detector (resolution of 144.5 eV at Mn K-alpha line, 40 microsecond time constant, 10 eV/channel, 40 or 100 second spectra acquisition times, 45 degree takeoff angle). For EDS analysis, the TEM was operated at 60kV, spot sizes 10-11, with objective aperture removed. Elemental ratios were

calculated from spectra using the EDAX MX-TEM program "Materials Thin" that employs a thin-section approximation analysis strategy. When appropriate, substrate support film background spectra were subtracted from particle spectra.

6.4 Results and Discussion

In this work we focus on the characterization of the nuclei and accumulation modes of DPM as defined previously (Kittelson, 1998). Under normal operating conditions for this engine, the nuclei mode is absent and the accumulation mode consists of agglomerates of elemental carbon spheres, with hydrocarbons and other trace species condensed/adsorbed onto the surfaces of the agglomerates. As iron is added to the system, surface deposition of iron vapors initially increases, but at a certain threshold level of iron doping, vapor deposition cannot keep up with the locally high cooling rate and the super-saturation ratio of iron rises quickly. Self-nucleated metallic nanoparticles are subsequently created and begin coagulating with other particles. These processes result in the evolution of distinct new particle morphologies which are outlined and discussed below.

6.4.1 Identifying Common Particle Morphologies

Five particle types were identified, representing the most common particle morphologies observed in samples. Each of the particle types are described below, including comments on the processes of condensation, nucleation and coagulation as they relate to the fate of iron in the system. These processes may occur for other species as well, most notably for carbon, and the formation of carbon agglomerates is therefore

covered first to provide a baseline for subsequent discussions of the interaction between metals and carbon in such a system.

"Type 1" Particles: Carbon Agglomerates (accumulation mode of soot)

Under normal operating conditions, most particles are carbon agglomerates formed by coagulation of "spherules" of elemental carbon. The spherules are formed from soot precursors near the flame front, where temperatures are high and combustion chemistry dominates (Wagner, 1980, pp.1-28). The extremely high concentration of free carbon and numerous collisions result in the formation of these 20-80nm clusters of atoms and molecules consisting mainly of elemental carbon (Siegmann, et al, 2002). Due to the enhanced molecular mobility at high temperatures, these clusters arrange themselves into a spherical shape and have been shown to have a layered structure (Roessler, et al, 1980, pp. 57). The carbon agglomerates are subsequently formed at lower temperature when these spherules begin to coagulate into larger chain-like particles and eventually take on other more volatile species by surface interactions.

For the undoped case, most particles observed are these "typical" carbon agglomerates (Figure 6.1) with mean mobility diameter of around 80nm. The diameter of the primary particles varies somewhat but appears to have a mean of about 20-30 nm as reported earlier (Pipho, et al, 1992). Since the fuel is not doped, metal content is relatively low and virtually no "pure" metallic particles are observed. The trace metals in the system, derived from fuel contaminants, lube oil additives and engine wear, likely react in gas phase to form metallic compounds and as the system subsequently cools they adsorb or condense relatively evenly onto carbon particles. For this undoped case the

amount of metals residing on carbon particles is generally too low for detection using EDS. However, using particle induced x-ray analysis (PIXE) on size-selected samples of Fe-doped soot (Figure 6.2), we can detect that in addition to the iron, there are also other metals (fuel, oil, and engine wear related) present in smaller quantities. Others have done bulk analysis of diesel soot samples using ICP with similar results (Barris, et al, 1991).

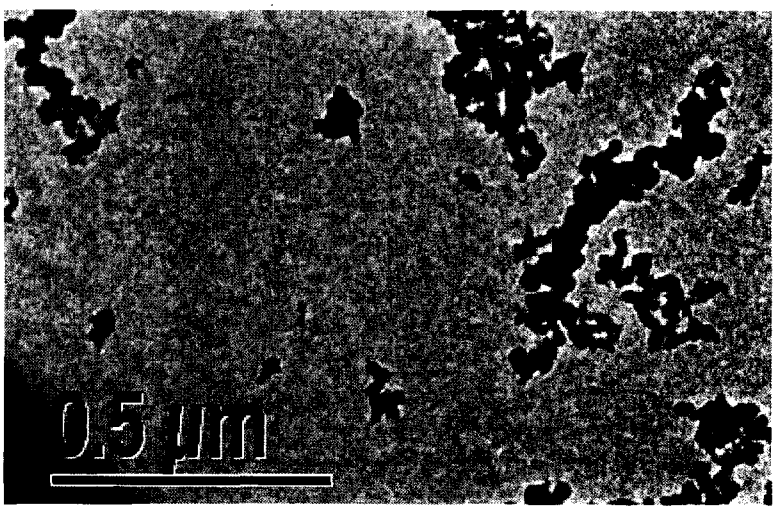

Figure 6.1 - Image of undoped soot.

"Type 2" Particles: Primary Particles of Metal (self-nucleated)

When the fuel is doped with just enough iron to trigger self-nucleation we see the appearance of a nuclei mode of small (<10nm mobility diameter) metallic "primary particles" as evidenced by the beginnings of a nuclei mode for the 20ppm doping case in Figure 6.3. At and above this threshold condition, the amount of metal in the system is much higher than for the undoped case, and the EDS technique can now be used to

measure the metal on individual particles. For the lowest doping condition (20ppm), EDS spectra from large particles show small amounts of Fe, but TEM images show no visibly dense regions indicating concentrated iron content. It is concluded that for this case the Fe on the particles is mainly from vapor deposition, with perhaps some coagulation of very fine nanoparticles or molecular clusters and is thus not visible on the images.

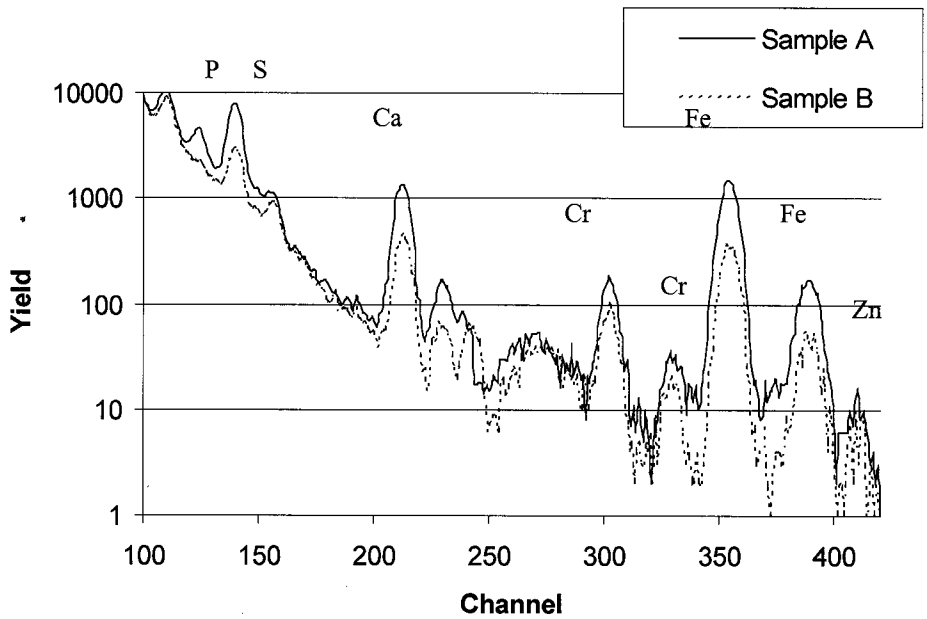

Figure 6.2 - PIXE data for Fe doped case, also shows presence of lube-oil additive metals (P, S, Ca, Zn) and engine wear metal (Cr).

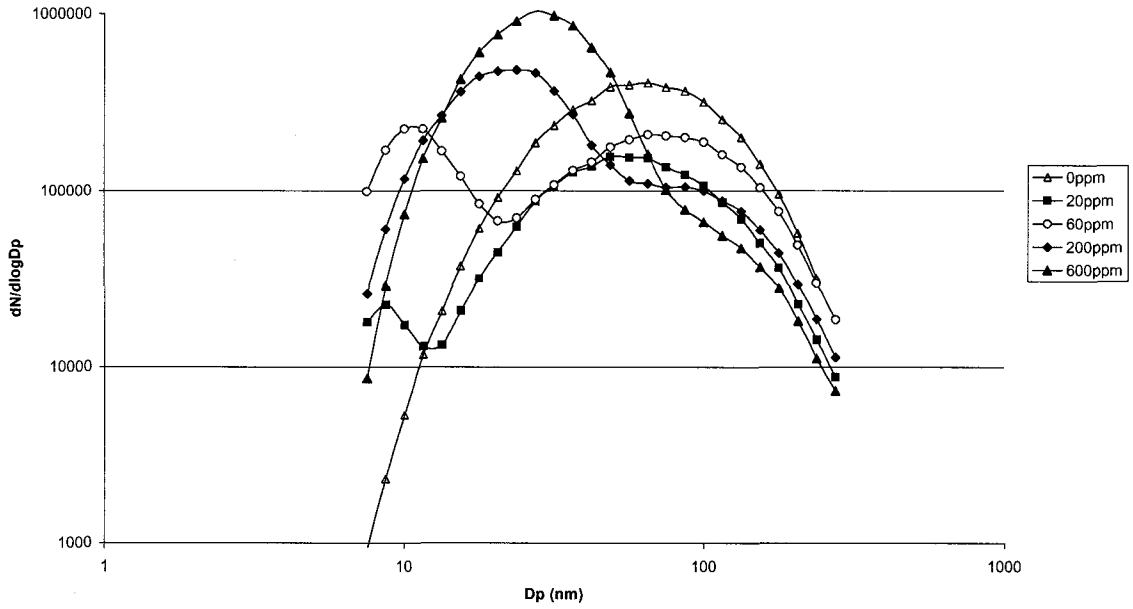

Figure 6.3 - Effect of iron doping level on the size distribution of diesel particles. Engine load of 0kw and dilution ratio of approximately 700:1 for all cases.

As the metal content in the system increases, more and more self-nucleated metallic particles are generated. The primary particle size is initially less than 10nm as evidenced by both SMPS data (20ppm case in Figure 6.3), and TEM images such as in Figure 6.4. Analysis of small particles such as those in Figure 6.4 using EDS yields background levels of all species except Fe, indicating they are composed mainly of iron. Note that the primary particle size appears to increase slightly with increase in doping levels, especially notable for the 600ppm doping case. This may be a result of higher super saturation ratios during piston retraction, which would accelerate the self-nucleation process and prolong the time period in which it occurs, leading to increased primary particle size.

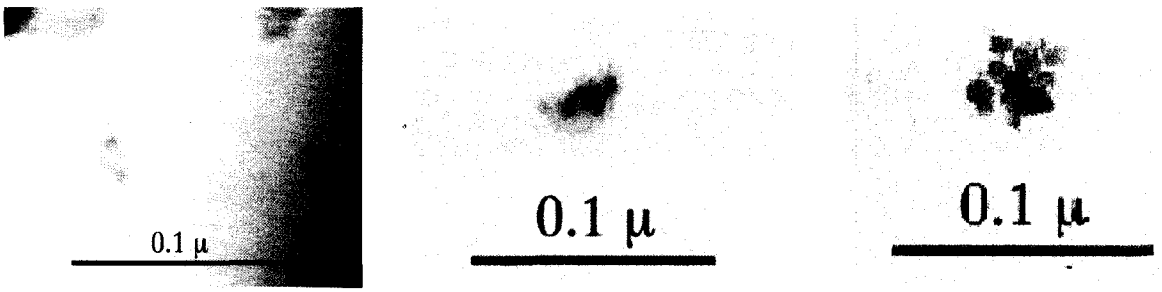

a) b) c)

Figure 6.4 - TEM images of small iron agglomerates, roughly indicating primary particle size and agglomerate diameters for three doping conditions: a) 60ppm, b) 200ppm, and c) 600ppm.

At lowest doping level (20ppm), it is difficult to observe the primary iron particles using TEM. The SMPS data confirm their existence and the shapes of particles such as those in Figure 6.4a suggest that they coagulate into larger particles. However, they are so small that even when they coagulate into particles such as in Figure 6.4a, it was not possible to resolve the primary particles with our TEM. At higher doping rates, the primary iron particles are larger and it was then possible to resolve the individual primary particles within the agglomerates.

The potential role of iron oxide primary particles that may form early in the combustion process, perhaps even in the core of the diffusion flame as described in an earlier work, is unclear. For premixed flames (Ritrievi, et al, 1987), addition of ferrocene was shown to trigger the self-nucleation of iron oxide nanoparticles, which formed prior to the soot, and in fact reportedly enhanced soot production since their high surface reactivity encouraged soot deposition. These soot particles were described as then being immune from surface oxidation as they passed through the remainder of the flame, since the metal could not diffuse through the carbon and reach the surface fast enough. On the

other hand, laminar diffusion flames (Bonczyk, 1991) have been shown to display the same behavior, i.e., early generation of metal-oxide nanoparticles. However (perhaps due to reduced oxygen availability) this process appeared to be limited, leaving sufficient metal in the system to form metal oxide coatings on the soot particles. This was evidenced by their high rate of oxidation later in the flame. Neither of these studies indicated that metal played a role in suppression of soot during the combustion process. However, a later study (Miyamoto, et al, 1987), in which soot concentration was measured in the cylinder as a function of crank angle, suggested that during diesel combustion of metal-doped fuel, soot oxidation is not only enhanced due to its metallic surface film, but that its formation is also suppressed. The validity of that approach may be in question, however, since the soot measurements were not taken inside the diffusion flame, but rather in the prechamber, i.e., where the flame initiated.

The creation of iron oxide particles during diesel combustion is suggested by EDS data such as in Figure 6.5, which shows a distinct oxygen peak for a 78nm metallic agglomerate. However, analysis of the relative mol fractions of iron and oxygen on a number of such particles did not yield consistent stoichiometric ratios commensurate with FeOx compounds.

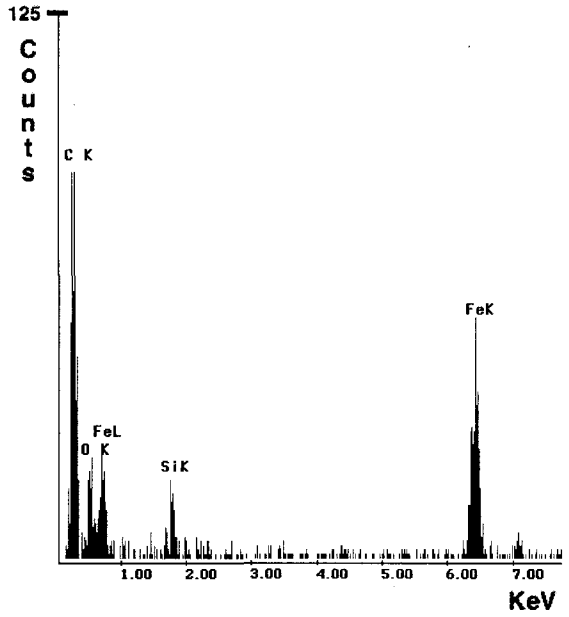

Figure 6.5 - EDS spectrum of metallic nanoparticle showing iron and oxygen.

It is also possible that the self-nucleated metallic particles are pure iron and that they oxidize enroute to the TEM. This is supported by lack of O peaks in the single particle mass spectra described in chapter 5. Since the boiling point of iron is high, it is probable that the Fe primary particles form only after Fe passes through the diffusion flame. In that case, the local oxidizing environment near the flame should encourage the formation of oxides, which does not explain our observation of "pure" iron nanoparticles. I therefore concluded that the observed nanoparticles that are pure iron particles may be self-nucleating in the cooler reducing environment away from the flame. I also concluded that such primary particles subsequently coagulate to a self-preserving size distribution, which is in fact the lognormal distribution making up the nuclei mode for the doped cases.

"Type 3" Particles: Carbon Agglomerates Decorated with Iron Nanoparticles

It is believed that before or during the mutual coagulation of the primary iron particles, they also individually collide with carbon agglomerates and "decorate" the agglomerate surfaces with "nano-nuggets" of relatively pure iron. This is confirmed by observation of very small nuggets of dense material visible on TEM images of carbon agglomerates (Figures 6.6a-b). The dense nuggets are assumed to be self-nucleated primary particles of iron attach directly to carbon surfaces. This process is also documented for the case of Ce-doped diesel combustion (Jung, et al, 2003). This decorating of carbon agglomerates may also explain the observation of minute dark specks on some carbon agglomerates at lower doping levels. For this case, the size of primary iron particle is potentially so small that they are not easily resolved in the TEM images, but rather appear as tiny specks (Figure 6.6c).

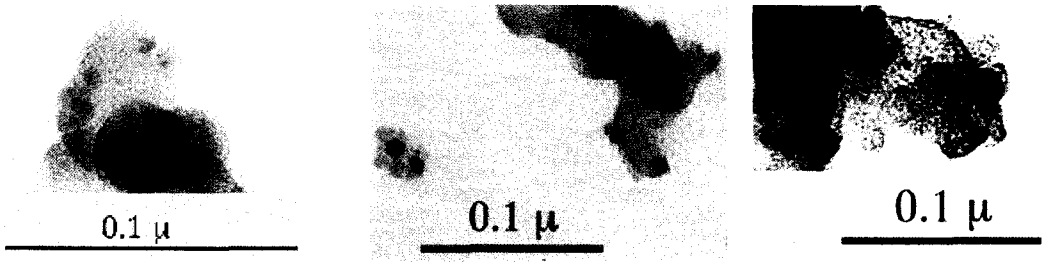

Figure 6.6 - TEM images showing metallic primary particles, i.e., the darker spots/specks that decorate lighter colored carbon agglomerates at Fe concentrations of: a) 1.8mg/m^3, b) 0.92 mg/m^3, and c) 0.54 mg/m^3.

"Type 4" Particles: Metal Agglomerates

After self-nucleation of iron is established, further increase in metal above the threshold level simply creates more (and slightly larger) primary particles. High numbers of such monodisperse particles drives coagulation and this creates the growing "nuclei mode" of metallic (agglomerate) particles we see in Figure 6.3. The mean diameter of this nuclei mode of metal agglomerates depends on the quantity of metal available. For example, at 600ppm doping (Figure 6.4) the mean mobility diameter of such agglomerates increases up to approximately 30nm (see Figure 6.5c which is typical of such particles).

The fact that the growing nuclei mode is a direct result of metal nucleation and agglomeration is shown in Figure 6.7. The linear growth of particulate volume (mass) in

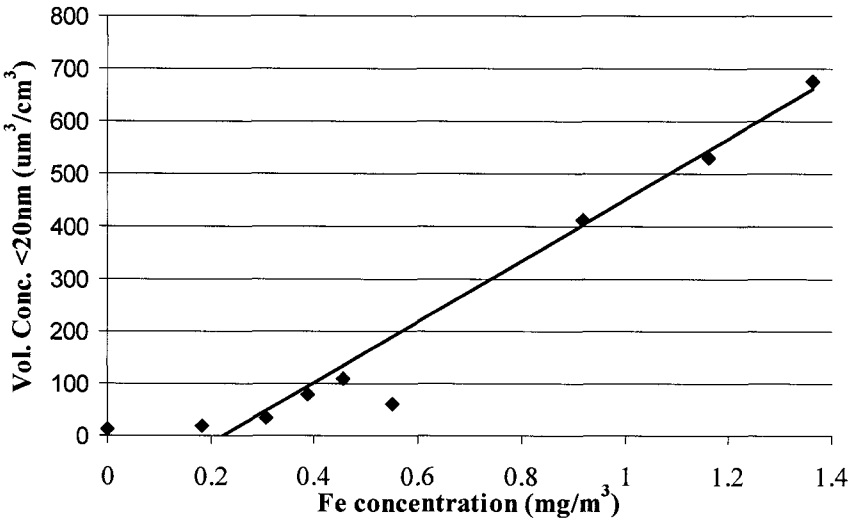

Figure 6.7 - Volume of nuclei mode particles (<20nm) as a function of Fe concentration.

the nuclei mode corresponds directly to the increase in mass concentration of Fe in the system. As noted in the interpretation of Figure 5.6, this represents a high recovery rate

of iron, suggesting that much of the iron is contained in the nuclei mode. For this figure the nuclei mode volumes were calculated from SMPS size distributions and the Fe concentrations were calculated as the product of fuel flow rate and doping level, divided by the volumetric flow rate through the engine. For the conditions of our tests, the "threshold" Fe concentration for the onset of self-nucleation is at about 0.25 mg/m^3 i.e. where the trend line crosses the x-axis in Figure 6.7. Since the threshold is also affected by the availability of carbon surfaces for metal deposition, I use the (baseline/undoped) carbon mass measurements presented later in section C to calculate a "threshold iron-to-carbon ratio" of 0.013 for onset of self-nucleation. In Figure 6.8, the calculated Fe/C ratios for all loads are seen to be well above this threshold for the 60ppm doping case, which is supported by experimental results, while the Fe/C ratio at 0kW and 20ppm doping is near the threshold of nucleation. The latter was observed experimentally and is reflected in Figure 6.3.

Note that due to the wide range of metal to carbon ratios used to derive the trend line, the Fe/C ratio at 0kW actually appears slightly below the threshold in Figure 6.8, while the existence of a nuclei mode for the 20ppm case in Figure 6.3 confirms that it is in fact above the threshold. The increase in mean diameter of the nuclei mode with doping level, shown in Figure 6.3, is confirmed by the TEM images of Figure 6.5. Those images show increase in the size of "typical" type-3 particles for the cases of 60, 200 and 600ppm doping. The increase in size with doping is a function of both primary particle size and number of primary particles in each cluster. Both these are observed to increase as more metal is added to the system.

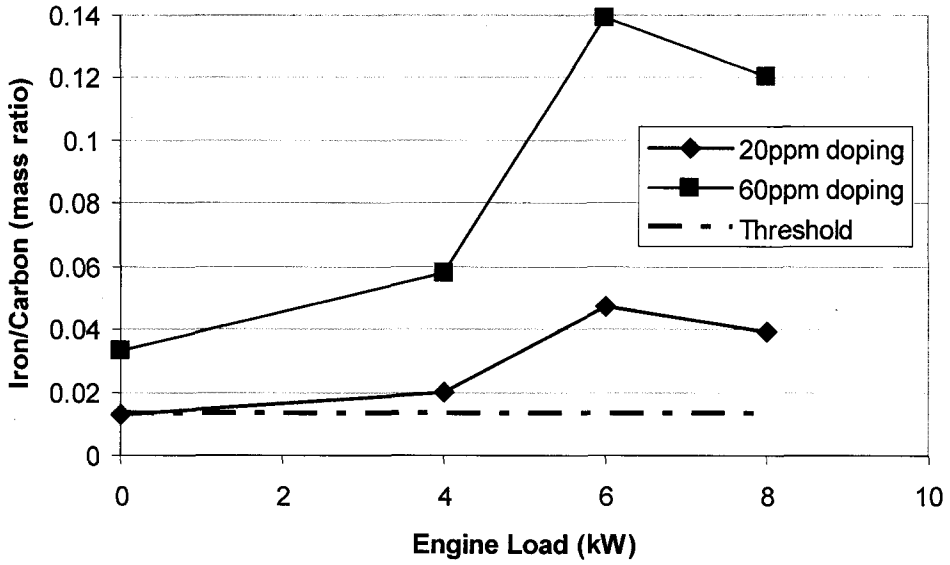

Figure 6.8 – Data for four different engine loads and two doping levels, showing how iron to carbon ratio increases with doping level and engine load.

As metal levels increase, coagulation of metallic particles leads to the formation of larger metal agglomerates. This is evidenced by particles such as that shown in Figure 6.9, and further supported by observation of occasional ~100nm "pure" iron particles in the single particle mass spectra for the case of 60ppm doping (Lee, et al, 2004). For the lowest doping rate (20ppm), such particles are virtually non-existent, but for the highest doping rate (600ppm), they are fairly common.

For iron doping levels at and above 60ppm, we observe agglomerates with significant amounts of iron and carbon. An example is shown in Figure 6.10a. Three consecutive localized EDS scans of this particle (Figure 6.10b-d) show clearly the association between morphology and chemistry.

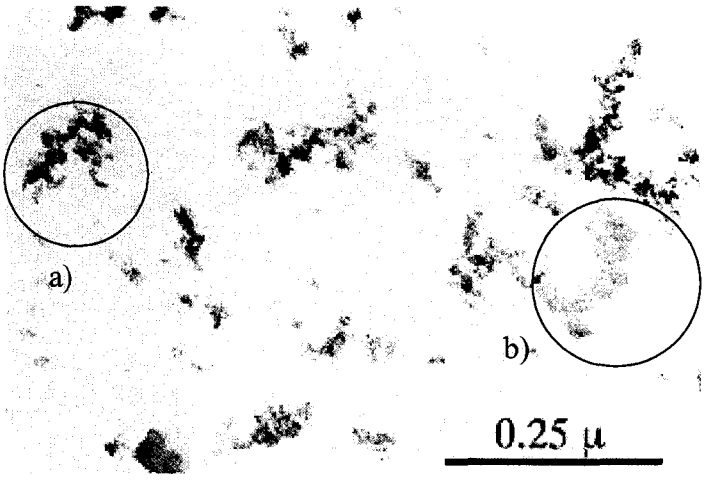

Figure 6.9 - ESP sample for 60ppm doping case showing large agglomerates of: a) iron and b) carbon.

"Type 5" Particles: Combined Metal/Carbon Agglomerates

The upper end of this particle consists of a carbon agglomerate structure with a few very small metallic primary particles visible and the spectrum of Figure 6.10b shows a relatively small iron peak for this case. The spectrum of Figure 6.10c shows an even smaller iron peak for the low-density (carbonaceous) central portion of that particle. Finally, Figure 6.10d shows a very large iron peak suggesting that this end of the particle was formed by coagulation with a type-4 metallic agglomerate.

Figure 6.10a thus demonstrates coagulation for metallic and carbon species during the complex particle formation process. First, the iron primary particles on the upper left end of the chain show how self-nucleated particles attach to carbon surfaces. Second, the structure on the lower right indicates coagulation of metallic agglomerates with carbon particles, an observation supported by earlier data (Lee, et al, 2004). Both processes are collision driven and will increase as the concentration of metallic particles increases.

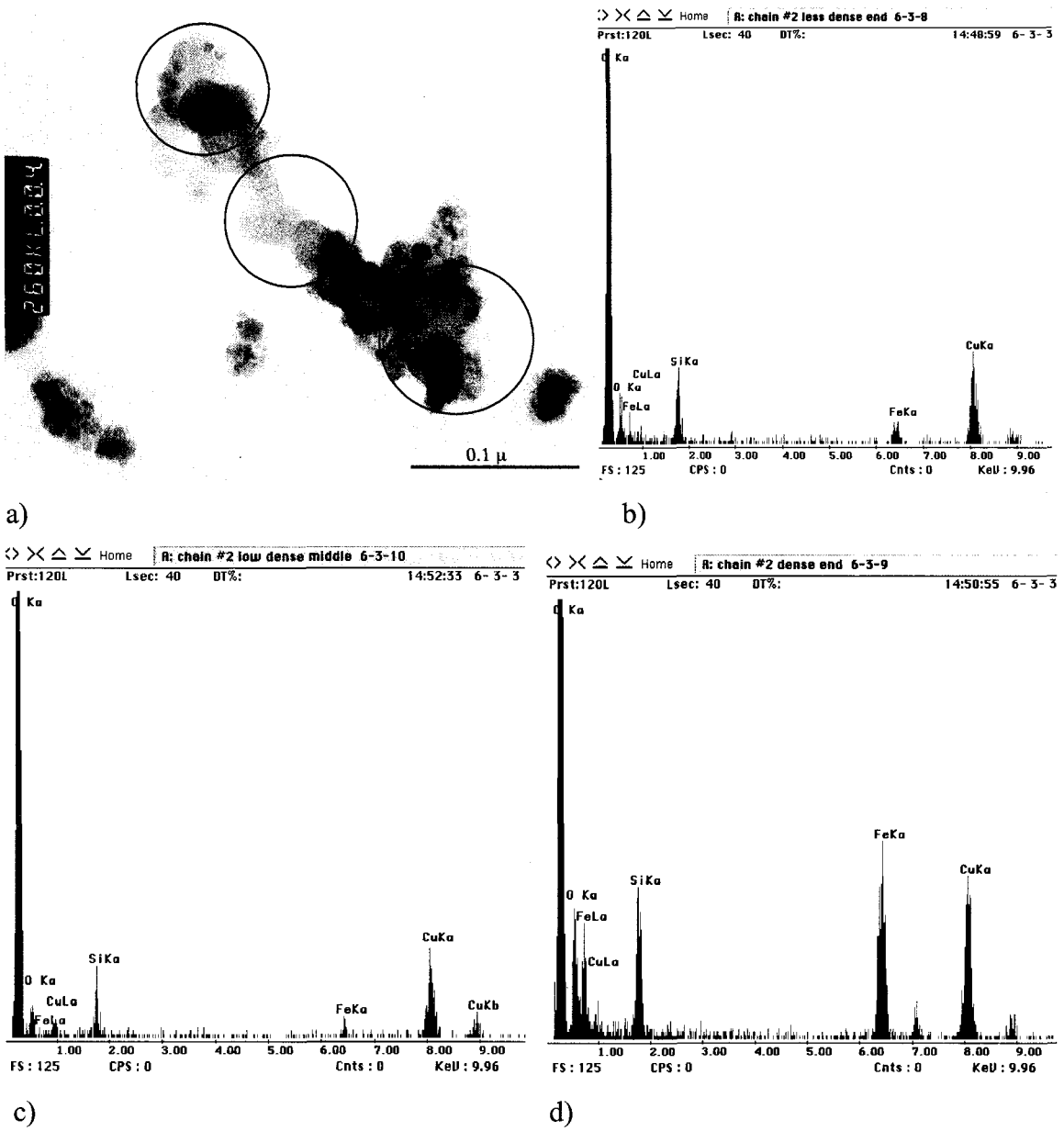

Figure 6-10 - TEM image and EDS spectra show how iron content is related to morphology. a) Image of combination iron-carbon particle, b) EDS spectrum for upper end of particle, c) Spectrum for mid section, and d) Spectrum for lower section.

Figure 6.11 further demonstrates the variation in particle size and morphology for the metal bearing exhaust aerosol. This sample was collected from raw exhaust (using 60ppm Fe doping) with an electrostatic precipitator. This collection method favors

highly charged particles so the sample is not necessarily representative, but it does clearly show the variation in particle morphologies that occur at these doping levels.

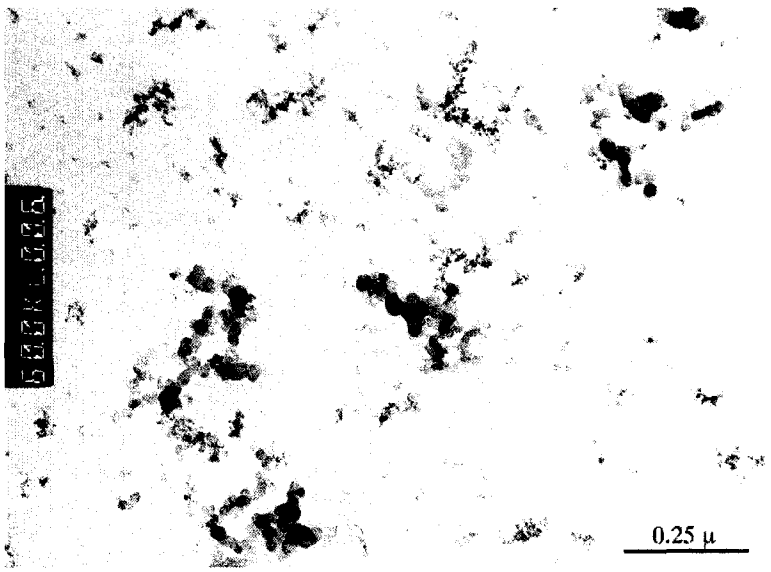

Figure 6.11 - Sample taken with ESP shows the great variety in particle morphologies for the case of 60ppm Fe doping of fuel.

6.4.2 Relative Frequency of Particle Types as a Function of Metal Concentration

The five particle types described above appear with varying frequencies depending on doping level. This is best visualized by comparing TEM images of particles collected on the eighth stage of the LPI at different doping levels (Figures 6.12-6.15). Note that the particle number density in the photos is not necessarily representative, due to variable loading of the TEM grids. In the following descriptions, references to iron content were verified by EDS analysis.

At the highest doping condition of 600ppm (Figure 6.12), "pure" type-1 carbon particles do not exist, while there are numerous type-4 metal agglomerate particles and type-5 combined particles. This is the only condition at which the large type-4 metal agglomerates are readily found, and we also see considerable numbers of type-3 Fe-decorated carbon particles. For the latter, the Fe appears as tiny dots on the larger carbon particles, as seen in Figure 6.12b.

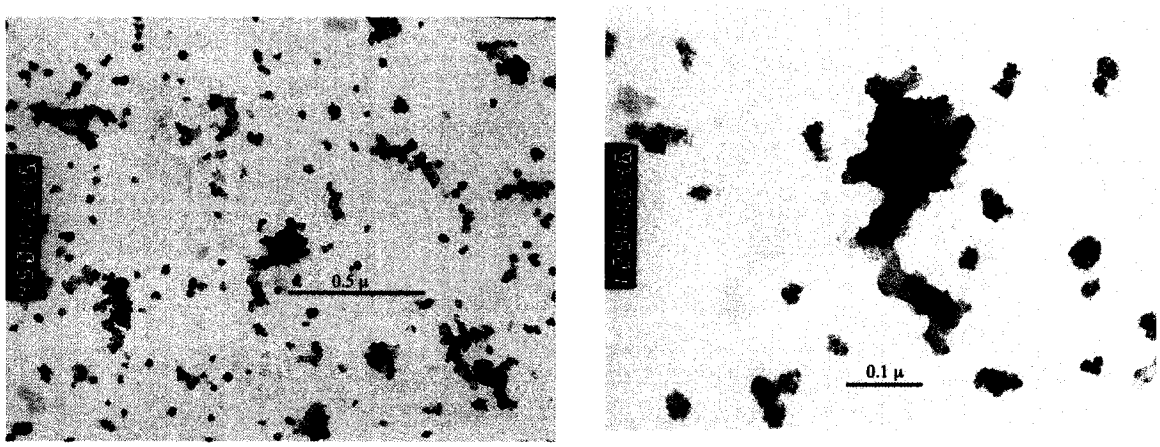

a) b)

Figure 6.12 - TEM images from LPI stage 8 (600ppm doping rate and 0kW engine load). a) Shows prevalence of iron agglomerate particles (type 3) and combination iron/carbon particles, and b) Shows iron nanoparticles (type 2) decorating a carbon agglomerate.

Figure 6.13 shows that at the next lower doping level (200 ppm), the type-4 metal agglomerate particles are still prevalent. The type-5 combined particles are now less prevalent, and the number of primary metal particles attached directly to carbon agglomerates is also reduced (Figure 13b).

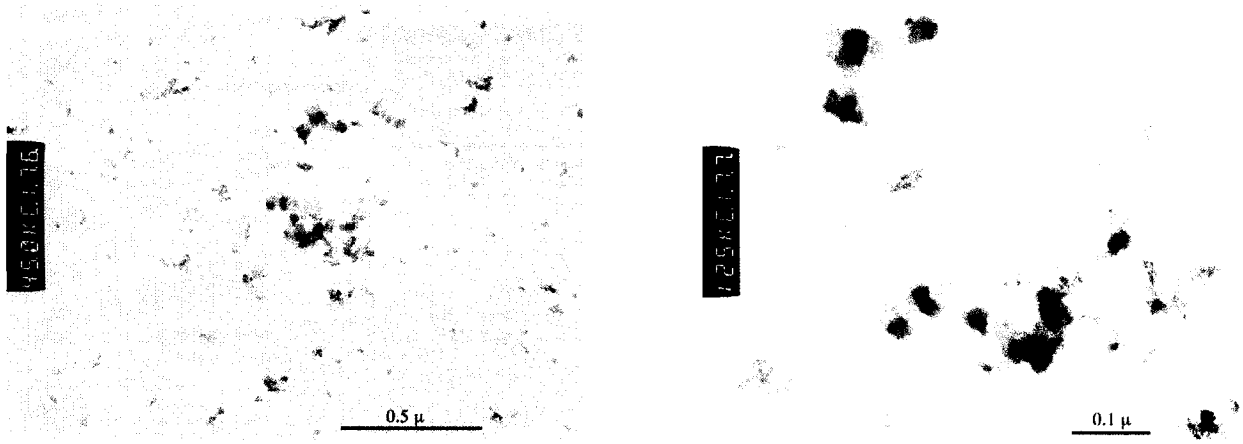

Figure 6.13 - a) LPI stage 8 sample, 200ppm doping, 6kW load, and b) Zoom of same showing small iron agglomerates and iron nanoparticles decorating a carbon agglomerate.

At the 60-ppm doping level (Figure 6.14), the type-4 metal agglomerate particles are still fairly prevalent. The type-1 carbon agglomerates are plentiful, while type-5 particles are now infrequent. Direct attachment of primary metal particles to carbon agglomerates is still evident but infrequent and since the primary particles are very small, they are sometimes hard to resolve on TEM images such as in Figure 6.14b.

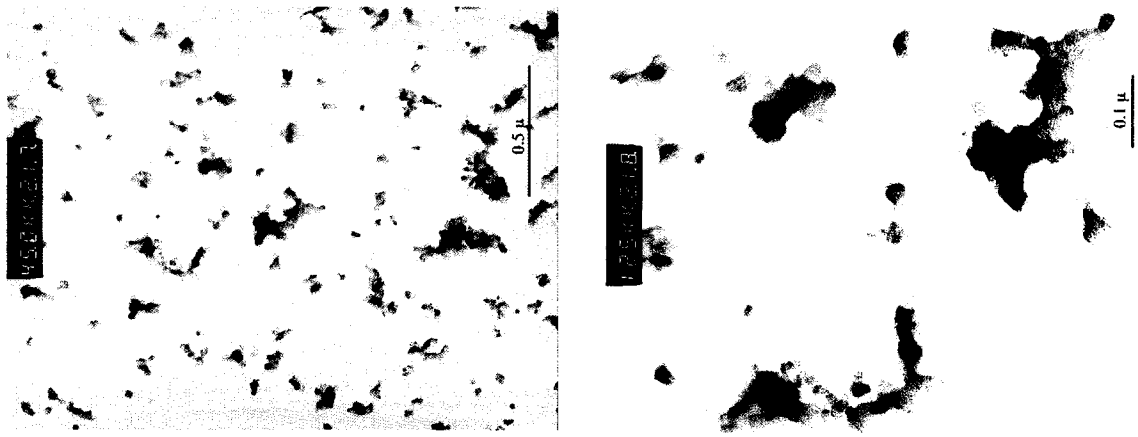

Figure 6.14 - a) LPI stage 8 sample, 60ppm doping, 6kW load, and b) Zoom of same showing small metal agglomerates and very fine iron nanoparticles decorating a carbon agglomerate (upper right corner).

At the lowest doping level (20 ppm), the type-5 particles are gone and the type-4 particles are rare (Figure 6.15). Since few if any type-2 particles exist, the nanoparticles observed in these images are carbonaceous (this was confirmed using EDS). At this condition, most of the particles are type-1 particles. These particles contain small amounts of iron but their appearance is similar to the undoped particles of Figure 6.1. A potential exception to that similarity is the possibility of greater variation in primary particle size for the 20ppm-doped particles.

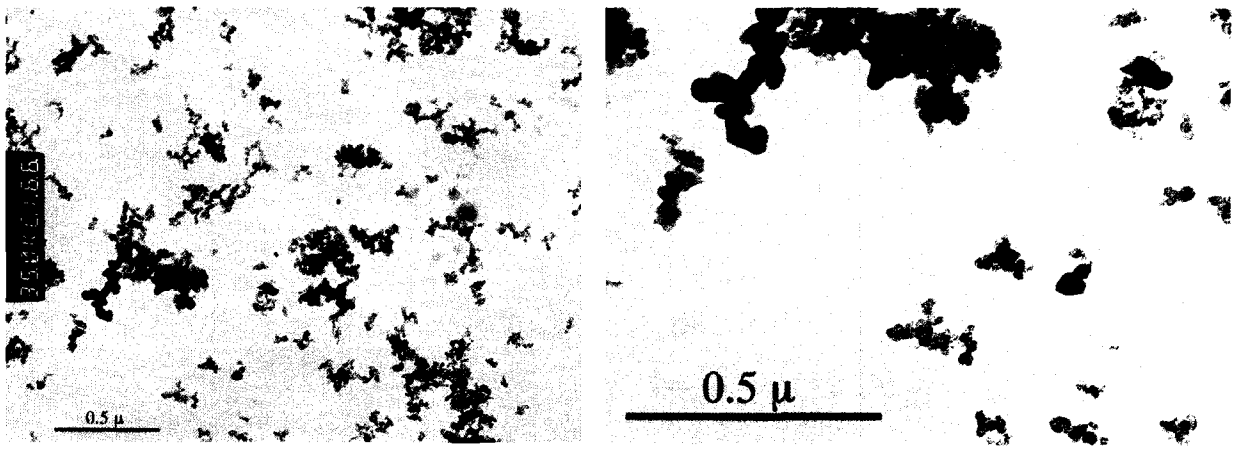

Figure 6.15 - a) LPI stage 8 sample, 20ppm doping, 6kW load, and b) Zoom of same showing carbonaceous agglomerates and nanoparticles, as well as variation in size of carbon primary particles.

This disparity in the size of primary carbon particles could be related to the enhanced post-combustion oxidation of the doped particles as they make their way through the exhaust system. For the case of no doping the carbon primary particles have a fairly narrow lognormal distribution in size (Pipho, et al, 1992). Since the relative amount of vapor-deposition of both metallic and hydrocarbon species would favor

smaller particles due to their high surface to volume ratio, these particles are likely to oxidize faster than their larger neighbors, leading to the skewed size distribution (greater number of smaller particles) observed in Figure 6.15, as compared to Figure 6.1. Further work should be done to confirm this statistically.

6.4.3 Metal Enhanced Soot Reduction

The addition of ppm levels of metals to diesel fuel has been shown to reduce soot emissions (Du et al. 1998). I confirmed this result for the case of 60ppm iron doping by using the NIOSH Standard Method 5040 (Birch 2002) to measure elemental carbon (EC) and organic carbon (OC) in the raw exhaust. In Figure 6.16 is a comparison of the baseline (undoped) values of total carbon (TC=EC+OC) with the case for the doped condition. Reductions in total carbon are on the order of 20-40%, which is commensurate with metal-induced soot reductions reported earlier (Jung et al. 2003).

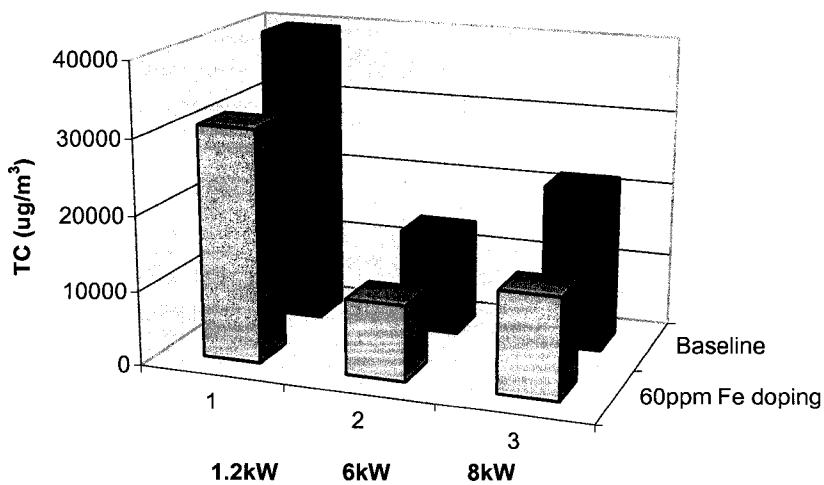

Figure 6.16 - Comparing TC=EC+OC measurements with and without 60ppm Fe doping.

Using the NIOSH method 5040 allowed me to look separately at metal-induced reductions in EC and OC. Notably, OC is reduced significantly and in fact accounts for most of the reduction in total carbon. Figure 6.17 shows OC reductions on the order of 65-85% for the three engine loads tested.

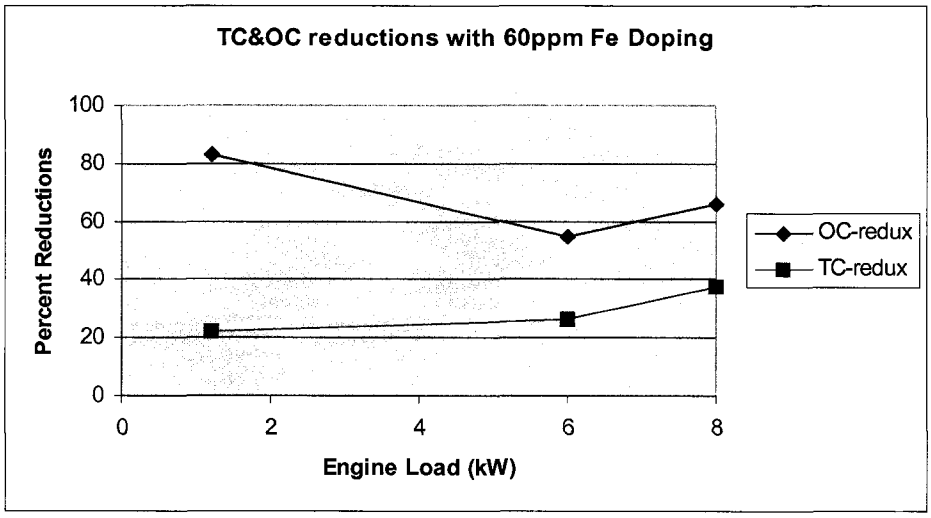

Figure 6.17 - Reductions of total carbon (TC) and organic carbon (OC), with engine load for the case of 60ppm doping.

For the two tests with highest OC reductions, it was also noted that measured EC levels increased from the baseline. This is counter intuitive since it is noted in Figure 6.3 that accumulation mode volumes decrease significantly and this is normally assumed to reflect oxidation of EC. Although this issue may require additional research to clarify, there are two plausible explanations for it:

1) The data may be reflective of a complex relationship between the formation of EC and the level of metal in the system. One argument to support this would be that

metal oxide formation in the diffusion flame robs oxygen during the critical stage of particle precursor oxidation, resulting in more soot formation.

2) It is possible that the presence of metal on the filter samples may influence the "split" between OC and EC during the method 5040 quantification process i.e. since the metal may cause the EC to oxidize at a lower temperature than it normally would. In that case, the differing reductions in EC and OC may be in question, but the overall reduction of total carbon would still be valid.

The trend of increasing total carbon reductions with engine load (Figure 6.17) is also reflected in the data of Figure 6.3, which indicate a decrease in accumulation mode particles for higher doping. Although the data of Figure 6.17 are for 60ppm doping only, the absolute throughput of iron increases about 2.5 times between the lower and higher engine load conditions due to increased fuel flow, and this may account for the increase in carbon reduction indicated by the data.

6.5 Summary

Combining measurements of carbon output of the engine taken simultaneously with particle size distribution measurements, I showed that above a threshold iron to carbon ratio of approximately 0.013, iron nanoparticles form during diesel combustion and subsequently coagulate with each other as well as with larger carbon agglomerates. Following are descriptions of plausible formation pathways for the resulting particles.

Using the assumption of a quasi-steady-state combustion process (Flynn, et al, 1999), the ferrocene-doped fuel exits the injection nozzle at high velocity and forms a plume of fuel vapors with a diffusion flame at its periphery. The plume entrains hot air and

temperatures inside reach about 1600K. Since the ferrocene decomposes at around 750K (Du, et al, 1998), it is probable that as the fuel droplets vaporize, the ferrocene also vaporizes. Subsequent thermal decomposition of ferrocene vapor would then lead to the existence of iron vapor at or near the hotter (~2500K) flame front, creating the conditions for vapor deposition and/or self nucleation of iron particles just outside the flame front.

During the short time period when the piston is near top dead center, the iron vapors build up outside the flame and interact with a growing population of soot particles and hydrocarbon vapors. Around the time that the concentration of these combustion products reaches a peak, the downward piston motion cools the system. As the saturation ratio of iron rises, vapors begin adsorbing and condensing onto existing particle surfaces. If the amount of iron vapor is high compared to available surface area (mainly carbon agglomerates), condensation cannot convert the vapors fast enough (since it is rate limited) and the saturation ratio rises quickly, triggering self-nucleation of primary particles. The absolute amount of a given species, in this case iron, along with local temperature and cooling rate, would determine the extent of these processes and thus affect the size of primary particles. During and after formation of the primary particles of iron, they coagulate with each other and with larger carbon agglomerates leading to the five particle types described above.

The presence of iron in the system leads to measurable reductions in soot output. There are two probable causes for this:

1) The first is the suppression of soot inside the diffusion flame. This is suggested in earlier work (Miyamoto et al. 1987) but a definite mechanism was not identified. It could possibly result from iron vapors (thermally-decomposed from ferrocene),

interacting with free carbon and/or local soot precursors (carbon fragments) and catalyzing their destruction. My data was inconclusive in this regard.

2) The second cause is the iron-accelerated oxidation of organic carbon in the cooler region outside the flame (and after the flame goes out). This would include both gas phase reactions as well as the (later) oxidation of organic compounds attached to the surfaces of carbon agglomerates. The plausibility of the latter has been demonstrated in earlier work (Jung, et al, 2003), and is supported by the data of Figure 6.17.

The demonstrated result that the formation of metallic nanoparticles will occur at a threshold metal to carbon ratio has important implications. It suggests that as engine combustion technologies improve, the "cleaner" engines i.e. those that generate less soot, will be more likely to generate metallic nanoparticles. The source of metals for such particle generation could be from fuel impurities, lube oil consumption (lube oil often contains significant metal additives), or metals derived from engine wear. Due to their small size and thus efficient lung penetration, the generation of such metallic nanoparticles may introduce a new health concern, perhaps even more serious than the issue of exposure to combustion related soot.

6.6 References

Aust, A.E., J. C. Ball, A. A. Hu, J. S. Lighty, K. R. Smith, A. M. Straccia, J. M. Veranth, and W. C. Young. Particle Characteristics Responsible for Effects on Human Lung Epithelial Cells. Research Report-Health Effects Institute, (110) pp. 1-65, discussion pp. 67-76, 2002.

Barris, M.A., S. B. Reinhart, and F. H. Wahlquist. The Influence of Lubricating Oil and Diesel Fuel on Ash Accumulation in an Exhaust Particle Trap. SAE Tech Paper 910131, pp. 19-28, 1991.

Birch, M. E. Analytical Instrument Performance Criteria: Occupational Monitoring of Particulate Diesel Exhaust by NIOSH Method 5040. Applied Occupational and Environment Hygiene 17(6), 400 – 405, 2002.

Bonczyk, P. A. Effect of Ferrocene on Soot in a Prevaporized Iso-Octane/Air Diffusion Flame. Combustion and Flame, Vol. 87, pp. 233-244, 1991.

Cheng, Y.S., H. C. Yeh, and G. M. Kanapilly. Collection Efficiencies of a Point to Plane Electrostatic Precipitator. Am Ind Hyg J., (42) 8/81, pp. 605-610, 1981.

De Petris, C., V. Giglio, and G. Police. Some Insights on Mechanisms of Oil Consumption. SAE Tech Paper 961216, 1996.

Du, C. J., J. Kracklauer, and D. Kittelson. Influence of an Iron Fuel Additive on Diesel Combustion. SAE Tech Paper 980536, pp. 1-13, 1998.

Flynn, P., R. Durrett, G. Hunter, A. Loye, O. C. Akinyemi, J. Dec, and C. Westbrook. Diesel Combustion: An Integral View Combining Laser Diagnostics, Chemical Kinetics, and Empirical Validation. SAE Technical Paper 1999-01-0509, 14 pp., 1999.

Ghio, A.G., J. H. Richards, J. D., Carterr, and M. C. Madden. Accumulation of Iron in the Rat Lung After Tracheal Instillation of Diesel Particles. Toxicologic Pathology, 28 (4), pp. 619-27, 2000.

Hering, Susanne K., Sheldon K. Friedlander, John J. Collins, and L. Willard Richards. Design and Evaluation of a New Low-Pressure Impactor 2. Environmental Science and Technology, Vol. 13, No. 2, February 1979.

Jung, H., D. B. Kittelson, and M. R. Zachariah. The Influence of Cerium Additive on Kinetics of Diesel Nanoparticle Oxidation. Article in preparation.

Kittelson, D., Engines and Nanoparticles: A Review. J. Aerosol Sci. 1998, Vol. 29, No. 5/6, pp. 575-588.

Lee, D. G., A. L. Miller, M. R. Zachariah, and D. B. Kittelson. Characterization of Metal-Bearing Diesel Nanoparticles Using Single Particle Mass Spectrometry. Submitted to Journal of Aerosol Science, April 2004.

Miyamoto, N., H. Zhixin, A. Harada, H. Ogawa, and T. Murayama. Characteristics of Diesel Soot Suppression with Soluble Fuel Additives. SAE Paper 871612, 7 pp., 1987.

Pipho, M. J., D. B. Kittelson, L. Luo, and D. Zarling. Injection Timing and Bowl Configuration Effects on In-cylinder Particle Mass. SAE Tech. Paper 921646, pp. 111-126, 1992.

Pope, C. A., III, M. J. Thun, M. M. Namboodiri, D. W. Dockery, J. S. Evans, F. E. Speizer, and C. W. Heath, Jr. Particulate Air Pollution as a Predictor of Mortality in a Prospective Study of U.S. Adults. Am. J. Respir. Crit Care Med., 151, pp. 669-674, 1995.

Ritrievi, K. E., J. P. Longwell, and A. F. Sarofim. The Effects of Ferrocene Addition on Soot Particle Inception and Growth in Premixed Ethylene Flames. Combustion and Flame, Vol. 70, pp. 17-31, 1987.

Roessler, D. M., F. R. Faxvog, R. Stevenson, and G.W. Smith. Optical Properties and Morphology of Particulate Carbon: Variation with Fuel/Air Ratio, Proceedings of Int. Symp. on Particulate Carbon, Formation During Combustion, GM Res. Lab., Edited by Donald Siegla and George Smith, October 15-16, 1980, pp. 57-84.

Siegmann, K., K. Sattler, and H. C. Siegmann. Clustering at High Temperatures: Carbon Formation in Combustion. J. Electron Spectroscopy and Related Phenomena, Vol. 126, pp. 191-202, 2002.

Utell, M. J., and M. W. Frampton. Acute Health Effects of Ambient Air Pollution: The Ultra-fine Particle Hypothesis. Journal of Aerosol Medicine, 13, pp. 355-359, 2000.

Wang, Y. F., K. L. Huang, C. T. Li, H. H. Mi, J. H. Luo, and P. J. Tsai. Emissions of Fuel Metals Content from a Diesel Vehicle Engine. Atmospheric Environment, 37, pp. 4637-4643, 2003.

Wagner, H. G. Soot Formation-An Overview. Proceedings of Int. Symp. on Particulate Carbon, Formation During Combustion, GM Res. Lab., Edited by Donald Siegla and George Smith, October 15-16, 1980, pp. 1-28.

Chapter 7 - Characterizing Exhaust Particles Containing Metal Lube Oil Additives, Using the SPMS and the ATOF-MS

It has been shown that measurable amounts of inorganic material are in DPM and that such material originates from sources including fuel and lube oil (Okada, et al, 2003; Wang, et al, 2003). Since there are several metallic additives in the engine lube oil as shown in Section 3.3, much of the trace metal in DPM originates from such additives. The work described in this chapter entails doping of the fuel with lube oil to increase the amount of such metals in the DPM to levels detectable using single particle mass spectrometry. For this study, DPM was generated by a 1.5 liter diesel engine and lube oil containing a known formulation of metallic additives was doped into the fuel. The exhaust particles were analyzed in real time using a recently developed single particle mass spectrometer (SPMS), as well as a commercial aerosol time of flight mass spectrometer (ATOF-MS). Results show that when the fuel is doped with lube oil, metal-rich nanoparticles are emitted and their number and size increase along with the concentration of metal in the system. Metal-bearing particles that span a larger size range are also emitted and the metal to carbon ratios measured for individual particles indicate significant agglomeration of metallic and carbon particles. Hydrogen to carbon ratios were also measured, which leads to the identification of organic-carbon type particles. Results show that the H/C ratios increase for smaller sized particles, verifying a similar result presented in Chapter 5.

7.1 Background

The dynamics of particle formation during and after combustion is a topic of much interest and investigation. A recent summary of the diesel combustion process (Flynn, et al, 1999) describes how soot particles are formed during diffusion flame combustion when the piston is near top dead center. As the piston subsequently moves downward, the system cools rapidly. At this stage, if there are other low volatility gaseous species (such as metals) with high concentrations, they may self-nucleate (if the rapid cooling drives their saturation ratios high enough), and/or deposit onto the existing carbon particles. As the resulting aerosol travels through the exhaust system coagulation takes place and further cooling causes semi-volatile species such as polycyclic aromatic hydrocarbons (PAH's) to adsorb and condense onto the agglomerate particles. When the aerosol exits the tailpipe it again cools rapidly and other more volatile species condense suddenly and/or self-nucleate into nanoparticles. The resulting complex mixture of particles is what we call DPM.

Adverse health effects have been shown to be associated with DPM and one theory suggests that the ultrafine and nano-sized particles i.e. particles less than about 100 nm in diameter, may play a key role in this (Utell and Frampton, 2000). Although new techniques have been developed to characterize the size and morphology of such small particles, the issue of chemical composition and its links to particle formation scenarios is complex and remains elusive. The role of trace metals is of particular interest due to their possible toxicity as well as their potential roles in atmospheric chemistry, and this dissertation therefore focuses on the origin and fate of metals in DPM.

Metals in diesel exhaust may originate from sources such as trace metals in the fuel or from the use of metallic fuel additives for enhancing regeneration of diesel particulate filters, but under normal operating conditions most are believed to originate from lube oil additives that enter the combustion chamber via reverse blow-by of the piston rings. This is evidenced by data showing metallic lube oil additives appearing in bulk DPM samples (Bugarski, 1999), and in fact has been evaluated as a way to estimate lube oil consumption (Okada et al, 2003). The addition of lube oils to diesel fuel has been used as an oil-recycling method and a device was recently developed by the Cummins engine company to inject used oil into the fuel stream to extend the period between oil changes. Recent work (Jung et al, 2003A) describes how this could affect particle oxidation rates, leading to reductions in soot emissions, but little information is available concerning other, potentially deleterious effects.

The role of such metals in the chemistry of DPM formation remains a challenging topic of investigation. The metallic particles created during such combustion may have human health implications so there is a need to better understand the chemistry of diesel particulate formation when metals are involved. The research reported here aims at providing insight into this issue by investigating the formation of metal-rich nanoparticles via self-nucleation as well as the overall distribution of metals across a wider range of particle sizes due to vapor deposition and coagulation.

7.2 Research Approach

The main goals of this work are to quantify the fate of lube-oil-borne metals during diesel combustion and to investigate how metal levels during combustion may

affect the chemistry of particle formation. The research approach taken was to use a diesel engine to generate exhaust particles and to dope the fuel supply with lube oil (containing metal additives) to introduce additional metals into the combustion process. It is important to note that the levels of metal originating from normal lube-oil consumption are sometimes not high enough to detect by using the SPMS. For this reason, we enhanced the levels of metals by adding 1wt% lube oil to the fuel. This resulted in metal levels in the fuel of about 4-33 ppm, for the first five metals listed in Table 7.1.

Table 7.1 - Information on elements detected in diesel particles.

Element/ Compound	wt. % in oil	Molecular weight	Mole %	IP kJ/mol	P_{sat}	
					torr	°C
Ca	0.29	40	0.007	590	$\sim 10^{-8}$	282
Zn	0.14	64	0.002	906	8×10^{-4}	280
P	0.13	31	0.004	419	1	261
Mg	0.04	24.3	0.002	738	$\sim 10^{-5}$	282
S	0.33	32	0.100	1000	1	189
C		12		1087	$\sim 10^{-8}$	1657
Fe		56		762	$\sim 10^{-8}$	892

The resulting metal-bearing diesel exhaust particles were analyzed using a recently developed single-particle mass spectrometer (SPMS) that is capable of determining the elemental composition and size of nanoparticles (Mahadevan, et al, 2002; Lee, et al, 2004), as well as an ATOF-MS instrument made by the TSI Company (Gard, et al, 1997).

Lab testing entailed running the diesel engine and routing a sample of the diluted exhaust aerosol to the SPMS or the ATOF-MS for analysis. The size distribution of the diesel aerosol was also measured using a scanning mobility particle sizer (SMPS). (Please note the similarity in acronyms). Both the SPMS and ATOF-MS generated mass spectra for large numbers of individual particles. Subsequent analysis of the spectral data provided insight into not only the elemental composition of particles that make up the DPM aerosol, but also the size-preference of the elements. Additional particle analysis was conducted using transmission electron microscopy (TEM) and energy dispersive spectroscopy (EDS).

The following section describes the experimental setup and sampling arrangement. Section 7.4 includes various presentations of the SPMS and ATOF-MS data that show elemental composition of particles and subsequent discussion of those results. The final section summarizes the highlights of the data analysis.

7.3 Experimental Setup and Procedures

The engine and particle sampling setup used for this experiment were the same as those described in Chapter 5 (Figure 5.1). The engine is a 1.5 liter Isuzu engine controlled by an electronic governor actuator that maintains a constant engine speed of 1800 rpm. The load on the engine is provided by loading the generator outlet with a resistive load bank made by the Simplex Company. For the purposes of our experiments, the engine was run at four conditions, i.e., 0 kW, 2 kW, 4 kW, and 6 kW load. The corresponding fuel flow rates were 1.1, 1.4, 1.8, and 2.2 kg/hr. The fuel used for all tests

was #2 diesel fuel with a nominal sulfur level of 350 ppm, doped with 1% lube oil, yielding a fuel mixture containing ppm levels of several metals as outlined in Table 7.1.

The particulate matter for sampling/analysis was drawn from the tailpipe as described in Chapter 5. For measurements of particle size distribution with the SMPS, the flow was diluted as in previous experiments and all SMPS data in this report have been dilution-corrected to represent actual tailpipe conditions. It should also be noted that the size distribution of particles generated by this engine varies somewhat from that of typical heavy-duty engines. Under normal operating conditions it produces no discernable nuclei mode and the accumulation mode does not increase significantly with engine load as it does for larger engines.

7.3.1 Data Collection Using the Two Different Particle Mass Spectrometers

The SPMS used in this study has been discussed in detail elsewhere (Mahadevan, et al, 2002; Lee, et al, 2004; Rents and Schnabel, 2001) and is shown in schematic form in Figure 5.2 of Chapter 5. The primary components of this system consist of an aerodynamic lens inlet, a three-stage differential pumping system, a free-firing dissociation/ionization laser and optics system, a linear time-of-flight mass spectrometer, and a data acquisition system composed of a high-speed digital storage oscilloscope and a PC.

The size distribution of the inlet aerosol was correlated to the range of signal intensities of particle mass spectra as discussed in previous work (Lee, et al, 2004), and this correlation is used to derive a volume-equivalent diameter associated with each particle mass spectrum. The smaller particles, due to their high diffusivity, have poor

collimation in the aerodynamic lens, and therefore poor transmission efficiencies to the ablation laser. We note that mobility sizing (SMPS) measurements under all four engine load conditions show high concentrations of particles less than 30 nm for which our mass-spectrometer did not observe any hits.

The ATOF-MS used in this study has also been discussed elsewhere (Gard, et al, 1997). It differs from the SPMS in that it incorporates a laser doppler velocimeter that allows determination of the size and speed of incoming particles. Knowing the particle speed allows firing of the ablation laser at the exact time when the particle transits the laser focal volume. This gives very high hitting rates but has the drawback of only identifying particles greater than about 200 nm in diameter, since the doppler laser will not give a dependable signal for smaller particles. As part of this work, spectra from ultrafine particles (50-100 nm) were obtained by circumventing the doppler system and free-firing the laser. To get size information as well (since the doppler system was not in use during free firing), the aerosol was first run through a DMA set to a pre-determined voltage. Unfortunately it was found that the aerodyamic lens inlet on the ATOF-MS passed virtually no particles smaller than 40 nm (mobility diameter) and for the small particles the hitting rate was very low (for 40 nm particles the hitting rate was about one hit every 5-10 minutes). This was in part due to the design of the aerodynamic lens, which was not optimized for nanoparticle penetration.

It should be noted that the ATOF-MS has a smaller ablation laser than the SPMS. Unlike the SPMS, which creates an intense plasma ball resulting in generation of near-unipolar atomic ions of individual elements, the ATOF-MS creates bi-polar ions of elements, compounds and atomic clusters. The drawback of this is that the elemental

ratios can not be determined from the ATOF-MS spectra, but in turn it has the advantage of allowing identification of atomic clusters as well as some compounds. In this work, that advantage was the key to in-situ verification of the existence of metallic oxides on particles.

7.3.2 Mass Spectra for Individual Particles

Examples of typical SPMS particle mass spectra are shown in Figures 7.1a-c. Note that although there are some molecular fragments (C_x, CaO, N_2, O_2/S), the particles were generally ablated to their elemental constituents. The peaks at m/z = 32 are likely a combination of O2 derived from dilution air and sulfur derived from the fuel or oil. Though much of the sulfur (~ 98 %) leaves the tailpipe as SO_2, a few percent of sulfur is known to convert to particulate sulfate and could thus contribute to that peak.

Examples of ATOF-MS spectra are shown in Figures 7.2a-d. These spectra were collected with the ATOF-MS set to free fire. By using a DMA before the inlet and setting it to a predetermined voltage, we were able to estimate the size of the particles hit by the laser. The particles in Figure 7.2 are approximately 40, 60, 75, and 90 nm in aerodynamic diameter. It is immediately obvious that there are many more spectral peaks than in the SPMS spectra. This is a result of the partial ablation of particles by the laser. Some of these peaks indicate the existence of metallic oxide compounds such as CaO, PO3, and HSO4, a result not attainable using the SPMS.

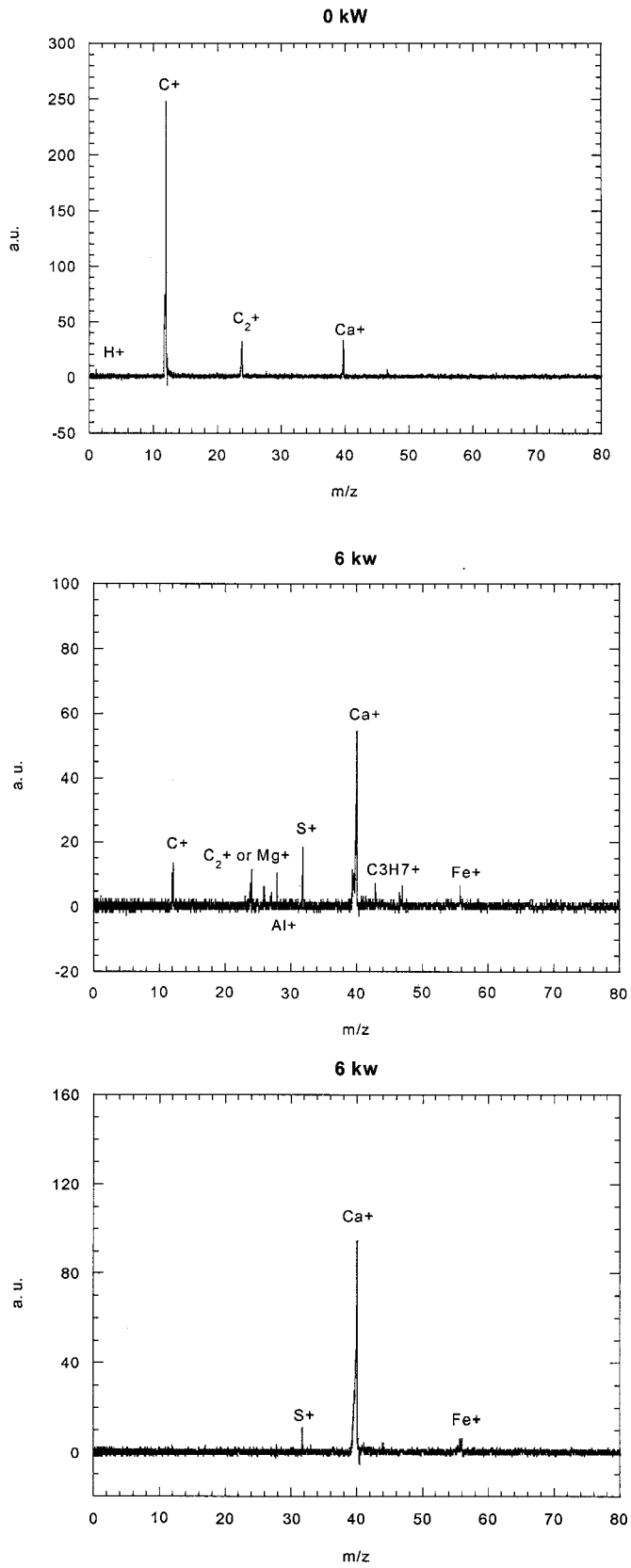

Figure 7.1 - Three classified examples of diesel SPMS (a) agglomerate particle (low load so no metals), (b) carbonaceous particle with metals, and (c) Ca nanoparticle.

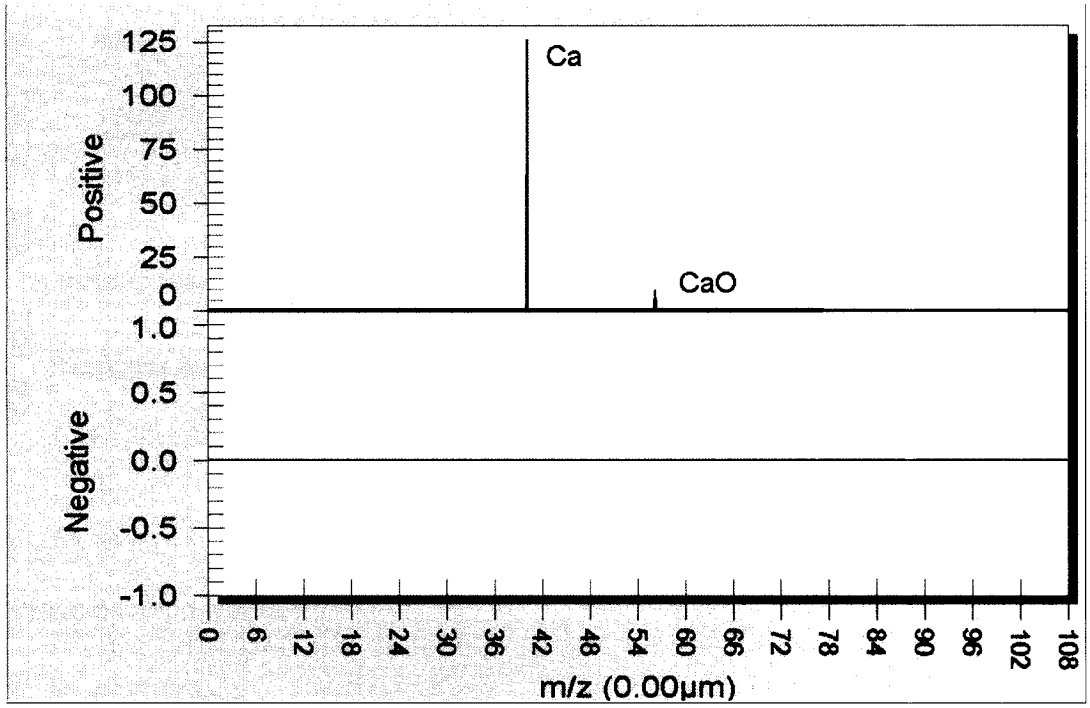

a) 40 nm Ca nanoparticle

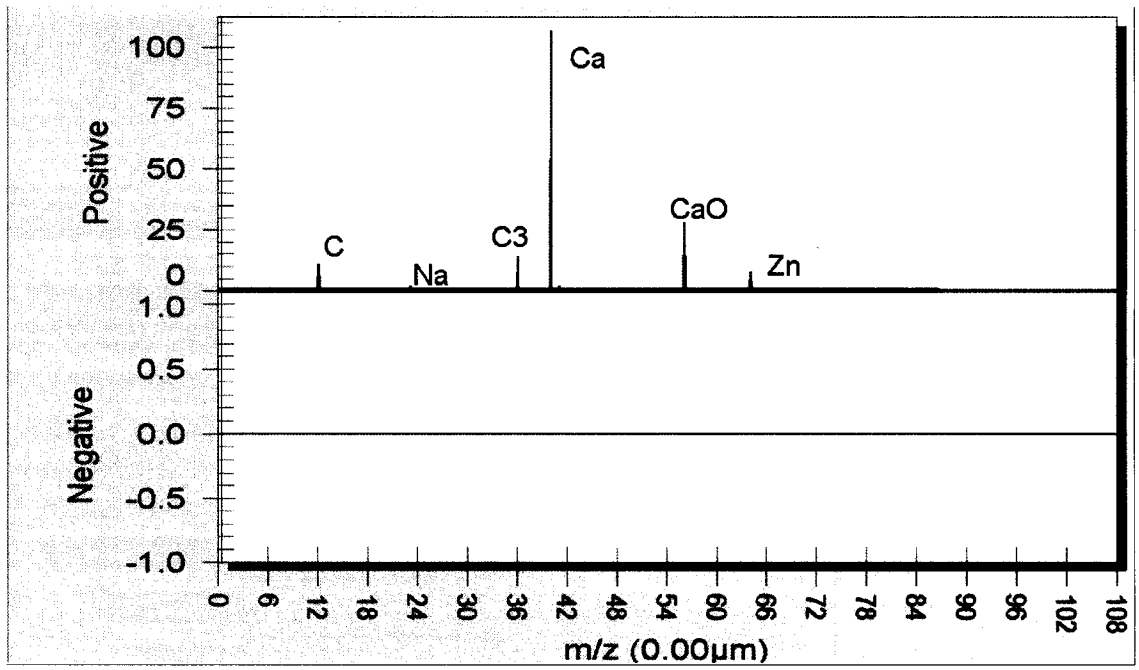

b) 60 nm particle

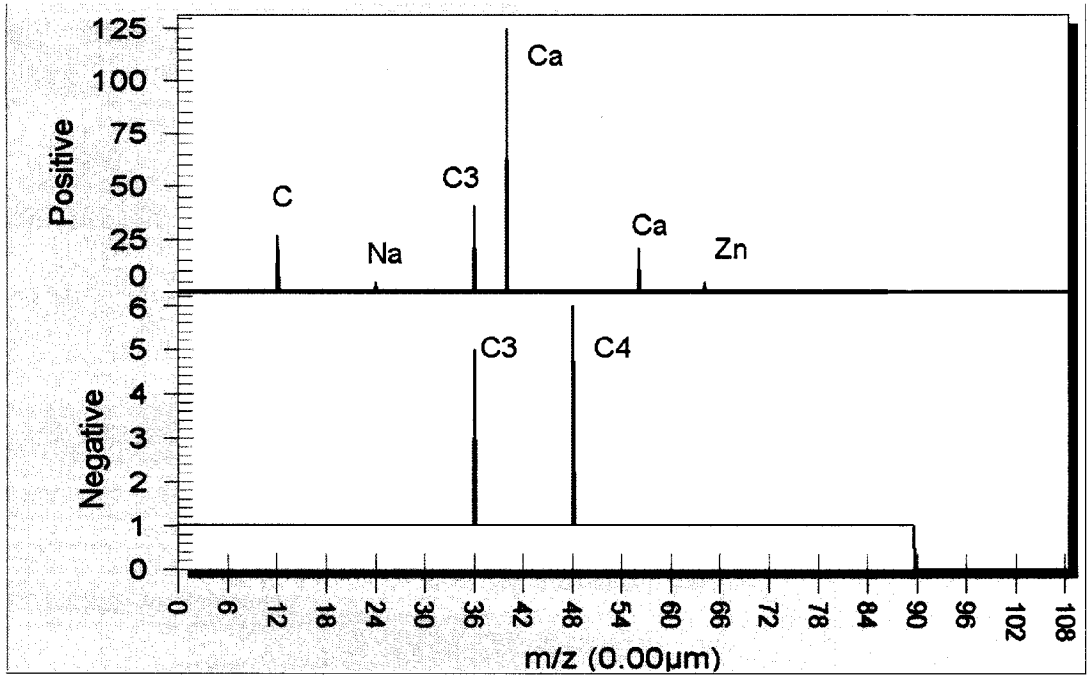

c) 75 nm particle

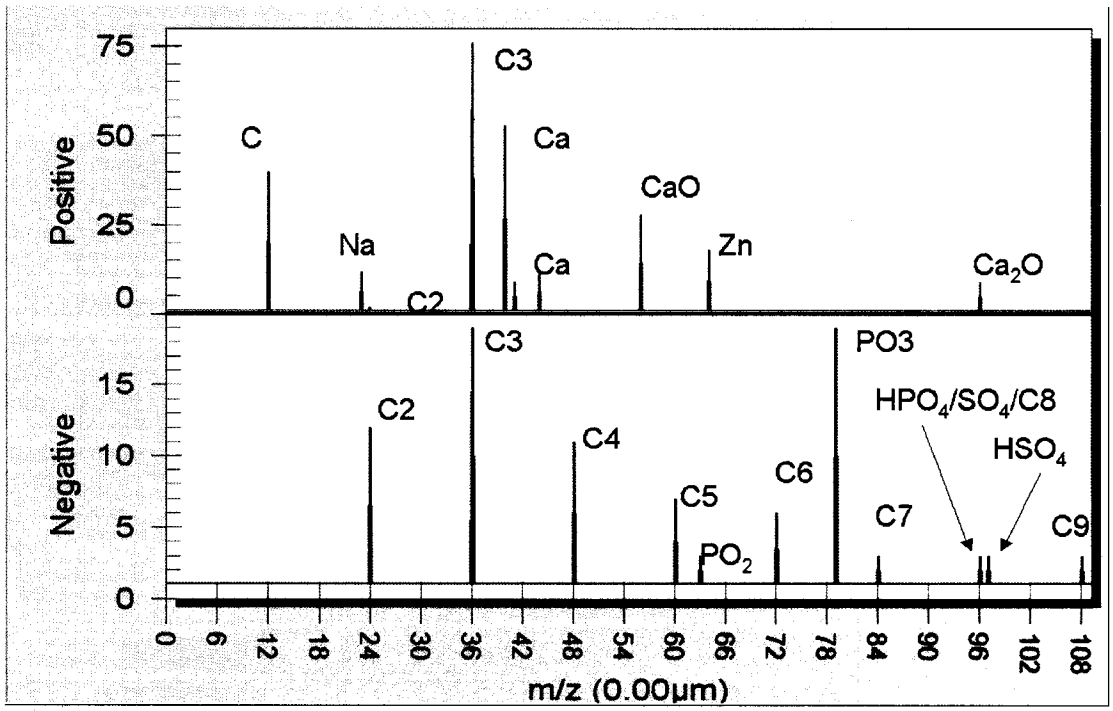

d) 90 nm particle

Figure 7.2 - ATOF Spectra: a) 40 nm particle (Ca nanoparticle), b) 60 nm particle, and c) 75 nm particle, and d) 90 nm particle ("typical" agglomerate particle).

Thousands of spectra were collected during the course of this work. Each spectrum is unique, as is each particle. Key to the analysis of the particles is the application of customized software to help sort and analyze the numerous individual particle spectra collected during lab tests. Toward this end, Dr. Dong Geun Lee (Lee, et al, 2004) developed software for use with our SPMS that provides a method for quickly sorting hundreds of data files and providing statistical analysis of the relative size of all spectral peaks for multiple elements. The software also allows for rejection of "bad hits," which are spectra containing only background (BG) signals, or dominated by BG noise. For analysis purposes, all O_2 and N_2 signals were considered to be noise, induced by the presence of air in the aerosol stream. The ATOF-MS also has dedicated software which allows sorting of data files and a variety of post analyses on the data. Analysis of the ATOF-MS data gathered in this experiment will be presented in a future publication (Miller, et al, 2005).

7.4 Results and Discussion

In this section, I first discuss the determination of particle composition from the SPMS data, with an eye toward quantifying the distribution of metal on particles of various sizes. The relative proportions of the main elements found in each particle were derived from the ratios between peak areas in the particle mass spectra. The validity of this assumption has been reported in a prior work (Mahadevan, et al, 2002). I thus determined both the size and elemental composition for each of many particles and used this to investigate the distribution of a particular element across the measured particle

size range. Note that calcium is quite prevalent in the data. This is due to its abundance in the oil, as well as its apparent propensity to readily self-nucleate.

The data from ATOF spectra were not as useful for assessing the elemental ratios, due to the lack of total ablation of particles. However, this incomplete ablation presents an advantage when looking for the presence of compounds such as oxides, (which may shed light on the particle formation process).

7.4.1 Single Particle Mass Spectra Sorted by Class

Due to the great variety in aerosol composition as observed in the mass-spectra, I found it useful to sort the spectra into three classes of particles. In the ensuing discussion, I will refer only to the sorting of SPMS spectra. Although the ATOF spectra were not sorted by class, the three classes of particles were readily apparent in that data as well (Figure 7.2a-d). For the purposes of the following discussion, the SPMS spectra were sorted into classes as follows.

1) "Ca-rich" particles are defined as those where Ca was >90% of particle mass. These are typically agglomerates of Ca primary particles that were self nucleated in the engine.
2) "Organic Carbon" particles are those where H/C >1. They are typically nanoparticles or small agglomerates containing fuel or oil residues rich in organic carbon i.e. rich in hydrogen.
3) "Elemental Carbon" particles are those with H/C <1 and <90% Ca content. This class of particles is dominated by large carbon agglomerates with peak diameter around 110 nm.

Note that the values of C, H, and Ca, as well as other elements referred to in this chapter, are molar ratios and are obtained from the areas under the elemental peaks of the individual mass spectra.

Before looking at detailed particle stoichiometry, I present the SPMS results for these three particle types, in terms of the frequency distribution of each type as a function of particle size. Figures 7.3a-d show the number-weighted volume-equivalent size distribution, for each of the three classes at four different engine conditions. Although these particle classes are by no means definitive, some significant trends are noticeable.

For the lowest load (and thus lowest relative Ca throughput), Figure 7.3a shows the appearance of relatively large Ca-rich particles even before a nuclei mode is established (see 0kW curve in Figure 7.4). This is quite different from earlier work for Fe doping (Lee, et al, 2004) in which a strong nuclei mode of Fe nano-agglomerates was established well before any coagulation with the larger carbon agglomerates took place (Section 5.3). As load is increased to 2 kW, an accumulation mode of Ca rich particles (which were defined as particles containing more than 90% Ca in composition) begins to form. Note the right-most circle in Figure 7.3a. Even at relatively low engine load such as 2kW, Ca generation is high and both a nuclei and accumulation mode appear to be forming. It is unclear how a large accumulation mode can be forming, since the nuclei mode is relatively small. More research is required to clarify this. There are a few possible explanations that could be investigated including: 1) That the Ca particles are forming in zones where the C has burned out. 2) That the Ca catalyzes the burnout of C so only Ca survives, as suggested by earlier research (Kittelson et al., 1978). 3) That the Ca or CaOx primary particles form differently than iron, particularly in terms of the time

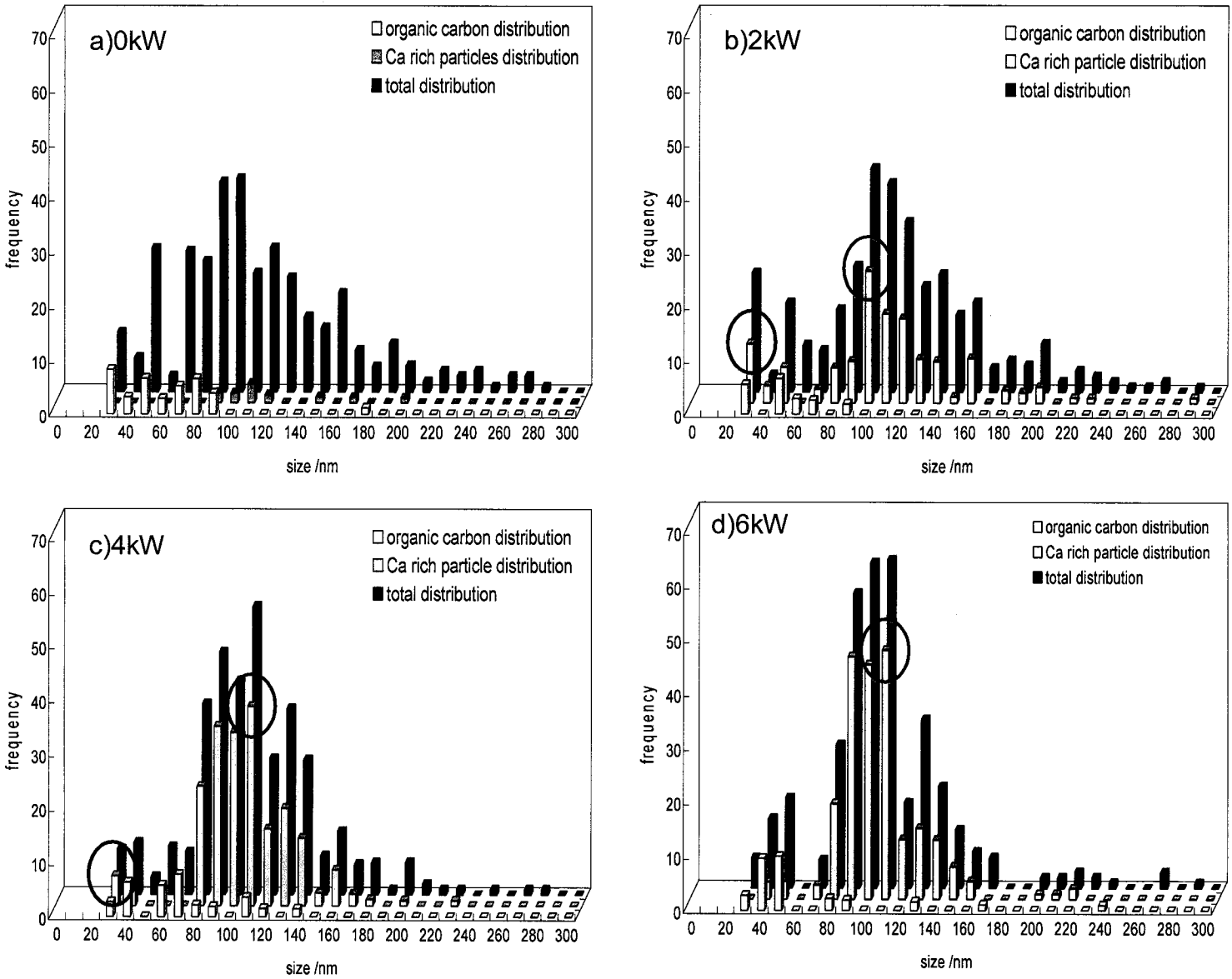

Figure 7.3a-d. Size distributions for three classes of diesel exhaust particles at:

a) 0 W load, b) 2 kW load, c) 4 kW load, and d) 6 kW load.

Note values on y-axis refer to frequency of occurrence.

history. They may form later, after the carbon already has reached a self preserving size distribution (SPSD). If so, as soon as they are forming, they are also coagulating with each other and with carbon particles. In comparison, Fe may form an SPSD before or simultaneously with carbon particles.

This is in line with theories of early FeOx formation in previous papers (Ritrievi, et al, 1987; Bonczyk, 1991). More convincing perhaps, is that the very low vapor pressure and the high boiling point of Fe both suggest that Fe will convert to particles much sooner than Ca. The difference between Ca and Fe laden particles might be explained by considering the kinetics of the process. Since the vapor pressure of Ca is much higher than Fe, it may not self nucleate at localized hot temperatures near the flame, but may wait until later in the process (during piston retraction) where cooling rates are typically not as high and more time is available for coagulation. This would favor coagulation with larger particles as opposed to growth in size of the nuclei mode.

The fact that Ca appears in large particles at the engine load of 2 kW (Figure 7.3) is indicative. It demonstrates that even as "nucleation" starts (as defined by first appearance of >7nm particles in the SMPS scans of Figure 7.4), the Ca is already creating large agglomerate particles. The mechanism for this is unclear, and it is suspected that perhaps these particles represent the remains of large soot particles that have burned out due to metal-enhanced oxidation. This is an issue which begs further research.

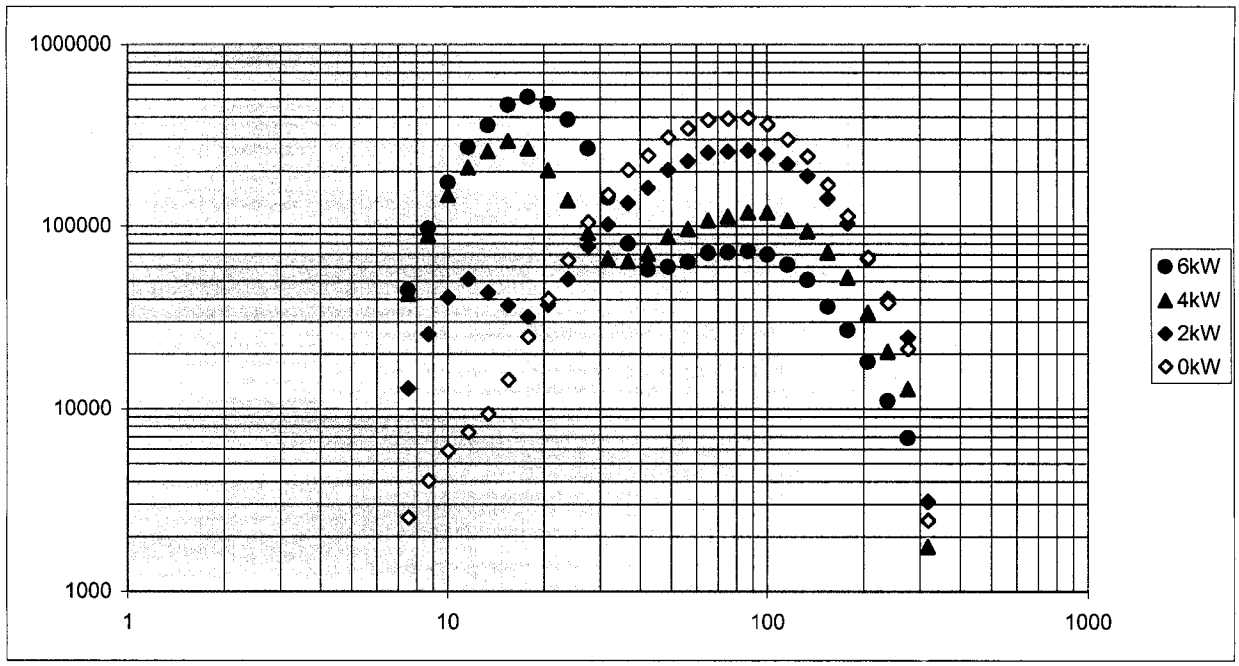

Figure 7.4 - Number-weighted size distribution of diesel particulate for different engine loads (for 1% lube oil doping of fuel). (Note that the 0 kW data in this figure are similar to the data for undoped combustion shown in Figure 6.3).

Using the data of Figure 7.3, the increase in frequency of Ca particles with engine load is plotted and shown in Figure 7.5. Note that at high load the Ca particles actually outnumber carbon particles. This trend may be in part due to the presence of Ca causing oxidation of carbon species, enhanced by the increased temperatures at higher engine loads. Such a reduction in carbon is also suggested by the decrease in the accumulation mode at higher loads, as reflected in the data of Figure 7.4. Also contributing to this trend is the fact that this particular engine produces more carbon at lighter loads (which is unlike most larger engines).

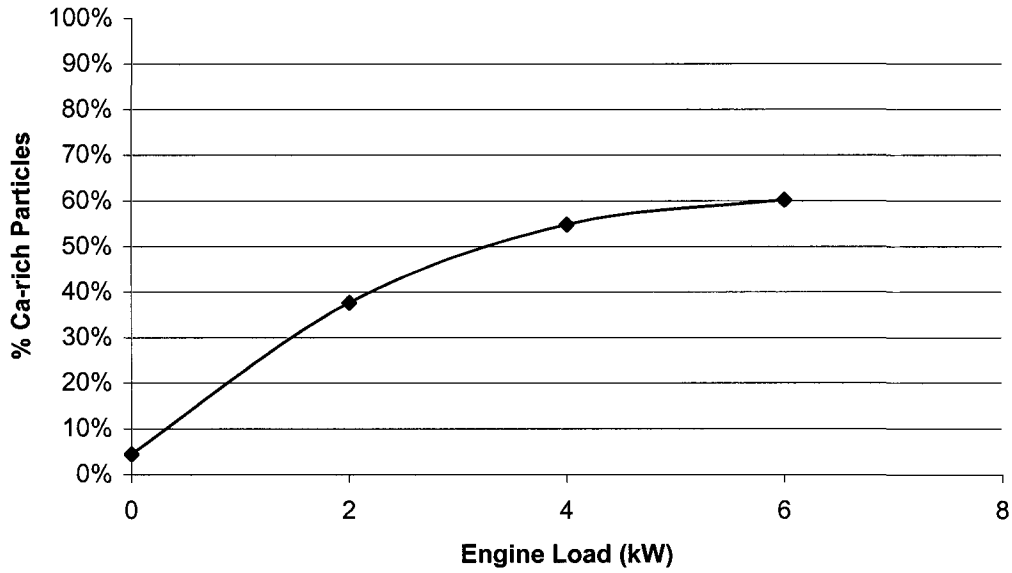

Figure 7.5 - Increase in the percentage of Ca-rich particles with engine load.

Among the additives in the mixed fuel (Table 7.1), Ca has the lowest saturated vapor pressure at the exhaust gas temperature of ~240°C in the tailpipe. This means that Ca may be the most probable species capable of adsorbing onto the preexisting nuclei or forming nuclei themselves. The other species such as Zn, P, Mg (because they have higher vapor pressure), might leave the tailpipe partly in the gas phase (as products of gas-phase reactions), or may condense only minimally onto particles as the combustion products cool (relatively slowly) in the exhaust system. This is certainly true of sulfur, which although it is much more abundant than Ca in the fuel mix, appears only in very small amounts on particles. EDX data suggest very small Zn amounts on large agglomerate particles, but the peak is close to the copper "pollution" from the copper TEM grids, and is difficult to quantify. This supports the assertion that the species

having large vapor pressure (Zn, Mg, P, S) are still there but that they are more randomly detectable, and in smaller amounts than might be expected.

7.4.2 Detailed Elemental Composition

In the following discussion I will focus on the composition of the particles analyzed with the SPMS. I will present results (Figures 7.6-7.8) that illustrate the analysis of numerous mass spectra to observe trends in particle properties, namely the amount of various elements in each particle. Each point on a graph represents the area under one elemental peak from one unique mass spectrum (i.e., one particle). The x-axis reflects the size of the particle analyzed, i.e., the volume-equivalent diameter calculated using the correlation described in a previous related work (Lee, et al, 2004). The values on the y-axis reflect the relative amount of each element determined by calculating the area under that elemental peak. For carbon, due to molecular fragments, there was sometimes more than one peak and in that case the area under all carbon-containing peaks was summed to give the amount of carbon for that particle. These area summations represent the relative contribution of each element in the particle, and therefore give mole fraction or particle elemental stoichiometry. The validity of this has been discussed in the literature (Mahadevan, 2002).

The relative volume of each element in various sized particles is represented in Figure 7.6. It is immediately apparent that the doped lube oil contributes a number of trace elements to the particles and that other than carbon, calcium is the dominant species. The data indicate that at the lowest engine load (Figure 7.6a), there are

numerous particles with considerable volumes of Ca, but very few that are "pure" Ca, as in Figures 7.6b-d. This is reflected in Figure 7.3a also, and suggests that when enough

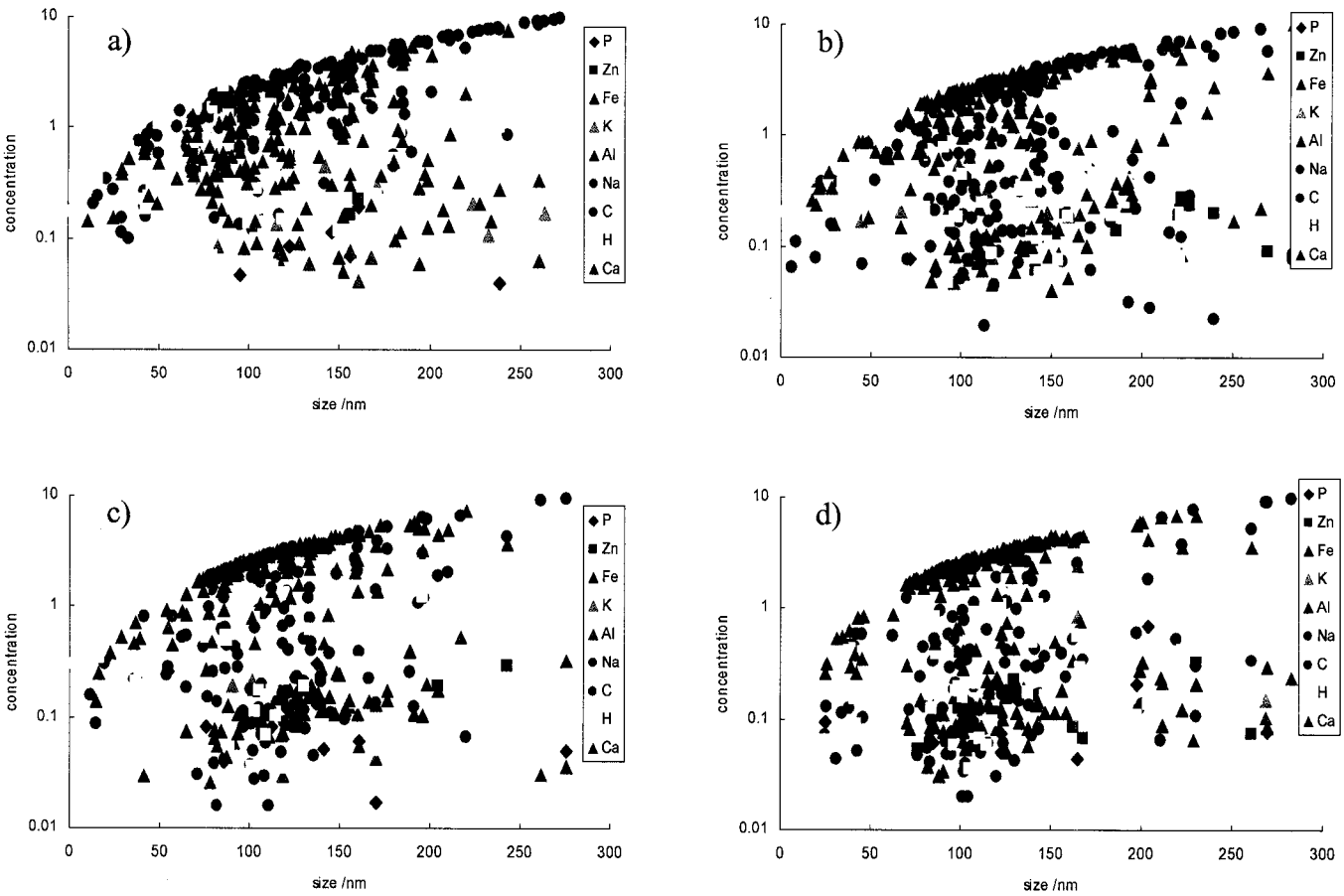

Figure 7.6 - Distribution of various elements across particle size range for four different engine loads: a) 0 kW, b) 2 kW, c) 4 kW, and d) 6 kW (fuel doped with 1wt% lube oil).

calcium is present, it may coagulate and form its own self-preserving size distribution. Conversely, when insufficient Ca is available, this process would be cut short and over the relatively long time span in the exhaust system, the undersized calcium particles

would eventually coagulate with carbon to form larger agglomerates of carbon and calcium or "combination particles."

The data of Figure 7.6 also show the apportionment of hydrogen on various sized particles. Note that the volume of hydrogen is inversely proportional to particle size, which supports a theory of hydrocarbon condensation onto particles as suggested in an earlier paper (Lee, et al, 2004). It appears that other (non-Ca) species may also display this trend, but since they occur in amounts near the limit of detection for the SPMS, the trend is not as obvious.

The data suggest that there are two main types of "accumulation mode" particles. Particles of the first type are not unlike the carbonaceous particles for undoped diesel combustion. The second type appear to be very high in the metals associated with lube oil, almost as if the lube oil were somehow being concentrated onto these particles. This is not likely, since the doped lube oil traverses the diffusion flame along with the fuel and is surely completely volatilized and decomposed. The formation pathway for the second type of particles is unclear at this time and that topic warrants further research.

The ratio Ca/(C+metal) was determined for many particles and the data are presented in Figure 7.7. At low load the data are scattered considerably, suggesting coagulation and numerous "combination particles" as noted above. At higher load, more and more particles are nearly pure calcium, and the most frequent size of these is around 100nm. Note that this peak size spreads slightly at higher loads, which is consistent with the flatter peaks for the SMPS data of Figure 7.4. Similarly to the data of Figure 7.3, the data of Figure 7.7 suggest that at low load, mainly "combination particles" exist, while at higher load, numerous Ca-rich particles exist.

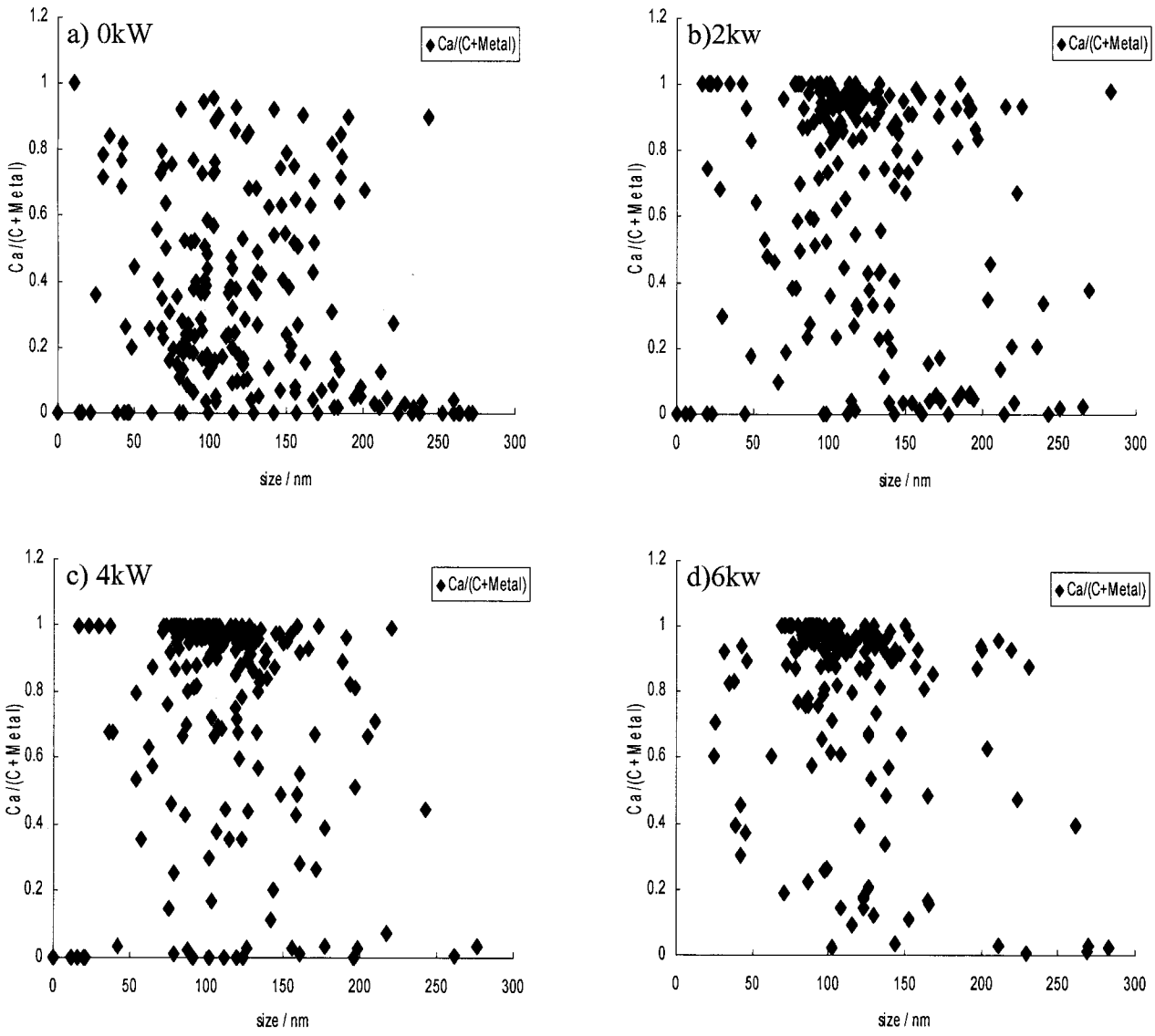

Figure 7.7 - Ca fraction in particles as a function of size.

7.4.3 Effect of Metals on Particle Formation

Figure 7.4 shows that when the fuel is doped with 1% lube oil, the size distribution of particles contains a distinct nuclei mode that increases with engine load. This nuclei mode is a direct result of increase in metal content due to increased fuel flow and thus higher throughput of metals from the doped lube oil. At the lowest load the metal content is at a minimum and the nuclei mode nearly disappears as seen in the figure. If the appearance of the nucleation mode is directly attributable to self-nucleation of metals then there should be a direct correlation between the mass concentration of metals in through the system and the volume of nuclei mode particles (~ less than 20 nm) for each condition. Figure 7.8 shows the relationship between Ca mass concentration and total volume of particles (less than 20 nm) measured for several different engine conditions. For this case, since Ca is by far the most abundant metal, I assume that it alone self nucleates, therefore only include the Ca mass concentration. The concentration was obtained for each operating condition as the product of doping level (Table 7.1) and fuel flow rate, divided by the volumetric flow through the engine. It is evident from the first two data points on the left that there is a "baseline" volume of small particles for this engine that is independent of the presence of metal. I attribute this baseline to the "tail" of the non-metal containing accumulation mode. The next three data points show that starting at a "threshold" value of about 0.35-0.4 mg/m^3 of Ca, the volume (and thus mass) of self- nucleated particles increases proportionally with the higher Ca concentrations in the exhaust aerosol. This threshold value corresponds to a critical M/C ratio at which

self-nucleation of metallic particles first begins. Further increase in Ca simply adds to the number of such nucleated particles.

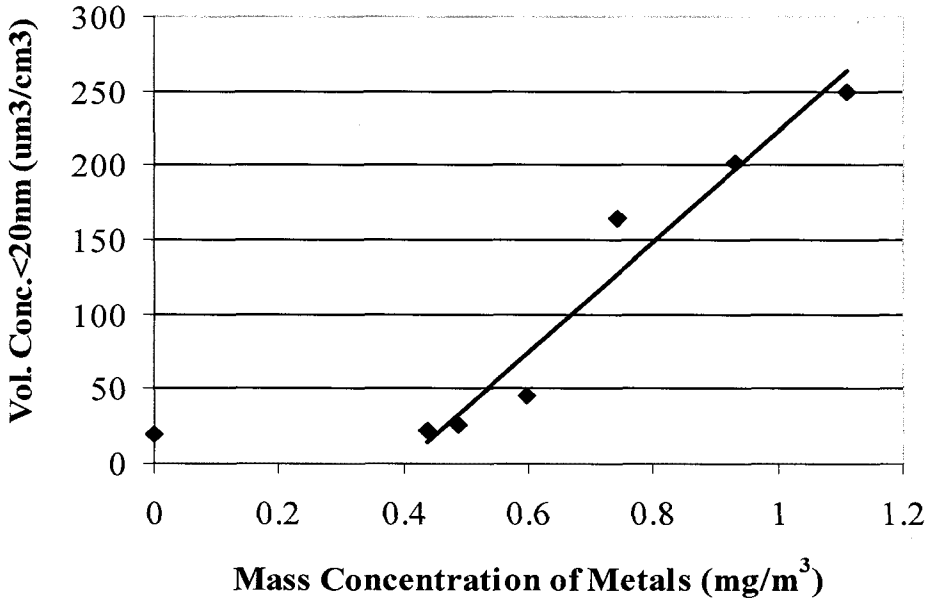

Figure 7.8 - Total volume of nuclei mode particles (<20 nm) as a function of the mass concentration of metal (only Ca in this case) in the exhaust aerosol.

Note that this process may occur for other elements, but it is unclear whether elements such as Zn and Mg are contributing to the nuclei mode for this case. Figure 7.9 shows nanoparticles collected using an electrostatic precipitator. Several of these were characterized using energy dispersive spectroscopy (EDS) and found to contain mainly Ca. It is possible that a few percent of such particles are also Zn or Mg nanoparticles, but this was not substantiated. In Figure 7.8, the inflection point at the Ca concentration of about 0.75mg/m^3 (which corresponds to the jump from 2 kW to 4 kW engine load), may suggest that another species such as Zn or Mg has started self nucleating, causing the

sudden jump in the volume of nuclei particles. This conclusion is clouded by the fact that fuel flow simultaneously increased, with corresponding increase in Ca concentration and engine temperature. Both of these could lead to more metal-driven oxidation of carbon particles during combustion, which would favor increased nucleation, i.e., by reducing available surface area for vapor deposition. (The inherent reduction in carbon at higher loads for this engine certainly plays a role here also).

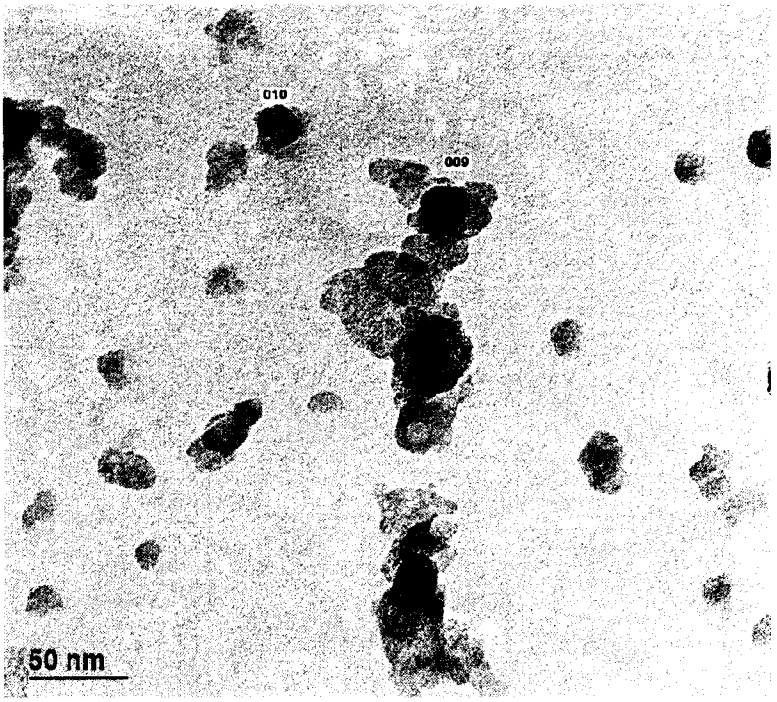

Figure 7.9 - Calcium-rich nanoparticles (<50 nm) and carbonaceous agglomerates (>100 nm), collected with the ESP.

The role of metals in soot reduction is elusive. Figure 7.3 shows a notable reduction in accumulation mode particles, which translates into a reduction in the mass of soot emissions. This has been shown to correlate directly to the lowering of activation energy required for oxidation of soot particles due to the presence of metals (Jung, et al,

2003b) and is believed to reflect the oxidation of soot late in the expansion stroke. It is also suggested that the unique low-temperature (above 600 deg C) oxidation rates of diesel soot as compared to flame soots, may in fact be related to the presence of trace metals derived from lube oil consumption (Jung, et al, 2004b).

Another process which may play a role in soot reduction is the suppression of soot formation, presumably inside the diffusion flame. It is possible that the jump in nuclei mode volume evident in Figure 7.8 is partly a result of such suppression. The following discussion supports this assertion:

For the case of iron doping of fuel as described in Chapter 5, the increase in nuclei mode volume with engine load is approximately linear, which means it follows the linear increase in iron concentration in the system. For that case, the soot gathers iron fairly early in the combustion cycle due to the low vapor pressure and high boiling point of iron. The iron on the soot may then lead to oxidation of soot as indicated above (Jung, et al, 2003), but the resulting reduction in surface area will not affect self nucleation since the iron has already nucleated. Therefore, there is no direct link between self nucleation and soot oxidation, and the nuclei volume simply follows the iron content of the system. However, for the current case of Ca presence (via lube oil doping), the Ca has higher vapor pressure and much lower boiling point, so will appear on particles much later in the cycle (which should reduce soot oxidation), yet I measured as much or more soot reduction for that case. This could be a result of soot suppression in the diffusion flame. Suppression may be favored because the lower boiling point of Ca would produce significant Ca-vapors in the flame, which would assist carbon reactions and suppress soot formation. If this happens, the reduced surface area of soot would lead to the later

increase in self-nucleation of Ca. For such a case, the volume of nucleated Ca is not linked directly to Ca throughput (which is tied to the (linearly increasing) fuel flow rate). Rather, it may be linked to the suppression process which is likely not linear since it involves reaction rates. This, as well as experimental error, may explain the jump in nuclei mode volumes evident in Figure 7.8. Based on this explanation, it is possible that the Ca enhances both suppression and oxidation of soot.

Another way of looking at the role of metals during the particle formation process is to investigate the potential chemical equilibrium states that might occur during the combustion cycle. This can be done by performing calculations of equilibrium chemistry under conditions representative of the combustion cycle. For such work, the logical choice for a metal would be calcium, since it is generally in the lube oil as an additive and is combusted continually, entering the combustion chamber via various pathways. Calculations of equilibrium chemistry for simulated diesel combustion including the presence of calcium have been done previously (Abdul-Khalek et al., 1998) using the NASA Program Flame (Gordon and McBride, 1976). Results indicated that production of solid CaO was in fact predicted in the temperature range of about 1300-1700 K, which is typical of the temperature in the cool region of the diffusion flame plume in a diesel engine (Flynn et al., 1999). The calculations by Khalek et al. however, assumed an equivalence ratio of 0.36, which is leaner than would be expected inside the flame. A similar calculation was recently done (Jung, H., 2005), and yielded similar results (Figure 7.10). In that work, Jung calculated the equilibrium chemistry for a higher pressure (shown to have little effect) and a higher equivalence ratio (phi=4.0), as might be expected inside the diffusion flame. The results of those calculations (for the most

prominent Ca species) are shown in Figure 7.11 and indicate that CaO(cr) is produced at temperatures as low as about 1200 K and CaOH at around 1500 K, while the other major Ca species are formed at slightly higher temperatures starting around 1800 K.

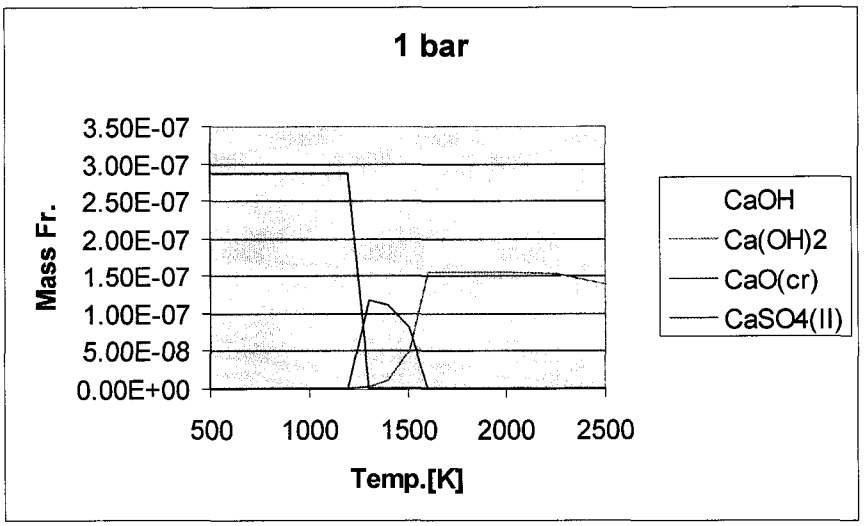

Figure 7.10- Results of equilibrium chemistry calculations (Jung, 2005) which confirm those done earlier (Abdul-Khalek et al., 1998).

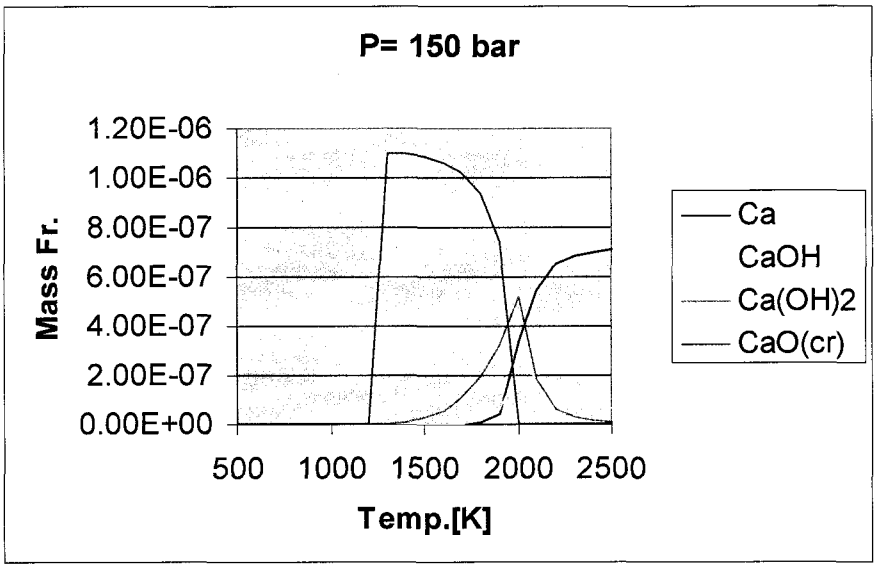

Figure 7.11- Results of equilibrium chemistry calculations (Jung, 2005) using elevated pressure (150 bar) and equivalence ratio (phi=4.0).

This result suggests that CaO could be formed inside the flame at temperatures ranging from 1200 to 2000+K and where the equivalence ratio is high. If that were the case, and the CaO survived the higher temperatures across the flame front, they might subsequently participate in the particle formation process. That explanation is supported by the data of Figure 7.2, which show significant amounts of Ca and CaO associated with representative particles of various sizes. Jung also made additional calculations, attempting to simulate conditions that might be found outside the flame (i.e. using equivalence ratio of 0.01), which yielded no Ca and only small amounts of CaO(cr) at relatively higher temperatures (Fig 7.12). The combination of high temperatures and low equivalence ratio might possibly be found in a small region just outside the flame front, so it is possible that some CaO could be forming outside the flame front as well.

The above technique of comparing single particle mass spectra with results predicted equilibrium chemistry calculations was shown to be a useful tool to investigate potential particle formation pathways. Another technique which may shed light on this issue would be to integrate the results of predicted equilibrium chemistry as input into a solution of the general dynamic equation for particle creation and growth from superheated vapors. Further research is warranted in both these areas.

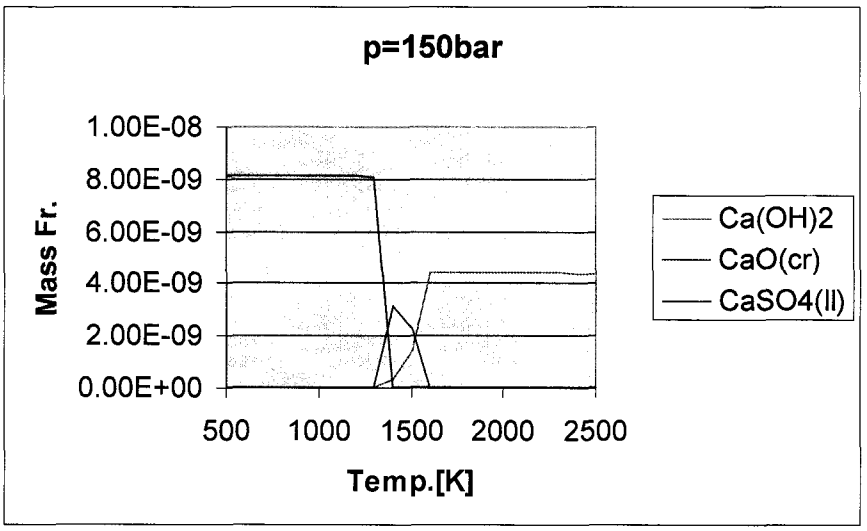

Figure 7.12- Results of equilibrium chemistry calculations (Jung, 2005), at conditions simulating the low equivalence ratio (phi=0.01) outside the diesel diffusion flame.

7.4.4 Implications Concerning Lube Oil Additives

The long-term goal of my research is to investigate the effect of metals (such as those from lube oils), on engine emissions under normal operating conditions. However there are two things which make this (lube-oil doping) work important. First, it is not uncommon to recycle waste oil by burning it in engines, and second, there is a new technology coming to the market that injects used oil into the fuel stream and then replaces it with fresh oil from a reservoir, in order to increase the time between oil changes.

The research described in this chapter, while it only indirectly sheds light on the issue of normal operation, gives a very clear picture of how particulate emissions are affected by burning small amounts of lube oil in the engine. The lube oil contains several metals both from additive packages and from engine wear. These metals likely have

different pathways by which they form into particulate matter, which will determine where and how they show up in (or on) particles.

A key issue which will be addressed in the next chapter is the difference in pathways and resulting morphology resulting from metals which participate in the "main" combustion, such as they do when they are doped into the fuel, versus how they behave when they originate from "normal" lube oil consumption, where their origin may be from droplets shed by the cylinder walls, which only peripherally take part in the combustion process.

We know that even under normal engine operation, metallic lube oil additives appear on diesel particles. In a recent work (Okada et al, 2003) a direct correlation was shown between the mass of Ca and organic carbon (OC) on bulk particulate samples, due to their common origin being lube oil. This is consistent with previous diesel particulate data showing that the OC originates from hydrocarbons associated with lube oil (Sakurai, et al, 2003). A similar correlation could probably be made for other lube-oil borne metals, but has not been done to my knowledge, perhaps since the smaller amounts of such metals hinder dependable quantification.

The particle formation pathways of metallic emissions have potential health implications. The concentration of metals on the soot and the potential for metallic nanoparticles are both closely tied to engine technology. For example, the newer "cleaner combustion" engines, i.e. low in soot production, combined with high (or even normal) oil consumption, will result in a higher metal to carbon ratio in the engine. Such engines will therefore generate particles with higher metallic content, and could also produce great numbers of metal-rich nanoparticles.

7.5 Summary

In this chapter I have shown that when lube oil is added to the fuel in a diesel engine, the metallic additives in the oil participate directly in the combustion process and subsequently exit the engine in particulate form. This has been shown to be true for Ca, P and Zn. Depending on their physical properties such as melting point, boiling point and reactivity, they may take a variety of pathways during this process. It has been shown that if metal to carbon ratios are high, metals (in this case Ca) can and do self nucleate and form metallic nanoparticles that have primary particle size in the 7-20 nm range, and that such metallic primary particles can coagulate to form larger (20-200 nm) agglomerate particles. Depending on the amount of metal in the system and on the relative time history of self nucleation of metals and carbon, metallic primary particles and/or their agglomerates may coagulate with carbon particles and form a population of "combined agglomerate" particles. The morphology of such particles appears to be a function of the time history of formation for the participating species, and may also be influenced by other forces such as particle charges or elemental affinities. Since coagualtion is a strong function of number density, it is likely that the coagulation process will be dominant during time periods when total number count is highest.

My current understanding of the particle formation process can be summarized as follows. The formation process begins inside a plume shaped diffusion flame (Flynn, et al, 1999). Carbonaceous agglomerates are formed in the fuel-rich jet and largely burned out in high temperature regions surrounding the jet. At about two milliseconds from the onset of ignition, when cylinder pressures are about 150 atmospheres and flame

temperatures reach a peak of around 2500K (Flynn, et al, 1999), most of the carbon in the fuel is oxidized, and only a small amount of carbon fragments survive (about 0.1% of the original fuel mass). As temperature drops into the 1100-1500K range from a combination of mixing with air surrounding the jet and near adiabatic expansion resulting from piston motion, equilibrium shifts favor the formation of solid metal compounds and gas to particle conversion must take place, either by homogeneous nucleation or adsorption onto existing carbon particles. This happens about 10 milliseconds after ignition at pressures of about 20 atmospheres (Flynn, et al, 1999). The relative timing of this will depend on the material properties of the individual species. Homogeneous nucleation is favored by a high metal to carbon ratio and should be very small under normal conditions, but will be enhanced for conditions representing an increase in the metal to carbon ratio.

As the resulting aerosol travels through the exhaust system, further cooling causes condensation of less volatile hydrocarbon species (such as heavy hydrocarbons from lube oil and trace PAH's) onto the particles, roughly in the order of their volatility. When the aerosol exits the tailpipe about one half second after ignition, at temperatures of around 600K, it again experiences rapid cooling, and any remaining semi-volatile species condense and/or self-nucleate into nanoparticles. Thus, if the concentration of metallic species is high enough, and the presence of volatile species great enough, the nuclei mode may contain both solid and volatile nanoparticles. Under such conditions, agglomerate particles will also contain metals, both from vapor deposition and from coagulation events with metal nanoparticles.

7.5.1 Key Findings

- The SPMS gives excellent tracking of metal to carbon elemental ratios in individual particles for metal content above about 0.25 mol%.
- The ATOF-MS has similar sensitivity, but due to incomplete ablation by the smaller laser, does not typically yield elemental ratios. It does however give signatures of some compounds (notably metal oxides), which is in this case very illuminating.
- At 1% lube oil doping of fuel and low engine load, self-nucleated Ca particles (about 10nm diameter) are detectable by the SMPS. This "threshold" condition corresponds to a Ca mass concentration of approximately 0.35-0.4 mg/m^3.
- As more metal is added to the system, above this threshold level, much of it will self-nucleate into nanoparticles during the combustion and/or expansion processes, and these nanoparticles will start coagulating with each other and with carbon particles.
- Mass spectra of Ca-rich agglomerates were measured with both mass spectrometers in the estimated range of 30-200 nm mobility diameter at high engine load.
- At all loads, the relative amount of hydrogen on each particle increases for smaller sized particles. This increase is non-linear in diameter suggesting condensation deposition of moderately volatile hydrogen-rich species onto existing particles (driven by the inherent cooling as they make their way out of the cylinder and through the exhaust system). Data also suggest the same for other (non-Ca) species.
- For modern engines with combustion systems optimized to produce low solid carbon emissions, a given metal content in the fuel will produce a higher metal to carbon ratio, and therefore a greater tendency to produce metal-rich nanoparticles in the exhaust.

7.6 References

Abdul-Khalek, I.S., Kittelson, D.B., Graskow B.R., and Wei , Q., 1998. Diesel Exhaust Particle Size: Measurement Issues and Trends, SAE tech. paper series 980525, pp1-14.

Bonczyk, P. A. Combustion and Flame. Vol. 87, pp. 233-244, 1991.

Bugarski, A. D. Characterization of Particulate Matter and Hydrocarboin Emissions from In-use Heavy-duty Diesel Engines. Ph.D. Dissertation -W. VA University, 1999, 254 pp.

Flynn, P., R. Durrett, G. Hunter, A, Loye, O. C. Akinyemi, J. Dec, and C. Westbrook. SAE Technical Paper 1999-01-0509, 14 pp.

Gard, E., and J. E. Mayer, et al. Real-Time Analysis of Individual Atmospheric Particles: Design and Performance of a Portable ATOFMS. Analytical Chemistry 69(20): 4083-4091, 1997.

Gordon, S., and McBride, B.J., "Computer Program for Calculation of Complex Chemical Equilibrium Compositions, Rocket Performance, Incident and Reflected Shocks, and Chapman-Jouguet Detonations, NASA SP-273, 1976.

Jung, H., "Calculations of Chemical Equilibrium for Simulated Diesel Combustion Including Presence of Calcium. Personal communication to the author, Feb, 2005.

Jung, H., D. B. Kittelson, and M. R. Zachariah. The Influence of a Cerium Additive on Ultrafine Diesel Particle Emissions and Kinetics of Oxidation. *Combustion and Flame, Volume 142, Issue 3, August 2005, Pages 276-288*

Kittelson, D.B., Dolan, D.F., Diver, R.B., Aufderheide, E., 1978. Diesel Exhaust Particle Size Distributions- Fuel and Additive Effects. SAE Technical Paper 780787, 11pp.

Lee, D. G., A. L. Miller, M. R. Zachariah, and D. B. Kittelson. Characterization of Metal-Bearing Diesel Nanoparticles Using Single Particle Mass Spectrometry. Approved for publication by the Journal of Aerosol Science, April 2005.

Mahadevan, R., D. G. Lee, H. Sakurai, and M. R. Zachariah. J. Phys. Chem. A. 2002, 106, pp. 11083-11092.

Miller, A., K. Park, D. G. Lee, D. Dutcher, D. B. Kittelson, M. R. Zachariah, and P. H. McMurry. Quantifying the Fate of Metallic Lube Oil Additives During Diesel Combustion using Single Particle Mass Spectrometry. Paper in preparation, 2005.

Reents, W. D., and M. J. Schabel. Anal. Chem. 2001, 73, 5403-5414.

Ritrievi, K. E., J. P. Longwell, and A. F. Sarofim. Combustion and Flame. 1987, Vol. 70, pp. 17-31.

Sakurai, H., H. J. Tobias, K. Park, D. Zarling, K. S. Docherty, D. B. Kittelson, P. H. McMurry, and P. J. Ziemann. Atmos. Environ. 2003, Vol. 37, pp. 1199-1210.

Okada, S., C. Kweon, J. Stetter, D. Foster, M. Shafer, G. Christensen, J. Schauer, A. Schmidt, A. Silverberg, and D. Gross, D. Measurement of Trace Metal Composition in Diesel Engine Particulate and its Potential for Determining Oil Consumption. SAE paper 2003-01-0076, 2003.

Utell, M. J., and M. W. Frampton. Journal of Aerosol Medicine, Vol. 13, pp. 355-359, 2000.

Wang, Y. F., K. L. Huang, C. T. Li, H. H. Mi, L. H. Luo, and P. J. Tsai. Emissions of Fuel Metals Content from a Diesel Vehicle Engine. Atmospheric Environment, 37, pp. 4637-4643, 2003.

Chapter 8 - Characterizing the Nuclei Mode of Exhaust Particles for a Modern Heavy Duty (CAT) Engine

Modern diesel engines emit less particulate matter (by mass) than their predecessors, but research shows that they sometimes emit a higher number of nanoparticles. According to my dissertation hypothesis, such particles may originate from self nucleation in the engine. In order to investigate that possibility, I designed an experiment to characterize such nanoparticles and investigate their origin. In this chapter I describe that experiment and discuss the experimental data. I specifically address the potential sources of both volatile and nonvolatile (solid) nanoparticles. I hypothesized that nanoparticles are formed when the cooling rate is high and available surface area (for vapor deposition) is low. I support this hypothesis by demonstrating that solid nanoparticles are in fact formed when the engine is idling and that they may be carbonaceous and/or may contain metals derived from the lubricating oil.

8.1 Introduction

Under normal operating conditions, diesel engines produce a tri-modal size distribution of diesel particulate matter (DPM), (Kittelson, 1998). In this chapter I discuss the two most common modes i.e. the accumulation mode which consists mainly of carbon agglomerate particles approximately 20-200 nm in diameter and the nuclei mode, made up of much smaller particles approximately 5-30 nm in diameter. The nuclei mode tends to be quite variable and can be attributed in many cases to the self-nucleation of volatile species during the dilution and simultaneous cooling of the exhaust aerosol as

it exits the tailpipe. It has also been shown that a separate population of nanoparticles may form prior to dilution and that this phenomenon can be enhanced by introducing trace amounts of metals into the fuel (Du, et al, 1998; Higgins, et al, 2002). The increase in nuclei mode particles is thought not to be a direct function of how "clean" the engine is, but rather to depend on the ratio between carbon (soot) and the nucleating species.

Improvements in technology have made modern diesel engines more efficient and clean burning than ever before. The mass-based emissions of DPM are now just a fraction of what they were a decade ago. These DPM reductions are mainly a result of reduced soot output. Modern electronically controlled, high pressure fuel injection systems accurately control the quantity and timing of fuel injection into the cylinders, leading to more complete combustion and therefore less soot.

Such reductions of soot have a significant influence on DPM formation in the engine. During gas to particle conversion after combustion, gases adsorb and condense onto the available surface area of existing particles. When soot is reduced, this available surface area shrinks, changing the dynamics of gas to particle conversion. The impact of this is most pronounced during periods of rapid cooling in the engine. When cooling is sudden such as during piston retraction, gas to particle conversion is limited by the condensation rate and available surface area. The saturation ratios of gaseous species may rise quickly, potentially triggering self-nucleation and subsequent nanoparticle formation.

The diesel combustion process has been fairly well characterized (Flynn, et al, 1999), but the details of particulate formation are still unclear. Based on previous research, the

current understanding of gas to particle conversion in a diesel engine might be summarized as follows:

Following the ignition event, a diffusion flame is established and at temperatures above 2000K, primary particles or "spherules" of carbon are formed at or near the flame (Roessler, et al, 1980; Siegmann, et al, 2002). The numerous spherules rapidly coagulate to form agglomerate particles. If other species of very low volatility exist, (such as fuel borne metals), they may vaporize in the flame and self nucleate as they transit the high temperature gradient outside the flame. Other reactions taking place outside the flame include combustion of materials derived from lube oil, which may also include metals. The result is a highly compressed aerosol of gases and particles in the slightly cooler region outside the flame. As the piston retracts, the system cools adiabatically and gases begin converting into/onto particles, roughly in the order of their volatility. Since temperatures are still on the order of 1000K, only the lesser volatile species such as metals and very heavy hydrocarbons will condense at this time and since the cooling rate is high, these may also have the opportunity to self-nucleate, especially if available surface area is low (Jung, et al, 2003). As the gases and aerosol leave the tailpipe, the cooling rate again is very high, and other volatile and semi-volatile hydrocarbon species will condense rapidly onto existing particles and may also self nucleate if conditions are favorable. The resulting aerosol mixes quickly with ambient aerosols, and becomes part of the atmosphere we breath (Finlayson-Pitts and Pitts, 1986).

The goal of the work described in this chapter is to shed further light on the topic of particle formation and to demonstrate how reductions in overall soot levels in the engine can lead to increased nanoparticle formation. This is accomplished through investigation of the nuclei mode of particles emitting from a modern (clean burning) heavy duty truck engine.

8.2 Experimental Set Up and Procedures

The experimental set up used for this work is sketched in Figure 8.1. The engine is a 1995 Caterpillar 3176 C-12 Diesel engine designed for use in over the road trucks.

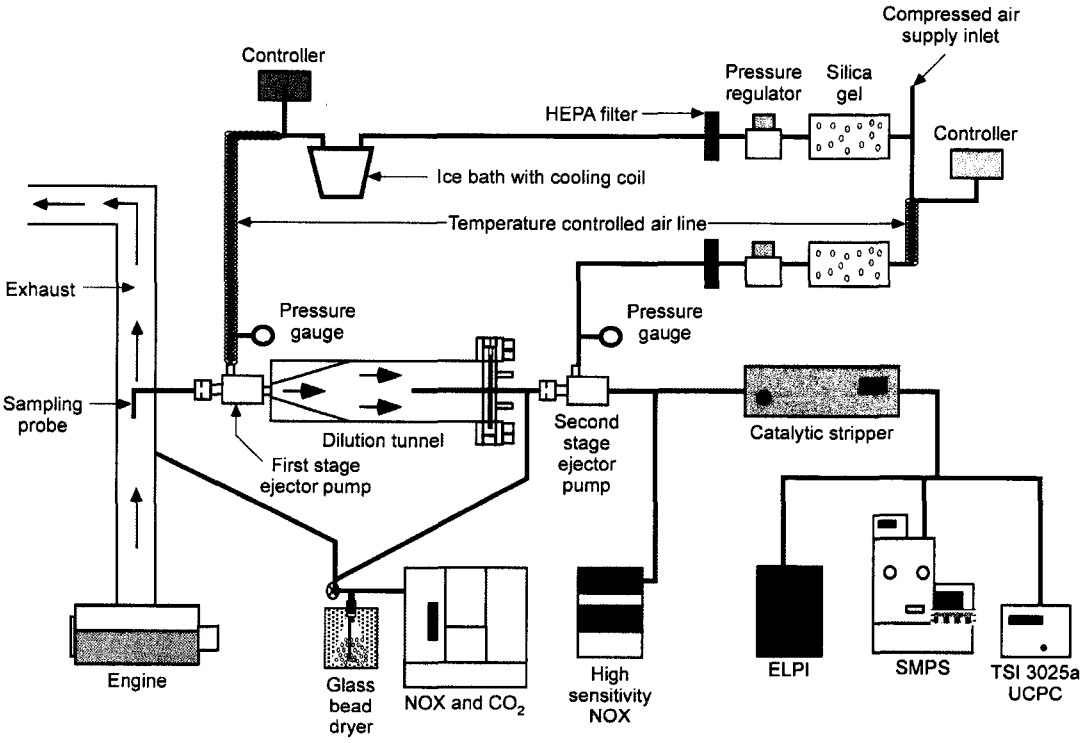

Figure 8.1- Experimental setup.

This engine has been reconfigured and reprogrammed to meet the post consent decree 1998 standards. It is an electronically controlled, direct injection, 6 cylinder, 12 liter, turbocharged and aftercooled engine, which has been derated to 265-kw (355 hp). Load is applied to the engine by an eddy current dynamometer. The dynamometer utilizes an open loop control system so that by adjusting the engine "throttle" and dynamometer load, one is able to achieve a desired operating condition. The load is controlled by a Digalog dynamometer controller.

8.2.1 Dilution

To provide a stable aerosol for sampling, engine exhaust is diluted using a two-stage micro-dilution tunnel adapted from an earlier study (Abdul-Khalek, et al, 1999). In this system, exhaust is diluted with dry, filtered, temperature controlled air using Air-Vac TD-110 air ejectors. A portion of the exhaust is routed through an insulated, stainless steel transfer line (20-cm long, 4-mm inside diameter) to the first stage of dilution. Here a TD-110 air ejector mixes dry filtered air at a constant temperature of 21°C with the sampled exhaust aerosol. After first stage dilution, the mixture passes through the residence time portion of the dilution tunnel where the aerosol is allowed to age. The residence time in this tunnel can be varied by means of a moveable sample inlet within the tunnel that leads to the secondary ejector. Residence times for the current tests are about one second. The sample is then diluted again using a second TD-110 air ejector. Dilution air for the second stage ejectors is controlled at 25°C.

During each test the primary dilution ratio is monitored by measuring the NO concentration before and after the primary ejector using a Thermo Environmental Instruments (TEI) NO gas analyzer. The secondary dilution ratio is monitored using a separate high sensitivity Monitor Labs (ML) NOx analyzer. Both of these instruments draw a small sample of exhaust and use chemilluminescence to measure the concentration of nitrogen oxides in the sample. For all tests the TEI instrument used calibration points of 0 ppm and 985 ppm, while the ML instrument used calibration points of 0 ppm and 9.6 ppm.

The NO measurements were used to calculate dilution ratios for each test. Dilution ratios for the first stage ejector ranged from about 22:1 – 29:1, with an exhaust sample flow rate of about 2-3 l/min. The second stage dilution ratios ranged from 22:1 – 26:1. All particle size distribution data was multiplied by the appropriate simultaneously measured dilution ratios to correct it back to the original tailpipe conditions.

8.2.2 Sample Conditioning

One of the main goals of the investigation is to characterize the non-volatile nuclei mode particles. To this end, a catalytic stripper is used to remove the volatile hydrocarbon material from the exhaust aerosol as demonstrated earlier (Abdul-Khalek, et al, 1995). The stripper used for these tests incorporates two substrate coatings, one for catalytic hydrocarbon oxidation and a second for removing sulfur. The stripper was operated at temperatures between 30 and 450 deg C for the various tests. Particle losses through the stripper due to processes including diffusion and thermophoresis were estimated using loss data developed for this stripper and published elsewhere (Kittelson

and Stenitzer, 2003). As with the dilution ratios, all size distribution data was corrected for these losses so as to reflect conditions at the tailpipe.

8.2.3 Experimental Equipment for Particle Sizing and Characterization

The instrument used for particle sizing was an SMPS, i.e., scanning mobility particle sizer (Wang and Flagan, 1989). The SMPS system I used is a modified home-built version of a TSI instrument and employs a long-column differential mobility analyzer (DMA), a model 3010 condensation particle counter (CNC) made by TSI inc, and an IBM personal computer running Microsoft Excel macro-based software.

To measure carbon output of the engine, filter samples of raw exhaust were collected for analysis by the NIOSH Standard Method 5040, (Birch, 2002) which determines the mass of elemental and organic carbon (EC/OC) on the filters. The samples were collected on pre-fired quartz filters held in 37 mm plastic cassettes. Using "ELF" portable pumps made by MSA, the aerosol was drawn through an isokinetic probe inserted through the wall of the exhaust pipe and routed through a silica dryer enroute to the filters.

Using an MSP Model 100 Micro-Orifice Uniform Deposit Impactor with nanoparticle attachment, i.e., NanoMOUDI (Marple, et al, 1991), size selected particle samples were collected on 3-mm-dia TEM grids for analysis by transmission electron microscopy and energy dispersive spectroscopy (TEM/EDS). The impactor was used in the non-rotating mode and the upper nine stages were sprayed with silicon grease to prevent particle bounce. On the four lower impactor stages (with aerodynamic cutpoints

of 56, 32, 18, and 10 nm), TEM grids were attached near the center of the impactor plates by carefully taping down the grid edges.

The sampled particles were analyzed using a Philips TEM machine with EDS capabilities. TEM images and EDS spectra were taken on impaction plumes and individual particles. Elemental ratios were calculated from spectra using the EDAX MX-TEM program "Materials Thin" that employs a thin-section approximation analysis strategy. When appropriate, substrate support film background spectra were subtracted from particle spectra.

8.2.4 Experimental Procedures

Since the number of nuclei mode particles varies greatly at different engine conditions, this investigation included three separate engine settings, i.e., idle, cruise, and acceleration. The torque and engine speed for these three settings were as follows:

Idle: 80 N-m @ 900 rpm

Cruise: 520 N-m @ 1500 rpm

Acceleration: 1450 N-m @ 1250 rpm

For each setting I measured baseline particle size distributions using the SMPS as well as total carbon emissions using filter samples analyzed by the NIOSH Standard Method 5040 (Birch, 2002). I then set the catalytic stripper to a given operating temperature (200, 350, or 450 deg C) and repeated the size distribution measurements, to determine what portion of the measured nuclei mode particles were "volatile."

Using this procedure I identified that the idle engine setting produces a significant nuclei mode of non-volatile particles. The origin and composition of such solid

nanoparticles is uncertain and is of great interest, so subsequent tests focused on their characterization.

With the engine at idle and the stripper set to maximum temperature (450 deg C), I collected size-selected samples using a NanoMOUDI cascade impactor (with no rotation). The particles were collected onto copper mesh style TEM grids coated with silicon monoxide films. The collected particles were analyzed by TEM and EDS to evaluate their morphology and elemental content.

8.3 Results and Discussion

Results are presented here in two parts. The first part is a review of how, for the three different engine settings, the particle size distributions change as the aerosol is passed through the catalytic stripper. The second part describes the particle characterization and shows how morphologies and metal to carbon ratios change under different conditions.

8.3.1 Particle Size Distributions

For measuring particle size distributions at the three engine settings, the exhaust aerosol was diluted approximately 500-800:1 with clean dry air, routed through the stripper set at a specific temperature, and then directed to the sizing instrumentation. The stripper was unheated for the first series of tests and those data constitute a baseline. For subsequent tests the stripper temperature was increased and the resulting changes in size distribution measured.

Baseline Particle Size Distributions

Baseline number weighted size distributions (SMPS data) for the three engine settings are shown in Figure 8.2. Each size distribution represents the average of three separate measurements taken over the course of about 30 minutes with the engine running at steady state. Note that for the acceleration setting, most particles are in the accumulation mode while for the idle setting most are in the nuclei mode. For cruise conditions, the number of particles is divided somewhat evenly between the two modes. Employing the assumption of spherical particles the SMPS data is used to estimate the total volume of particles emitted for each engine setting.

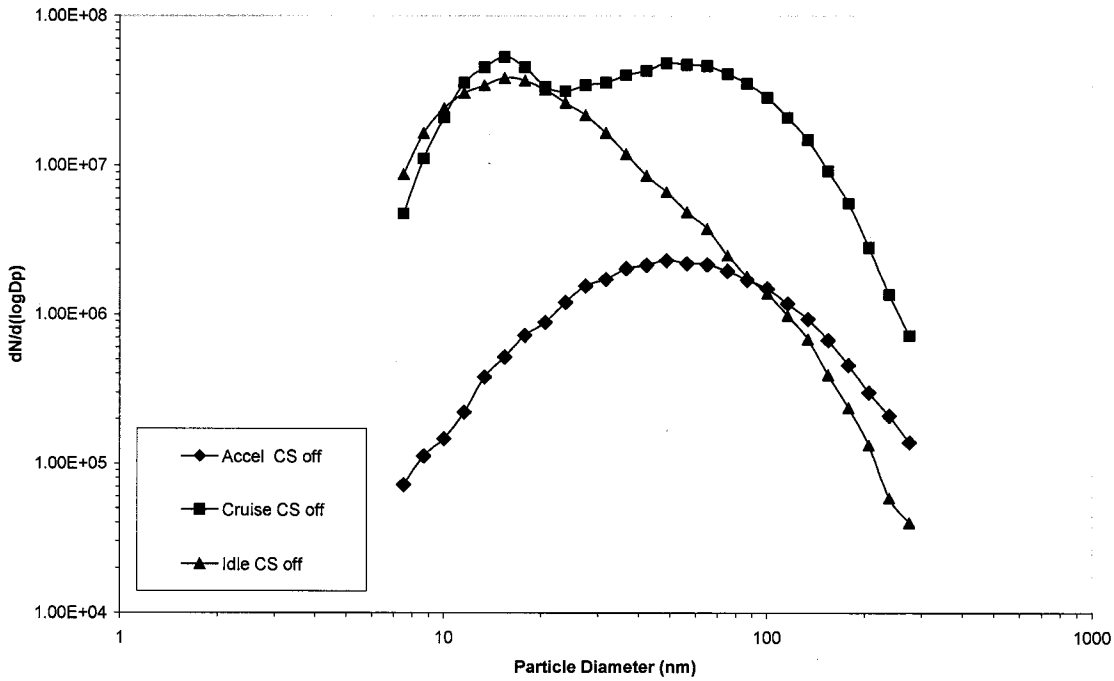

Figure 8.2- Comparing size distributions with CS at room temperature, for 3 engine settings (Idle: 80 N-m @ 900 rpm, Cruise: 520 N-m @ 1500 rpm, and Acceleration: 1450 N-m @ 1250 rpm).

Figure 8.3 shows how these volume estimates compare to measurements of total carbon mass, derived from filter samples of raw exhaust (analyzed using the NIOSH Method 5040). Neglecting the error from the spherical particle assumption, this data can be used to estimate the effective density of particles for each engine setting (by simply taking the ratio of bar heights in Figure 8.3).

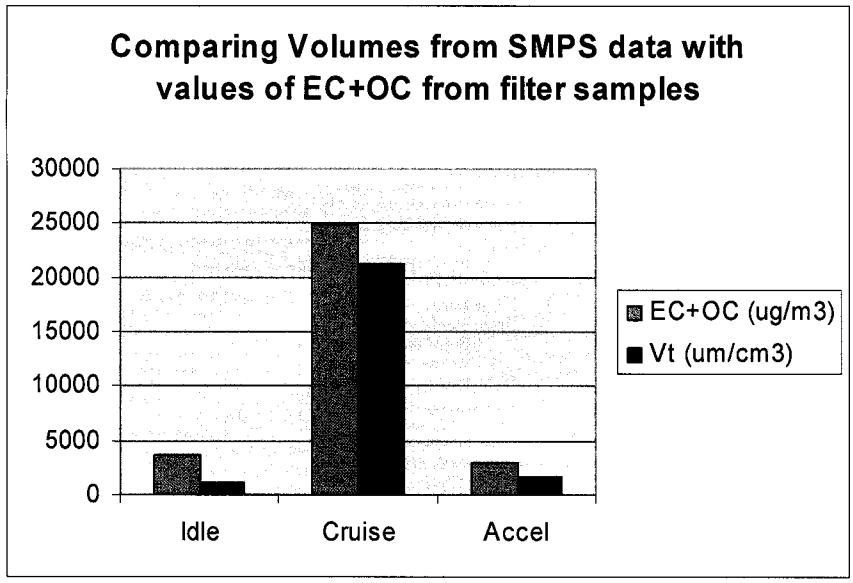

Figure 8.3 - Comparing total carbon (EC/OC data) for the three engine settings, to total particle volumes estimated using SMPS data.

This estimate yields effective densities of approximately 2.3, 1.1, and 1.5 for the idle, cruise, and acceleration settings respectively. Although these values are indicative of the relative density of particles at these conditions, they do not agree with the more detailed assessments of DPM densities in the literature (Park et al 2002). This is not surprising since the volumes estimated from SMPS data are typically rather low, which would suggest that these estimates of effective density are likely a bit high. The lower

density particles at cruise may be reflective of the great number of highly agglomerated particles, while the higher density at idle may reflect the high proportion of the (more dense) nuclei mode particles at that condition.

Another way of looking at the data is to to compare just the EC portion of the carbon measurements with the total volume of particles measured for the accumulation mode. This was done and the results presented in Figure 8.4. Note that for this case, the EC represents only a fraction of the volume of particles in the accumulation mode, reflecting that the OC also contributes to the volume.

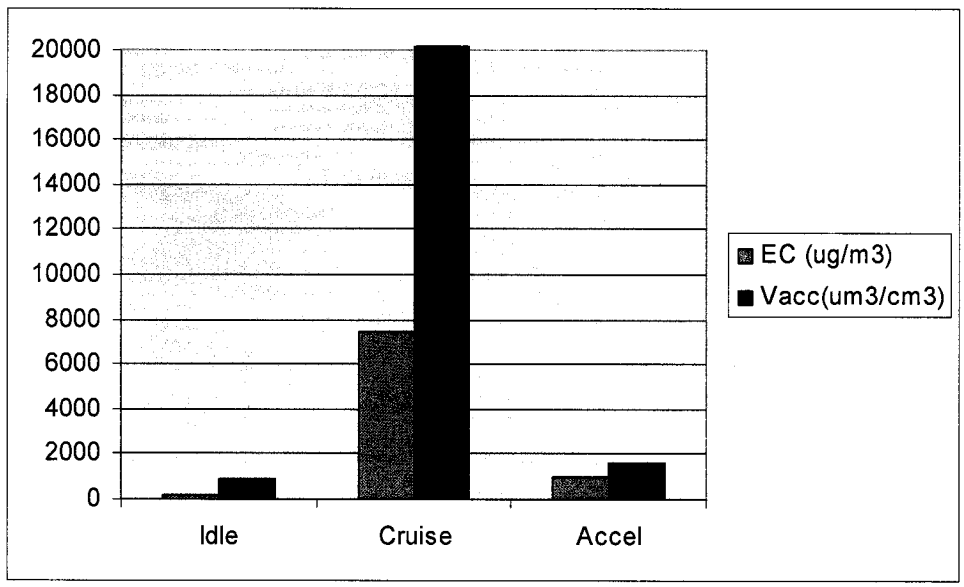

Figure 8.4 – Comparing EC measured from filter samples with particle volumes calculated from the accumulation mode of SMPS-measured size distributions.

From Figures 8.2, 8.3, and 8.4 it is observed that the acceleration setting is nearly as "clean" as the idle setting in terms of total mass of particles, it has virtually no nuclei

mode, and particles have higher density compared to the cruise setting. All these may be related to the higher engine temperature for that setting, which will be discussed further in Section 8.4. Note that exhaust gas temperatures were approximately 100, 300 and 500 deg C for idle, cruise, and acceleration respectively.

Post-Stripper Particle Size Distributions

To investigate the role of volatile materials, especially how they affect the content of the nuclei mode particles, the catalytic stripper (CS) temperature was increased for subsequent tests. An example of how this affects particle size distributions for the three engine settings is shown in Figure 8.5. The data indicate that as temperature is increased, the removal of volatile material reduces the size and number of nuclei mode particles. The fact that both size and number are reduced suggests there may be two main types of particles i.e., those that are "purely volatile" i.e., those formed by self nucleation during dilution cooling, and those that have non-volatile cores with volatile coatings. The former type are removed by the stripper while the latter survive but shrink somewhat. At the stripper temperature of 300 deg C (Figure 8.5), the nuclei mode nearly disappears for the cruise setting but remains quite large for the idle. This demonstrates that the engine produces more non-volatile nanoparticles at the idle setting. The composition of this unique class of particles is of great interest and subsequent data analyses were done to further address that issue.

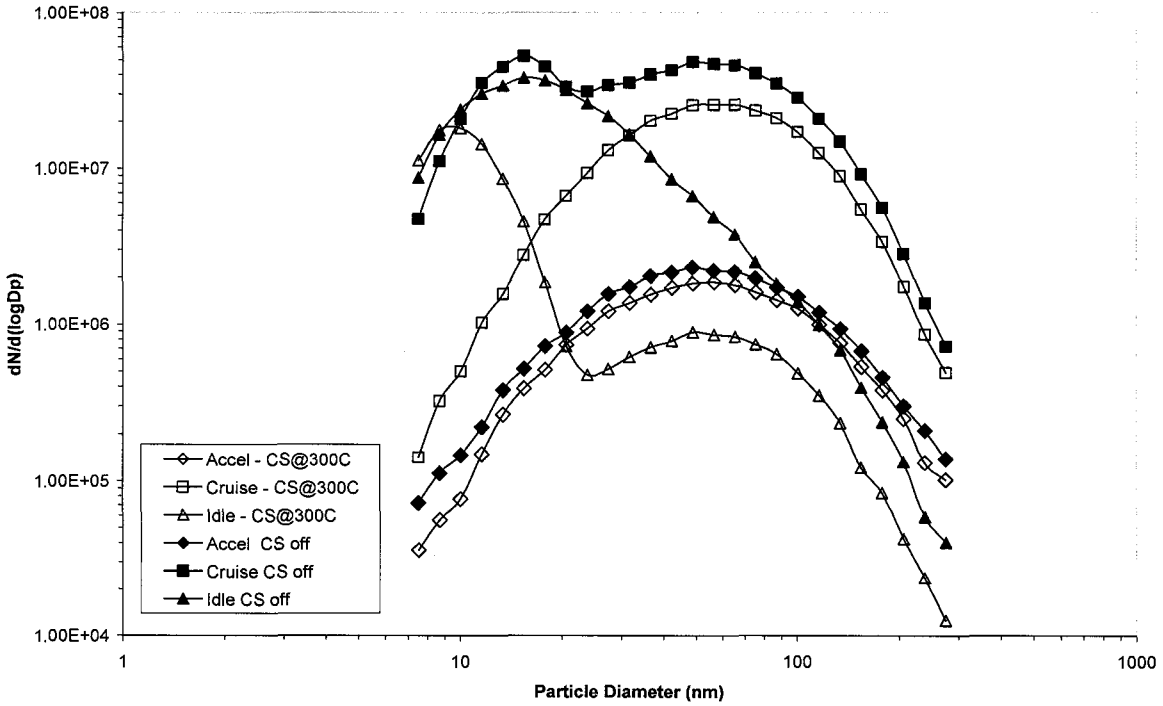

Figure 8.5 - Corrected SMPS data for three engine conditions, with catalytic stripper at room temperature and at 300 deg C.

To further investigate the effect of the stripper on both accumulation mode and nuclei mode particles, a curve fitting algorithm was developed and used to massage the size distribution data. The algorithm entails a statistical assessment and minimization of the "matching error" between the data and an idealized lognormal curve fit. Figure 8.6 shows that the fitted data matches well to the original (loss corrected) SMPS data, and also shows the idealized (lognormal) nuclei and accumulation modes for the idle engine setting.

This curve fitting technique was used to analyze the effect of the stripper on the nuclei mode particles at the idle engine setting. Figure 8.7 shows how the nuclei mode

changes as the temperature of the catalytic stripper (CS) goes from room temperature to 300 deg C. Many particles are lost and the mean size shrinks significantly. If we assume

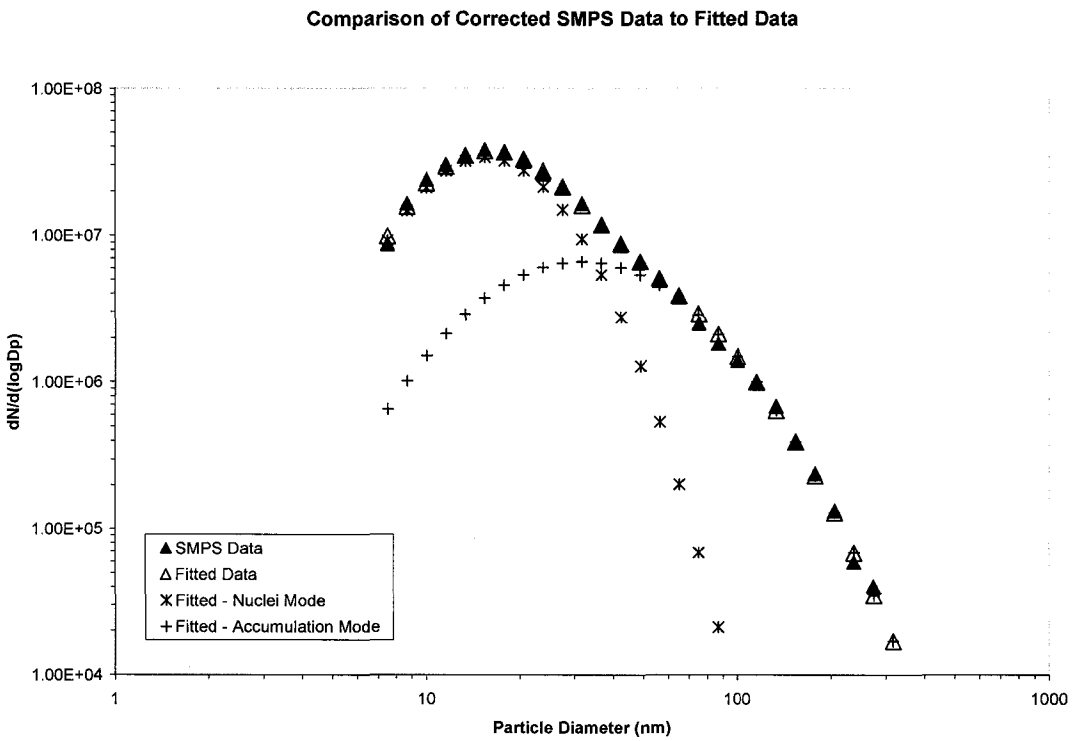

Figure 8.6 - Fitted SMPS data show that at engine idle, more nuclei mode particles survive the stripper.

that all the lost particles were completely "volatile" and therefore entirely oxidized, then the "difference" graphed in Figure 8.7 represents those volatile particles. The data indicates that under that assumption, the particles removed are approximately twice the size of the remaining "non-volatile" particles, suggesting two distinct types of particles. Additional (fitted) nuclei mode data at engine idle (Figure 8.8), clearly show the reduction in number and size as the stripper temperature increases. The mean particle diameter appears to be reducing linearly with temperature (Figure 8.9), suggesting that the smallest "non-volatile" particles may in fact be shrinking.

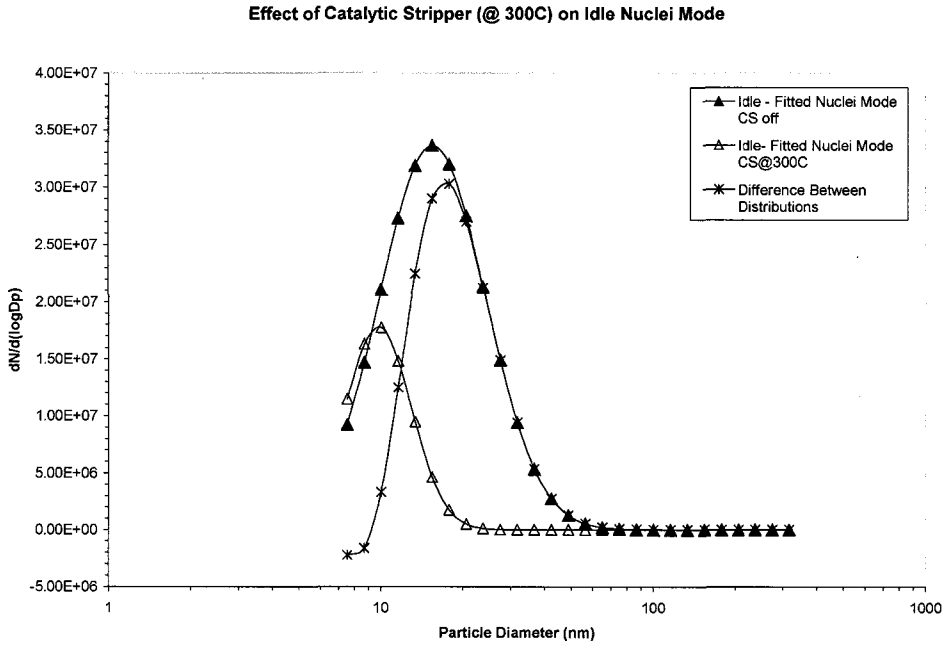

Figure 8.7 - Calculating the "difference" between the size distributions before and after the stripper ("difference" may be the "lost" volatile particles).

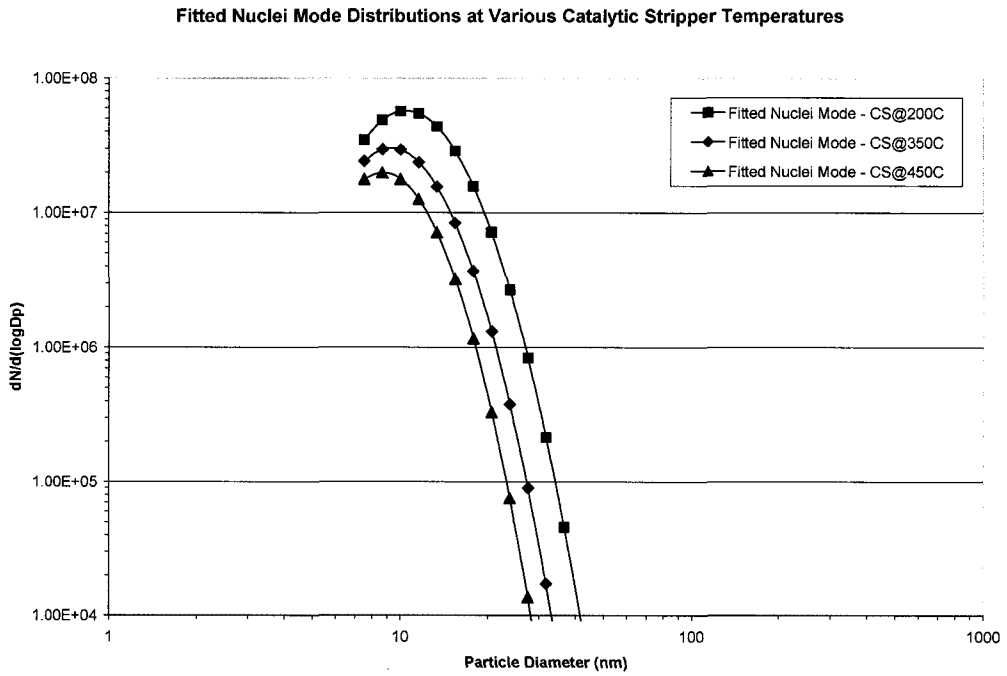

Figure 8.8 - Effect of the stripper on the nuclei mode (stripper at 200-450C).

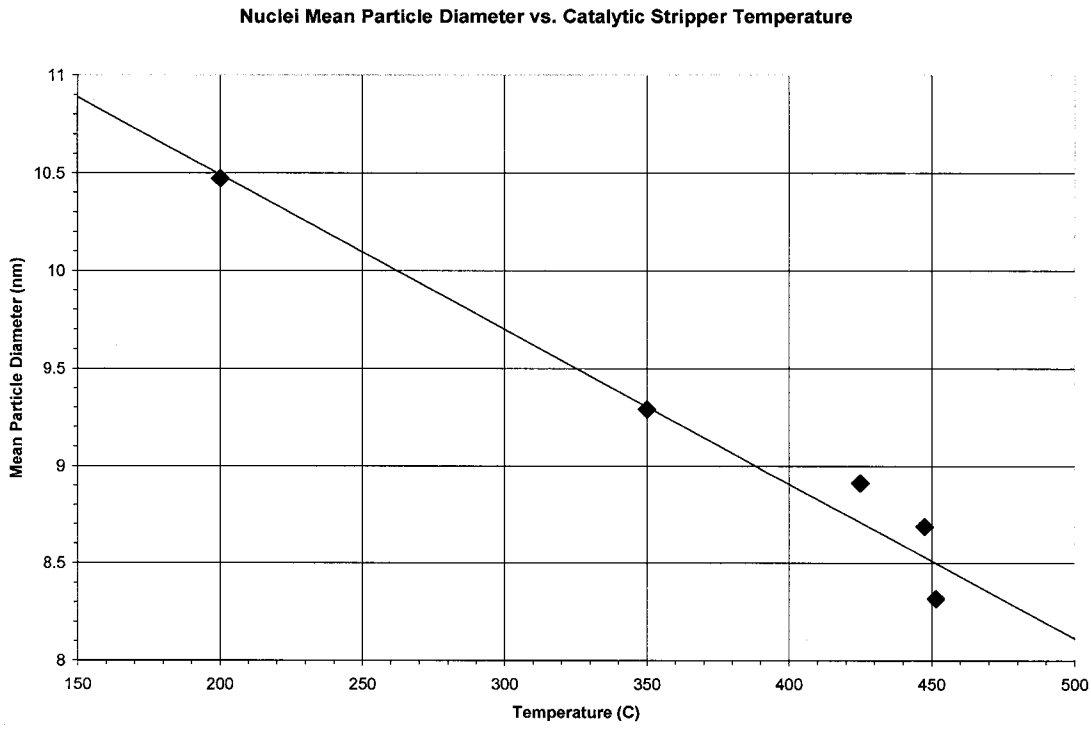

Figure 8.9 - Reduction in peak of nuclei mode volume is linear with stripper temperature for the idle engine setting.

The volatile material removed by the catalytic stripper is related to that defined as "OC" by the Method 5040. This relationship is evident in Figure 8.10, which correlates relative volume reductions by the stripper (derived from SMPS data), with relative OC fractions in the raw exhaust for four different engine conditions, as derived from filter samples analyzed by the Method 5040. Note that the slope of the fitted line suggests a reasonable correlation but the line is offset vertically. Extrapolating the line until it crosses the x-axis suggests that a fairly high percentage of OC is unaccounted for. There are four possible contributors to this. First, the volume reductions calculated from the SMPS data may not directly represent mass reduction since the removed particles may have different density than those that remain. Second, the non-carbon contribution to

particle volume may lower the measured volume reductions, especially at idle where ash content is high. Third, at temperature of only 300, the stripper may not be removing all the organic carbon. The remainder may in part reflect organic carbon that is "bound up" in the observed solid nuclei mode. If that material is derived from self nucleation of extremely low-volatile hydrocarbons, the increased surface tension of these very small particles may render them resistant to re-volatilization in the stripper. This effect would be greater for the idle setting. Finally, part of the offset may be due to differences in the two methods of oxidizing organic carbon. In the stripper, OC is oxidized catalytically but at temperatures of only 300 deg C, while in the NIOSH Method 5040, the OC is volatilized in a helium atmosphere at maximum temperature of 870 deg C. It is expected that the Method 5040 removes virtually all OC, while the stripper may not.

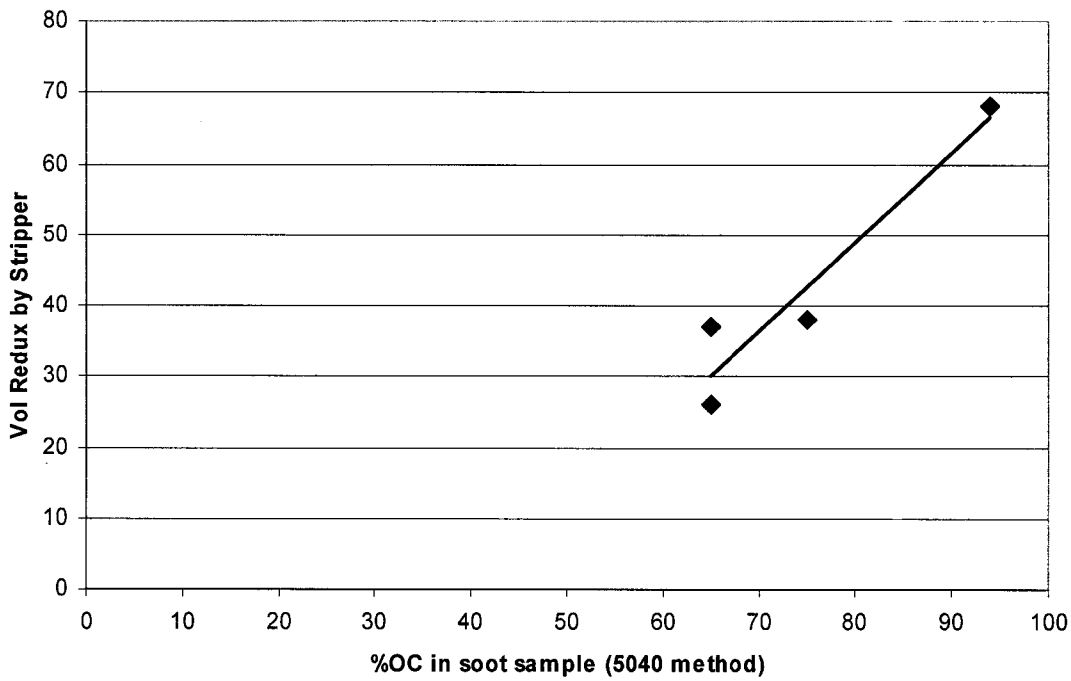

Figure 8.10 - Volume reductions by stripper (using SMPS data) versus OC% from EC/OC data at four different engine conditions.

It is also possible that a small portion of the offset may be due to a fraction of the organic carbon being bound up in the "non-volatile" nuclei mode and that these particles are self nucleated during the piston retraction event. For this to be true, in addition to the sudden cooling during piston retraction, the self nucleation of heavy hydrocarbons would require a high proportion of hydrocarbon vapors relative to the particle surface area available for surface deposition. To investigate this further, the ratios of OC mass to available particle surface area were calculated for the three engine settings, using the OC values derived from filter samples and using the surface area of accumulation mode particles left after the stripper as a measure of available surface area for vapor deposition. The ratios are plotted in Figure 8.11 and show a higher ratio for the idle setting. This suggests that the "non-volatile" nanoparticles observed for the idle setting may well be the result of self nucleation of heavy hydrocarbons (like PAH's) during piston retraction.

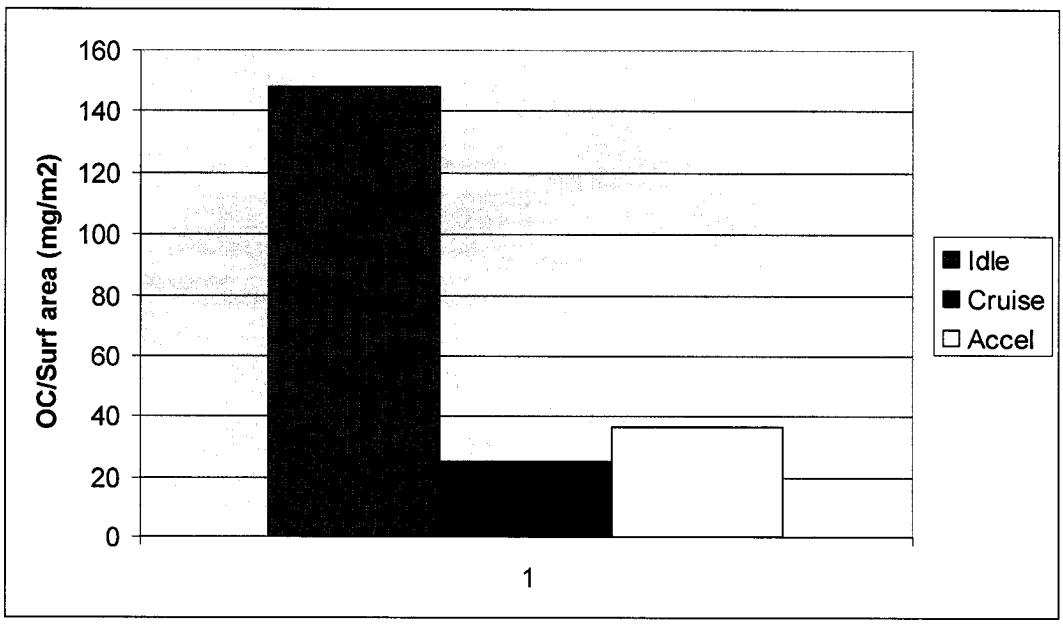

Figure 8.11 - Estimated ratio of available OC to available surface area prior to piston retraction.

8.3.2 Particle Characterization

Since the origin and content of the non-volatile nuclei mode became the focus of this experiment, particle characterization was mostly done on samples taken at engine idle. Particle samples were collected on TEM grids using a NanoMOUDI cascade impactor and characterized using TEM/EDS. The grids are 3 mm in diameter which is somewhat larger than the impactor orifice (jet) spacing, so each grid typically contains several impact plumes, each corresponding to a single jet (Figure 8.12).

The plumes generally have a starburst shape caused by the flow patterns resulting from the many (up to 2,000) closely spaced impactor jets. Although the plume centers are a solid mat of particles, near the edges there is usually a discernable pattern of large clumps of particles (Figure 8.13). At first glance it appears that these clumps are very large particles which "bounced" from the upper impactor stages. This is considered unlikely since for such a case it is probable that the large particles would impact into the mat of particles near the center of the plume, although they could hypothetically bounce outward and stick to the grid at the plume periphery. An alternate explanation for the patterns of clumps is that many particles have a horizontal trajectory at the plume periphery and when one particle sticks to the surface it presents an obstacle to other laterally moving particles and thus may collect others and "grow" into the large clumps we see. This may explain the observed patterns of clumps near the periphery but unfortunately does not help differentiate between large potentially bounced particles and the large particles which are in fact clusters of many smaller particles. For this reason it is not possible to estimate the relative mass of "properly sized" and "bounced" particles on a given grid.

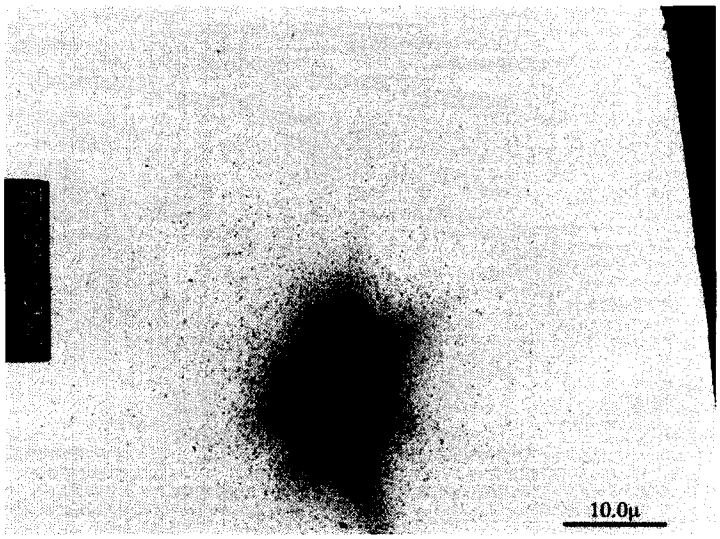

Figure 8.12 - Typical plume of particles deposited on TEM grid by impactor jet. Note the copper grid bar at right edge of image.

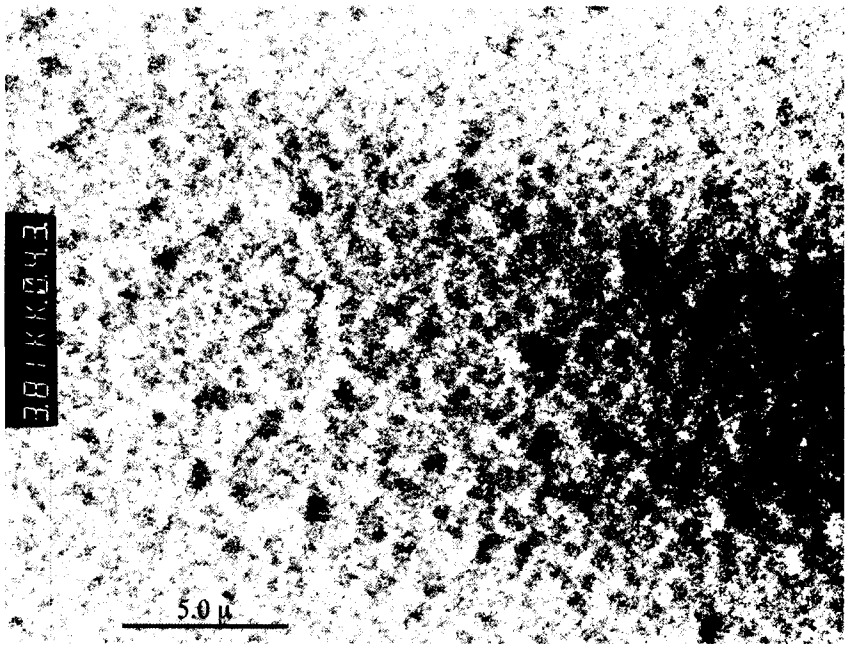

Figure 8.13 - Deposition patterns observable at periphery of impact plume.

For characterizing individual particles we chose particles at the far periphery of the plume (as shown in Figure 8.14a and b). Note from the figure that even at the

periphery there are often particles which are much smaller or larger than the designed cut-point range of the impactor.

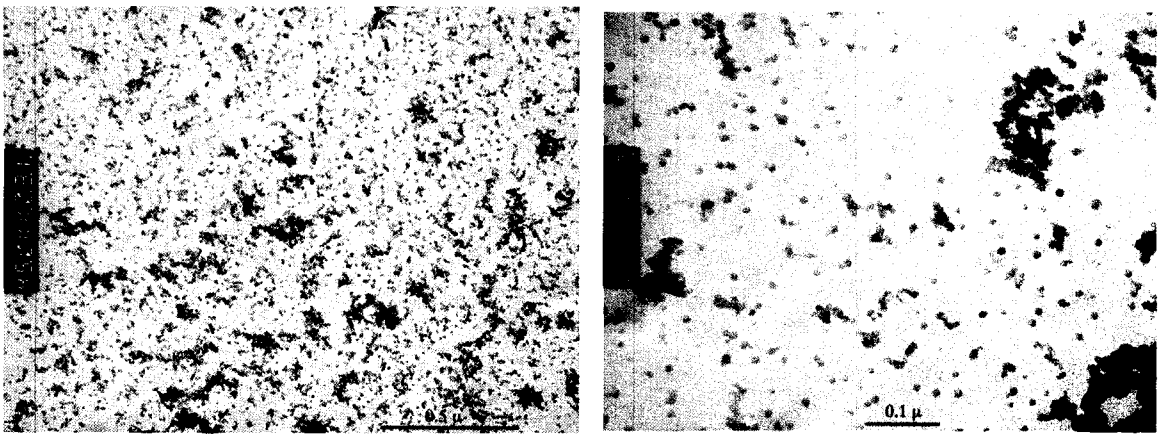

Figure 8.14 - Particle deposition at far periphery of plume typically includes many particles or clusters which are larger than the design cut point of the impactor.

Particle Morphology- TEM Images

Since the idle engine setting produces the most non-volatile nanoparticles, I chose to focus much of the TEM/EDS analysis on the samples taken at engine idle. The observed particles fall into three main categories as shown in Figure 8.15.

a) Carbon Agglomerates (~30-300 nm).

These particles constitute the bulk of the DPM, and are agglomerates of relatively spherical "primary particles" of elemental carbon (Roessler, et al, 1980, pp. 57). The diameter of primary particles varies somewhat but appears to have a mean of about 20-30 nm as reported earlier (Pipho, et al, 1992). The mean mobility diameter of the agglomerates is shown in Figure 8.2 to be about 70 nm.

b) Spherical Particles (~50-150 nm)

These particles are very high in metals, i.e., those derived from lube oil additives. Their origin is unclear, but it is possible that unburned oil droplets created by piston slop do not completely evaporate or burn but instead coalesce into these spheres. This type of particle is similar to those observed in the previous chapter where the diesel fuel was doped with lube oil, so it is possible that they form from vapors during piston retraction.

c) Non-agglomerated Nanoparticles (~5-30 nm)

This may include uncoagulated primary carbon particles, residue "cores" of oil droplets which partially combusted, and particles that self nucleated from vapors. Since all samples were run through the catalytic stripper, it is unlikely that the self nucleated particles are from volatile material but may be from any of a variety of more non-volatile vapors such as metals or very heavy hydrocarbons.

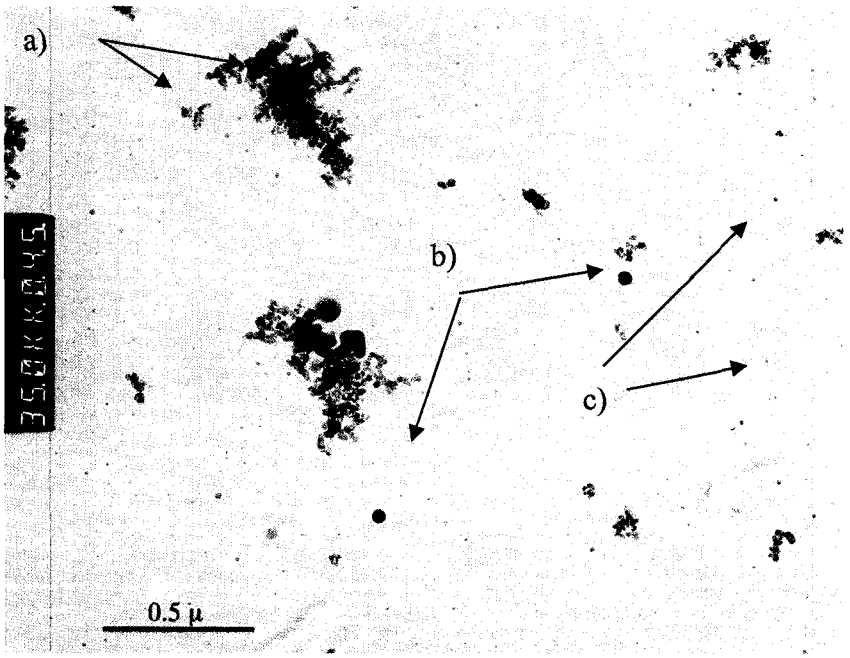

Figure 8.15 - Particle types: a) carbon agglomerates, b) metal spheres, and c) nanoparticles.

Particle Elemental Analysis- EDS spectra

The primary goal of the EDS analyses was to quantify the non-carbonaceous content of particles with an eye toward determining the fate of metals from lube oil additives. EDS analysis was conducted on the impact plumes and on individual particles and results are presented here.

In order to get the best sensitivity, EDS analysis was done on the dense center regions of plumes such as the one shown in Figure 8.12. Even using this technique, the sensitivity was marginal for samples taken at the cruise and acceleration settings. For the samples taken at idle, three EDS scans were done on a single representative plume from each of the four impactor stages i.e., for the four cut sizes 56, 32, 18, and 10 nm. Figure 8.16 is a typical spectrum from these analyses. Note that in this and other similar figures, the large Si and O peaks are assumed to come mainly from the silicon monoxide grids, while the Cr peak may be derived in part from noise generated by the sample holder. Using such spectra, the relative amounts of carbon and several metallic elements were estimated from peak areas using EDAX MX-TEM software and are expressed as metal to carbon (M/C) ratios in Figure 8.17. Note that there is considerable variability in the M/C ratios, especially at the lowest cut size, and a slight trend toward lower M/C for smaller sized particles. It is deduced that the combination of the somewhat random metallic spheres (details in next section) and the possibility of bounced particles may have combined to mute this trend, but certainly would not have reversed it.

I originally hypothesized that self nucleated metallic nanoparticles would dominate the lower size fractions yielding higher M/C ratios, but in looking at Figure 8.17, this does not appear to be the case. Nor does it appear that the higher surface to

volume ratio of the smaller particles has led to higher M/C ratios from condensing metals, as might be expected (Lee, et al, 2004).

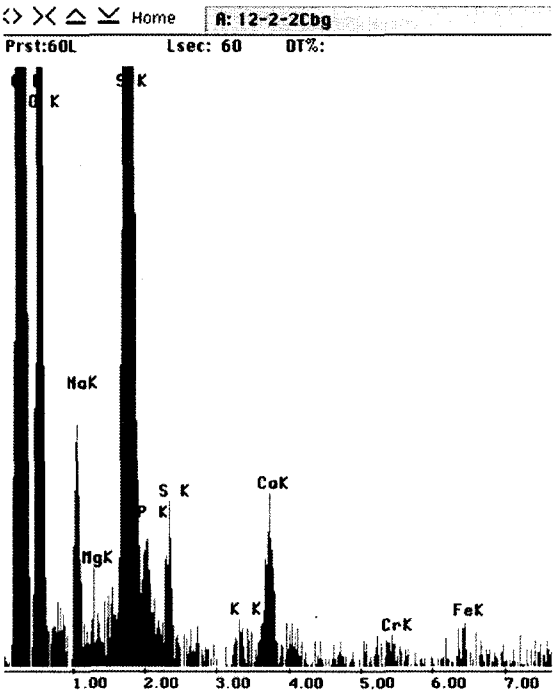

Figure 8.16 - Typical EDS spectrum of impaction plume.

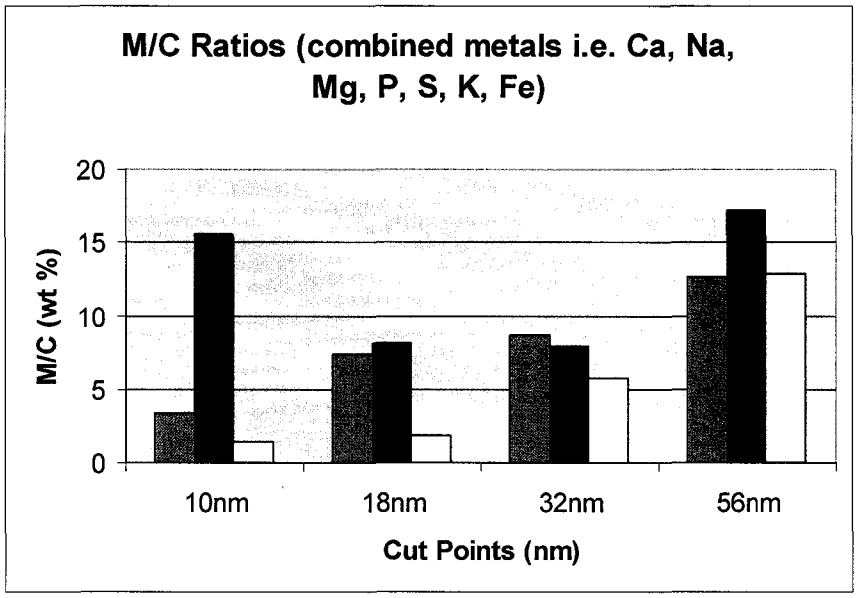

Figure 8.17 - Metal to Carbon ratios from impactor plumes at various impactor cut sizes. The three bar colors represent EDX quantification at 3 different locations of each sample.

In fact the data indicate just the opposite, suggesting that perhaps many of the nanoparticles form after metal deposition is partially or fully completed. This supports a theory of time dependent vapor deposition of species during piston retraction i.e. based on their volatility, concentration and the local instantaneous cooling rate. For the case at hand, such a process would entail deposition of metallic vapors early in the piston retraction event. This would be followed by deposition (and potentially self nucleation) of very low volatile hydrocarbons, while the more volatile hydrocarbons remain in vapor form until after piston retraction, when the system cools further.

Since Ca is the most abundant metal in all the samples, I calculated a bulk Ca/C ratio for the idle setting, and compared it to the estimated "threshold" Fe/C ratio for iron nucleation, cited in a previous work (Miller, et al, 2004). We found that the Ca/C ratio for our case was only slightly above the nucleation threshold, which supports the above argument that the self nucleation of Ca and other metals would likely be negligible under these conditions. The heavy hydrocarbons however, may easily be in higher concentration than the calcium, and so could be above their own nucleation threshold, which would explain the many carbonaceous nanoparticles observed.

Spherical particles in the size range of about 50-150 nm were observed frequently in the samples at idle, but virtually non existent in other samples. Such spheres contained mainly metals as indicated by the spectrum of Figure 8.18 (note that the S and O peaks are from the silicon monoxide grid films). The metals were typically those derived from lube oil (Ca, P, Zn, and Mg) but were not usually observed in the same relative amounts as they occur in the lube oil. In contrast, bulk M/C ratios for these four metals, derived from soot samples, showed a close correlation to their relative abundance in the virgin

lube oil (Figure 8.19). The origin of the spherical particles is unclear. One theory is that they are a product of oil "slobbering" at low engine load. That is supported by recent work (Dutcher, 2005), where 500nm+ oil droplets were emitted by this same engine at idle. If one assumes that the metals make up about 1% of the droplet mass, and the oil is assumed to combust/evaporate, these droplets would possibly shrink (by the cube root of 100 i.e. by a factor of about 4.5), yielding metal-rich residue particles on the order of 50-150nm as I observed. The fact that such particles were also found in DPM derived from combustion of lube-oil-doped fuel in the smaller engine described in chapters 5-7 suggests that this phenomenon is not unique to this engine.

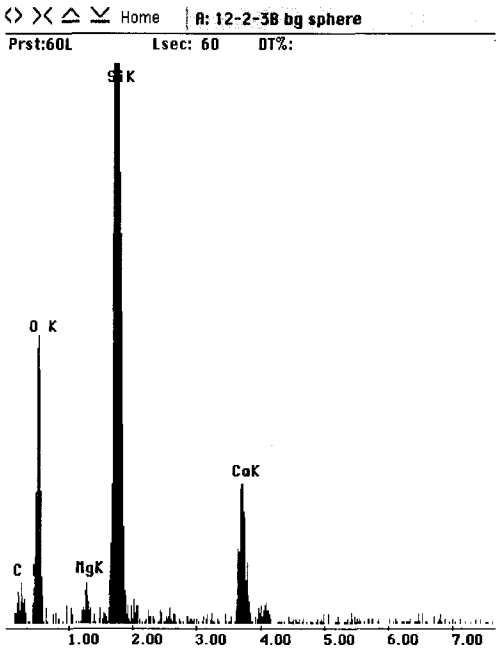

Figure 8.18 - EDS spectrum from a metallic sphere.

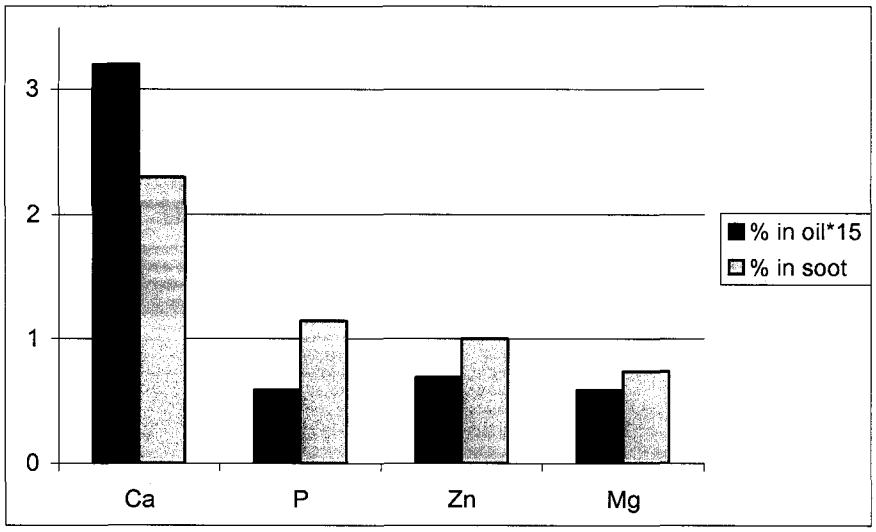

Figure 8.19 - Chart comparing % metals measured in soot samples (using EDS) and in the lube oil (using ICP-MS).

The vast majority of the nanoparticles are fairly spherical particles which look similar to one another (Figure 8.14b). EDS scans done on individual and groups of such nanoparticles suggest that they are carbonaceous. The very small mass makes it difficult to derive a dependable signal from the noise, but background subtracted spectra often show a small carbon peak and no other peaks. There are also occasional nanoparticles which have other morphologies and for which EDS analysis yields non-carbon peaks such as Fe and Al, but these are relatively rare.

Based on EDS spectra and previously observed morphologies of self nucleated particles, it is concluded that the bulk of the non-volatile nanoparticles are carbonaceous and are either "primary particles" of carbon or are hydrocarbon particles self-nucleated during piston retraction.

The fact that both the spherical particles and the carbonaceous nanoparticles are abundant at idle may be related to slobbering, i.e., excess oil consumption, which would result in increased amounts of both hydrocarbons and metals. It is hypothesized that the oil droplets may coalesce into spherical particles while most of their hydrocarbon compounds volatilize, (the latter creating a source of highly supersaturated hydrocarbons from which the carbonaceous nanoparticles then form during piston retraction). Since it has been shown that PAH's build up in the engine oil, that their survivability is 40-100 times greater for oil than for fuel and that they are released during combustion (Schramm et al. 1994), it is possible that the release of PAH's from oil much later in the expansion stroke (when temperatures are lower and cylinder surface area exposed to exhaust gases is higher), may contribute to the formation of such nanoparticles. More research is needed to verify this.

8.4 Summary

In this chapter I presented results of an experiment designed to investigate the generation of non-volatile (solid) nuclei mode particles by a heavy-duty diesel engine. Initial tests using a catalytic striper to pre-treat the particles before sampling, showed that a significant population of solid nanoparticles are generated at the idle engine setting. I first hypothesized that the particles were metallic, originating from lube oil additives. Subsequent measurement of metal to carbon ratios on size selected particle samples showed that this was not the case.

Size selected samples were used for EDS analysis of the solid nanoparticles and results suggested that the nanoparticles are carbonaceous. To further clarify this, data for

carbon emissions were collected and analyzed using the NIOSH method 5040 i.e. for assessing the EC and OC of samples. These data were used with calculated estimates of available particle surface area (from SMPS data) to yield a ratio of organic carbon in the sample to the available surface area of particles at the corresponding engine setting. Results showed that this ratio was higher for the idle setting, suggesting conditions may exist for the nucleation of hydrocarbons. Other conditions that would contribute to this are low cylinder temperature and sudden cooling during piston retraction, both of which are characteristic of an idling engine. It is hypothesized that all these factors may be working together to form this unique population of nanoparticles.

In addition to the solid nanoparticles, another unique particle type was observed in samples collected at the idle engine setting. This type of particle was extremely spherical and very rich in metals, specifically some of those derived from lube oils. The formation pathway for such particles is unclear and more research is warranted to elucidate their origin.

8.5 References

Abdul-Khalek, I.S., and D. B. Kittelson. Real Time Measurement of Volatile and Solid Exhaust Particles Using a Catalytic Stripper. SAE Paper No. 950236, 1995.

Abdul-Khalek, I. S., D. B. Kittelson, and F. Brear. The Influence of Dilution Conditions on Diesel Exhaust Particle Size Distribution Measurements. SAE Paper No. 1999-01-1142: 1-9, 1999.

Bagley, S. T., K. J. Baumgard, L. D. Gratz, J. H. Johnson, and D. G. Leddy. Aftertreatment Device Effects on Diesel Emissions. Health Effects Institute, Cambridge, MA, Research Report No. 76, 1996.

Birch, M. E. Analytical Instrument Performance Criteria: Occupational Monitoring of Particulate Diesel Exhaust by NIOSH Method 5040. Applied Occupational and Environment Hygiene 17(6), 400 – 405, 2002.

Du, C. J., J. Kracklauer, and D. Kittelson. Influence of an Iron Fuel Additive on Diesel Combustion. SAE Tech Paper 980536, pp. 1-13, 1998.

Flynn, P., R. Durrett, G. Hunter, A. Loye, O. C. Akinyemi, J. Dec, and C. Westbrook. SAE Technical Paper 1999-01-0509, 14 pp.

Higgins, K., H. Jung, D. B. Kittelson, J. T. Roberts, and M. Zachariah. Size-Selected Nanoparticle Chemistry: Kinetics of Soot Oxidation. Journal of Physical Chemistry, Vol. 106, No. 1, January 10, 2002, p. 96-103, 2003.

Jung, H., D. B. Kittelson, and M. R. Zachariah. The Influence of Cerium Additive on Kinetics of Diesel Nanoparticle Oxidation. Article in preparation 2003

Finlayson-Pitts, B.J., and J. N. J. Pitts. Atmospheric Chemistry: Fundamentals and Experimental Techniques. New York, N.Y., John Wiley and Sons, 1986.

Kittelson, D. B., and M. Stenitzer. A New Catalytic Stripper for Removal of Volatile Particles. Proceedings of 7th ETH Conference on Combustion Generated Nanoparticles, Zurich, August 2003.

Kittelson, D. J. Aerosol Sci. 1998,Vol. 29, No. 5/6, pp. 575-588.

Knutson, E. O., and K. T. Whitby. Aerosol Classification by Electric Mobility: Apparatus, Theory, and Application. Journal of Aerosol Science. 6:443-451, 1975.

Lee, D. G., A. L. Miller, M. R. Zachariah, and D. B. Kittelson. Characterization of Metal-Bearing Diesel Nanoparticles Using Single Particle Mass Spectrometry. Submitted to Journal of Aerosol Science, April 2004.

Marple, V., K. Rubow, and Steven Behm. A Microorifice Uniform Deposition Impactor (MOUDI): Description, Calibration and Use. Aerosol Sci & Tech, Vol. 14, pp. 434-446, 1991.

Miller, A. L., G. Ahlstrand, D. B. Kittelson, and M. R. Zachariah. The Fate of Metal (Fe) During Diesel Combustion: Morphology, Chemistry and Formation Pathways of Nanoparticles. Paper in preparation 2004.

Pipho, M. J., D. B. Kittelson, L. Luo, and D. Zarling. Injection Timing and Bowl Configuration Effects on In-Cylinder Particle Mass. SAE Tech. Paper 921646, pp. 111-126, 1992.

Roessler, D. M., F. R. Faxvog, R. Stevenson, and G. W. Smith. Optical Properties and Morphology of Particulate Carbon: Variation with Fuel/Air Ratio. Proceedings of Int. Symp. on Particulate Carbon, Formation During Combustion, GM Res. Lab., Edited by Donald Siegla and George Smith, October 15-16, 1980, pp. 57-84.

Schramm, J., S. Hori, and T. Abe. The Emission of PAH from a Diesel Engine Operating on Fuels and Lubricants with Known PAH Content. SAE Paper 940342, Diesel Combustion Processes and Emission Control, SP-1028, February 1994.

Siegmann, K., K. Sattler, and H. Siegmann. Clustering at High Temperatures: Carbon Formation in Combustion. J. Electron Spectroscopy and Related Phenomena, Vol. 126, pp. 191-202, 2002.

Wang, S.C. and R.C. Flagan [1989]. "Scanning Electrical Mobility Spectrometer". Division of Engineering and Applied Science, CA Institute of Technology, Pasadena, CA 91125, pp138-178.

Chapter 9 - Conclusions

This dissertation research was conducted to address a potential health concern regarding diesel particulate matter (DPM). The first chapter provides background information on the toxicology and adverse health effects of DPM. The second chapter outlines the basic engineering principles regarding particle formation and behavior while the third chapter focuses on the details of DPM formation. The material in the first three chapters provide a backdrop for Chapter 4, which is a simple statement of the dissertation hypothesis, reprinted here:

Dissertation Hypothesis

It is hypothesized that as a part of the diesel combustion process, trace amounts of metals from the fuel, lube oil and/or engine wear will vaporize and subsequently adsorb or condense onto the surfaces of carbon particles during and after combustion, and if the metal to carbon ratio during combustion reaches a critical level, self nucleated metallic nanoparticles will form.

The remainder of the chapters describe a series of experiments designed to address that hypothesis. Chapter five reports the results of experiments in which I employ a single particle mass spectrometer (SPMS) to investigate the fate of small amounts of metal (Fe) doped into the diesel fuel. Chapter 6 follows directly from that work and describes the analysis of the Fe-doped DPM using TEM/EDS. Chapter 7 also describes the analysis of DPM using the SPMS, but for that work the fuel was doped with small amounts of lube oil to raise the level of several metals in the system, i.e., those

which would originate from lube oil consumption under normal operating conditions. Chapter 8 is the culmination of this work and describes the characterization and analysis of DPM for an engine operating under normal conditions (no doping of fuel).

9.1 Overall Summary of Research Results

In the first three chapters, evidence is cited that indicates potential toxicity from the inhalation of metallic particles, and that such toxicity is enhanced by the increased surface area of ultra-fine and nano-sized particles. Research presented in subsequent chapters demonstrates that diesel engines do in fact produce ultra-fine and nano-size particles that contain varying amounts of metals. The following paragraphs summarize that research and provide rationale for the final section of this document, which is a statement of the conclusions to my dissertation hypothesis.

In the experiments described in Chapter 5 that entailed doping of the diesel fuel with iron, it was shown that when using 20 ppm iron doping, self-nucleated iron particles are formed and are detectable by both the SMPS and SPMS. As iron content is increased, the iron nanoparticles grow in size and number (in size range 20-40 nm). At low engine load, (or lesser iron availability), the proportion of iron on small particles increases non-linearly, suggesting condensation of iron onto the particles. When more iron is available, self-nucleated particles increase in number and the amount of iron on larger particles is more variable, indicating coagulation of the iron nanoparticles with the larger carbon agglomerates.

For the experiments discussed in Chapter 6, exhaust particles from Fe-doped combustion are analyzed using TEM/EDS. Electron micrographs and EDS spectra are used to identify the following distinct types of particles for this case:

1) Carbon Agglomerates
2) Self Nucleated Metallic Primary Particles (Fe)
3) Carbon Agglomerates Decorated with Metallic Primary Particles
4) Metal Agglomerates
5) Combination Metal/Carbon Agglomerates

As part of that work, combining measurements of carbon output of the engine taken simultaneously with particle size distribution measurements, I showed that above a threshold iron to carbon ratio of approximately 0.013, iron nanoparticles form during diesel combustion and subsequently coagulate with each other as well as with larger carbon agglomerates.

Showing how the presence of iron leads to a variety of particle morphologies gave me insight into particle formation pathways and led to the design of a subsequent set of experiments in which the diesel fuel was doped with lube oil. The idea was to introduce some of the same metals (metallic lube oil additives) that would be present under normal operating conditions.

For that work, described in chapter seven, the exhaust particles were analyzed using the SPMS and results demonstrated that when lube oil is added to the fuel in a diesel engine, the metallic additives in the oil (including Ca, P, S, and Zn) participate directly in the combustion process and subsequently exit the engine in particulate form.

It is also shown that if metal to carbon ratios are high, metals (in this case Ca) can and do self nucleate and form metallic nanoparticles that have primary particle size in the 5-20 nm range, and larger (20-200 nm) metal-rich particles are also formed. Depending on the amount of metal in the system and on the relative time history of self nucleation of metals and carbon, metallic primary particles and/or their agglomerates may coagulate with carbon particles and form a population of "combined agglomerate" particles. The morphology of such particles appears to be a function of the time history of formation for the participating species, and may also be influenced by other forces such as particle charges or elemental affinities.

At low engine load, using 1% lube oil doping of fuel, self-nucleated Ca particles (about 10 nm diameter) are first detectable by the SMPS. This "threshold" condition corresponds to a Ca throughput of approximately 0.03-0.04 g/hr. As more metal is added to the system above this threshold level, much of it self-nucleates into nanoparticles during the combustion and/or expansion processes, and these nanoparticles may then coagulate with each other and with carbon particles. This work suggests that for modern engines with combustion systems optimized to produce low emissions of solid carbon, a given metal content in the fuel (or lube oil) will produce a higher metal to carbon ratio during combustion, and therefore a greater tendency to produce metal-rich nanoparticles in the exhaust.

A final set of experiments, described in chapter eight, entailed no doping of the fuel. Since the levels of the metals were likely to be too low for easy detection with the SPMS and because much of the analysis was done on particles too small to penetrate the aerodynamic lens of the SPMS, offline analysis by TEM/EDS was used. Size-selected

particle samples were analyzed metal to carbon ratios measured for each sample. Results showed that the metal levels were enhanced greatly at the idle engine setting.

Initial tests using a catalytic stripper to pre-treat the particles before sampling, showed that a significant population of solid nanoparticles were generated at the idle engine setting. I first hypothesized that the particles were metallic, originating from lube oil additives. Subsequent measurement of metal to carbon ratios on size selected particle samples showed that this was not the case.

Size selected samples were then used for EDS analysis of the solid nanoparticles and results suggested that the nanoparticles were carbonaceous. To further clarify this, data for total carbon emissions were collected and analyzed using the NIOSH standard method 5040 i.e. for assessing the EC and OC of samples. These data were used along with calculated estimates of available particle surface area (from SMPS data) to yield a ratio of organic carbon in the sample to the available surface area of particles at the corresponding engine setting. Results showed that this ratio was much higher for the idle setting, suggesting that conditions may exist for the self nucleation of heavy hydrocarbons. Other conditions that would contribute to this are low cylinder temperature and sudden cooling during piston retraction, both of which are characteristic of the idling engine. It is hypothesized that all these factors may be working together to form this unique population of nanoparticles.

In addition to the solid nanoparticles, another unique particle type was observed in samples collected at the idle engine setting. This type of particle was extremely spherical and very rich in metals, specifically some of those derived from lube oils. The

formation pathway for such particles is unclear and more research is warranted to elucidate their origin.

9.2 Conclusion to the Dissertation Hypothesis

It has been shown that for the case of diesel combustion at low engine load using iron-doped fuel (20 ppm Fe), the metal to carbon ratio is below the threshold for self nucleation, but iron appears to condense onto particles. At a higher doping level (60 ppm) and higher engine load, a significant population of iron nanoparticles is formed. Similar results were derived from experiments where the fuel was doped with lube oil, adding metals to the fuel in the form of metallic lube oil additives. For undoped diesel combustion, it was shown that for a typical modern heavy duty engine, operating under a lean fuel mixture condition (idle mode), the metal to carbon ratio is at or just below the threshold for self nucleation, so few if any metallic nanoparticles are formed. However for this undoped case, the exhaust particles contain much higher metal content than for the rich (undoped) operating conditions. Although significant numbers of metallic nanoparticles are not formed, a new (and large) population of solid nanoparticles is in fact formed, as well as a smaller population of ultrafine metallic spheres. The solid nanoparticles are carbonaceous and are believed to be derived mainly from unburned lube oil which produces relatively high levels of organic carbon under these conditions. The origin of the metallic spheres is unclear, but appears to be directly associated with greater relative oil consumption. These unique particle types may potentially represent a new health concern. It is hoped that the results of this work will assist epidemiological studies that investigate the impact of such particles on human health.